Thermal Modeling and Performance Investigations of Metal Hydride Based Heat Pumps

A thesis
submitted in partial fulfillment of the
requirements for the degree of

Doctor of Philosophy

by

A. Satheesh
(06610301)

Department of Mechanical Engineering
Indian Institute of Technology Guwahati
Guwahati
February 2011

THESIS CERTIFICATE

This is to certify that the work contained in the thesis entitled **Thermal Modeling and Performance Investigations of Metal Hydride Based Heat Pumps** by **A. Satheesh**, a student of the Department of Mechanical Engineering, Indian Institute of Technology Guwahati, for the award of the degree of **Doctor of Philosophy** has been carried out under our supervision and that this work has not been submitted elsewhere for any degree.

Dr. P. Muthukumar
Associate Professor
Department of Mechanical Engineering
Indian Institute of Technology Guwahati
Guwahati – 781039, Assam
INDIA

Dr. Anupam Dewan
Professor
Department of Applied Mechanics
Indian Institute of Technology Delhi
New Delhi – 110016
INDIA

Dedicated to

my

Beloved Mother

ACKNOWLEDGEMENT

First and foremost, I would like to express my sincere gratitude and thanks to my supervisors **Dr. P. Muthukumar** and **Dr. Anupam Dewan** for their admirable guidance, advice encouragement and generous throughout my study. I have no doubts that finishing my degree in a proper and timely manner was impossible without their helps, suggestions and advices. I am extremely fortunate to work under them.

I express my heartfelt thanks to **Dr. –Ing. Manfred Groll, IKE, University of Stuttgart, Germany** for providing valuable technical suggestions and ideas at every stage of the research work. I am also very grateful to my doctoral committee members **Dr. U. K. Saha**, **Dr. A. Srinivasan** and **Dr. Anil verma** for sparing their precious time to evaluate the progress of my work.

I would like to express my sincere thanks to **Dr. D. Chakraborty** the Head of the Department and other faculty members for their kind help in carrying out this work. I am also grateful to all the members of the research and technical staff of the department without whose help I could not have completed this thesis.

My deepest gratitude goes to my family for their continuous love and support through out my studies. The opportunity that they have given me and their unlimited sacrifices are the reasons where I am and what I have accomplished so far.

I should take this opportunity to thank my friend **Mr. K. Ravi Kumar** who insisted me to apply for Ph.D at IIT Guwahati. I am extremely grateful to **Dr. D. Santhosh Kumar** for teaching the basic of C language, and useful discussions and suggestions throughout my research work. I extend my thanks to **Mr. U. Madhavakrishna, Mr. A. Harish,** and **Mr. M. M. Umekar** for their invaluable help during the initial stage of my research work. I express my thanks to **Mr** and **Mrs. Ratanakar Das** for their affection and encouragement have supported by morale and made my stay at IIT Guwahati a memorable and most delightful experience. I cherish their friendship.

I would like to thank **Dr. S. P. Lakshmanan, Dr. D. Senthil kumar, Mr. S. Anbarasu** and **Mr. B. Satya Sekhar** with whom I had academic discussions and shared personal feeling during my entire stay at IIT Guwahati. I am sincerely thanks to **Dr. Vijay pantangi, Dr. D. A. Perumal, Mr. C. Subramaniam, Mr. M. Eswaran, Mr. E. Sureshpandian, Mr. C. Shyam Anand, Mr. N. Rama Krishnan, Mr. Anto Pradeep, Mr. P. Monash, Mr. Ashok, Mr. Satheesh , Mr. G. Suresh babu, Mr. P. Suresh Kumar, Ms. Sumitra, Dr. Arpananath, Mrs. P. Sangeetha** and during this four years at IITG, I have many friends who helped me in several ways, I would like to say a gratitude to all of them for their friendship and support.

Finally, I am very much grateful to my dear friends **Mr. N. Gnanasekaran, Mr. K. Lakshmi Narayanan, Mr. B. Nethaji**, **Mr. Radha Krishnan, Mr. K. Munusamy** and **Ms. N. R. Devi** whose continuous support and motivation to complete the thesis work.

ABSTRACT

The use of Chloro-Fluro-Carbon refrigerants (CFCs) is a significant source of pollution to the global environment and an attempt is being made to minimize this problem through the promotion of the alternative refrigeration and air-conditioning systems. One of the most promising alternatives is the use of hydrogen as a refrigerant in the thermally driven metal hydride based heating and cooling systems. These systems provide a wide operating temperature range and use low grade thermal energy (e.g., waste heat from industries, heat from the exhaust flue gases and solar energy) to produce high quality thermal energy and cooling outputs. Further, these systems are environment friendly, contain no moving parts, have a compact construction and offer noise free operation. Absorption and desorption of hydrogen to/from the metal hydride are exothermic and endothermic reactions, respectively. The performance of such devices highly depends on the rate at which the heat is removed/supplied from/to the metal hydride beds. Development of an efficient and economic design of such devices requires highly sophisticated computational methods. Therefore, it is necessary to carry out the mathematical modeling before conducting the expensive experiments. Many investigators have predicted the heat and mass (hydrogen) transfer characteristics of metal hydride beds [e.g., Mayer *et al*. (1987), Groll *et al*. (1987, 1993), Gopal and Murthy (1992, 1995)] using various simplifying assumptions, such as, the use of one-dimensional model without considering the effect of hysteresis and plateau slope in the pressure-concentration-temperature (PCT) curve, neglecting the variation in the heat transfer fluid temperature along the axial direction of the reactor, etc. Such simplified models reported in the literature have limited scopes. Further, there is a lack of literature on thermal modeling of metal hydride heat pump (MHHP).

A transient coupled heat and mass transfer model in cylindrical coordinates for predicting the performance of metal hydride based heat pumps is developed in the present thesis. Effects of hysteresis and plateau slope on the PCT characteristics of the metal hydrides and variation in the heat transfer fluid temperature along the axial direction of the reactor are considered in the model. The objectives of the thesis are;

- to predict the performance of a single-stage metal hydride heat pump (SS-MHHP) at different operating conditions employing different alloy pairs
- to predict the performance of a double-stage double-effect metal hydride heat pump (DSDE-MHHP) at different operating conditions

- to evaluate the performance of cross van't Hoff metal hydride based heat pump at different operating conditions.

Accuracy of a thermal model used for predicting the performance of MHHP highly depends on the precise determination of the thermo-physical properties, such as, the activation energy, reaction rate constant, enthalpy of formation and entropy of formation. To begin with, the hydriding kinetics of some commonly used metal hydrides for the heat pump applications, such as, $LaNi_5$, $LaNi_{4.7}Al_{0.3}$ and $LmNi_{4.91}Sn_{0.15}$ alloys are investigated at different temperatures. Two widely used reaction kinetics models, namely, Jander diffusion model (JDM) and Johnson-Mehl-Avrami (JMA) model are considered for the analysis. Two variants of JMA model, namely, JMA model 1 in which the order of the reaction is assumed as unity and JMA model 2 in which the rate constant is calculated by estimating the order by fitting the reaction kinetics data with a reaction kinetics equation, are considered. The activation energy and pre-exponential constants of the above-mentioned alloys are estimated by constructing the Arrhenius plot. Activation energies estimated using different models are compared. The accurate values of activation energy for different alloys considered are determined by comparing the reaction kinetics data obtained from these models with the corresponding experimental data. The present results show that the predictions using JDM model closely match with the experimental data for all three alloys and therefore, the rate-controlling mechanism in the (α+β)-phase region is the diffusion of the hydride atom into the metal hydride. The estimated activation energies of $LaNi_5$, $LaNi_{4.7}Al_{0.3}$ and $LmNi_{4.91}Sn_{0.15}$ hydride alloys are 27.7, 29.1 and 28.0 kJ/mol of H_2, respectively, using Jander diffusion model.

A computational investigation of a single-stage metal hydride cooling system working with $MmNi_{4.6}Al_{0.4}$ / $MmNi_{4.6}Fe_{0.4}$ hydride pair has been performed in the present thesis. The system of equations is solved by the fully implicit finite volume method (FVM) using the central difference scheme. The computational results are compared with the experimental data reported in the literature [Ni and Liu (2007)] for $LaNi_{4.61}Mn_{0.26}Al_{0.13}$ / $La_{0.6}Y_{0.4}Ni_{4.8}Mn_{0.2}$ hydride pair and a good agreement between the two is observed. The effects of constant and variable wall temperature convective boundary conditions on the reaction bed temperature distribution, hydride concentration, and equilibrium pressures of the reactors are investigated. The heat interactions (cooling/heating) between the hydride beds and heat transfer fluids are also studied for a complete cycle. A dynamic correlation of the PCT plot is presented and a large deviation between the static and dynamic van't Hoff plots is observed. At the given operating temperatures of 363, 298 and 278 K of heat source, heat sink and refrigeration, respectively, the cycle time for the constant and

variable wall temperature convective boundary conditions of a single-stage metal hydride system are found to be 1470.0 s and 1765.6 s, respectively.

The mathematical model developed for a single-stage metal hydride heat pump (SS-MHHP) is extended to study the performance of the system working with five different alloy pairs, namely, $MmNi_{4.6}Al_{0.4}$ / $MmNi_{4.6}Fe_{0.4}$ (AP1), $LaNi_{4.61}Mn_{0.26}Al_{0.13}$ / $La_{0.6}Y_{0.4}Ni_{4.8}Mn_{0.2}$ (AP2), $LmNi_{4.91}Sn_{0.15}$ / $Ti_{0.99}Zr_{0.01}V_{0.43}Fe_{0.09}Cr_{0.05}Mn_{1.5}$ (AP3), $LaNi_{4.6}Al_{0.4}$ / $MmNi_{4.15}Fe_{0.85}$ (AP4) and $Zr_{0.9}Ti_{0.1}Cr_{0.9}Fe_{1.1}$ / $Zr_{0.9}Ti_{0.1}Cr_{0.6}Fe_{1.4}$ (AP5). The influences of the operating temperatures, such as, heat source (T_H), heat sink (T_M) and refrigeration (T_C) temperatures on the coefficient of performance (COP) and specific cooling power (SCP) of the system are presented. The optimum operating temperatures of all the selected metal hydride pairs are found out. From the selected hydride alloy pairs, the maximum COP is found to be 0.66 for $Zr_{0.9}Ti_{0.1}Cr_{0.9}Fe_{1.1}$ / $Zr_{0.9}Ti_{0.1}Cr_{0.6}Fe_{1.4}$ at the operating temperatures of 393/298/288 K ($T_H/T_M/T_C$) and the highest SCP of 53.25 W/kg of total mass of the system is obtained from the $LmNi_{4.91}Sn_{0.15}$ / $Ti_{0.99}Zr_{0.01}V_{0.43}Fe_{0.09}Cr_{0.05}Mn_{1.5}$ hydride pair at the operating temperatures of 413/298/293 K, respectively.

The performance investigation of a double-stage double-effect metal hydride heat pump (DSDE-MHHP) working with $LaNi_{4.1}Al_{0.52}Mn_{0.38}$ / $LmNi_{4.91}Sn_{0.15}$ / $Ti_{0.99}Zr_{0.01}V_{0.43}Fe_{0.09}Cr_{0.05}Mn_{1.5}$ as high / medium / low temperature alloys is presented. For comparing the present computational results, the operating temperatures of 568, 361, 296, and 289 K as heat driven (T_D), heat rejection (T_H), heat sink (T_M) and refrigeration (T_C) temperatures, respectively, chosen by Klein (2007) are considered. The variation of reaction bed temperatures during the hydriding and dehydriding processes is compared with the experimental data reported by Klein (2007) and a good agreement is observed between the two. The variations in hydride concentrations, equilibrium pressures, and temperatures within the hydride beds, and the heat exchange between the hydride beds with the heat transfer fluids are presented for a complete cycle. The operating cycle of a DSDE-MHHP is explained on the dynamic PCT plot. For the given operating temperatures of 568 / 361 / 296 / 289 K (T_D / T_H / T_M / T_C), the average COP and SCP of the system are found to be 0.471 and 28.4 W/kg of total hydride mass, respectively.

Further, this model is extended to study the effects of half cycle time (θ), hydride mass ratio (M_R), sensible heat exchange factor (ϕ) and operating temperatures, such as, heat source (T_D), heat sink (T_M), and refrigeration (T_C) temperatures on the amount of hydrogen transferred between the paired reactors, coefficient of performance (COP) and

specific cooling power (SCP) of a DSDE-MHHP system. The numerical results show that the effects of heat source and refrigeration temperatures on system COP are more significant than that of the heat sink temperature. Based on the operating conditions, the half cycle time is fixed as 15 min and the optimum operating temperatures are 578 / 373 / 298 / 283 K. The COP and SCP of the system for the above-mentioned optimum operating temperatures are found to be 0.81 and 48.1 W/kg of total alloy mass, respectively. It is observed from the numerical results that a decrease in the mass ratio from 1.35 to 0.3 enhances the COP and SCP by approximately 17.5% and 46.3%, respectively. Recovery of 50% sensible heat improves the COP by 32%. Therefore, to achieve a good (optimum) performance one has to give attention to the design and optimization of the reaction beds, heat and mass transfer issues, and the internal heat recovery between high and intermediate pressure reactors. However, additional heat exchangers are necessary for the utilization of the sensible heat and hence, the economic feasibility of internal heat recovery should be evaluated before its implementation.

The operating feasibilities of a SS-MHHP working on cross van't Hoff line concept is investigated by employing two different hydride alloy pairs, namely, $V_{0.846}Ti_{0.104}Fe_{0.05}$ / $Fe_{0.9}Mn_{0.1}Ti$ and $V_{0.855}Ti_{0.095}Fe_{0.05}$ / $MmNi_{4.7}Al_{0.3}$. The importance of cross van't Hoff MHHP is to utilize the enthalpy of formation of refrigeration alloy for driving the system. The influences of heat source (T_H) and refrigeration (T_C) temperatures on the amount of hydrogen transferred between the paired reactors, COP and SCP of the system are studied. For the given operating temperatures of 373/303/291 K, the COP and SCP of SS-MHHP working on the cross van't Hoff line concept are found to be 0.89 and 30.8 W/kg of total system mass, respectively for $V_{0.846}Ti_{0.104}Fe_{0.05}$ / $Fe_{0.9}Mn_{0.1}Ti$ hydride pair. While, for $V_{0.855}Ti_{0.095}Fe_{0.05}$ / $MmNi_{4.7}Al_{0.3}$ hydride pair, these values are 0.86 and 30.3 W/kg of total system mass at the operating temperatures of 400/303/283 K. For the same operating temperatures and geometric conditions, COP of the conventional SS-MHHP is found close to 0.6.

In general, by using these thermal models one can obtain the optimum operating parameters, such as, heat source, heat sink and refrigeration temperatures, and half cycle time, and design parameters, such as, hydride mass ratio, hydride bed thickness, and sensible heat exchange factor without conducting the expensive experimental studies. Further, the results of the present thesis will also be useful in developing an economic and efficient reaction bed which can deliver a short cycle time.

CONTENTS

LIST OF FIGURES

LIST OF TABLES

NOMENCLATURE

A	Surface area [m^2]
C	Reaction rate constant [s^{-1}]
C_p	Specific heat capacity [J/kg-K]
COP	Coefficient of performance
E	Activation energy of the reaction [J/mol H_2]
f	Reacted fraction
k	Thermal conductivity [W/m-K]
K	Coefficient of Darcy law [m^2]
L	Length of the reactor [m]
m_f	Mass flow rate of the heat transfer fluid [kg/s]
$\dot{m}_{H_2}$	Mass flow rate of hydrogen [kg/m^3-s]
M	Molecular weight [g/mol]
M_R	Hydride mass ratio
n	Order of reaction, number of moles of hydrogen [mol]
P	Pressure [bar]
Q	Heat interaction [J]
r	Radius of the reactor [m]
R_u	Ideal gas constant [J/mol-K]
SCP	Specific cooling power [W/kg]
t	Time [s]
T	Temperature [K]
u	Velocity [m/s]
U	Overall heat transfer coefficient [W/m^2-K]

V	Free Volume [m^3]
x	Concentration (H/M)
Z	Compressibility factor

Greek symbols

ΔH	Enthalpy of formation[J/mol H_2]
ΔS	Entropy of formation [J/mol H_2-K]
ρ	Density [kg/m^3]
μ	Dynamic viscosity [N-s/m^2]
v_g	Kinematic viscosity [m^2/s]
ε	Porosity
φ, φ_o	Slope factors
β	Hysteresis factor
ϕ	Sensible heat exchange factor
θ	Half cycle time [min]

Subscripts

a	absorption
A,B	hydrides
C	refrigeration
d	desorption
D	driving
e	effective
eq	equilibrium

f	final, fluid
fi	heat transfer fluid inlet
fo	heat transfer fluid outlet
g	gas
h	hydride
H	rejection
i	inner, inital
m	metal
M	sink
max	maximum
min	minimum
P	connecting pipe
r	reactor
s	supply, solid
ss	saturation
T	total
I	first half cycle
II	second half cycle

CHAPTER 1

INTRODUCTION

1.1 HYDROGEN ENERGY ECONOMY

We are living in a fossil fuel dominated world. These fuels have limited resources and their use has a negative impact on the environment. The recent increase in energy demand has put an additional pressure on the energy scenario in the world over. Therefore, the ways of making the energy economy more environment friendly are intensively discussed in the literature (Winter, 2009). There is a need to use clean energy sources, especially with respect to the global warming. Not only renewable energy sources are discussed, but also the sequestration of CO_2 from the fossil fuel based power stations is considered. Lately, hydrogen has received renewed interest as an ideal zero emission secondary energy carrier with a potential of replacing fossil fuels in the transportation sector and various industrial applications for heating and cooling. With a strong possibility of an increased hydrogen usage, the issues of safety, and efficient and economical storage of hydrogen are of significant importance.

Hydrogen is traditionally stored as a compressed gas or as a cryogenic liquid (Züttel, 2003). Both of these storage methods exhibit a reasonable gravimetric storage capacity. However, a great amount of high grade energy is required to compress or liquefy the hydrogen. Table 1.1 lists the basic hydrogen storage options with detailed information about the gravimetric (ρ_m) and volumetric (ρv) densities (Züttel, 2003; Fu, 2007) at different working pressures and temperatures. Hydrogen storage in metal hydrides seems to be a good solution compared to high pressurized tanks or liquid hydrogen system due to their high inherent safety and high volumetric storage density. However, most metal hydrides available for applications under the working conditions of pressures of approximately 10.0 bar at near ambient temperatures have a comparably small gravimetric storage capacity. Besides hydrogen storage, the metal hydride systems are used in a wide range of applications, such as, thermal energy storage, hydrogen compressor, water pump, heat pump, refrigerator and heat upgrading systems. Among these applications, metal hydride heat pumps are used for both heating and cooling applications.

Table 1.1 Basic hydrogen storage methods with gravimetric and volumetric densities at different working pressures and temperatures (Züttel, 2003; Fu, 2007)

Storage method	**ρ_m wt%**	**ρ_v kgH_2/m^3**	**Temp. °C**	**Pr. bar**	**Remarks**
High-pressure gas cylinders	4(13)	<40	~25	300 (800)	Energy for compression: ~2 to 3 kWh_{el}/kgH_2
Liquid hydrogen in cryogenic tanks	Size dependent (eg. ~5wt% for a can tank)	70.8	-252	1	Energy for liquefaction: ~10 to 12 kWh_{el}/kgH_2
Adsorption	~2	20	-80	100	e.g., CNT, CNF
Absorption	2	150	<100	>1	Intermetallic compounds
	7.6	135	>300	~1	Mg
	<18	150	>100	1	Complex compounds, e.g., Alanates, Borates

1.2 METAL HYDRIDES

Metal hydrides are chemical compounds formed when the hydrogen gas reacts with metals. Such metal-hydrogen reactions can take place in a wide range of equilibrium temperatures and pressures. The most useful metal hydrides react with hydrogen near room temperature just above the atmospheric pressure. When metal hydride forming metals or metal alloys (usually in granular form) are exposed to hydrogen at a certain pressure and temperature, they can absorb large quantities of hydrogen by liberating great amounts of heat during formation of metal-hydrogen compounds (exothermic reaction). During absorption, the hydrogen atom is uniformly bound in the interstitial sites in the metal (alloy) lattice:

$$Metal + H_2 \rightarrow Metal\ hydride + Heat \tag{1.1}$$

The above-mentioned process results in the distribution of hydrogen throughout the metal lattice and hydrogen gets stored in the form of a solid solution. Similarly, when the metal hydride is heated to a certain temperature at a certain pressure, the metallic bonds between the hydrogen and metal hydride breaks and the hydrogen gets desorbed (endothermic reaction):

$$Metal + H_2 \leftarrow Metal\ hydride + Heat \tag{1.2}$$

The detailed thermodynamics of metal hydride formation is discussed in the following section.

1.3 THERMODYNAMICS OF METAL HYDRIDE FORMATION

Metal hydrides are formed when metal hydride forming metals or alloys are exposed to hydrogen at certain pressures and temperatures. Initially, the hydrogen molecules physically come in contact with the metal surface. Then, the hydrogen molecules dissociate into the hydrogen atoms and penetrate into the surface of the metal or alloy.

The hydrogen dissolves randomly in the metal lattice forming a solid solution of hydrogen in the metal and after reaching a saturation level hydrogen atoms arrange themselves in a specific configuration along with the metal atoms by forming a metallic bond between the metal and hydrogen atoms. The process of hydrogen uptake by the metal is represented by the following equation

$$M + \frac{X}{2} H_2 \underset{desorption}{\overset{absorption}{\rightleftharpoons}} MH_X . \tag{1.3}$$

The thermodynamic equilibrium of hydrogenation and dehydrogenation can be depicted in a diagram, correlating equilibrium pressure, temperature, and hydrogen concentration, called the pressure-composition-temperature (PCT) curve. The ideal PCT diagram is shown in Fig. 1.1(a). Three distinct parts can be observed in the PCT diagram. The initial steep slope corresponds to the hydrogen diffusion in the metal lattice (α-phase). As the α-phase reaches saturation, a second solid phase (β-phase) begins to form. According to the Gibbs phase rule, for a given temperature, the pressure remains constant as the concentration of hydrogen increases with progressive conversion of the α-phase into the β-phase. When all the hydride is converted to β-phase, the pressure starts rising steeply as more hydrogen is added to the system. The flat (α+β)-region is the most important part of the PCT diagram as most of the hydrogen is absorbed in this region under a constant pressure. The initial steep slope during the transformation of the α-phase to the (α+β)-phase and the later pressure rise during the (α+β)-phase to the β-phase obeys the Sieverts law (Sieverts, 1914).

$$x_{H_2} = \sqrt{P_{H_2}} \tag{1.4}$$

According to Eq. (1.4), a strong increase in pressure only leads to a rather small amount of dissolved hydrogen (α-phase). Within this range, there exist two components, metal and hydrogen, and two phases, a gaseous phase (hydrogen) and solid phase (metal).

Therefore, according to Gibbs' phase rule (Eq. 1.5), the number of degrees of freedom is two, viz., pressure and temperature.

$$f = C - P + 2 \tag{1.5}$$

If the temperature remains constant, i.e., during an isothermal condition, the amount of absorbed hydrogen is only related to the pressure (given in the Eq. 1.4). During the formation of metal hydride [(α+β)-phase], there exist three phases, one gaseous phase (hydrogen) and two solid phases (metal and metal hydride). According to Eq. (1.5), there is only one degree of freedom. If the temperature is the independent variable, the other parameters can be determined as a function of temperature under the equilibrium conditions. The degree of freedom during the β-phase can be determined using Eq. (1.5). Thus two components (hydrogen and metal) and two phases (solid and gaseous) exist and therefore, the degree of freedom (pressure and temperature) is two as in the α-phase.

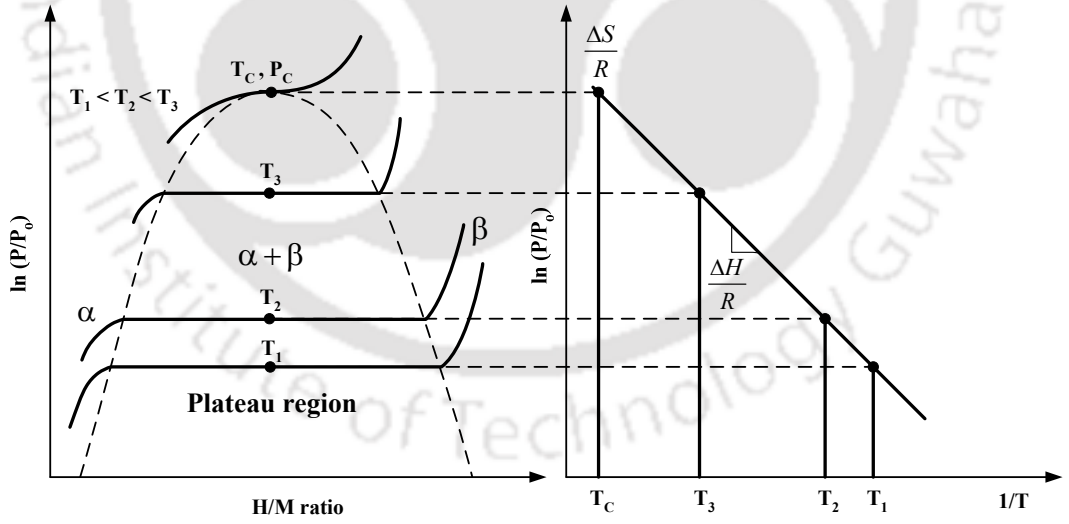

Fig. 1.1(a) Ideal pressure-concentration-temperature diagram.

Fig. 1.1(b) Ideal van't Hoff plot.

Metal hydrides with wide plateau region are advantageous as they absorb large amount of hydrogen under a constant pressure. It can be observed that the width of the plateau reduces as the temperature increases, and altogether vanishes at the critical temperature T_C where the α-phase is converted directly into the β-phase. The hydrogen storage capacity of a metal hydride is formulated as either atomic hydrogen to metal ratio (H/M ratio) or wt%. Generally, hydrogen storage capacity is represented as wt% and this parameter can be easily compared for different metal hydrides. At a given temperature, the value of the plateau pressure is the direct indication of the thermal stability of the metal hydrides. Highly stable metal hydrides are characterized by small plateau pressures and vice versa. A correlation between the equilibrium pressure and the inverse of absolute temperature (1/T) is represented in Fig. 1.1 (b) and is called van't Hoff plot. The negative slope and the intercept from the plot give the enthalpy of formation (ΔH) and entropy of formation (ΔS), respectively.

The actual PCT diagram is shown in Fig. 1.2(a) and 1.2(b). The plateau slope and hysteresis effect significantly affect the performance of the metal hydride based thermal machines. Hysteresis was initially predicted by Holt (1913). Many physical systems naturally exhibit hysteresis. This effect is also predicted in the reversible hydrogen storage in metal hydrides. For a given temperature, hysteresis is referred as the logarithmic pressure ratio between the absorption and desorption ($\ln (P_a/P_d)$) at the mid point of the (α+β)-region (Huston and Sandrock, 1980). This asymmetry varies widely from alloy to alloy. Fig. 1.2(a) shows that the width of the hysteresis decreases with higher isothermal conditions, and finally, it vanishes at the critical temperature (T_C). Apart from the hysteresis, another irreversibility that reduces the system efficiency is the sloped plateau and it is characterized by the expression

$$\varphi = \frac{d \ln P}{dx_{H_2}}. \tag{1.6}$$

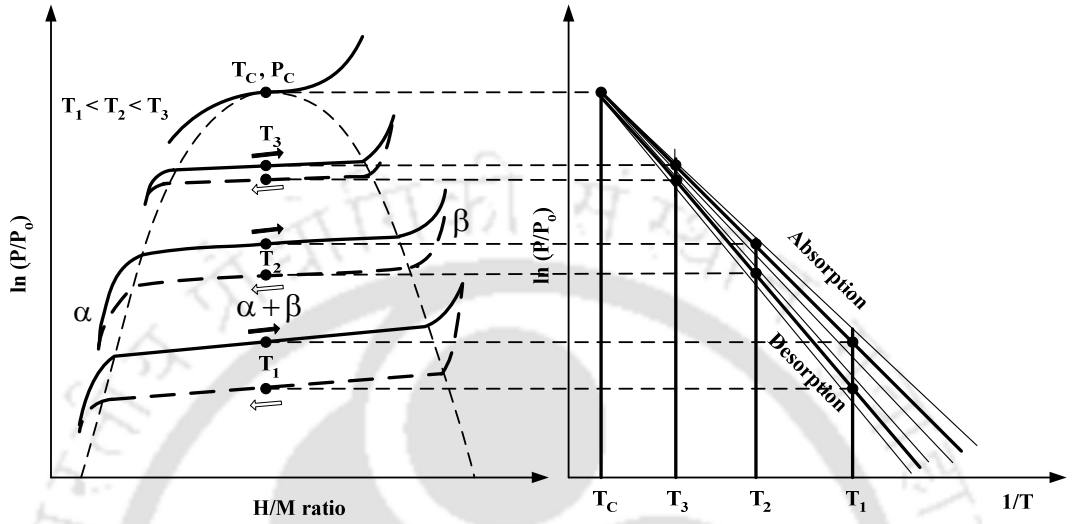

Fig. 1.2(a) Actual pressure-concentration-temperature diagram.

Fig. 1.2(b) Actual van't Hoff plot.

In actual systems all the hydrides possess sloped plateaus and this effect is not desirable in the practical applications. The magnitude of the sloped plateau region depends strongly on the material considered. Because of the plateau slope, the equilibrium pressure in the (α+β)-region increases with concentration during the absorption, and decreases with concentration during desorption. This behavior reduces the usable hydrogen capacity. As a result, the system performance is reduced. These irreversibilities can be varied by tailoring the hydride alloys. Important properties of metal hydrides required for the thermodynamic analysis are, the enthalpy of formation (ΔH), entropy of formation (ΔS), equilibrium pressure (P_{eq}), equilibrium temperature (T), hydride concentration (x), slope factors (φ, φ_o) and hysteresis factor (β). The fundamental equation, which relates equilibrium pressure to the reference pressure (P_o) with the other properties, is the van't Hoff equation and it is given as (Nishizaki *et al*., 1983)

$$ln\left(\frac{P_{eq}}{P_o}\right)=\left[\frac{\Delta S}{R_u}-\frac{\Delta H}{R_u T}+(\varphi\pm\varphi_o)\tan\left(\pi\left(\frac{x}{x_f}-\frac{1}{2}\right)\right)\pm\frac{\beta}{2}\right] \quad (1.7)$$

where, '+' sign indicates absorption and '–' sign indicates desorption. The slope factor is expressed in terms of the hydrogen concentration.

1.4 CLASSIFICATION OF METAL HYDRIDES

Metal hydrides can be classified on the basis of the type of bonding between the alloy and hydrogen atoms. The bonds can be: (1) ionic, (2) covalent and (3) metallic. Of these types, the covalent hydrides cannot be formed by the direct reaction of hydrogen with metals unless under very special conditions (Gopal, 1996). All other ionic hydrides except magnesium hydrides (MgH_2) are too stable for use in practical hydride systems (Reilly, 1979). Hence, only the metallic hydrides offer the necessary behavior for storing large quantities of hydrogen reversibly, as well as faster reaction kinetics, ease of formation and economical costs. Therefore, these alloys and intermetallics are of special interest from the heat pump (both heating and cooling) and energy storage points of view.

Another important classification of metal hydrides is with respect to the number of alloy atoms in one mole of material. Based on this classification, different types of metal hydrides are characterized. They are: AB, AB_2, A_2B, and AB_5 (Dantzer and Orgaz, 1986). First element (A) denotes the element with strong hydriding properties which contributes mainly to the hydrogen storage and the second element (B) denotes the element with weak hydriding properties, which acts as the catalyst to accelerate the hydriding kinetics. These classifications are used to help organizing the hydride alloys for different metal hydride applications.

1.5 APPLICATIONS OF METAL HYDRIDES

The unique advantage of metal hydride systems is that a wide range of operational requirements (pressures and temperatures) can be met by suitably changing the alloy composition, e.g., by changing the amount of aluminium in $LaNi_{5-x}Al_x$ compound from x = 0 to 1.0, the equilibrium temperature (for the same equilibrium pressure of 1 bar) increases approximately from 16°C to 160°C. The corresponding enthalpy of formation changes from 31.78 kJ/mol H_2 to 47.67 kJ/mol H_2 (Dantzer and Orgaz, 1986). The application of metal hydride based systems range from storing hydrogen for use in automobiles to energy conversion, such as, heating or cooling systems, heat up gradation, thermal energy storage, etc. and the applications can cover temperatures range from deep freezing to over 600°C. Some of desired properties of metal hydrides used for engineering applications are:

1. high hydrogen storage capacity.
2. satisfactory absorption-desorption kinetics (in many cases this means the equilibrium pressure above 1.0 bar for the respective equilibrium temperature).
3. easy activation at moderate temperatures and pressures.
4. desorption of hydrogen at moderate temperatures (e.g., for automotive applications, temperature must be less than 100°C).
5. low hysteresis and negligible plateau slope.

Even though all these properties may not be found in a single metal hydride, a judicious combination of various factors will determine its suitability for various applications. Moreover, different applications demand different properties of metal hydrides. Muthukumar *et al*. (2003) have studied more than hundred metal hydride alloys for the suitability for different engineering applications viz., hydride heat pumps and heat

transformers, hydrogen compressors, hydrogen storage and energy storage applications. Muthukumar *et al*. (2003) grouped the metal hydride alloys in enthalpy of formation (ΔH) vs. entropy of formation (ΔS) plot and divided the plot into four regions as shown in Fig. 1.3.

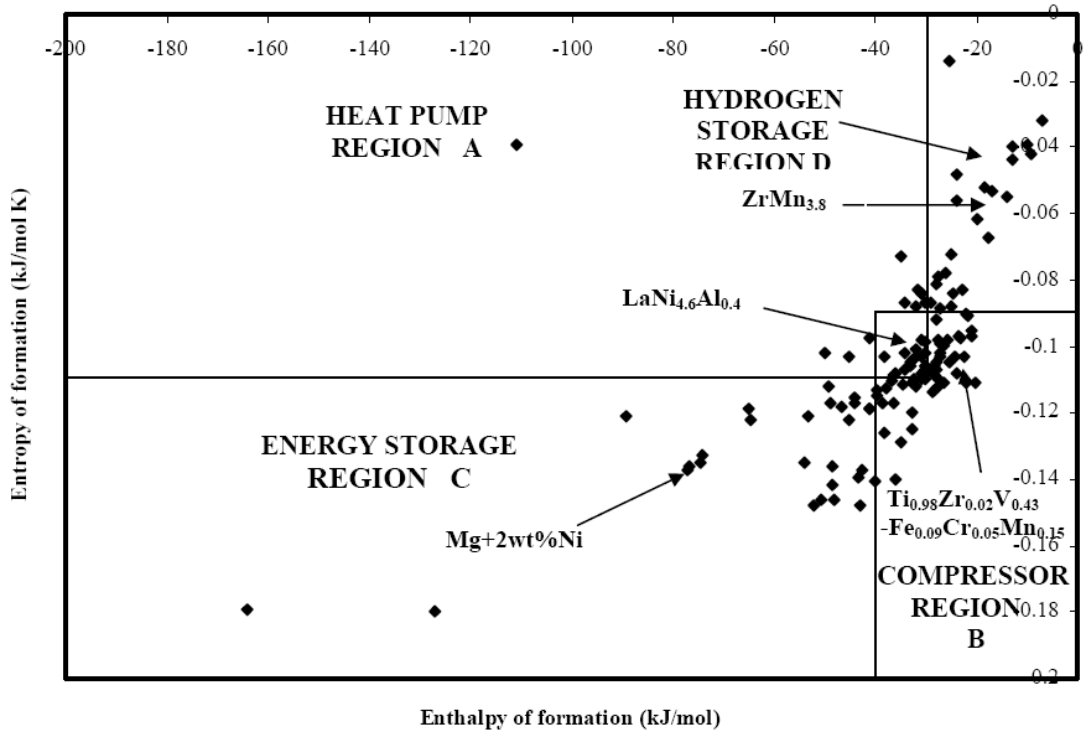

Fig. 1.3 Thermodynamic properties of different metal hydride applications (Muthukumar *et al.,* 2003).

Further applications of metal hydrides include batteries, isotope separation, hydrogen purification and remote temperature sensors. For all the above-mentioned applications, long life cycle stability and low cost are also important characteristics.

1.6 MOTIVATION FOR THE PRESENT WORK

Primary motivation comes from the idea to use hydrogen as a universal secondary energy carrier, the use of which has no negative impact on the environment. This idea of an environment friendly energy technology with hydrogen as a major secondary energy

carrier has renewed the interest of researchers to develop and investigate safe, an efficient and economical production and storage of hydrogen. The metal-hydrogen (metal hydride) systems have a good potential in the application fields of heat pumps, refrigeration and air-condition applications.

A typical metal hydride based energy systems comprise reactor (reaction beds) as the core component. The design, especially consideration of heat and mass transfer to/from these reactors, along with the selection of suitable metal hydride alloys is extremely important. In the present thesis, the performance of metal hydride based heat pumps and their basic components, which include the reaction bed, is studied. A major emphasis is given to the heat and mass transfer processes associated with the reaction beds.

1.7 STRUCTURE OF THE PRESENT THESIS

As mentioned earlier, the performance of metal hydride based heat pumps and refrigeration systems is dependent on the proper selection of the hydride alloy pairs for the required operating conditions. The objective of the present thesis is to study the performance of a single-stage and double-stage metal hydride heat pumps based on the coupled heat and hydrogen transfer between the reaction beds and heat transfer fluids. The present chapter begins with an introduction to metal hydrides and their applications.

The published research work on metal hydrides is reviewed in Chapter 2. The importance of hydriding and dehydriding rates, coupled heat and hydrogen transfer characteristics of the hydride bed related to some specific engineering applications, such as, metal hydride heat pumps, refrigeration and air-conditioning are also presented in Chapter 2.

Studies on hydriding kinetics using the well-known reaction kinetics models are presented in Chapter 3.

Chapter 4 describes the thermal modelling and performance investigation of single-stage; double-stage metal hydride based heat pumps and crossed van't Hoff line concept heat pumps.

Chapter 5 discusses the results obtained from the reaction kinetics and heat and mass transfer studies, and the performance of metal hydride based heat pumps.

In Chapter 6, major outcome of the present research work and conclusions are described.

CHAPTER 2

STATE-OF-THE-ART

Since early 1970s extensive research work has been carried out in the field of metal-hydrogen technology. As a result, many thermally driven metal hydride systems, such as, heat pump, refrigerator, heat transformer, hydrogen compressor, hydrogen storage, and purification, etc. were built and tested. Of these, heat pump and refrigeration are the most widely investigated applications.

The absorption and desorption of hydrogen in metal hydrides are exothermic/endothermic processes, i.e. associated with release of heat from the reaction bed or uptake of heat into the reaction bed. The operation of metal hydride based heating and cooling systems is essentially determined by these heat and mass transfer characteristics. In this chapter, a detailed state-of-the-art on the intrinsic reaction kinetics of hydriding and dehydriding mechanisms, coupled heat and hydrogen transfer aspects during absorption/desorption of

hydrogen to/from metal hydride beds are presented. Further, a detailed literature survey on two major topics of the present thesis, namely, single-stage and double-stage metal hydride based heat pumps is presented.

2.1 STUDIES ON HYDRIDING AND DEHYDRIDING KINETICS

The absorption and desorption kinetics of hydrogen in a metal hydride bed is one of the important areas on which many investigators have carried out extensive research. To begin with, Boser (1976) investigated the hydriding and dehydriding kinetics of $LaNi_5$ in the operating temperature and pressure ranges of 0-90°C and 0-5 bar, respectively. The reported activation energy of $LaNi_5$ was about 31.8 kJ/mol of H_2. The rate controlling step was found as the phase transformation between the metal to hydride phase. Later, Goodell *et al*. (1980) slightly changed the composition of AB_5 alloy and presented the reaction kinetics of $LaNi_5$, $LaNi_{4.9}Al_{0.1}$ and $LaNi_3Co_2$. At 25°C absorption temperature, $LaNi_5$ was found to be extremely active. They found that the reaction rates of investigated alloys could be reduced by substitution of cobalt and aluminium for nickel. Rudman *et al*. (1983) discussed the nucleation and growth (N-G) transformation during the hydriding and dehydriding processes. They investigated the thermal behavior of the kinetic system using a mathematical model and provided a detailed discussion on the aspects of activation, intrinsic kinetics, and heat flow effects. The intrinsic kinetics was further divided into three processes in series, namely, surface process, diffusion and phase transformation. They discussed the problem of determining the rate limiting intrinsic process from time-temperature-pressure dependence of the different processes. They showed the importance of the interaction between the intrinsic kinetics and heat flow effects.

Miyamoto *et al*. (1983) developed an experimental setup for investigating the reaction kinetics of hydrogen absorption in $LaNi_5$ at a constant hydrogen pressure and in the temperature range of 15-80^oC. A simple first order reaction kinetics model was taken into consideration. The activation energy of 32.24 kJ/mol of H_2 was observed from the Arrhenius plot. The rate controlling step in the (α+β)-phase region was assumed to be chemical reaction.

Goudy *et al*. (1983) performed reaction kinetics studies for desorption of hydrogen in $LaNi_5$, $LaNi_{4.7}Al_{0.3}$, (CFM) Ni_5 (CFM = cerium-free misch metal) and $MNi_{4.5}Al_{0.3}$ hydride alloys. It was reported that the desorption of hydrogen from $LaNi_5$ follows first order kinetics in the low temperature range of 25-45°C with the activation energy in the range of 35-40 kJ/mol of H_2. Whereas, in the temperature range of 70-90°C, a second order reaction kinetics model was adopted. Supper *et al*. (1984) discussed the experimental investigations of the reaction kinetics of various AB_5 type alloys and also studied the influence of different heat and mass transfer enhancement techniques on the reaction kinetics of $LaNi_{4.7}Al_{0.3}$ hydride alloy. They studied the effects of bed thickness ranging from 1.0 mm to 6.0 mm and absorption temperatures ranging from 20-50°C. They reported that the porous aluminium foam improves the reaction rate substantially leading to a significant improvement in the hydrogen transfer.

Koh *et al*. (1989) compared the hydriding and dehydriding kinetics of $LaNi_5$ in the (α+β)-phase region. During these processes, the sample was maintained at nearly isothermal condition and the ratio of supply pressure to the equilibrium pressure at the mid-point of the pressure plateau ($P_S/P_{eq} = 0.5$) was varied from 2 to 5. In both processes, the reaction rate was controlled by the phase transformation. Activation energies were found to be 27

and 37 kJ/ mol of H_2 for the absorption and desorption processes, respectively, at a pressure ratio of 2. Wang and Suda (1990) characterized the dehydriding kinetics of $LaNi_{4.7}Al_{0.3}$ using a stepwise method under both constant and variable pressure conditions. They developed the rate equation by considering both hydrogen pressure and concentration. They showed that the rate constants are independent of pressure and concentration in the (α+β)-phase region. Subsequently, Mungole *et al*. (1998) investigated the hydrogen desorption kinetics of $MmNi_{4.2}Al_{0.8}$ at three temperatures of 15, 25 and 35^oC. The reaction rate was based on the first order equation. They estimated the activation energy for hydrogen desorption reaction to be 48.09 kJ/mol of H_2.

Skripnyuk *et al*. (2003) studied the desorption kinetics for the commercial hydride forming alloys C2, $C5_1$ and $C5_2$ at the temperature range of -20 to 20^oC. First order reaction kinetics was assumed to compute the reaction constants. The estimated activation energies for the hydrogen desorption of C2, $C5_1$ and $C5_2$ alloys were 33, 40 and 30 kJ/mol of H_2 at 20^oC, respectively. Recently, Kumar *et al*. (2008) studied the absorption kinetics of $MmNi_5$, $MmNi_{4.7}Al_{0.3}$, $MmNi_{4.5}Al_{0.5}$, $MmNi_{4.2}Al_{0.8}$ and $MmNi_4Al$ at the temperature range of 20-80^oC and the pressure ratio was maintained at 2. They showed that the addition of aluminium decreases absorption kinetics and it results in an increase in the activation energy.

.

A summary of the above-mentioned literature on hydriding and dehydriding kinetics is presented in Table 2.1.

2.2 HEAT AND MASS TRANSFER IN HYDRIDE BEDS

Many researchers have reported on heat and mass transfer studies in metal hydride beds during absorption and desorption of hydrogen. In this sub-section, important literature on this topic is presented.

Lucas and Richards (1984) developed a mathematical model for predicting the performance of hydrogen storage in a metal hydride reaction bed. They solved the one-dimensional transient heat conduction equation but did not include the heat of reaction, Hence, there was large disagreement between their numerical results and experimental data. Later, Mayer *et al*. (1987) discussed the properties of metal hydrides as well as the necessary requirements for their usage in hydrogen storage applications. Subsequently, the same research group developed a two-dimensional numerical model for the transient heat and mass transfers in the metal hydride beds. Their numerically predicted reaction kinetics behavior showed good agreement with the experimental data reported by them. Sun *et al*. (1990) presented an unsteady, two-dimensional mathematical model describing the dynamic behavior of the metal hydride beds in rectangular and cylindrical coordinates and one-dimensional heat and mass transfer problems in cylindrical, rectangular and spherical coordinates. They used the finite difference method with the alternate-direct implicit scheme. They validated the predicted transient hydriding and dehydriding behavior of $MmNi_{4.5}Mn_{0.5}$ filled cylindrical reactor with their experimental data.

Gopal and Murthy (1992) investigated the effects of bed parameters, such as, bed thickness and effective thermal conductivity and operating parameters, such as, cooling and heating temperatures on hydriding and dehydriding characteristics of $LaNi_{4.7}Al_{0.3}$ using a one-dimensional mathematical model. They concluded that for a good metal hydride system the heat transfer characteristics must be improved by keeping the bed

thickness as small as possible or by improving the thermal conductivity of the hydride bed. Subsequently, the same research group (Gopal and Murthy, 1995) presented the experimental results of $LaNi_{4.7}Al_{0.3}$ hydride reactor during both the absorption and desorption processes at different cooling and heating fluid temperatures. Gambini (1993) developed a two-dimensional mathematical model for predicting the dynamic behaviour of heat and hydrogen transfer in metal hydride bed considering the variation in heat transfer fluid temperature along the axial direction. However, there was no information about the effect of variation of the heat transfer fluid temperature on the parameters, such as, hydride concentration, bed temperature and hydrogen absorption rate at different axial locations. Groll (1993) investigated the heat and mass transfer characteristics of typical reaction beds for dry sorption machines. Since, powder beds are usually not suitable (k < 1 W/m-K), four different types of heat transfer augmentation techniques, namely Aluminium-foam, Copper-helical band (W band), Aluminium-star shaped band and Copper-cassette were used to improve the performance of the reaction beds. Depending on the addition of Al powder a maximum thermal conductivity of 23 W/m-K was achieved. He observed that the permeability of the porous metallic-matrix hydride bed decreases with increase of Al powder content.

Jemni and Nasrallah (1995a, 1995b) predicted the dynamic behaviour of heat and mass transfer in a metal hydride reaction bed during absorption/desorption of hydrogen using a two-dimensional mathematical model considering the effects of convection and variation of gas pressure inside the reactor. They showed that solving the problem with a single-phase model does not significantly change the result and the effect of convection is significant during the initial stage of the hydriding process. Isselhorst (1995) numerically studied the heat and mass transfer characteristics of $LmNi_{4.85}Sn_{0.15}$ and

$LmNi_{4.49}CO_{0.1}Mn_{0.21}Al_{0.21}$ hydride alloys. He predicted the transient behavior of coupled heat and mass transfer characteristics, such as, hydride bed temperature, concentration, pressure distribution and the amount of hydrogen absorbed/desorbed in a metal hydride bed at differential radial and axial positions. His numerical results showed good agreement with the experimental data reported by him.

Nakagawa *et al*. (2000) developed a two-dimensional mathematical model for evaluating the transient heat and mass transfer in $LaNi_5$ hydride bed using the finite element method. They tested the predictions of Jemni and Nasrallah (1995a and 1995b) and validated the local thermal equilibrium (local gas temperature and bed temperature) and found a small variation of hydride bed temperature and rate of absorption due to the incorporation of convection term in the energy equation. They compared the numerically obtained averaged reaction (reaction rate) profiles during hydriding process with the standard hydriding equations and a reasonably good agreement was observed between the two. Mat and Kaplan (2001) developed a two-dimensional mathematical model for analyzing the hydride formation in $LmNi_5$. The governing equations were solved with a fully implicit finite volume method using the commercial code PHOENICS. It was observed that the hydride formation is quicker at regions with lower equilibrium pressure or low bed temperature regions. The absorption of hydrogen increases exponentially during the early stage of the hydriding process and slows down after the temperature of the reaction bed increases due to the release of the heat of reaction. Their theoretical results agreed satisfactorily with experimental data reported in the literature by Mayer *et al*. (1987).

Aldas *et al*. (2002) extended the two-dimensional numerical model of Jemni and Nasrallah (1995a) to a three-dimensional situation. They used the momentum equation

instead of Darcy's law to find out the hydrogen pressure and solved the governing equations using the PHOENICS code. They compared the hydrogen storage profiles with and without considering the convection effect (fluid flow) in the energy equation. Their numerical results showed that the convection significantly influences the temperature profile; however, the hydride formation was not affected by the fluid flow. They also showed that the hydriding process is uniform all over the bed, but it was slower at the core region and quicker near the boundary walls. Their numerical results showed good agreement with the experimental results reported by Jemni and Nasrallah (1995a).

Askri *et al*. (2003) investigated the dynamic behaviour of heat and mass transfer during both absorption and desorption processes in $LaNi_5$ and Mg based metal hydride reaction beds using a two-dimensional mathematical model considering the effects of convection and radiation. They observed that the effect of radiative heat transfer is significant for Mg based alloys (at higher operating temperatures, order of 300°C) while for $LaNi_5$ alloy (at lower temperatures, about room temperature) it is negligible. Subsequently, the same research group (Askri *et al*., 2004a) developed a two-dimensional mathematical model to describe the transient heat and mass transfer during desorption of hydrogen in a porous lanthanum misch metal bed of cylindrical configuration using the control volume finite element method. They presented the results of temperature, composition distribution and velocity inside the reactor. Further, the hydrogen flow was described by the general momentum conservation equations instead of Darcy's law (Askri *et al*., 2004b). The effects of the reactor dimensions, inlet diameter, volume of expansion part, tank volume, inlet pressure and amount of hydrogen in the tank on the heat and hydrogen transfer were reported. They compared their predictions with their own experimental data and found a good agreement between the two.

Dougan *et al*. (2004) developed a two-dimensional mathematical model by considering a complex heat and mass transfer model during the hydriding process. The coupled differential equations were solved numerically with a fully implicit scheme using the commercial code PHOENICS. The driving force was considered to be the pressure difference between the supply pressure and equilibrium pressure. Increase in heat transfer fluid flow was found to enhance the hydriding rate in the system. The numerical results were found to agree satisfactorily with the experimental data reported by Jemni and Nasrallah (1995a). Ha *et al*. (2004) developed a two-dimensional mathematical model for unsteady heat and mass transfer in metal hydride bed during the hydriding process using a finite volume method and investigated the physical mechanisms occurring in the bed. Their results showed that the whole process occurring in the bed is governed and controlled by the heat transfer from the bed to the surrounding cooling fluid. Higher thermal conductivity, smaller bed thickness and the presence of fins in the bed provide enhanced heat transfer rate from the bed. Their computational results showed good agreement with the experimental data.

Demicran *et al*. (2005) presented a two-dimensional mathematical model during absorption of hydrogen by metal hydride bed considering the complex heat and mass transfer with internal heat generation. The system of equations was solved numerically with a fully implicit scheme using the PHOENICS code. They also performed experiments by varying the supply pressure from 6 bar to 10 bar. The numerical results were compared with the experimental data with two different types of reactor geometries. Kikkinides *et al*. (2006) developed a two-dimensional mathematical model for predicting the hydrogen storage capacity in $LaNi_5$ hydride bed. Optimization of coupled heat and hydrogen transfer systems improves about 60% of the storage time than the case where

the system is not optimized. They compared the predicted numerical results with the experimental data reported by Jemini and Nasrallah (1995a) and found a good agreement between them. Donald and Rowe (2006) investigated a two-dimensional transient model to determine the impact of external fins on the ability of metal hydride tank to deliver the hydrogen at a specific flow rate. Marty *et al*. (2006) presented a numerical approach for the prediction of heat and mass transfer in a hydride reactor during the absorption of hydrogen. Although they used a two-dimensional geometry, they showed that the design of an industrial reactor needs the use of a three-dimensional modeling.

Phate *et al*. (2007) developed a coupled heat and mass transfer model in hydride bed during the absorption of hydrogen in cylindrical coordinates using the commercial software FLUENT 6.2. Mohan *et al*. (2007) studied unsteady, two-dimensional behavior of a cylindrical metal hydride storage device using the multiphysics commercial code COMSOL. The hydride alloy used for the simulation was $LaNi_5$. They studied the effects of geometric and operating parameters on hydriding performance of the storage reactor.

Muthukumar *et al*. (2007) presented a two-dimensional mathematical model for predicting the behavior of coupled heat and mass transfer processes in a cylindrical hydrogen storage device filled with $MmNi_{6.4}Al_{0.4}$ and numerically studied its behavior by using FLUENT 6.1.22. The mathematical model was able to account for the plateau slope and hysteresis effect of the alloy. They studied the effect of operating parameters, such as, supply pressure and absorption temperature, bed parameters, such as, the bed thickness and overall heat transfer coefficient on the performance of the hydrogen storage device. They showed that at the supply condition of 30 bar and 25°C, $MmNi_{6.4}Al_{0.4}$ stores about 13.1 g of hydrogen per kg of alloy. Further they extended their model (Muthukumar *et*

al., 2008) to study the effects of hydrogen concentration, hydride equilibrium pressure and hydride bed temperature along the axial direction by employing variable wall convective boundary condition. They showed that the effect of variable wall temperature on absorption time is found to be significant for hydride beds of thickness more than 7.5 mm.

Førde *et al*. (2009) developed an unsteady, one-dimensional mathematical model for the prediction of hydrogen absorption and/or desorption rate in a $La_{0.83}Ce_{0.10}Pr_{0.04}Nd_{0.03}Ni_{4.40}Al_{0.60}$ hydride alloy. They conducted the experiments at 7 bar pressure and 20°C temperature for absorption process and 2.5 bar pressure and 30°C temperature for desorption process. They observed that the rate of absorption and desorption is mainly dependent on the operating pressures and temperatures. They validated their numerical results with their own experimental data and observed a good agreement between the two. Askri *et al*. (2009) investigated the transient, three-dimensional, coupled heat and mass transfer characteristics in a cylindrical hydrogen storage tank equipped with fins and filled with $MmNi_{4.6}Fe_{0.4}$ hydride alloy. They studied the effects of different parameters, such as, length, thickness and thermal conductivity of fins and overall heat transfer coefficient on the hydrogen storage performance of the tank. Results for hydrogen absorption at different supply pressures were compared with the experimental data reported by Muthukumar *et al*. (2005) and a good agreement was observed between them. They showed that the use of fins enhances the heat transfer rate by about 40% for the hydrogen storage. For the operating conditions of 35 bar at 15°C, the maximum hydrogen storage capacity of $MmNi_{4.6}Fe_{0.4}$ was observed as 1.6 wt%.

Krokos *et al*. (2009) developed a three-dimensional mathematical model in the Cartesian coordinate system. The rate of hydrogen absorption and absorption time were predicted with different heat transfer fluid velocity and the effects of number of metal hydride tubes and the position of the hydride tubes on the reaction kinetics were presented. The metal hydride tank was designed to store enough amount of hydrogen for 25 km range in a fuel cell vehicle. But they did not discuss about the total amount of hydrogen required (total mass of $LaNi_5$) for traveling 25 km distance.

Recently, Mellouli *et al*. (2010) presented a two-dimensional mathematical model to optimize the heat and mass transfer in metal hydride storage tanks for fuel cell vehicles equipped with finned spiral tube heat exchangers. The effect of geometric parameters, such as, fin thickness, length, pitch and the arrangement of fins on the charging process was studied. They showed that the use of circular fins enhances heat transfer by about 66% compared with the case without fins. The predicted numerical results of hydride pressure were compared with the experimental data reported by them and a reasonably good agreement was observed between the two. Melnichuk *et al*. (2010) investigated the performance of cylindrical metal hydride container using both experiments and numerical modelling. The heat transfer in the radial direction was simulated by a one-dimensional finite difference method. A 0.5 kg $MmNi_{4.7}Al_{0.3}$ hydride alloy was filled in a stainless steel container of 50 mm inner diameter. Equilibrium pressure, temperature and hydrogen discharge capacity were predicted and were compared with the experimental data and a good agreement between the two was observed.

Veerraju and Gopal (2010) described a two-dimensional transient model for predicting the heat and mass transfer characteristics of plate fin and elliptical tube type metal

hydride reactors. Use of elliptical metal hydride tubes in place of circular tubes provides compactness, decreases weight of the system and fan power considerably. Using 12.17 kg of $LaNi_{4.7}Al_{0.3}$ hydride mass, maximum reversible hydrogen storage capacity of 0.139 kg was achieved. However, their study was limited to unsteady, two-dimensional situation with only the conduction term in the energy equation.

Ye *et al*. (2010) numerically studied the hydrogen absorption in a cylindrical metal hydride storage tank containing $Ti_{0.98}Zr_{0.02}V_{0.43}Fe_{0.09}Cr_{0.05}Mn_{1.5}$ hydride alloy. They predicted heat and mass transfer by solving the transient, unsteady two-dimensional equations using the finite difference method. They studied the effects of hydrogen supply pressure, cooling fluid temperature, overall heat transfer coefficient and height to the radius ratio of the tank (H/R) on the hydrogen absorption of the selected metal hydride. The volume of the metal hydride tank considered was 270 ml and the radius and height of the tank were 35 mm and 70 mm, respectively. The tank was filled with approximately 1.0 kg of hydride alloy. A comparison of the predicted numerical results with experimental data provided a good agreement. For 30 bar supply pressure and 20°C cooling fluid temperature, a maximum hydrogen storage capacity of 1.8 wt% was reported. The effect of overall heat transfer coefficient was significant up to 1000 W/m^2-K. They showed that at H/R = 2, the average bed temperature reached a maximum temperature of about 76°C and the hydride bed takes the longest time (6000 s) to reach the initial temperature.

A summary of the above-mentioned literature on heat and mass transfer studies in hydride beds is presented in Table 2.2.

2.3 SINGLE STAGE METAL HYDRIDE HEAT PUMPS

Heat pumps have been known for a long time, but, until the energy crisis during 1973-74, there were only a few studies dealing with heat pumps. Subsequently, in addition to alternative energy sources, scientists and engineers have started studying heat pumps more earnestly. There are several kinds of heat pumps and their utilizations, but the most common one is the vapour-compression heat pump. In recent years researchers have started to give attention to the metal hydride based heat pumps. Based on the principle of reversible chemical reactions between a pair of alloys and hydrogen gas, a few researchers experimentally developed metal hydride heat pumps and tested their performances (e.g. Gruen *et al.,* 1978; Ron, 1984; Lee *et al*. 1995; Gopal and Murthy, 1999; Imoto *et al*. 1996; Kim *et al*. 1997; Ni and Liu, 2007; Qin, 2007). Few researchers investigated the performance of metal hydride heat pump using the numerical simulation of heat and mass transfer characteristics between the paired reactors (e.g. Gopal and Murthy, 1995a; 1995c; Kang and Kuznetsov, 1995; Fedorov *et al*., 1999; Jang *et al*., 2001; Mellouli *et al*., 2009). Important literature on this topic is discussed in the following section.

2.3.1 Experimental Studies on Single Stage Metal Hydride Heat Pumps

Experimental studies on single stage metal hydride heat pumps (MHHP) are presented in this section.

Gruen *et al*. (1978) developed a chemical heat pump of 15 kW cooling capacity, driven by solar heat sources at Argonne National Laboratory, USA, using $MmNi_{4.5}Fe_{0.5}$ and $LaNi_{4.7}Al_{0.3}$ as low and high temperature alloys, respectively. The operating temperatures

were 120°C for input, 29-50°C for heat rejection, and 0-20°C for refrigeration. During 1983, a similar kind of metal hydride heat pump was developed by Solar Turbines Inc. Research Laboratory, USA, to provide a refrigeration capacity of 3.5 kW with the operating temperatures of 93°C, 29°C and 4.4-10°C (heat source, heat sink and refrigeration temperatures) using $LaNi_5$ / $MmNi_{4.15}Fe_{0.85}$.

Ron (1984) built a MHHP that used waste heat of exhaust gases as the heat source temperature for a bus air-conditioner using $LaNi_{4.7}Al_{0.3}$ / $MmNi_{4.15}Fe_{0.85}$ hydride pair. Total alloy inventory was about 70 to 80 kg for achieving 3.6 kW cooling capacity. A special aluminium matrix was used for enhancing the thermal conductivity of hydride alloy. The specific cooling capacity (cooling capacity per unit hydride mass) of 680 to 900 W/kg of desorbing hydride mass was predicted with 2 min cooling time. The low temperature units were located within the space to be air-conditioned. The high temperature units were heated via arrangements simulating the hot exhaust gas of a bus. Compared to the conventional vapour compression systems, this heat pump reduces the fuel consumption of the bus up to 30%.

Suda et al. (1984) developed a metal hydride refrigeration system for producing cold air of 1.75 kW capacity using $LaNi_{4.65}Al_{0.3}$ and $MmNi_{4.0}Fe_{0.1}$ hydride pair. The four heat reactors of 18 reaction beds of 25 mm outer diameter and 360 mm length each filled with 0.55 kg of hydriding alloy. A total mass of about 10 kg hydride was filled in each heat exchanger (reactor). The maximum reported COP at 140°C was 0.4. The optimum cycle time of the system was found to be 13 min.

Lee *et al*. (1995) constructed a prototype of a MHHP using $Zr_{0.9}Ti_{0.1}Cr_{0.9}Fe_{1.1}$ and $Zr_{0.9}Ti_{0.1}Cr_{0.6}Fe_{1.4}$ as regeneration and refrigeration alloys, respectively. Tubular type reactors (each of 210 mm length and 19.1 mm inner diameter) were filled with the hydride masses of 2 kg (regeneration alloy) and 2.5 kg (refrigeration alloy). For enhancing the heat transfer characteristics 120 mesh brass screens were inserted in the hydride beds at the intervals of 2 mm. The reported maximum power output of 272 W/kg of desorbing hydride was obtained at the optimum operating conditions of 12.8-13.2 mol hydrogen exchange, 4 min heating time and 7-8 min cooling time. The lowest cooling temperature was found to be 18°C using 200°C heat source temperature and 30°C ambient air temperature. They found that the plateau pressure and reaction kinetics can be controlled by changing the relative composition of Cr and Fe.

Imoto *et al*. (1996) built a refrigeration system to generate temperature below -20°C using $La_{0.6}Y_{0.4}Ni_{4.8}Mn_{0.2}$ / $LaNi_{4.6}Mn_{0.3}Al_{0.3}$ pair. Total inventory of the hydride alloys were 90 kg. A heat source temperature range of 130-150°C was obtained from a solar collector. They employed the cylindrical reactors with internal aluminum fins. The maximum values of COP and SCP of the system were approximately 0.4 and 22.2 W/kg of total hydride mass for the cycle time of 40 min.

Izhvanov *et al*. (1996) developed a MHHP with cooling capacity of 150-200 W using $LaNi_{4.6}Al_{0.4}$ and $MmNi_{4.85}Fe_{0.15}$ hydride pair. They employed two pairs of cylindrical reactors (32mm diameter and 560 mm length), each filled with 1.5 kg of respective hydride. Corrugated aluminium foils were employed for heat transfer enhancement. The estimated COP of the system varied from 0.17-0.2 at the operating temperatures of 158°C heat source temperature, 30°C heat rejection and 0°C refrigeration temperature.

Gopal and Murthy (1999) tested a MHHP working with ZrMnFe / $MmNi_{4.5}Al_{0.5}$. They employed cylindrical reactors of 50 mm outer diameter and 250 mm length. They were of copper, into which a thick walled ceramic filter tube was inserted (OD 40 mm). The metal hydride was filled in the annular gap between Cu and filter tube, thus forming a thin bed of 5 mm thickness. External heat transfer was accomplished by a copper coil which was wrapped around the reaction bed. Depending upon the operating conditions (110–130°C, 25–35°C, and 10–20°C); the SCP was between 30 and 45 W/kg of desorbing alloy for the whole cycle, and the COP varied between 0.2 and 0.35. Chernikov *et al*. (2002) demonstrated a MHHP for producing ice from water available at 21.1°C using $LaNi_{4.6}Al_{0.4}$ and $MmNi_{4.15}Fe_{0.85}$ as high and low temperature alloys, respectively. Total hydride mass of 3 kg (each hydride mass of 1.5 kg) was used for the model. The reported COP and SCP of the system were 0.33 and 66.67 W/kg of total alloy masses, respectively for the whole cycle time at the operating temperatures of 130/25/1.5°C. Further they have also reported that an improvement of hydride bed thermal conductivity increases the rate of cold production and reduces the cycle time considerably.

Ni and Liu (2007) experimentally investigated the performance of a single-stage MHHP under the operating temperature of 150/30-32/20°C. The high pressure reaction bed was filled with $LaNi_{4.61}Mn_{0.26}Al_{0.13}$ while the low pressure reactor was filled with $La_{0.6}Y_{0.4}Ni_{4.8}Mn_{0.2}$ hydride alloys. They observed the lowest refrigerating temperature of 1.9°C for 150°C driving heat temperature. They found that the COP and cooling power output increase with an increase in the heat source temperature. For the selected operating temperatures of 150/30/20°C, the maximum COP and cooling capacity were found to be 0.3 and 240 W, respectively. Subsequently, Qin *et al*. (2007) used the same hydride pair ($LaNi_{4.61}Mn_{0.26}Al_{0.13}$ / $La_{0.6}Y_{0.4}Ni_{4.8}Mn_{0.2}$) for developing the exhaust gas driven

automotive air conditioner. The selected heat source, heat sink and refrigeration temperature ranges were 120–200 /20–50 /-10–0°C, respectively. The overall dimensions of the stainless steel reactors employed for their investigations were 75 mm outer diameter and 500 mm length. The reactors were filled with hydride masses of 2.75 kg each. The measured thermal conductivity of the hydride beds were in the range of 1.2-1.7 W/m-K. Oil and water were used as the heat transfer fluids for the high and low temperature reactors, respectively. A maximum cooling power of 639 W was achieved. For the selected operating conditions and the reactor geometries, the operating times of various processes were fixed as 850 s for regeneration, 1300 s for refrigeration, 650 s for sensible cooling and 800 s for preheating. The average cooling power and system COP were reported as 84.6 W and 0.26, respectively, at the operating temperatures of 150/30/0°C.

Payá *et al*. (2009) developed an experimental setup for a single-stage thermal driven cooling system operating between $LmNi_{4.91}Sn_{0.15}$ and $Ti_{0.99}Zr_{0.01}V_{0.43}Fe_{0.09}Cr_{0.05}Mn_{1.5}$ hydride pairs. Using capillary tube bundle reactors, fast reaction kinetics (95 s during desorption and 80 s for absorption) were achieved. The predicted numerical results were compared with their own experimental data and a reasonably good agreement was observed between the two. Their scopes were limited by solving a set of theoretical equations for approaching the approximate solutions. The driving power was waste heat removed at 130°C for producing the refrigeration effect at 20°C. For the selected operating temperatures, maximum and mean cooling powers of 736 W and 485 ± 40 W were reported during the refrigeration period. The average SCP and COP of the whole system were approximately 42 W/kg of total hydride masses and 0.22, respectively.

A summary of above-mentioned literature on numerical studies of single stage metal hydride heat pumps is listed in Table 2.3.

2.3.2 Numerical Studies on Single Stage Metal Hydride Heat Pumps

Some of the literature on the thermal modeling of single-stage metal hydride heat pumps is presented in this section.

Nishizaki *et al*. (1983) presented a model for calculating the COP of a metal hydride heat pump with four reaction beds using $LaNi_5$ / $LaNi_{4.7}Al_{0.3}$ hydride alloys. In this model, they introduced the concept of sensible heat exchange between the reactors for improving the COP of the system. Using the numerical calculations they showed that the design parameters, such as, system operating temperatures, PCT properties, reactor heat capacities and the efficiency of sensible heat exchange between the coupled reactors are essential for achieving a high COP. Dantzer and Orgaz (1986) presented a model of a hydride chemical heat pump based on the classical thermodynamic analysis. As a first step, they compared the model with other chemically driven heat pumps and found a good agreement between the two. Next, the model introduced the chemical constraints; these constraints were correlated to different processes encountered at the different steps in a cycle. The model was developed for two operating modes, isothermal and isobaric, and was tested using a $LaNi_{4.77}Al_{0.22}$ / $LaNi_5$ system.

Gopal and Murthy (1995a) numerically investigated the single-stage metal hydride cooling system working with ZrMnFe / $MmNi_{4.5}Al_{0.5}$ hydride alloy pair using a one-dimensional mathematical model. They studied the performance characteristics of the

system by varying the bed thicknesses, thermal conductivity and overall heat transfer coefficient. The bed thickness and effective thermal conductivity were found to influence the cycle time and the specific alloy output significantly. For the bed thickness of 3 mm, an optimum effective thermal conductivity was reported as 4 W/m-K. The optimum effective thermal conductivity was found to increase with bed thickness. The refrigeration temperature had considerable effect on the cycle time and specific alloy output. They predicted the performance of the metal hydride heat pump working with the same hydride pair (Gopal and Murthy, 1995c). The initial and operating cost of the system have to be minimized by optimizing the effective thermal conductivity, hydride bed thickness and overall heat transfer coefficients. Of the three operating temperatures, heat source and refrigeration temperatures were found to have the greatest influence on the performance of MHHP. The analysis was carried out for 1 kg of hydride mass in each reaction bed. The average COP was found to lie between 0.45 and 0.5. Then, Kang and Kuznetsov (1995) numerically predicted the performance of the metal hydride chiller by solving the transient transport processes of heat and hydrogen transfer between $LaNi_{4.5}Al_{0.5}$ (regeneration alloy) and $LaNi_5$ (refrigeration alloy) reaction beds. They solved the system of five first-order ordinary differential equations using the Runga-Kutta method. The effects of heat source, cooling water and chiller water temperature on the system performance were studied. The reported optimum operating cycle time for the regeneration and refrigeration processes were 500 s and 700 s, respectively for the operate temperatures of 423/303/282 K. Each reactor was filled with hydride mass of 1.13 kg. For the above-metioned operating temperatures, the system COP and SCP were reported to be 0.7 and 40 W/kg of desorbing hydride, respectively.

Kim *et al*. (1997a) presented the thermodynamic analysis of a heat driven hydride slurry heat pump by using different combinations of six refrigeration and three regeneration alloys. They showed that $Zr_{0.8}Ti_{0.2}Cr_{0.6}Fe_{1.4}$ and $Zr_{0.8}Ti_{0.2}MnFe$ hydride pair provides the highest coefficient of performance of about 1.59 with the desorption temperature nearly 0°C. Fedorov *et al*. (1999) presented the mathematical model of a MHHP using $LaNi_{4.5}Al_{0.25}H_x$ / $TiFe_{0.8}Mn_{0.2}H_y$ hydride pair. They carried out simulations without considering the effect of hysteresis and plateau slope on PCT isotherm. The operation temperature ranges were 80, 20, and 10°C, as the heat source, sink and refrigeration temperatures, respectively. They predicted the time dependent hydride bed temperatures and equilibrium pressures over a complete cycle. They reported the minimum refrigeration temperature as -5°C. The overall heat transfer coefficient between the hydride beds and heat transfer fluids was considered as 1000 W/m^2-K. However, they did not validate their numerical results and the performance of metal hydride heat pump was not analyzed. Later, Jang *et al*. (2001) developed an unsteady, one-dimensional mathematical model of MHHP working with $Zr_{0.9}Ti_{0.1}Cr_{0.9}Fe_{1.1}$ / $Zr_{0.9}Ti_{0.15}Cr_{0.6}Fe_{1.45}$ hydride pair. Initially, hydrogen was released from the hydrogen source tank to the hydride reactors at the operating conditions of 5 bar and 53°C. Their model was designed to operate at the heat source, heat sink and refrigeration temperatures of 200, 30 and 10°C, respectively. Duration of one cycle time was 12 min and the thermal conductivity of the hydride bed was taken as 1 W/m-K. They reported the change in hydrogen pressure, temperature and hydride concentration at the above operating conditions. They compared the predicted numerical results of hydriding kinetics over a cycle time with their own experimental data and obtained reasonably a good agreement between the two. They reported that the hydrogen pressure and hydrogen flow rate are the main controlling parameters.

Recently, Mellouli *et al*. (2009) investigated the performance of MHHP employing $MmNi_{4.5}Al_{0.5}$ / $MmNi_{4.2}Al_{0.1}Fe_{0.7}$ hydride pair using a thermal model by solving a set of equations. Effects of the operating parameters, such as, heat source and refrigeration temperatures and the reactor parameters, such as, efficiency of heat exchanger were studied. They did not report the dimensions of the reactors used for their model. Their model was focused on determining the optimum operating temperature range for the above selected hydride pair. Depending on the operating temperature ranges of 67-52 / 20-0 / –8 - –23°C (heat source/ heat sink/ refrigeration temperature), the COP and SCP of the system varied from 0.45 to 0.5, and 45 to 120 W/kg of desorbing hydride, respectively.

2.3.3 Studies on Compressor Driven Metal Hydride Heat Pumps

The performance of metal hydride heat pumps can be improved by employing a low speed isentropic compressor in place of a regeneration alloy. Performances of such systems are found to be attractive. Literature on compressor driven metal hydride heat pumps (CD-MHHPs) is presented in the section.

Kim *et al*. (1997b; 1997c) studied the performance of compressor driven metal hydride heat pumps. The reactors were copper tubes (diameter 12.7 mm, length 165 mm) with external fins for enhancing the outside heat transfer. Experiments were carried out with reactors employing copper coated porous metal hydride compacts of $LaNi_5$ and $Ca_{0.4}Mm_{0.6}Ni_5$. The SCP was about 1.5 kW/kg of desorbing hydride (130 s cooling time) for the $LaNi_5$ reactor, while, for $Ca_{0.4}Mm_{0.6}Ni_5$ hydride (150 s cooling time) had a higher SCP of 2.2 kW/kg (high desorption equilibrium pressure of $Ca_{0.4}Mm_{0.6}Ni_5$). Pressure ratio

of the compressor is 7.0. Life cycle tests with $LaNi_5$ were carried out (about 3000 cycles); the reduction in cooling capacity was about 55%.

Park *et al*. (2001) developed a CD-MHHP using $Zr_{0.9}Ti_{0.1}Cr_{0.55}Fe_{1.45}$. The maximum compressing pressure and minimum suction pressure are 20 and 0.5 atm, respectively. They employed a finned reactor of 15 mm diameter. Cooling power was found to increase by about 25% when the airflow was increased from $8m^3$/min to $11m^3$/min. The effect of room temperature beyond 24°C and the effect of airflow rate beyond $11m^3$/min had no significant influence. The hydrogen storage capacity of the hydride is 1.6 wt%. The maximum SCP of 0.29 kW/kg of desorbing hydride was obtained under the optimum operating conditions of cycle time 2.6 min and air flow rate $11m^3$/min. The same research group (Park *et al*., 2002) built an experimental set up (using 3.5 kg of $Zr_{0.9}Ti_{0.1}Cr_{0.55}Fe_{1.45}$) employing a commercial compressor and demonstrated the practical applicability for air-conditioning applications. The experimental results showed that the system could produce a maximum SCP of 0.41 kW/kg of alloy at 6°C cooling temperature and $7m^3$/min airflow rate. COP of the above system is about 1.8 with an optimum cycle time of 6 min.

Mazumdar *et al*. (2005) presented a detailed mathematical model of a CD-MHHP working under static and transient conditions. The analysis was carried out based on a model reported by Kim *et al*. (1997b; 1997c). The model takes into account the transient characteristics of the coupled metal hydride reactors with external fins, reciprocating compressor and air-conditioned space. For a cooling capacity of 1 kW, a reaction bed of cylindrical configuration (20 mm dia with internal radial aluminum fins of thickness 0.15 mm, fin spacing 316 fins/m) was selected. Two reactors were employed, both filled with

$Zr_{0.9}Ti_{0.1}Cr_{0.55}Fe_{1.45}$ hydride. COPs were obtained in the range of 1.7–2.2, depending on operating conditions, while the maximum SCP obtained was about 0.16 kW/kg of desorbing hydride with considering total cycle time.

Magnetto *et al*. (2006) developed a prototype of a CD-MHHP based air conditioning system for automotive applications. In order to support the heat transfer rates required for rapid hydrogen absorption and desorption, special type of reaction tubes (ring-manifold) were employed. The individual ring-manifold hydride tubes were integrated (called hydride heat exchanger) in the form of a circular disc of 203 mm diameter and 203 mm length. Each heat exchanger was filled with 3.5 kg of Mm based alloy. The hydride heat exchangers were designed for a hydrogen inventory of approximately 27 g and a half cycle time of approximately 1.5 min. The cooling capability of the system is approximately 2 kW. Performance tests were carried by varying the ambient temperature from 21-35°C and the respective reported average cooling capacity varied from 1.545 kW (COP = 2.76) to 2.095 kW (COP = 2.57).

2.3.4 Crossed van't Hoff line Single Stage Metal Hydride Heat Pumps

Libowitz *et al*. (1997) reported the principle of crossed van't Hoff line MHHP. They described the thermodynamic analysis of a novel heat driven MHHP system operating in a principle of a crossed van't Hoff line configuration. They showed that the enthalpy of formation of the cooling hydride (refrigeration alloy) contributes to the heat required to regenerate that hydride at high pressure (P_H). Due to utilization of absorption heat of refrigeration alloy, the theoretical COP of the crossed van't Hoff line heat pump significantly increased up to about 50% (including sensible heat exchange) higher than

the conventional MHHP system. They proposed four hydride alloy pairs, and among those, $V_{0.855}Ti_{0.095}Fe_{0.05}$ / $LaNi_5$ hydride pair gained maximum theoretical COP of 0.83 (conventional COP = 0.71). They showed that for this hydride pair, the system requires higher driving temperatures in the range of 135-175°C.

A summary of above-mentioned literature on numerical studies of single stage metal hydride heat pump is listed in Table 2.4.

2.4 DOUBLE STAGE METAL HYDRIDE HEAT PUMPS

2.4.1 Experimental Studies on Double Stage Metal Hydride Heat Pumps

A few experimental studies reported in the literature on the performance of double-stage metal hydride heat pumps are presented here.

Werner (1988) and Werner and Groll (1989) presented the operating behaviour and first results of a laboratory model of a two-stage metal hydride heat transformer using three different mischmetal-nickel alloys. The design temperatures of the model were 120°C (useful temperature), 80°C (heat input temperature) and 30°C (heat sink temperature). The cycle time of the system was reported to be 42 minutes and the specific alloy output was about 20 W/kg of total hydride mass. It was shown that in order to make the design more realistic, the metal hydride system design should be based on the dynamic PCT curve rather than static PCT curve. This is due to the increase in hysteresis and to a lesser degree the plateau slope with finite hydrogen flow conditions.

Suda *et al*. (1991) demonstrated a double-stage metal hydride heat pump with the capacities of 7.7 kW and 77 kW. The metal hydride employed in this system were $LaNi_{4.88}Al_{0.23}$, $MmNi_{4.57}Al_{0.46}Fe_{0.05}$ and $MmNi_{3.98}Fe_{1.04}$ hydride alloys as high, medium and low temperature alloys for heat upgrading to the range of 120-150°C using industrial waste water of 80°C. They discussed the experimental and analytical results of the performance of 7.7 kW capacity testing unit. The total weight of these three components was 230 kg. The number of heat exchangers employed was 6 and the system design temperature and pressure were 150°C and 5.0 MPa, respectively. They showed that thermal recovery between the heating and cooling processes improves the thermal output considerably. The maximum output obtained by the system was 98.5% (7.6 kW) of the designed value, the actual COP was 0.21 against COP_{ideal} of 0.36 and the specific alloy output was 33 W/kg of total mass of the alloy.

Isselhorst and Groll (1995) developed a prototype heat transformer with a capacity of about 8 kW depending on the operating parameters. They showed that an upgrading of thermal energy from temperatures of about 130-140°C up to temperatures of more than 200°C with a heat sink temperature of 30-40°C could be achieved. Metal hydrides used for the heat transformer laboratory model were $LmNi_{4.85}Sn_{0.15}$, $LmNi_{4.49}CO_{0.1}Mn_{0.205}Al_{0.205}$ and $LmNi_{4.08}Co_{0.2}Mn_{0.62}Al_{0.1}$ as high, medium and low temperature hydrides, respectively. They showed that the COP of 0.27 and specific alloy output of 38 W/kg of total hydride mass can be achieved.

Klein and Groll (2002) and Klein (2007) analyzed the possibility of a two-stage metal hydride sorption system, working with $LmNi_{4.91}Sn_{0.15}$, $LaNi_{4.1}Al_{0.52}Mn_{0.38}$ and $Ti_{0.99}Zr_{0.01}V_{0.43}Fe_{0.09}Cr_{0.05}Mn_{1.5}$ as a topping cycle with a double effect lithium bromide

water cycle as a bottom cycle. They employed 24 stainless steel reactors (8 reactors for each metal hydride), having 27 mm inner diameter with 1.5 mm thickness. Stainless steel porous sinter metal tube of 3 mm inner diameter (1.5 mm thickness, 1 mm pore size) was used as filter. Aluminum foam with 92% porosity was employed for heat transfer enhancement (k_e = 8 W/m-K). The system was designed to operate at a driving temperature of 310°C, heat release temperature for driving a bottoming cycle at 125°C and producing cold temperature of 2°C. The estimated cold production was about 1.8 kW and the heat generation was about 1.5 kW. The MHHP system COP is in the range of 0.9 and heat amplification was about 0.75.

A summary of the above-mentioned literature on the double-stage metal hydride heat pumps is provided in Table 2.5.

2.4.2 Numerical Studies on Double Stage Metal Hydride Heat Pumps

Balakumar *et al*. (1985) carried out a comparative thermodynamic study of metal hydride heat transformer (heat upgrading) and heat pump using different alloy pairs. They presented results in the form of nomograms to yield the operating temperatures, COPs, and exergetic efficiencies. Based on the nomograms the suitable alloy pairs can be selected for specific applications. Orgaz and Dantzer (1987) analyzed a ternary metal hydride heat pump based on the three hydride concept (DS-MHHP). Their results obtained from the thermodynamic analysis showed that under some physical conditions, the performance of these devices is better than that of the binary hydride heat pumps (SS-MHHP) working at the same temperatures. The authors proposed and analyzed some possible ternary heat pump cycles.

Murthy and Sastri (1992) presented the basic thermodynamic analysis of two-stage metal hydride heat pumps for five hydride pairs. The overall COP was reported as 2.4 for MNi_5, FeTi and $CaNi_5$ hydride pair at the operating temperatures of 185/50/-2°C. They showed that the double-stage metal hydride heat pump (DS-MHHP) (2 to 3.2) yields better COP than that of single stage heat pump (1.6 to 2.3).

Sun *et al*. (1992) presented a practical method to select the hydride alloys to be used in a double-stage metal hydride heat transformer ($LmNi_{4.85}Sn_{0.15}$, $LmNi_{4.49}Co_{0.1}Mn_{0.205}Al_{0.205}$ and $LaLmNi_{4.4}Co_{0.2}Mn_{0.2}Al_{0.2}$ as high, medium and low temperature alloys, respectively). They introduced three different evaluation criteria to compare the operating characteristics of heat transformers with different alloys, namely, COP, specific alloy output and temperature output. The influence of some metal hydride properties on the operating characteristics was also discussed. Further Sun (1996) performed a comparative study of a DS-MHHP working with six different operating cycles and presented the thermodynamic analysis of the systems. The effects of hydrogen exchange amount, weight ratio, specific heat capacity of the reactor vessel, and sensible heat exchange factor, and the various operating temperatures, such as, heat source, heat sink and refrigeration temperatures on COP of DS-MHHP systems is reported. They showed that the low-pressure-side two-stage heat pump is suitable for heat upgrading and the high-pressure-side two-stage heat pumps for heat amplifying and refrigeration applications.

Willers and Groll (1999) theoretically evaluated the performance of three combinations, namely, single stage (SS), double stage (DS) and multi hydride thermal wave (MHTW) heat pumps for heating and cooling applications. They described two types of DS-MHHP using star scheme connection of six reactors. Using a high performance reaction bed

(capillary tube bundle reactor), achievable SCP of 100 to 200 W/kg (SS) and 150 to 300 W/kg (DS) were reported.

A summary of the above-mentioned literature on the double-stage metal hydride heat pumps is provided in Table 2.6. Based on the above literature survey, a generalized reported is presented in Table 2.7.

Table 2.1 Summary of literature on reaction kinetics of metal-hydrogen reactions.

S. No.	Author (s) & Year	Operating conditions	Kinetic model	E_a (kJ/mol H_2)	Alloy
1	Boser (1976)	0 to 90°C	Pressure dependent model.	31.8 (a)	$LaNi_5$
2	Goudy *et al.* (1983)	25 to 45°C	JMA 1st order model.	38 (d)	$LaNi_5H_6$-Al
3	Miyamoto *et al.* (1983)	15 to 80°C	Shrinking core, JMA 1st order model.	32.2 (a)	$LaNi_5$
4	Goodell and Rudman (1983)	60 to 65°C	General reaction kinetics model.	45.6 (a)	$LaNi_5$
5	Reilly and Johnson (1984)	0 to 50°C	General reaction kinetics model.	11.1±1.04 (a)	$LaNi_5$-H_x
6	Han and Lee (1989)	0 to 50°C	--	--	$LaNi_5$ $LaNi_{4.7}Al_{0.3}$
7	Koh *et al.* (1989)	25 to 50°C P_r = 2, 3, 4 and 5	JMA 1st order	27 (a) 37 (d)	$LaNi_5$
8	Zarynow *et al.* (1991)	25 to 40°C P_r = 2, 3, 4 and 5	JMA 1st order	30 (a) 40 (d)	$LaNi_5$
9	Nahm *et al.* (1992)	20 to 50°C 50 to 200 kPa	Shrinking core	19.65 (a)	$LaNi_5$
10	Zhang *et al.* (1993)	40 to 70°C P_r = 3	JMA 1st order	19.5 (a) 44.0 (a)	$LaNi_5$ $LaNi_{4.7}Al_{0.3}$
11	Ming *et al.* (1997)	40 to 100°C P_r = 3	JMA 1st order	40 (a) & 37 (d)	$LaNi_5$
12	Dhaou *et al.* (2007)	20 to 40°C	Pressure dependent model	26.4 (a) & 39.8 (d)	$LaNi_5$
13	Wang and Suda (1993)	40.2 to 170.2°C	Pressure dependent model	36.8 (a) & 54.1 (d)	$LaNi_{4.7}Al_{0.3}$

a : absorption; d : desoption; Pr : pressure ratio

Table 2.2 Summary of literature on coupled heat and hydrogen transfer in metal hydride beds.

S.No.	Author(s) & Year	Contributions
1	Lucas and Richards (1984)	One-dimensional mathematical model by considering heat conduction equations for predicting the performance of a hydrogen storage system.
2	Mayer *et al*. (1987)	Numerical model for the transient heat and mass transfer within metal hydride reaction beds.
3	Sun *et al*. (1990)	Unsteady, two-dimensional mathematical model describing the dynamic behavior of metal hydride beds in rectangular and cylindrical coordinates.
4	Gopal and Murthy (1992)	One-dimensional mathematical model for investigating the effects of operating and bed parameters on hydriding and dehydriding characteristics of $LaNi_{4.7}Al_{0.3}$.
5	Gambini (1993)	Mathematical model for predicting the dynamic behaviour of heat and mass transfer in metal hydride bed.
6	Groll (1993)	Heat and mass transfer characteristics of typical reaction beds for dry sorption machines. Investigate the effects of four different types of heat transfer augmentation techniques on the performance of the reaction beds.
7	Jemni and Nasrallah (1995a, 1995b)	Predicted the dynamic behaviour of heat and mass transfer in a metal hydride reaction bed during absorption/ desorption of hydrogen using two-dimensional mathematical model considering the effects of convection and variation of gas pressure inside the reactor.
8	Isselhorst (1995)	Numerically studied the heat and mass transfer in $LmNi_{4.85}Sn_{0.15}$ and $LmNi_{4.49}CO_{0.1}Mn_{0.21}Al_{0.21}$ hydrides.
9	Nakagawa *et al*. (2000)	Two-dimensional mathematical model for evaluating the transient heat and mass transfer in metal hydride bed. Tested the validity of the local thermal equilibrium, and determined the effect of convection on the net heat transfer.
10	Mat and Kaplan (2001)	Two-dimensional mathematical model for analyzing the absorption of hydrogen in $LmNi_5$.
11	Aldas *et al*. (2002)	Extended the two-dimensional numerical model of Jemni *et al.* (1995a) to three-dimensional situation. The governing equations were solved using the commercial code PHOENICS.
12	Askri *et al*. (2003)	Dynamic behaviour of heat and mass transfer during both absorption and desorption processes in $LaNi_5$ and Mg based metal hydride reaction beds using a two-dimensional mathematical model considering the effects of convection and radiation.
13	Ha *et al*. (2004)	Two-dimensional mathematical model for unsteady heat and mass transfer in metal hydride bed during the hydriding process using a finite volume method.
14		Two-dimensional mathematical model considering

	Demicran *et al*. (2005)	complex heat and mass transfer with internal heat generation. The system of equations was solved numerically using a fully implicit scheme using the commercial code PHOENICS.
15	Marty *et al*. (2006)	Numerical approach for the prediction of heat and mass transfer in a hydride reactor during the absorption of hydrogen using the commercial software FLUENT.
16	Phate *et al*. (2007)	Coupled heat and mass transfer in hydride bed during the absorption of hydrogen in cylindrical coordinates using the commercial software FLUENT 6.2.
17	Mohan *et al*. (2007)	Unsteady, two-dimensional simulation of cylindrical metal hydride storage device using the commercial code COMSOL MULTIPHYSICS.
18	Muthukumar *et al*. (2007)	Two-dimensional computational model of coupled heat and mass transfer phenomena in cylindrical hydrogen storage device filled with $MmNi_{6.4}Al_{0.4}$ using the commercial code FLUENT 6.1.22.
19	Muthukumar *et al*. (2008)	Numerical investigation of two-dimensional heat and mass transfer during the absorption of hydrogen in a cylindrical metal hydride bed containing $MmNi_{6.4}Al_{0.4}$ with consideration of a variable wall temperature convective boundary condition.
20	Førde *et al*. (2009)	Unsteady, one-dimensional mathematical model for the prediction of hydrogen absorption and/or desorption rate of reactor filled with $La_{0.83}Ce_{0.10}Pr_{0.04}Nd_{0.03}Ni_{4.40}Al_{0.60}$ hydride alloy.
21	Askri *et al*. (2009)	Transient, three-dimensional coupled heat and mass transfer characteristics in a cylindrical hydrogen storage tank equipped with fins and filled with $MmNi_{4.6}Fe_{0.4}$ hydride alloy using the control volume finite element method.
22	Krokos *et al*. (2009)	Three-dimensional mathematical model in Cartesian coordinate system for predicting the behavior of complex metal hydride reactor as hydrogen storage tank for a fuel cell vehicle.
23	Mellouli *et al*. (2010)	Two-dimensional mathematical model to optimize the heat and mass transfer in four different types of metal hydride storage tanks for fuel cell vehicle equipped with finned spiral tube heat exchangers.
24	Melnichuk *et al*. (2010)	One-dimensional mathematical model to determine the heat transfer characteristics in radial direction using the finite difference method.
25	Veerraju and Gopal (2010)	Presented a transient two-dimensional model to predict the heat and mass transfer of elliptical metal hydride tubes and tube banks.
26	Ye *et al*. (2010)	Presented a two-dimensional mathematical model for cylindrical configuration to study the heat and mass transfer analysis using the finite difference method.

Table 2.3 Summary of literature on experimental studies of single-stage metal hydride heat pump.

S. No	Author(s) and Year	Contribution
1	Gruen *et al.* (1978)	• Presented the development of a chemical heat pump driven by solar or other low grade heat sources using $MmNi_{4.5}Fe_{0.5}$ and $LaNi_{4.7}Al_{0.3}$ as low and high temperature alloys. • Operating temperature range: 120/29-50/0-20°C (T_H /T_M /T_C); cooling capacity of 15 kW.
2	Ron (1984)	• A MHHP was designed and built for a bus air conditioner. Two pairs of $LaNi_{4.7}Al_{0.3}$ / $MmNi_{4.15}Fe_{0.85}$ hydride units were employed. • Total alloy inventory was about 70 to 80 kg for achieving the cooling capacity of 3.5 kW.
3	Suda *et al.* (1984)	• A metal hydride refrigeration system was developed for producing cold air of 1.75 kW capacity using $LaNi_{4.65}Al_{0.3}$ and $MmNi_{4.0}Fe_{0.1}$ hydride pair. • The maximum reported COP at 140°C heat source temperature was 0.4.
4	Lee *et al.* (1995)	• A prototype SS-MHHP operating with $Zr_{0.9}Ti_{0.1}Cr_{0.9}Fe_{1.1}$ and $Zr_{0.9}Ti_{0.1}Cr_{0.6}Fe_{1.4}$ as regeneration and refrigeration alloys, respectively, was constructed. • The reported maximum specific power output of 151 W/kg of desorbing hydride was obtained at the optimum operating conditions of 12.8-13.2 mol hydrogen exchange.
4	Imoto *et al.* (1996)	• SS-MHHP working with $La_{0.6}Y_{0.4}Ni_{4.8}Mn_{0.2}$ / $LaNi_{4.6}Mn_{0.3}Al_{0.3}$ hydride pair was built and tested. • Operating temperature range: 130-150/25-30/-20°C (T_H/T_M/T_C). • The maximum values of COP and SCP of the system were about 0.4 and 22.2 W/kg of total hydride mass (with a cycle time of 40 min)
5	Izhvanov *et al.* (1996)	• A MHHP with heating and cooling capacity of 150-200 W using $LaNi_{4.6}Al_{0.4}$ (high temperature alloy) and $MmNi_{4.85}Fe_{0.15}$ (low temperature alloy) hydride pair was developed and tested. • Total hydride alloy mass of 3.0 kg was used (each hydride 1.5 kg) for the system. • The estimated COP of the system varied from 0.17-0.2

		at the operating temperatures of 158°C, 30°C and 0°C.
6	Gopal and Murthy (1999)	• An experimental study was carried out on MHHP with the working pair ZrMnFe / $MmNi_{4.5}Al_{0.5}$. • Depending upon the operating conditions (110–130°C, 25–35°C, and 10–20°C); the SCP was between 30 and 45 W/kg of desorbing alloy for the whole cycle, and the COP varied between 0.2 and 0.35.
7	Chernikov *et al.* (2002)	• A SS-MHHP was built and tested for producing ice from water available at 21.1°C. • Hydride alloy pair employed in the system was $LaNi_{4.6}Al_{0.4}$ and $MmNi_{4.15}Fe_{0.85}$ as high and low temperature alloys, respectively. • Operating temperatures: 130/25/1.5°C ($T_H/T_M/T_C$). • The reported COP and SCP of the system were 0.33 and 66.67 W/kg of total alloy mass, respectively for the whole cycle time.
8	Ni and Liu (2007)	• The performance of a SS-MHHP was analyzed experimentally by employing $LaNi_{4.61}Mn_{0.26}Al_{0.13}$ / $La_{0.6}Y_{0.4}Ni_{4.8}Mn_{0.2}$ hydride alloy pair. • Operating temperature range: 150/30-32/20°C ($T_H/T_M/T_C$). • The maximum COP and cooling capacity were 0.3 and 240 W, respectively.
9	Qin *et al.* (2007)	• For developing the exhaust gas driven automotive air conditioner, the same hydride pair used by Ni and Liu (2007) was adopted. • Operating temperature range: 120–200 /20–50 /-10–0°C ($T_H/T_M/T_C$). • The average cooling power and system COP was reported as 84.6 W and 0.26, respectively, at the operating temperatures of 150/30/0°C.
10	Paya *et al.* (2009)	• An experimental setup for a single-stage thermal driven cooling system operating with $LmNi_{4.91}Sn_{0.15}$ / $Ti_{0.99}Zr_{0.01}V_{0.43}Fe_{0.09}Cr_{0.05}Mn_{1.5}$ hydride pairs was developed. • Operating temperatures: 130/30/20°C ($T_H/T_M/T_C$). • The average SCP and COP of the whole system were about 42 W/kg of total hydride mass and 0.22, respectively.

Table 2.4 Summary of literature on numerical studies of single-stage metal hydride heat pump.

S. No	Author(s) and Year	Contribution
1	Nishizaki *et al.* (1983)	• Presented a numerical model for calculating the COP of a MHHP with four reaction beds using $LaNi_5$ / $LaNi_{4.7}Al_{0.3}$ hydride alloys.
2	Gopal and Murthy (1995a & 1995c)	• SS-MHHP working with ZrMnFe / $MmNi_{4.5}Al_{0.5}$ hydride alloy pair using a one-dimensional mathematical model was numerically investigated. • The average COP obtained for this system was approximately 0.45 to 0.50.
3	Kang and Kuznetsov (1995)	• The performance of the metal hydride chiller was numerically predicted by solving the transient transport processes of heat and hydrogen between $LaNi_{4.5}Al_{0.5}$ (regeneration alloy) and $LaNi_5$ (refrigeration alloy) reaction beds. • A set of ordinary differential equations was solved by the Runga-Kutta method. • Operate temperatures: 150/30/10°C ($T_H/T_M/T_C$). • The system COP and SCP were reported to be 0.7 and 40 W/kg of desorbing hydride, respectively.
4	Kim *et al.* (1997)	• The thermodynamic analysis and experimental study of a heat driven hydride slurry heat pump was studied employing $Zr_{0.8}Ti_{0.2}Cr_{0.6}Fe_{1.4}$ / $Zr_{0.8}Ti_{0.2}MnFe$ hydride pair. • The highest coefficient of performance of about 1.59 was reported.
5	Fedorov *et al.* (1999)	• Reported the mathematical modelling of a SS-MHHP working with $LaNi_{4.5}Al_{0.25}H_x$ and $TiFe_{0.8}Mn_{0.2}H_y$ hydride pair. • The effect of hysteresis and plateau slope was not considered. • Operating temperatures: 80/20/10°C ($T_H/T_M/T_C$).
6	Jang *et al.* (2001)	• An unsteady, one-dimensional mathematical model of MHHP system working with $Zr_{0.9}Ti_{0.1}Cr_{0.9}Fe_{1.1}$ / $Zr_{0.9}Ti_{0.15}Cr_{0.6}Fe_{1.45}$ hydride pair was developed. • Operating temperatures: 200/30/10°C ($T_H/T_M/T_C$).
7	Mellouli *et al.* (2009)	• A set of theoretical equations was solved for predicting the performance of MHHP employing $MmNi_{4.5}Al_{0.5}$ / $MmNi_{4.2}Al_{0.1}Fe_{0.7}$ hydride pair. • Operating temperature range: 67-52/ 20-0/–8 - –23°C ($T_D/T_M/T_C$). • The COP and SCP of the system were in the range of 0.45 to 0.5 and 45 to 120 W/kg of desorbing hydride mass, respectively.

Table 2.5 Summary of literature on experimental studies of double-stage metal hydride system (heat transformer and heat pump)

S. No	Authors and Year	Contribution
1	Werner and Groll (1989) **(Heat Transformer)**	• A double-stage metal hydride heat transformer working with $LmNi_{4.85}Sn_{0.15}$, $LmNi_{4.49}CO_{0.1}Mn_{0.205}Al_{0.205}$ and $LmNi_{4.08}Co_{0.2}Mn_{0.62}Al_{0.1}$ as high, medium and low temperature hydride alloys was fabricated. • The design temperatures of the model were 120°C (useful temperature), 80°C (heat input temperature) and 30°C (heat sink temperature). • Specific alloy output was about 20 W/kg of total alloy mass.
2	Suda *et al.* (1991) **(Heat Transformer)**	• Built a double-stage metal hydride heat transformer employing $LaNi_{4.88}Al_{0.23}$ / $MmNi_{4.57}Al_{0.46}Fe_{0.05}$ / $MmNi_{3.98}Fe_{1.04}$ hydride alloys. • The operating temperatures were 120-150°C (useful temperature), 80°C (heat input temperature) and 30°C (heat sink temperature). • The actual COP of the system was 0.21and the specific alloy output was 33 W/kg of total alloy mass.
3	Isselhorst and Groll (1995) **(Heat Transformer)**	• A prototype heat transformer was developed for continuous power output of about 8 kW. • Hydride alloys employed in the systems were $LmNi_{4.85}Sn_{0.15}$, $LmNi_{4.49}CO_{0.1}Mn_{0.205}Al_{0.205}$ and $LmNi_{4.08}Co_{0.2}Mn_{0.62}Al_{0.1}$. • Upgrading temperatures from about 130-140°C to temperatures of more than 200°C with a heat sink temperature of 30 to 40°C were the design parameters. • The COP and specific alloy output of the system was about 0.27 and 38 W/kg of total alloy mass, respectively.
4	Klein and Groll (2002) **(Heat pump)**	• DS-MHHP working with $LmNi_{4.91}Sn_{0.15}$, $LaNi_{4.1}Al_{0.52}Mn_{0.38}$ and $Ti_{0.99}Zr_{0.01}V_{0.43}Fe_{0.09}Cr_{0.05}Mn_{1.5}$ hydride alloy pair, was built and tested. • The system was designed to operate at a driving temperature of 310°C, releasing heat at 125°C and producing cold temperature of 2°C. • The estimated cold production was about 1.8 kW and the heat generation was about 1.5 kW. • The COP and SCP of the continuous system was 0.49 and 28 W/kg of total hydride mass.

Table 2.6 Summary of literature on double-stage metal hydride system (heat transformer and heat pump)

S. No	Authors and Year	Contribution
1	Balakumar et al. (1985) **(Heat pump and heat transformer)**	• A comparative thermodynamic study of metal hydride heat transformer (heat upgrading) and heat pump using different alloy pairs were carried out.
2	Murthy and Sastri (1992) **(Heat pump)**	• Basic thermodynamic analysis of DS-MHHP for five hydride pairs was presented. • The overall COP was reported as 2.4 for MNi_5, FeTi and $CaNi_5$ hydride pair at the operating temperatures of 185/50/-2°C. • They showed that the double-stage metal hydride heat pump (DS-MHHP) (2 to 3.2) yields better COP (1.6 to 2.3) than SS-MHHP. •
3	Sun (1996) **(Heat pump and heat transformer)**	• A thermodynamic study of a DS-MHHP working with six different operating cycles was presented.
4	Willers and Groll (1999) **(Heat pump)**	• The performance of three combinations, namely, single stage (SS), double stage (DS) and multi hydride thermal wave (MHTW) heat pumps for heating and cooling applications is theoretically evaluated. • They described two types of DS-MHHP using star scheme connection of six reactors. • Using a high performance reaction bed (capillary tube bundle reactor), SCP of 100 to 200 W/kg (SS) and 150 to 300 W/kg (DS) can be achieved.

Table 2.7 Generalized literature survey on heat and mass transfer aspects of metal hydride based heat pumps.

S.No	Description	Literature	Remarks
1	Slope and hysteresis factors (φ, φ_o and β)	Nakagawa *et al.* (2000), Mat and Kaplan (2001), Aldas *et al.* (2002), Dogan *et al.* (2004), Demircan *et al.* (2005), Marty *et al.* (2006)[#], Phate *et al.* (2007)[#], Mohan *et al.* (2007)[#], Brown *et al.* (2008), Freni *et al.* (2009)[#], Mellouli *et al.* (2009)	The slope and hysteresis factors have been not considered in their models.
2	<u>Thermo-physical properties</u> 1. Thermal conductivity (k) 2. Overall heat	Mat and Kaplan (2001), Aldas *et al.* (2002), Ha *et al.* (2004), Botzung *et al.* (2008)[#], Mellouli *et al.* (2009)	Clear details about the thermo-physical properties used for their numerical studies are not available.

	transfer coefficient (U)		
3	Effect of activation energy (E_a) and reaction rate constants (C_a)	Nakagawa *et al.* (2000), Mat and Kaplan (2001), Ha *et al.* (2004), Demircan *et al.* (2005), Kikkinides *et al.* (2006)[#], Gondor *et al.* (2009), Melnichuk *et al.* (2010), Ye *et al.* (2010), Jang *et al.* (2001), Mellouli *et al.* (2009)	The activation energy and reaction rate constants were assumed and there is no proper justification for mathematical models used by them.
4	Effect of convection	Melnichuk *et al.* (2010), Ye *et al.* (2010), Jang *et al.* (2001)	Most authors have not considered the effect of convection in the energy equation. Such papers are discussed in the literature survey.
5	One-dimensional model	Gopa and Murthy, (1992a, 1992c), Melnichuk *et al.* (2010), Jang (2001), Mellouli (2009)	Many authors have presented one-dimensional model. Such papers are discussed in the literature survey.
6	Effect of hydride concentration on enthalpy formation	**Not considered so far.** (No ref. available)	So far, No researchers has been considered the effect of hydride concentration on the enthalpy of formation.
7	Variable convective boundary condition in axial direction	**Not considered so far.** (No ref. available)	So far, no researcher has incorporated the effect of variation in cooling fluid temperature along the axial direction of the reactor.
8	Validation	**No validation:** Dogan *et al.* (2004), Mohan *et al.* (2007)[#] **Validated their own experimental results** Askri *et al.* (2004a, 2004b), Ha *et al.* (2004), Demircan *et al.* (2005), Marty *et al.* (2006), Dhaou *et al.* (2007), Laurencelle and Goyette (2007), Botzung *et al.* (2008)[#], Brown *et al.* (2008), Førde *et al.* (2009), Gondor *et al.* (2009), Jang *et al.* (2001), Paya *et al.* (2009)*	Most of the authors have compared their own experimental results of hydrogen kinetics. Some researchers have not done any validation at all.

* Validated temperature profiles

[#] Softwares, such as, FLUENT, COMSOLE MULTIPHYSICS were used for the numerical analysis.

2.5 CLOSURE

The following conclusions may be drawn from the foregoing literature survey:

Many reaction kinetics models and reaction rate equations have been reported in the literature but there is a lack of availability of precise reaction kinetics data of metal hydrides used for heat pump applications. E.g. many investigators (Boser, 1976; Goudy *et al*., 1983; Miyamoto *et al*., 1983; Koh *et al*., 1989; Dhaou *et al*., 2007) have extensively studied the reaction kinetics of the $LaNi_5$ alloy. Table 2.1 shows that the activation energy (for absorption) of $LaNi_5$ reported in the literature varies from 11.1 to 45.56 kJ/mol H_2. Most of the researchers employed the JMA first order model (Goudy *et al*., 1983; Miyamoto *et al*., 1983; Koh *et al*., 1989; Zarynow *et al*., 1991; Zhang *et al*., 1993; Ming *et al*., 1997) and models which are based on supply pressure, concentration and temperature (Boser, 1976; Goodell and Rudman, 1983; Reilly *et al*., 1984; Han and Lee, 1989; Nahm *et al*., 1992; Dhaou *et al*., 2007) for studying the reaction kinetics of $LaNi_5$. Based on the agreement of the theoretical reaction kinetics data with experimental ones, the rate-controlling steps could be determined. They are dissociative chemisorption (Nahm *et al*., 1992), diffusion of hydrogen atoms (Han and Lee, 1989) and nucleation and growth (Goudy *et al*., 1983; Miyamoto *et al*., 1983; Koh *et al*., 1989; Zarynow *et al*., 1991; Zhang *et al*., 1993; Ming *et al*., 1997).

The reaction kinetics of $LaNi_{4.7}Al_{0.3}$ was also investigated based on the JMA first order model (Zhang *et al*., 1993) and using pressure and concentration dependent reaction kinetics equations (Martin *et al*., 1996; Han *et al*., 1989; Wang and Suda, 1993) for determining the reaction rate constant and activation energy. The reported different rate-limiting steps are diffusion (Martin *et al*., 1996; Han *et al*., 1989) and nucleation and

growth (Zhang *et al*., 1993; Wang and Suda, 1993). Hence there is no clear idea about the rate controlling step in the hydriding reaction. A detailed reaction kinetics study is necessary for determining the accurate values of activation energy and reaction rate constant.

- For efficient and economic design of metal hydride heat pump, it is necessary to study the heat and mass transfer characteristics between paired reaction beds operating under dynamic conditions. To optimize the operating and bed parameters of the metal hydride based heat pump, detailed theoretical investigation on the heat and mass transfer aspects of metal hydride reaction beds is needed. A few studies have been reported in the literature on this important aspect with simplifying assumptions. Hence, there is a need for more rigorous theoretical treatment in this area.

- Only few mathematical studies on single-stage metal hydride based heating and cooling systems have been reported in the literature. Hence there is a need for extensive parametric studies over a wide range of operating temperatures and performance of the system.

- No mathematical study on double-stage metal hydride heat pump has been reported in the literature. Therefore, a detailed numerical investigation is required for predicting the performance of the system.

- Heat and mass transfer aspects of crossed van't Hoff line metal hydride based heat pump have not been reported in the literature. Hence, there is a need for investigating the feasibility of cross van't Hoff line metal hydride based heat pump**.**

2.6 OBJECTIVES OF THE THESIS

In the view of above closure, the following aspects are considered in the present thesis.

- To study the reaction kinetics of metal hydride during absorption and desorption of hydrogen for predicting the accurate values of reaction rate constants and activation energies of metal hydride alloys used for heat pump applications.

- To develop a detailed mathematical model for predicting the performance of a single-stage metal hydride heat pump considering the variation in cooling fluid temperature along axial direction and slope and hysteresis factors of the PCT characteristics of the hydride pairs. To extend this model for comparing the performance of the system using different alloy combinations by varying their operating parameters.

- To develop a detailed mathematical model for predicting the performance of double-stage metal hydride heat pump at different operating conditions.

- To study the operating feasibility of crossed van't Hoff line single-stage metal hydride heat pump system.

In the next chapter, the hydriding kinetics studies using the well-known reaction kinetics models are presented.

CHAPTER 3

REACTION KINETICS STUDIES

As the behavior of metal hydride cooling/heating systems is inherently unsteady, to simulate such systems correctly it is essential to study hydriding and dehydriding kinetics, and the transient heat and mass transfer aspects of the coupled reaction beds. To begin with, the intrinsic reaction kinetics of hydrogen in metal hydrides is investigated for determining the rate controlling parameter and the reaction constants.

Fast reaction kinetics and high hydrogen storage capacity are the most important attributes of metal hydride alloys used for heat pump applications. The performance of these devices depends on the transient coupled heat and hydrogen transfer processes with internal heat generation in the hydride (reaction) beds. Large amount of research work has been devoted to predicting the performances of hydrogen storage device (e.g. Mayer *et al.,* 1987; Gopal and Murthy, 1992; Jemni and Nasrallah, 1995a; 1995b; Mat and Kaplan,

2001; Muthukumar *et al.,* 2007; 2008; Mellouli *et al*. 2010) and heat pumps (e.g. Gopal and Murthy, 1995a; 1995c; Kang and Kuznetsov, 1995; Fedorov *et al.,* 1999; Jang *et al.,* 2001; Ni and Liu, 2007, Qin *et al.,* 2007; Paya *et al*., 2009) using unsteady coupled heat and mass transfer thermal (mathematical) models. The accuracy of such thermal models depends on the knowledge of thermodynamic properties of the metal hydride alloys, such as, reaction enthalpies and entropies, activation energy, etc. In order to estimate the accurate values of the activation energy of the alloys, it is necessary to investigate the hydriding and dehydriding kinetics of the metal hydrides at different temperatures. Fig. 3.1 shows the five sequential processes of intrinsic hydriding kinetics, as presented by Martin *et al*. (1996).

i. Physisorption of hydrogen molecules.
ii. Dissociation of hydrogen molecules into atoms (Chemisorption).
iii. Diffusion of hydrogen atoms from the surface into the bulk through the surface layer.
iv. Diffusion of hydrogen atoms through the hydrid layer, and
v. Hydride formation at the metal hydride interface.

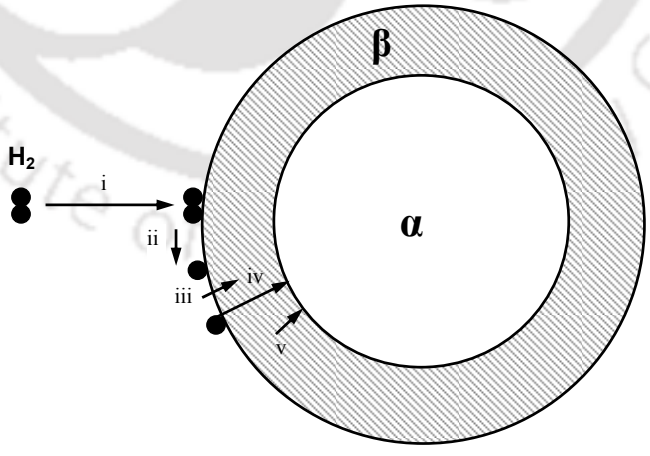

α - Metal phase **β - Hydride phase**

i. Physisorption ii. Chemisorption iii. Surface penetration
iv. Diffusion v. Nucleation and growth

Fig. 3.1 Different steps involved in the hydriding kinetics.

In the above-mentioned sequence, one of the processes (i to v) would be slower than the other processes. Hence, the slowest process governs the overall reaction kinetics. During hydride formation, the growing product (hydride) layer of β-phase proceeds from the surface of the hydride particle towards the centre.

The hydriding kinetics is greatly influenced by temperatures and supply pressures but mostly, the hydriding kinetics are investigated for the influence of temperature in order to determine the temperature independent reaction rate constant and the activation energy. Literature shows that there are two popularly used reaction kinetics models, namely, Johnson-Mehl-Avrami (JMA) model (Goudy *et al*., 1983; Miyamoto *et al*., 1983; Rudman 1983; Koh *et al*., 1989; Zarynow *et al*., 1991; Zhang *et al*., 1993; Ming *et al*., 1997; Srinivas *et al*., 2008; Anil Kumar *et al*., 2009) and Jander diffusion model (JDM) (Li *et al*., 2004; Cui *et al*., 2008) for predicting the activation energy and the reaction rate constant of the metal – hydrogen system. Hence, these two models are used in the present investigation. In the JMA model, the rate constant is calculated by assuming the first order reaction (case 1) and also by estimating the reaction order (case 2) from the experimental data.

3.1 JOHNSON-MEHL-AVRAMI (JMA) MODEL

This model comprises both diffusion, and nucleation and growth as the rate controlling mechanism. As explained earlier, two types of JMA models are considered for the analysis. The time-dependent reacted fraction (f) is expressed as

$$f(t) = 1 - \exp\left(-kt^n\right) \tag{3.1}$$

where, $k = k(T)$ denotes the temperature-dependent rate parameter and n the order of reaction.

3.1.1 First Order JMA Model

Consider $n = 1$, then Eq. (3.1) can be written as

$$-ln\left[1 - f(t)\right] = kt \tag{3.2}$$

The reaction rate constants are calculated from the slopes of the straight lines which fit the experimental ($-ln[1-f(t)]$ vs. t) plots.

3.1.2 Order Obtained From Experiment

Eq. (3.1) can also be written as

$$ln\left[-l\,n(1 - f(t))\right] = n\,l\,n\,t + n\,l\,n\,k. \tag{3.3}$$

A plot of $ln[-ln(1-f(t))]$ versus $ln\ t$ is a straight line with the slope n and the rate constant k as the intercept.

3.2 JANDER DIFFUSION MODEL (JDM)

It is a classical model used to analyze the reaction mechanism, in which the particles of the metal hydride are considered as spherical in shape. Diffusion is the only rate-controlling step.

$$\left[1 - (1 - f(t))^{1/3}\right]^2 = kt \tag{3.4}$$

where, $f(t)$ denotes the reacted fraction at any time t and k the rate constant, which depends on the temperature and supply pressure. The left side term in Eq. (3.4) is termed as the Jander diffusion parameter.

Experiments were carried out at IKE, University of Stuttgart, Germany (Muthukumar *et al*., 2009b). Three different hydride alloys commonly used for the metal hydride heat pump applications, namely, $LaNi_5$, $LmNi_{4.91}Sn_{0.15}$ and $LaNi_{4.7}Al_{0.3}$ were taken for the

hydriding kinetics measurement. The details of experimental setup and procedure are given in Appendix A. The experimental data obtained from IKE, University of Stuttgart was used for predicting the reaction kinetic data, such as, activation energy and reaction rate constant. During the experiment, the pressure ratio (supply pressure to equilibrium pressure at the mid-point of the pressure-concentration-isotherm) was maintained constant at 2 and the reaction conditions were nearly isothermal. The activation energy of the hydriding reaction was obtained through the Arrhenius plot drawn between ln k and inverse of absolute temperature ($1/T$).

$$k = C \exp\left(-\frac{E_a}{R_u T}\right) \tag{3.5}$$

where C denotes the pre-exponential factor and E_a the activation energy during the hydriding process. For validating the estimated activation energies and rate constants from the above models, a most general form of the hydriding equation is used (Mayer *et al*., 1987). The activation energies and reaction rate constants were substituted into Eq. (3.6) to determine the mass flow rate of the hydrogen.

$$\dot{m} = C \exp\left[\frac{-E_a}{R_u T}\right] \ln\left(\frac{P_s}{P_{eq}}\right)\left(\rho_{ss} - \rho_s\right) \tag{3.6}$$

The analytically predicted mass flow rates were compared with the experimental data. Based on the comparison, the best model was chosen and the hydriding process was considered to be the respective rate limiting step. Reaction kinetics is difficult to measure accurately at high hydrogen supply pressures due to the rapid hydriding reaction. Therefore, the pressure ratio (P_r) was maintained constant at 2 for all experiments. The variation of $LmNi_{4.91}Sn_{0.15}$ temperature during absorption is illustrated in Fig. 3.2 for different supply pressures and temperatures. It is seen that for high pressures (pressure ratios above 2) the deviation from the isothermal condition is significant.

Figs. 3.3 to 3.5 show the influence of operating temperatures on the hydriding kinetics of the activated $LaNi_5$, $LaNi_{4.7}Al_{0.3}$ and $LmNi_{4.91}Sn_{0.15}$ hydride alloys, respectively. The hydriding reaction rates increase with operating temperature for all alloys. For the given pressure ratio, the hydrogen storage capacity of $LaNi_5$, $LaNi_{4.7}Al_{0.3}$ and $LmNi_{4.91}Sn_{0.15}$ at 60°C is found to be approximately 1.4, 1.46 and 1.2 wt%, respectively. The reacted fraction (*f*), which is the ratio of the rate of hydrogen absorption to the maximum hydrogen storage capacity at the corresponding operating pressure and temperature, is calculated from the rate of hydrogen absorption. Figs. 3.6 to 3.8 show the reacted fraction (*f*) versus time (*t*) for $LaNi_5$, $LaNi_{4.7}Al_{0.3}$ and $LmNi_{4.91}Sn_{0.15}$ hydride alloys at different operating temperatures. In order to estimate the accurate values of the activation energy and to determine the mechanism for controlling the reaction rate, three reaction models are employed (Eqs. 3.2 to 3.4).

Figs. 3.9 to 3.11 show the Jander diffusion parameter, $[1-(1-f(t))^{1/3}]^2$, versus time *t* for $LaNi_5$, $LaNi_{4.7}Al_{0.3}$ and $LmNi_{4.91}Sn_{0.15}$ hydride alloys in the (α+β)- and β-phase regions at different temperatures. The reaction rate constant in the (α+β)-phase region is calculated from the slope of the interpolated straight line. Fig. 3.9 shows that the deviation of the JDM model fit from the experimental data is rather large for $LaNi_5$ at high temperature (60°C). For $LaNi_{4.7}Al_{0.3}$ and $LmNi_{4.91}Sn_{0.15}$, the agreement is good at high temperatures. For all cases, the agreement for the medium (40°C) and low (20°C) temperatures is relatively good and its correlation coefficients are close to 0.97.

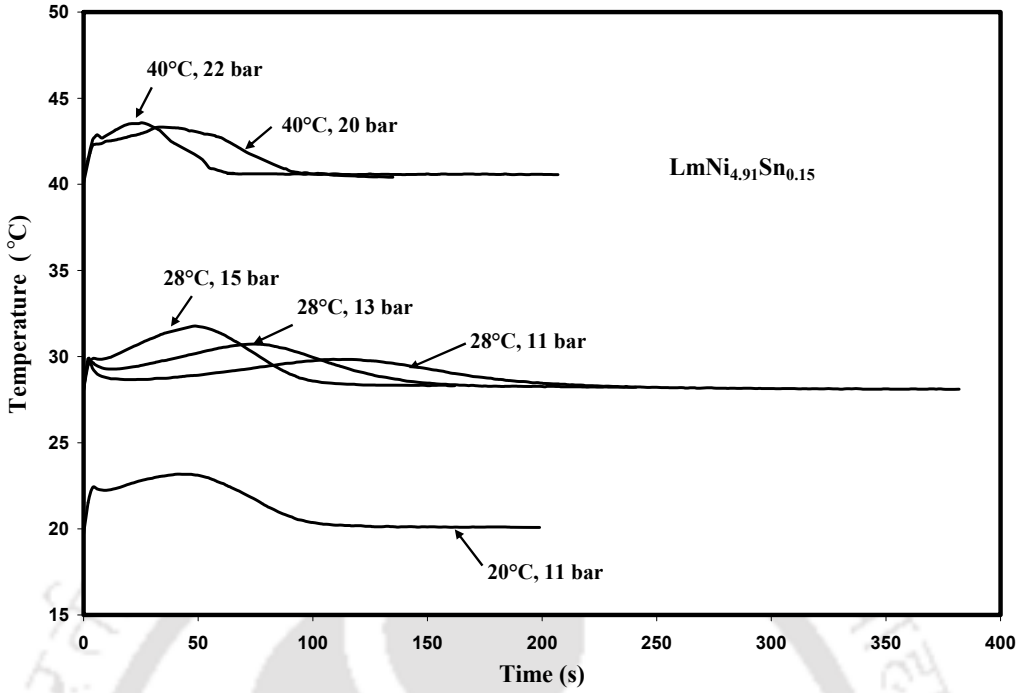

Fig. 3.2 Temperature variation in $LmNi_{4.91}Sn_{0.15}$ hydride alloy during absorption.

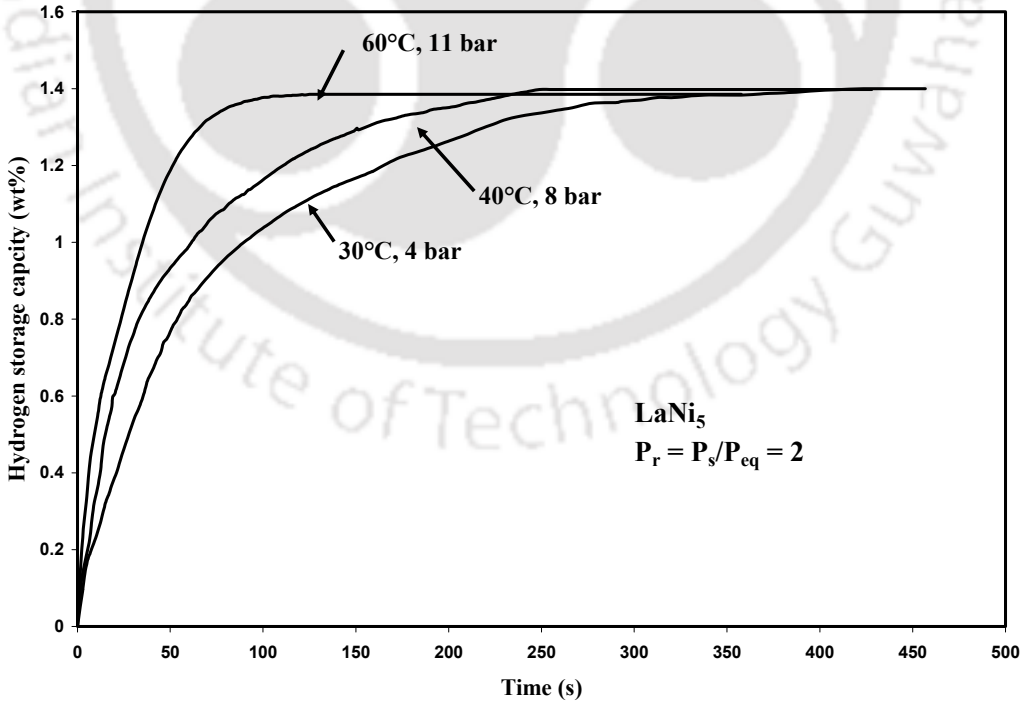

Fig. 3.3 Hydriding rate of $LaNi_5$.

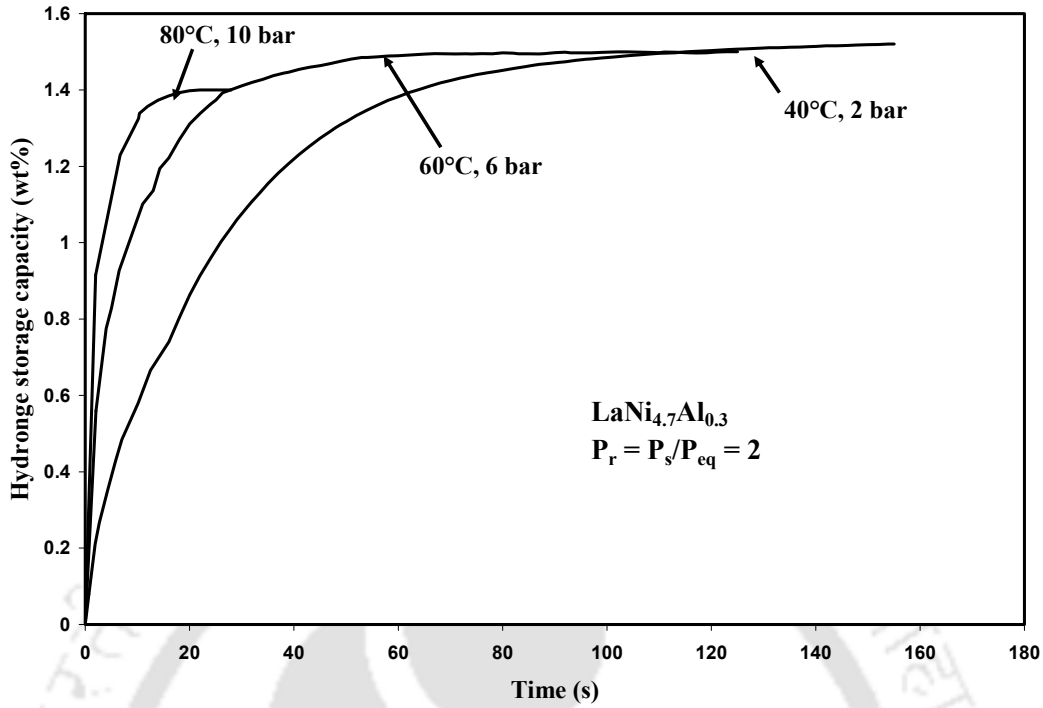

Fig. 3.4 Hydriding rate of $LaNi_{4.7}Al_{0.3}$.

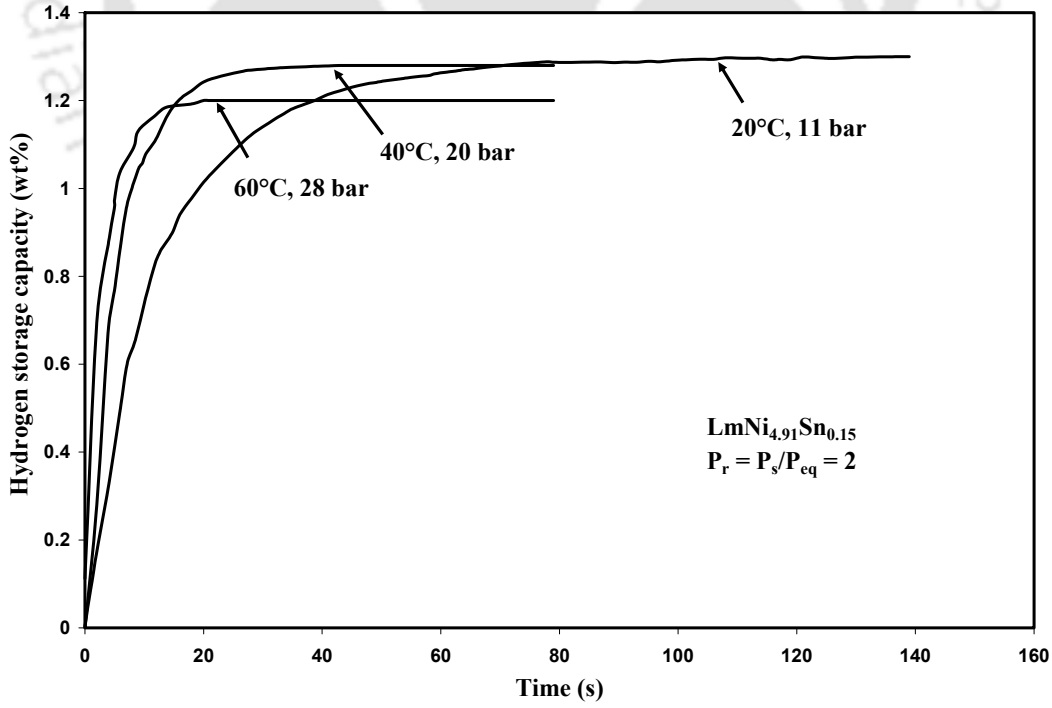

Fig. 3.5 Hydriding rate of $LmNi_{4.91}Sn_{0.15}$.

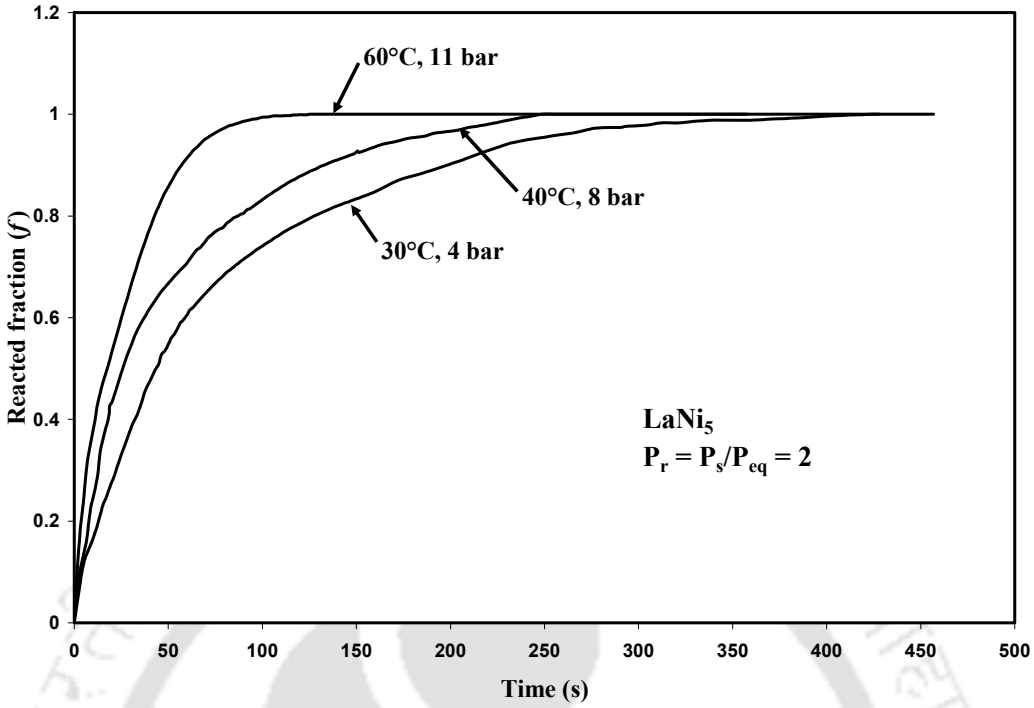

Fig. 3.6 Reacted fraction of $LaNi_5$.

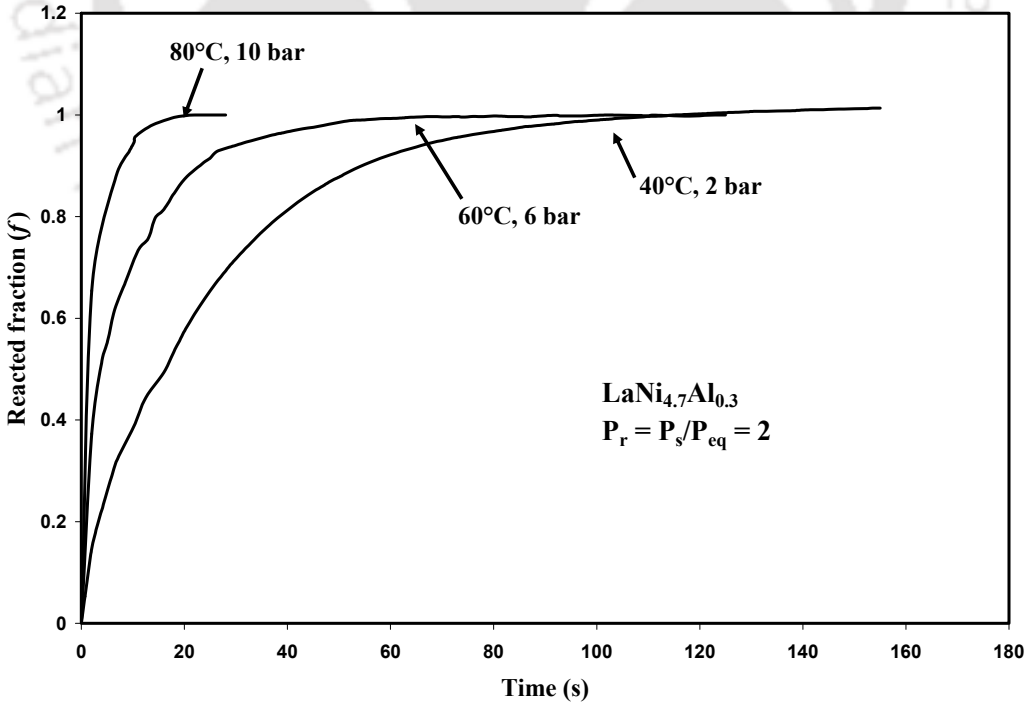

Fig. 3.7 Reacted fraction of $LaNi_{4.7}Al_{0.3}$.

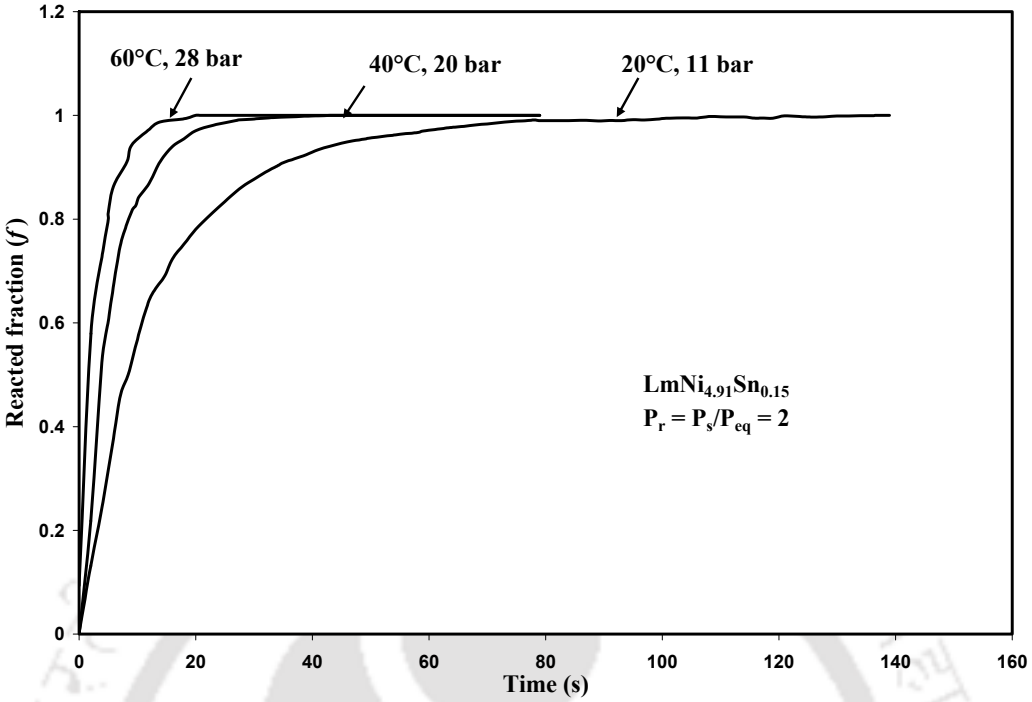

Fig. 3.8 Reacted fraction of $LmNi_{4.91}Sn_{0.15}$.

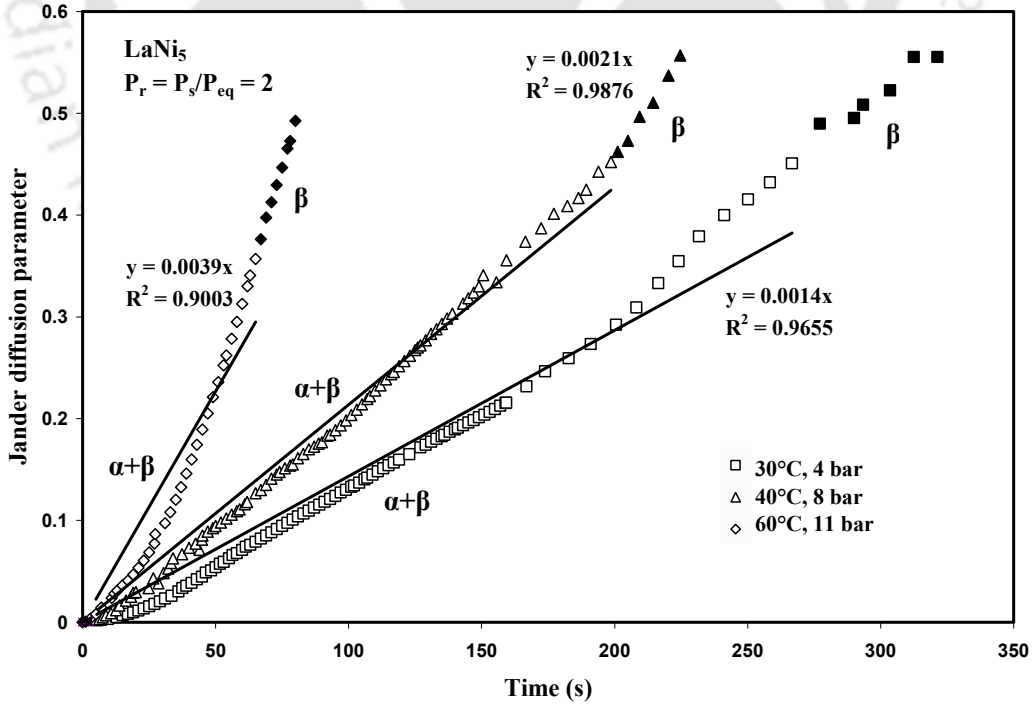

Fig. 3.9 Jander diffusion parameter $[1-(1-f(t))^{1/3}]^2$ vs. time (t) for $LaNi_5$.

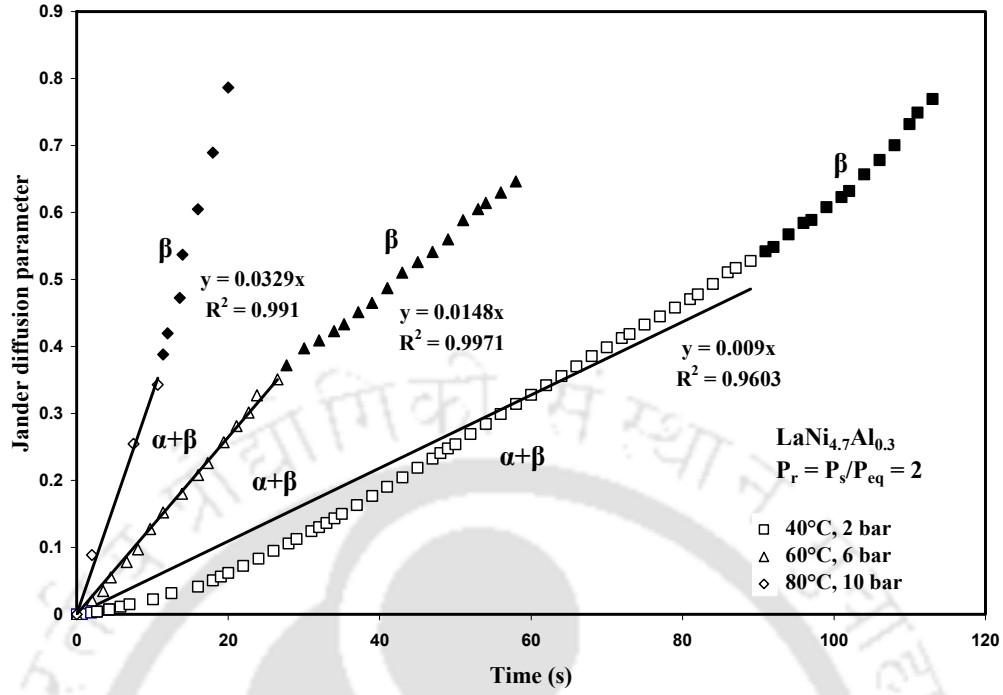

Fig. 3.10 Jander diffusion parameter $[1-(1-f(t))^{1/3}]^2$ vs. time (t) for $LaNi_{4.7}Al_{0.3}$.

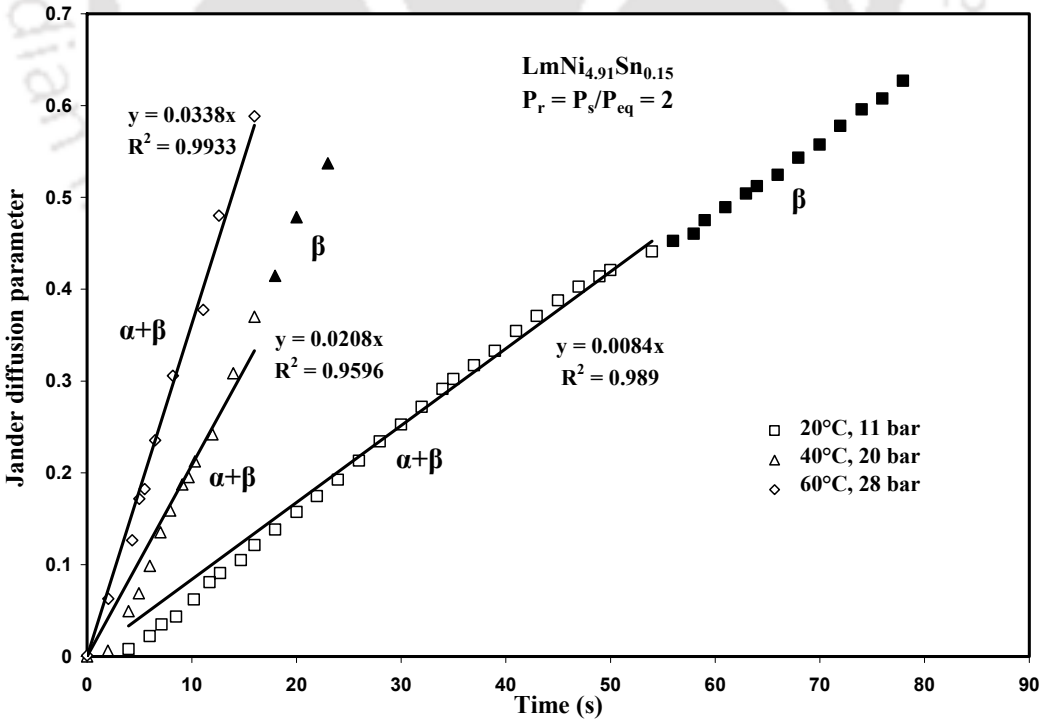

Fig. 3.11 Jander diffusion parameter $[1-(1-f(t))^{1/3}]^2$ vs. time (t) for $LmNi_{4.91}Sn_{0.15}$.

Figs. 3.12 to 3.14 show the results of three hydride alloys solved by Johnson-Mehl-Avrami model in which the order of equation is obtained by fitting the experimental data. A plot is drawn between $ln[-ln(1-f(t))]$ vs. $ln\ t$. It gives a straight line with slope n and intercepts k (rate constant). Each plot can be divided into three linear segments with different slopes, each of which represents a different zone of reaction, viz., α-, (α+β)- and β-phases. The slopes change for each phase transformation, viz., from α to (α+β) and from (α+β) to β. For a given pressure ratio, the reaction kinetics of $LaNi_5$ is slower than those of $LaNi_{4.7}Al_{0.3}$ and $LmNi_{4.91}Sn_{0.15}$ hydride alloys. The α-phase is clearly visible for the $LaNi_5$ alloy in the selected temperature range from 30°C to 60°C, whereas, for $LaNi_{4.7}Al_{0.3}$ and $LmNi_{4.91}Sn_{0.15}$ hydrides, the α-phase could not be observed.

In the first order Johnson-Mehl-Avrami (n = 1) model, the reaction rate constants are calculated from the slopes of the straight lines which fit the experimental $(-ln[1-f(t)]$ vs. $t)$ plots. Figs. 3.15 to 3.17 show these $(-ln[1-f(t)]$ vs. $t)$ plots for the JMA first order model for $LaNi_5$, $LaNi_{4.7}Al_{0.3}$ and $LmNi_{4.91}Sn_{0.15}$, respectively. It is observed that the reaction kinetics data of $LaNi_5$ and $LmNi_{4.91}Sn_{0.15}$ alloys show close agreement with the first order model and the accuracy of the fit is also close to 98% in the range of temperatures investigated. The temperature-dependent rate constants (k) are obtained from the slope of each of the straight lines obtained from the various kinetics equations. These rate constants are substituted into the Arrhenius equation (Eq. 3.5) for determining the hydriding reaction constants.

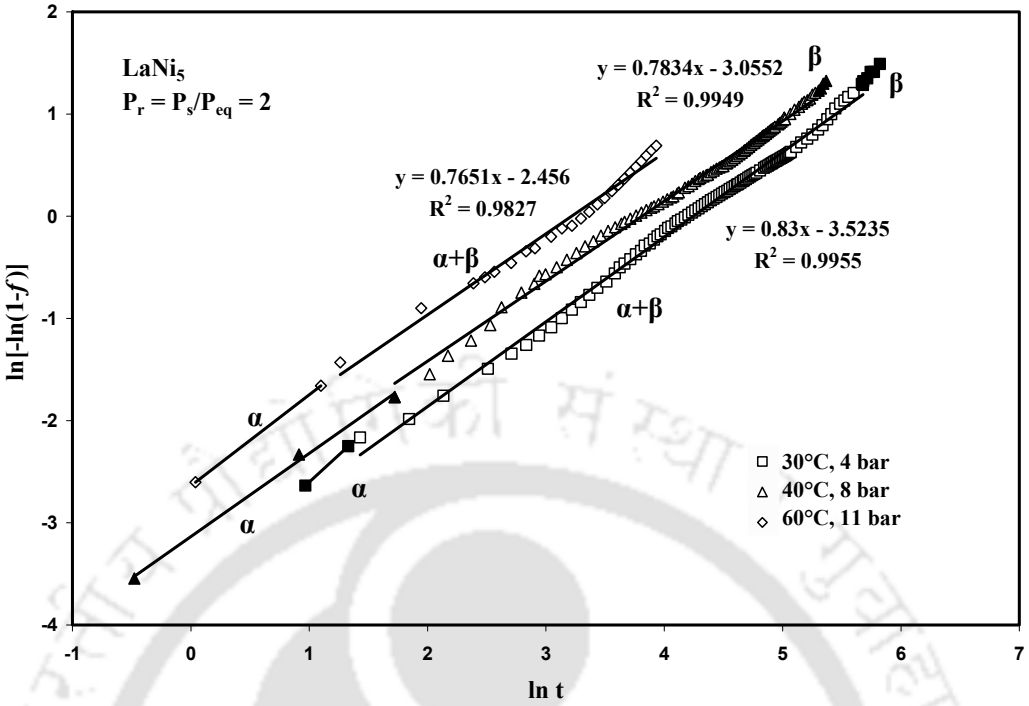

Fig. 3.12 ln[-ln(1-f(t))] vs. ln t for $LaNi_5$.

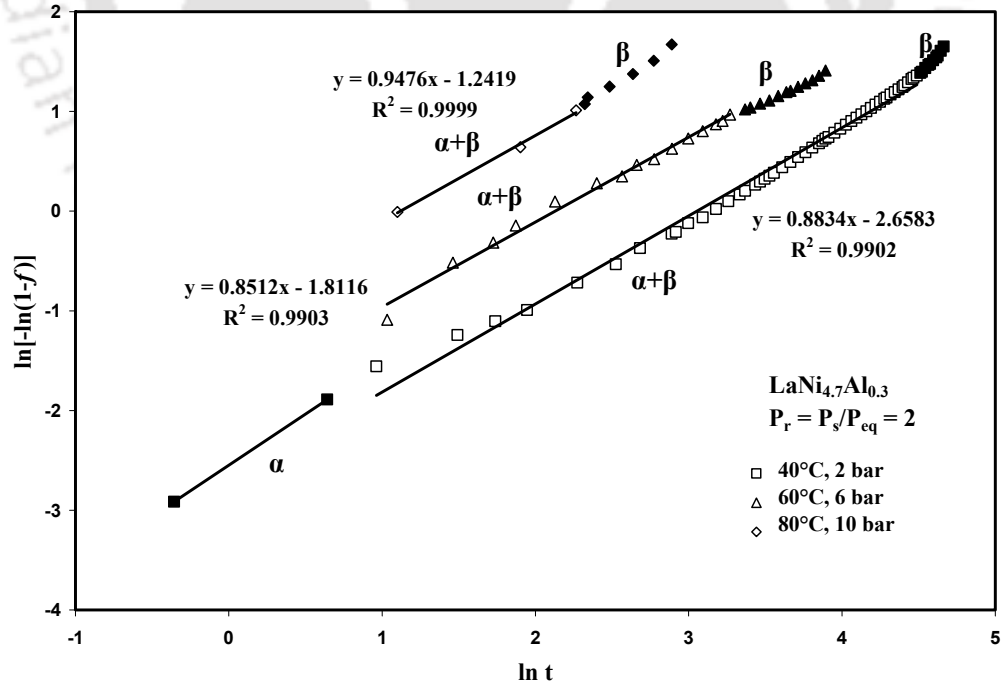

Fig. 3.13 ln[-ln(1-f(t))] vs. ln t for $LaNi_{4.7}Al_{0.3}$.

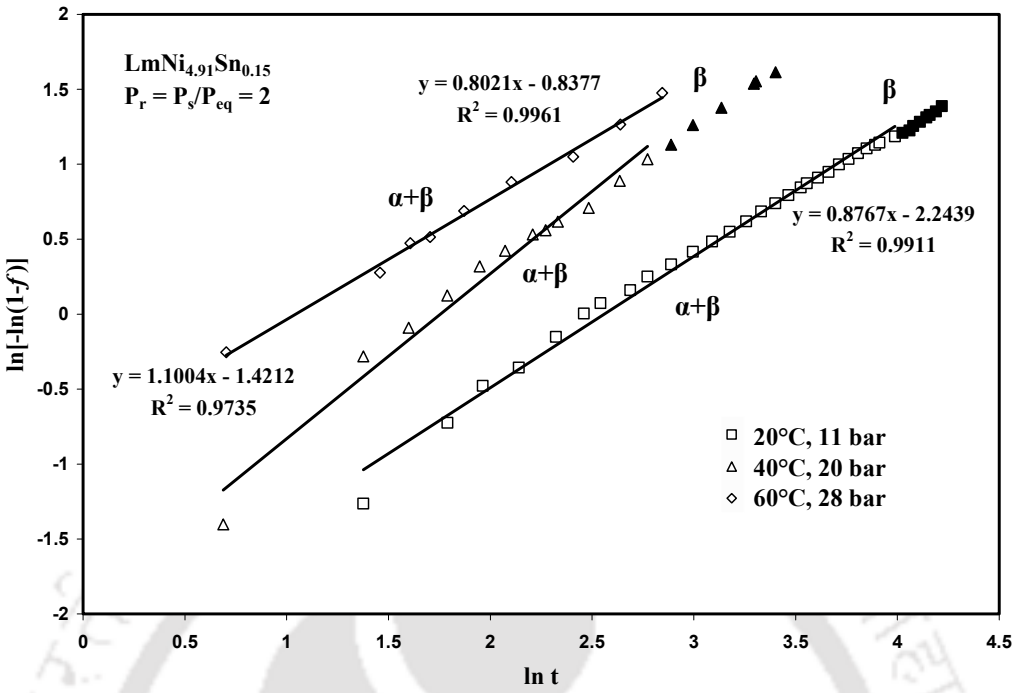

Fig. 3.14 ln[-ln(1-f(t))] vs. ln t for $LmNi_{4.91}Sn_{0.15}$.

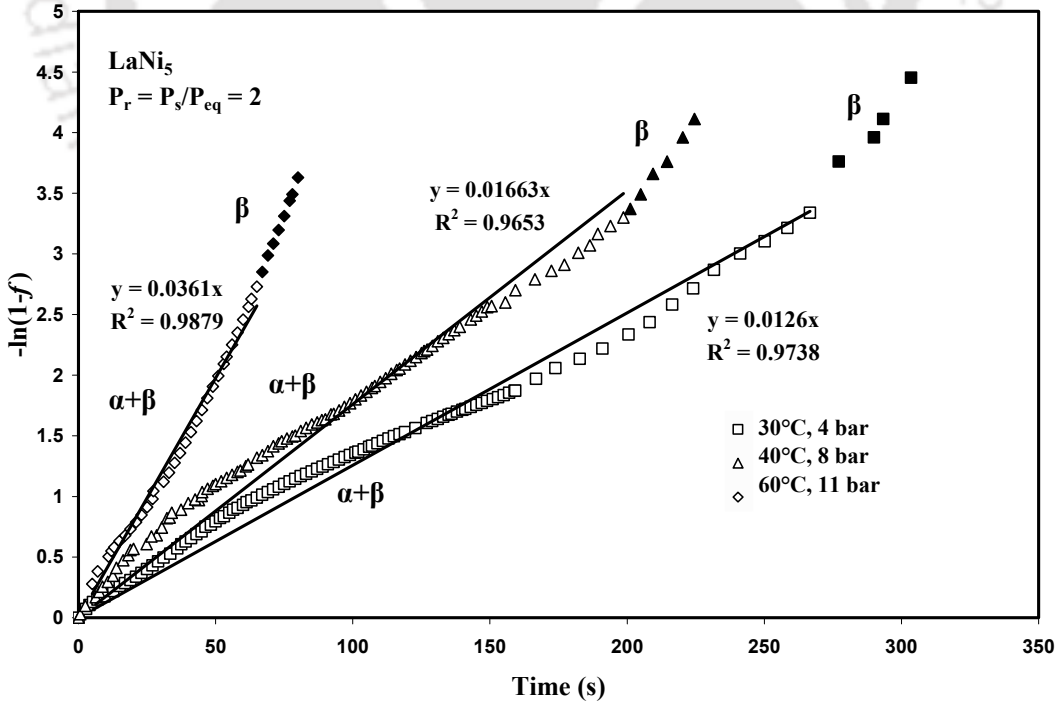

Fig. 3.15 -ln[1-f(t)] vs. time (t) for $LaNi_5$.

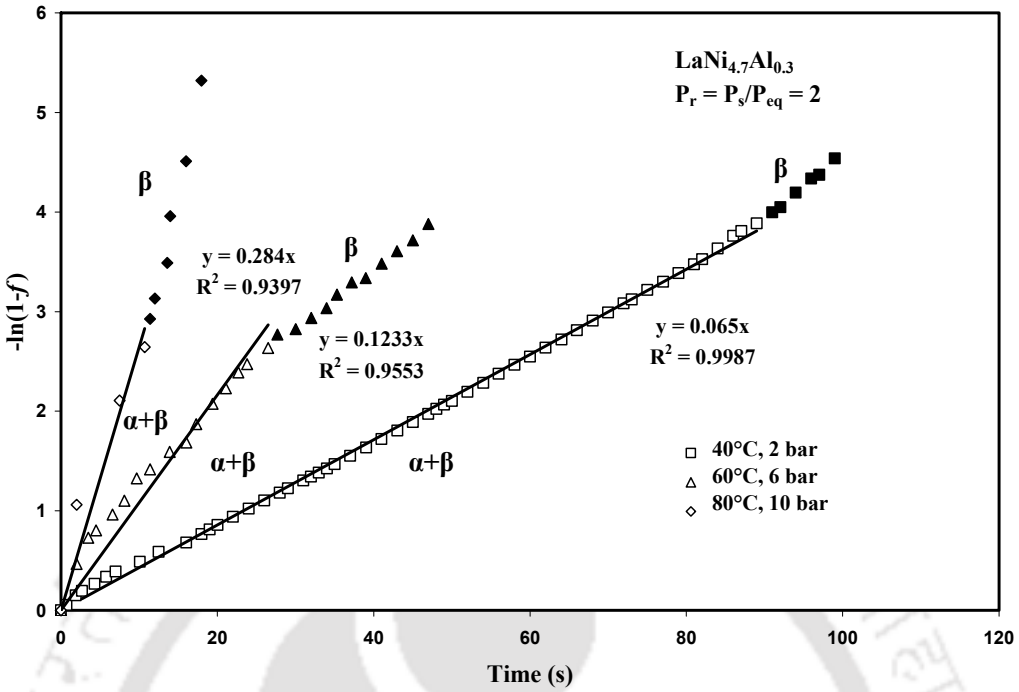

Fig. 3.16 -ln[1-$f(t)$] vs. time (t) for $LaNi_{4.7}Al_{0.3}$.

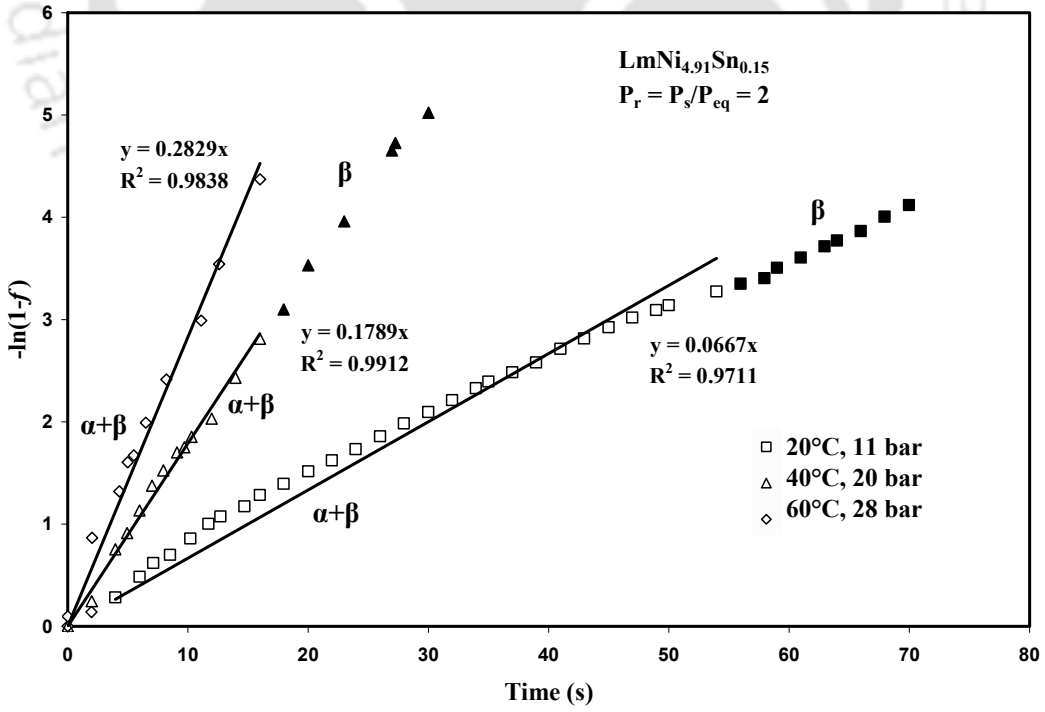

Fig. 3.17 -ln[1-$f(t)$] vs. time (t) for $LmNi_{4.91}Sn_{0.15}$.

Figs. 3.18 to 3.20 show the Arrhenius plots of ln k vs. $1/T$ for $LaNi_5$, $LaNi_{4.7}Al_{0.3}$ and $LmNi_{4.91}Sn_{0.15}$ (at $P_r = 2$), respectively. The slope and intercept of the straight lines give the ratio of activation energy to the universal gas constant ($-E_a/R_u$) and the pre-exponential factor (C), respectively. The calculated activation energy (E_a) and pre-exponential factor (C) for $LaNi_5$, $LaNi_{4.7}Al_{0.3}$ and $LmNi_{4.91}Sn_{0.15}$ from the JDM and JMA models are listed in Table 3.1. For validating the activation energies obtained from the various models, these estimated values of activation energy (E_a) along with the pre-exponential factor (C) are substituted in the most general form of the hydriding equation (Mayer *et al*., 1987) (Eq. 3.6) and then the rates of hydrogen absorption at different temperatures are calculated.

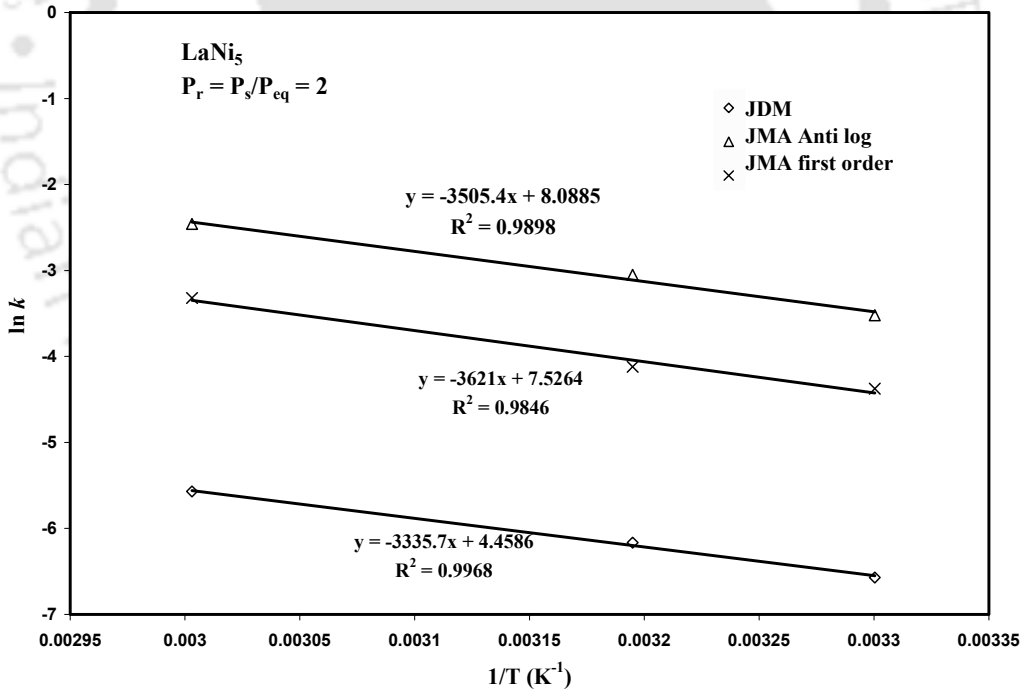

Fig. 3.18 Arrhenius plot for $LaNi_5$.

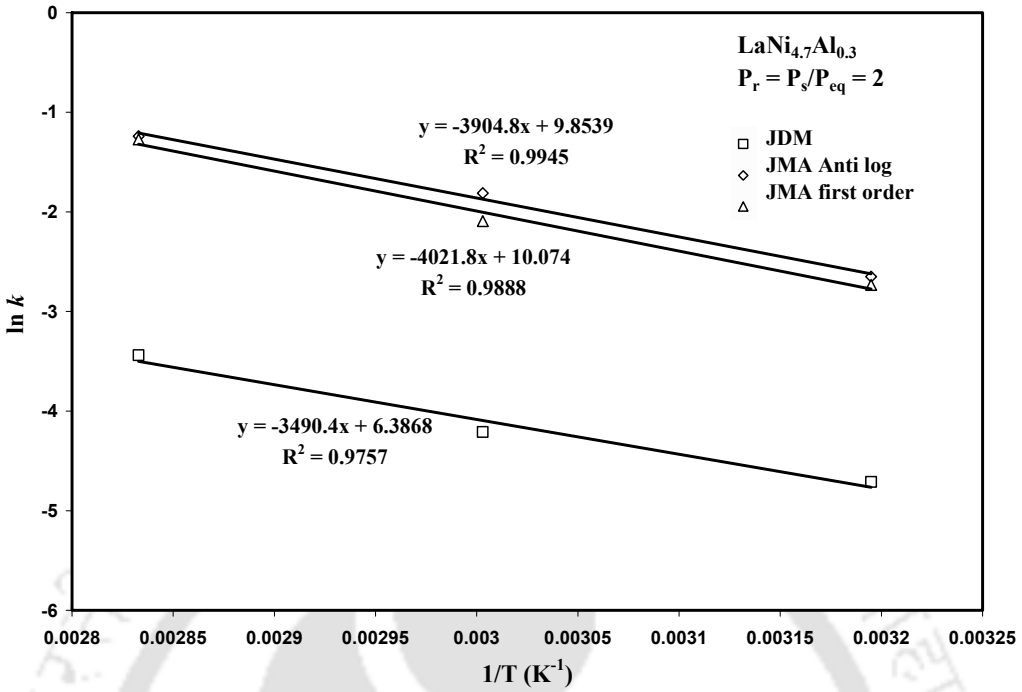

Fig. 3.19 Arrhenius plot for $LaNi_{4.7}Al_{0.3}$.

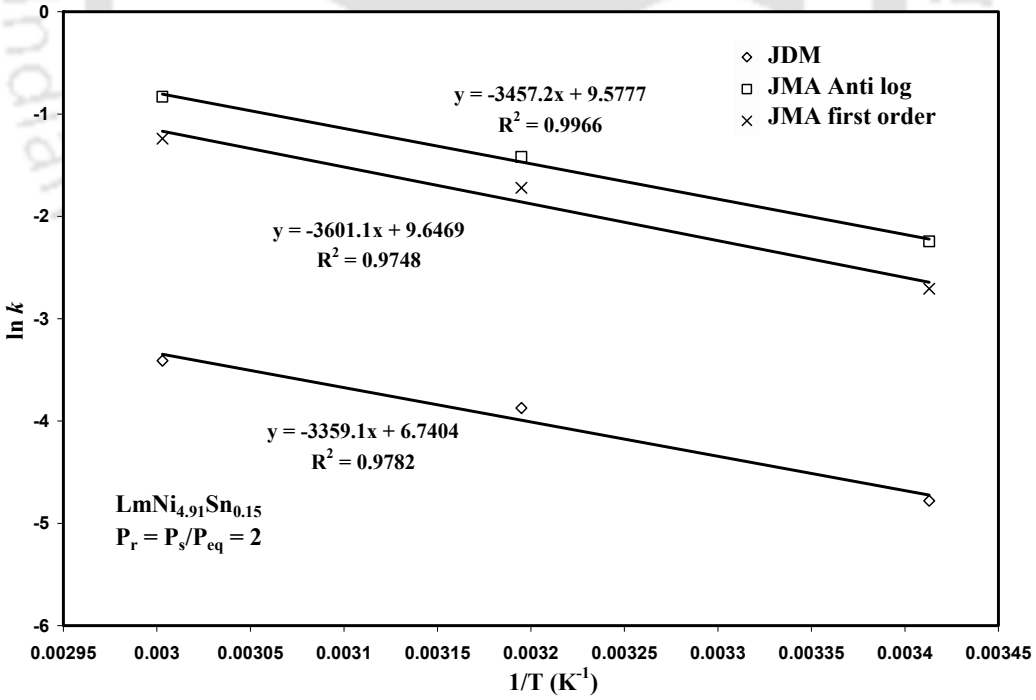

Fig. 3.20 Arrhenius plot for $LmNi_{4.91}Sn_{0.15}$.

Table.3.1 Activation energy and pre-exponential factor obtained in the (α+β)-phase region using different models.

Alloys		JDM	JMA Antilog	JMA First Order
$LaNi_5$	E_a **(kJ/mol H_2)**	27.7	29.1	30.1
	C **(s^{-1})**	86	3256	1856
$LaNi_{4.7}Al_{0.3}$	E_a **(kJ/mol H_2)**	29.1	32.45	33.4
	C **(s^{-1})**	594	19032	23718
$LmNi_{4.91}Sn_{0.15}$	E_a **(kJ/mol H_2)**	28.0	28.75	29.9
	C **(s^{-1})**	846	14440	15473

Fig. 3.21 shows a comparison of hydriding kinetics of $LaNi_{4.7}Al_{0.3}$ at 60 and 80°C for the Jander diffusion model. Figs. 3.22 to 3.24 show a comparison of hydriding kinetics of $LaNi_5$, $LaNi_{4.7}Al_{0.3}$ and $LmNi_{4.91}Sn_{0.15}$ for all three investigated reaction models. Among the three reaction kinetics models, the Jander diffusion model closely agrees with the experimental data. The largest deviation of the predicted result from the experimental data is about 8.4%, 4.7% and 3.4% for $LmNi_{4.7}Sn_{0.15}$ at 20°C, $LaNi_5$ at 40°C and $LaNi_{4.7}Al_{0.3}$ at 60°C, respectively. Hence, the diffusion of the hydrogen atom through the metal hydride is the rate-limiting step for $LaNi_5$, $LaNi_{4.7}Al_{0.3}$ and $LmNi_{4.91}Sn_{0.15}$. Using the Jander diffusion model the estimated activation energies of $LaNi_5$, $LaNi_{4.7}Al_{0.3}$ and $LmNi_{4.91}Sn_{0.15}$ are 27.7, 29.1 and 28.0 kJ/mol H_2, respectively.

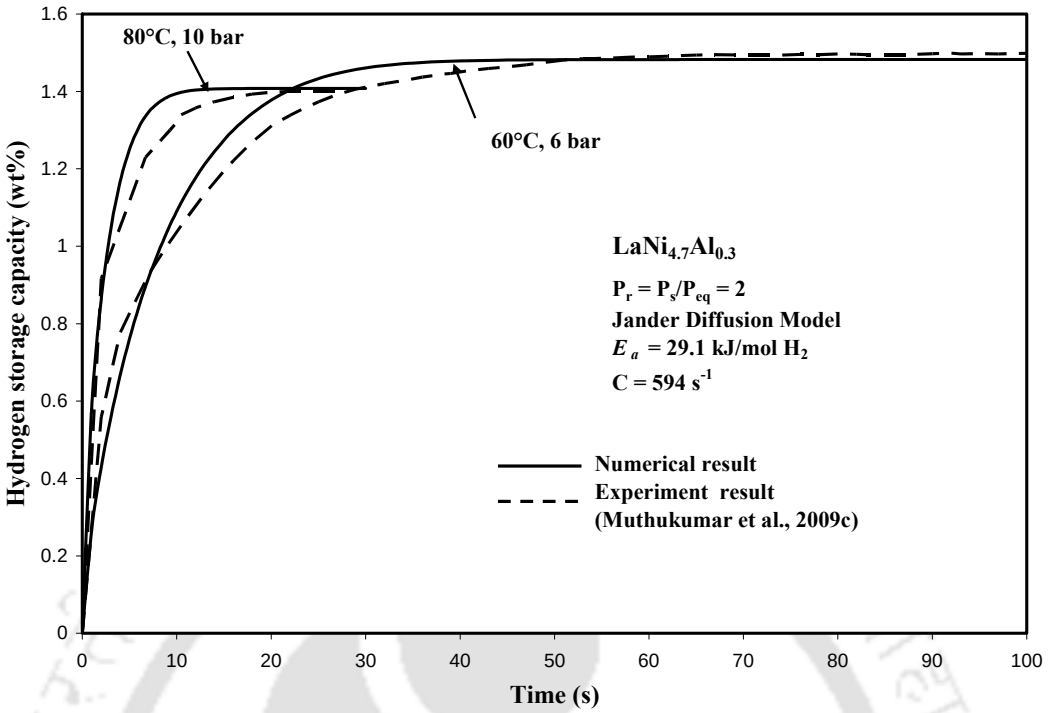

Fig. 3.21 Validation of reaction kinetics for $LaNi_{4.7}Al_{0.3}$ (JDM model).

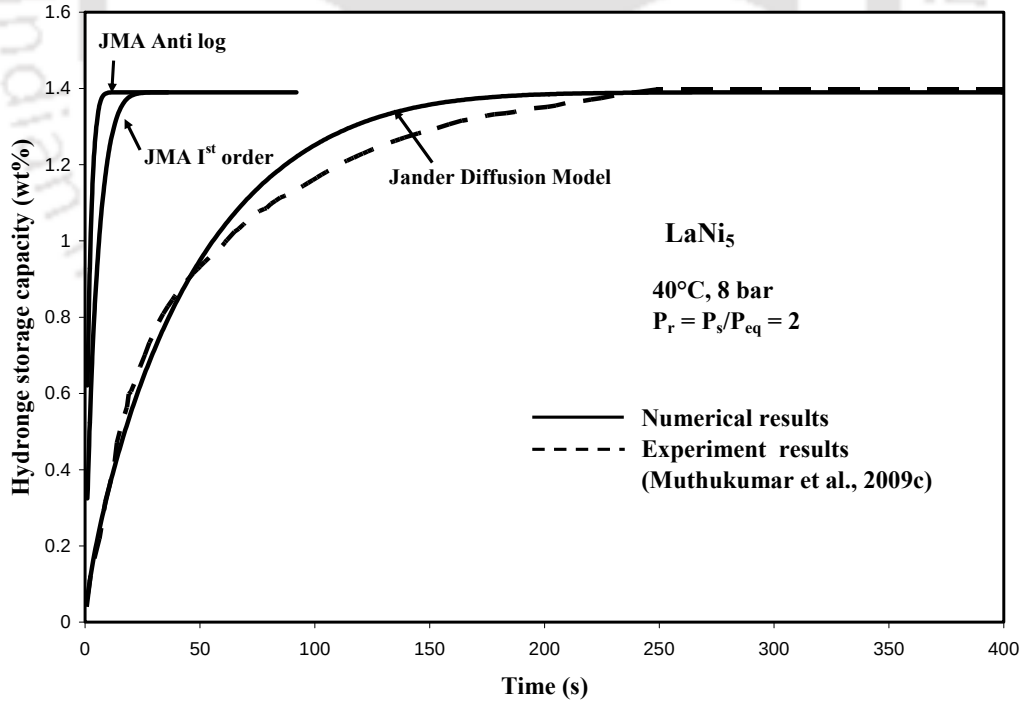

Fig. 3.22 Comparison of reaction kinetics of $LaNi_5$ for three different reaction kinetics models.

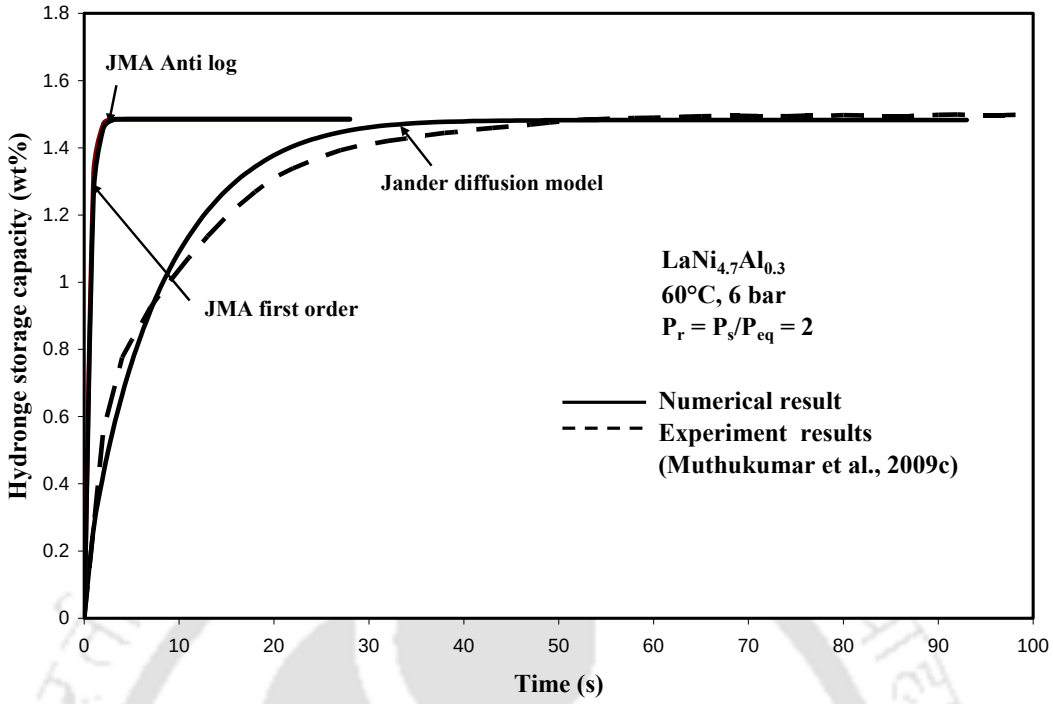

Fig. 3.23 Comparison of reaction kinetics of $LaNi_{4.7}Al_{0.3}$ for three different reaction kinetics models.

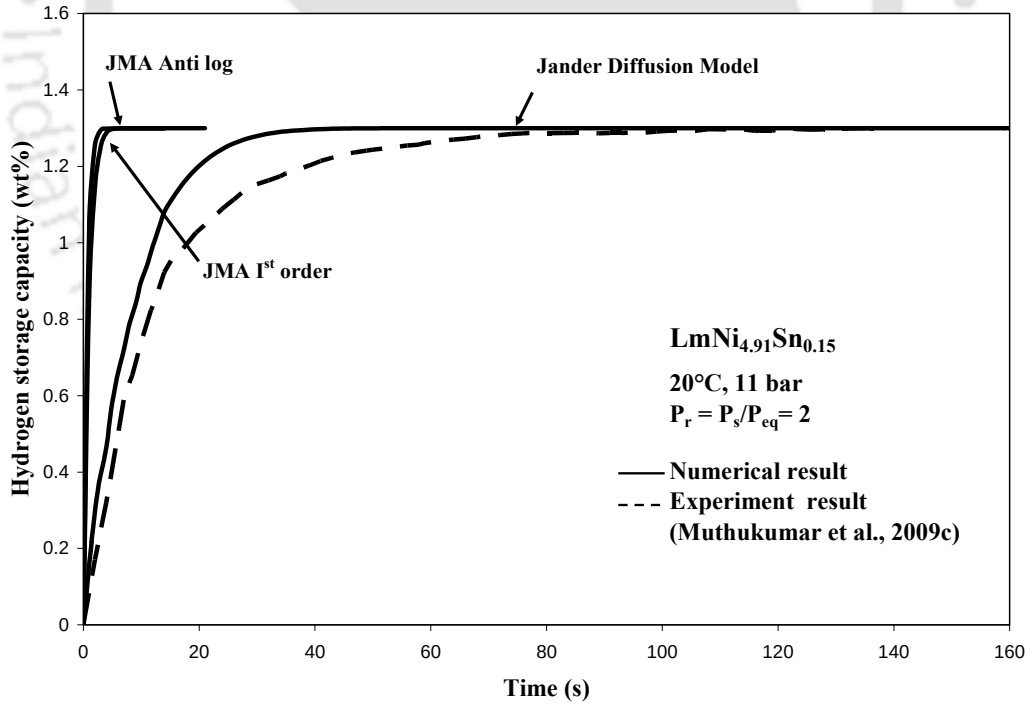

Fig. 3.24 Comparison of reaction kinetics of $LmNi_{4.91}Sn_{0.15}$ for three different reaction kinetic models.

3.3 SUMMARY

The hydriding kinetics of some commonly used metal hydrides for heat pump applications have been studied at different operating temperatures and pressures. Two widely used reaction kinetics models, namely, Jander diffusion model (JDM) and Johnson-Mehl-Avrami (JMA) model were considered for the present investigations. The activation energies and reaction rate constants of the above-mentioned hydride alloys were determined by constructing the Arrhenius plot. The activation energies estimated using different models were compared. The accurate values of activation energy were determined for the selected metal hydrides by comparing the reaction kinetics data obtained from these models with corresponding experimental data. The estimated activation energy and reaction rate constants are used for the further investigation in the single-stage metal hydride heat pump and the double-stage double-effect metal hydride heat pumps.

CHAPTER 4

HEAT AND MASS TRANSFER MODELS

Metal hydrides can be effectively utilized as working materials in a number of thermal machines which can contribute significantly the environmentally clean energy technologies. These systems use low grade thermal energy, for example, waste heat from industries, solar energy and heat from exhaust flue gases to produce high quality thermal energy and cooling outputs. Metal hydride heat pump is one of the promising applications of metal hydrides, which can be tailored to provide heating and cooling or temperature upgrading over a wide range of input and ambient temperatures. Development and optimization of such devices require highly sophisticated computational design methods. Though, many researchers have concentrated on the topic of metal hydride based cooling system, the commercial usage of these systems does not seem to be feasible yet. This is probably due to poor heat and mass transfer characteristics of metal hydrides, high initial cost of the hydride alloys and difficulty in achieving optimized heat and hydrogen

transfer in the reaction bed. In the following sub-section, the mathematical modelling of a single-stage metal hydride heat pump (SS-MHHP) is presented.

4.1 SINGLE STAGE METAL HYDRIDE HEAT PUMP (SS-MHHP)

The systems of equations are solved computationally for predicting the time dependent conjugate heat and mass transfer characteristics between the coupled reactors. The objectives of the present study are

- To investigate the hydride bed temperature distribution, hydrogen concentration, and equilibrium pressures of the selected hydride alloy pairs.
- To study the dynamic Pressure-Concentration-Isotherm (PCT) correlation during the heat and hydrogen exchange processes.
- To find the amount of hydrogen exchange between the paired reactors, cycle time, SCP and COP of the system.
- To investigate the effect of various operating temperatures, such as, heat source (T_H), heat sink (T_M) and refrigeration (T_C) temperatures on the performance of the SS-MHHP system.

4.1.1 Physical Model and Principle of Operation

Fig. 4.1 shows a schematic of a SS-MHHP used for producing the refrigeration effect at low temperature, T_C. It consists of a pair of two reactors A and B filled with a regeneration alloy (high temperature alloy) and a refrigeration alloy (low temperature alloy), respectively. The length of the reaction bed is 475.0 mm and outer diameter is 36.0 mm. A filter is used at the inner most tube of 12.0 mm outer diameter. Metal hydride is filled in the space between the inner tube and the filter tube. The cooling fluid flows

around the outer periphery of the tube of 1.0 mm gap. These two reactors are coupled by a connecting tube with a control valve through which hydrogen gas can flow freely between the reactors when the valve is opened. The dimensions of the connecting tube are taken as 300.0 mm length and 3.0 mm internal diameter. Fig. 4.2 shows the operating cycle on the van't Hoff plot. It consists of four processes and these are explained below.

4.1.1.1 Process *ab*

Initially, the reactor A is fully hydrided (X_{max}) and B is fully dehydrided (X_{min}) at their respective operating temperatures of T_H and T_M. Two reactors are coupled by a connecting tube with a valve (Fig. 4.1). Since the operating valve is initially closed, the equilibrium pressure difference exists between the reactors. Once the valve is opened, due to the difference in pressure, hydrogen gas starts to desorb from the reactor A by taking the heat from the reaction bed and heat transfer fluid, and reactor B starts to absorb hydrogen gas by rejecting the heat of absorption to the reaction bed and heat transfer fluid. This process continues till the fixed amount of hydrogen transfers from the reactor A to the reactor B.

4.1.1.2 Process *bc*

During this process, the valve between the reactors A and B is closed and no hydrogen transfer between the reactors takes place. Only the heat transfer takes place between the hydride bed and the cooling/heating fluids. This process is continued till the reactors A and B reach temperature T_M and T_C, respectively.

4.1.1.3 Process *cd*

Once the reactors A and B reach the respective medium and low (refrigeration) temperatures, the valve between the reactors is opened. Due to the existence of pressure difference, the hydrogen starts to desorb from the reactor B at temperature T_C by extracting the heat of desorption from the reaction bed and heat transfer fluid, yielding refrigeration effect. Simultaneously, the hydride A absorbs this hydrogen by rejecting the heat of absorption to the reaction bed and cooling fluid at the medium temperature, T_M. This process continues till the fixed amount of hydrogen is transferred (same as during the process *ab*).

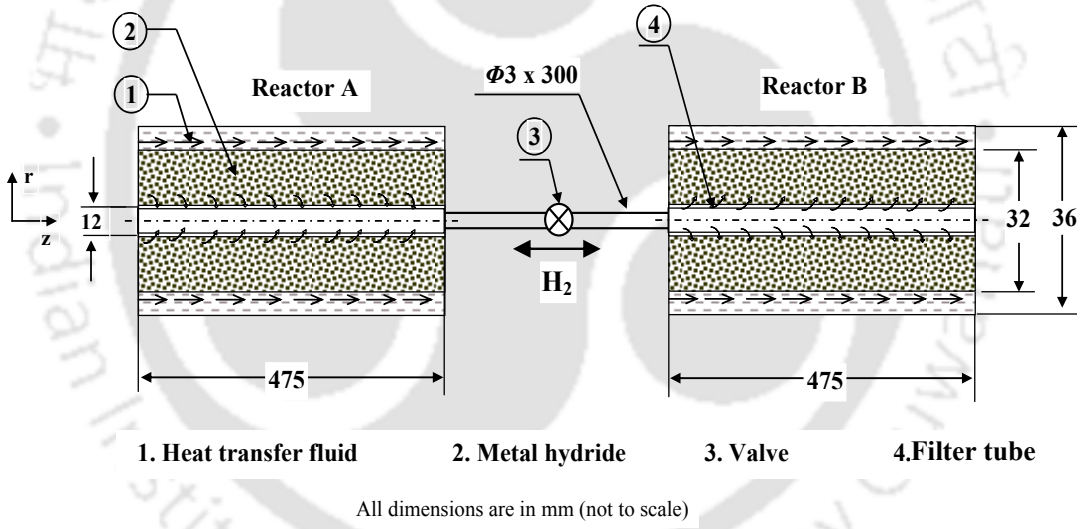

Fig. 4.1 Schematic diagram of coupled metal hydride reactors.

4.1.1.4 Process *da*

During this process the valve is closed. Reactors A and B are sensibly heated to T_H and T_M, respectively. Thus the first cycle operation is completed.

4.1.2 Selection of Metal Hydride Pairs

The dependence of the equilibrium pressure, P_{eq} on the reciprocal of the absolute temperature, $1/T$, which is an important characteristic of the two hydrides, is shown in Fig. 4.2. The selected hydride pairs are supposed to operate within the range of specified operating temperatures. Depending upon the application and availability of the heat source, the operating pressure and temperature range lies within 30 to 40 bar, and 130 to 170°C (driving temperatures) for the regeneration alloy and 0.1 to 5 bar and –10°C to 20°C (refrigeration temperatures) for the refrigeration alloy, respectively. Further, the selected alloy pairs should satisfy the following conditions.

1. The minimum desorption pressure of the regeneration alloy at T_H must be greater than the maximum absorption pressure of the refrigeration alloy at T_M.
2. Similarly, the maximum absorption pressure of regeneration alloy at T_M must be less than the minimum desorption pressure of refrigeration alloy at T_C.

With the above conditions, five hydride alloy pairs, namely, $MmNi_{4.6}Al_{0.4}$ / $MmNi_{4.6}Fe_{0.4}$ (AP 1), $LaNi_{4.61}Mn_{0.26}Al_{0.13}$ / $La_{0.6}Y_{0.4}Ni_{4.8}Mn_{0.2}$ (AP 2), $LmNi_{4.91}Sn_{0.15}$ / $Ti_{0.99}Zr_{0.01}V_{0.43}Fe_{0.09}Cr_{0.05}Mn_{1.5}$ (AP 3), $LaNi_{4.6}Al_{0.4}$ / $MmNi_{4.15}Fe_{0.85}$ (AP 4), and $Zr_{0.9}Ti_{0.1}Cr_{0.9}Fe_{1.1}$ / $Zr_{0.9}Ti_{0.1}Cr_{0.6}Fe_{1.4}$ (AP 5) are selected for the present investigations. The enthalpy and entropy of formation for the above selected alloy pairs during both the absorption and desorption processes are listed in Table 4.1.

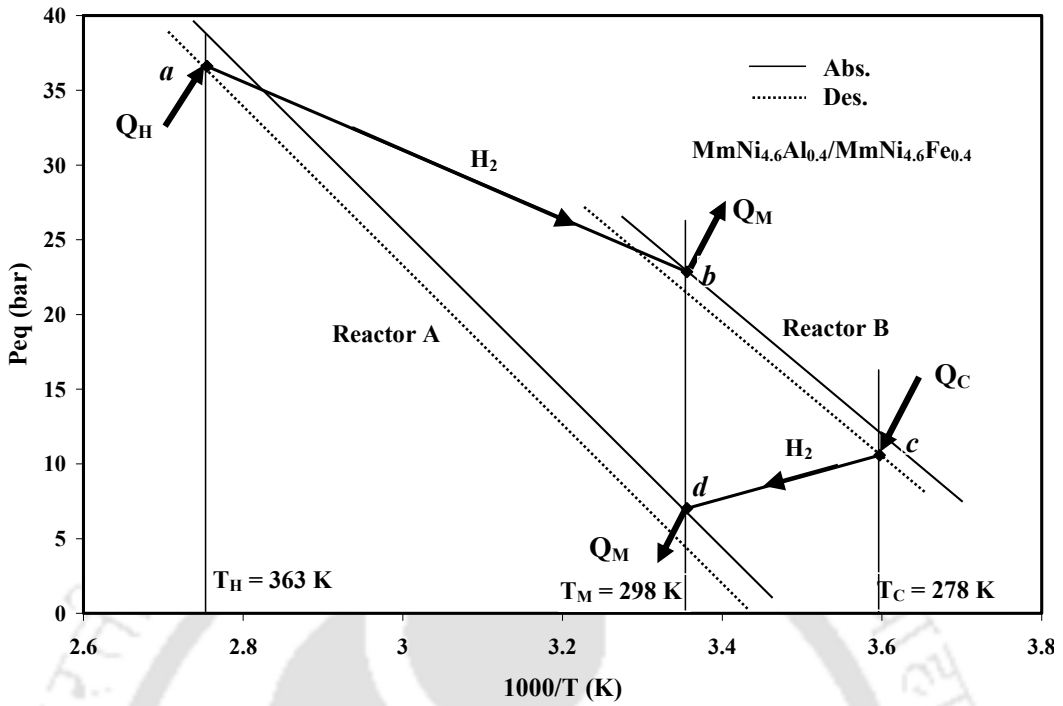

Fig. 4.2 Van't Hoff plot for a single stage metal hydride heat pump.

Table 4.1 Enthalpy and entropy of formation of the selected hydride alloy pairs

Alloy pairs		ΔH (kJ/mol H_2)		ΔS (J/mol H_2 K)		References
		Abs.	Des.	Abs.	Des.	
AP1	$MmNi_{4.6}Al_{0.4}$ (A) $MmNi_{4.6}Fe_{0.4}$ (B)	29.0 25.2	27.8 24.7	108.7 104.5	107.2 105.4	Satheesh *et al*., 2009
AP2	$LaNi_{4.61}Mn_{0.26}Al_{0.13}$ (A) $La_{0.6}Y_{0.4}Ni_{4.8}Mn_{0.2}$ (B)	36.9 26.9	37.6 26.6	109.7 102.3	108.2 97.4	Ni an Liu, 2007; Qin *et al.,* 2007
AP3	$LmNi_{4.91}Sn_{0.15}$ (A) $Ti_{0.99}Zr_{0.01}V_{0.43}Fe_{0.09}$- $-Cr_{0.05}Mn_{1.5}$ (B)	27.2 20.0	32.4 25.5	103.1 97.0	112.8 110.9	Payá, 2009
AP4	$LaNi_{4.6}Al_{0.4}$ (A) $MmNi_{4.15}Fe_{0.85}$ (B)	34.8 25.3	35.8 24.7	113.9 105.0	115.6 107.0	Izhvanov *et al.,* 1996; Chernikov *et al.,* 2002
AP5	$Zr_{0.9}Ti_{0.1}Cr_{0.9}Fe_{1.1}$ (A) $Zr_{0.9}Ti_{0.1}Cr_{0.6}Fe_{1.4}$ (B)	29.65 24.55	34.71 29.77	92.0 92.0	104.97 104.13	Park *et al.,* 1990; Lee *et al.,* 1995

For solving the present mathematical model, the following assumptions are made.

1. Hydrogen is considered to be a perfect gas.
2. Initially at process *ab*, the hydride beds of reactors A and B are in equilibrium with hydrogen gas.
3. Heat transfer through the hydride bed is by two-dimensional conduction and convection. The effect of radiation is negligible.
4. The thermo-physical properties of the metal hydride, such as, reaction enthalpy and entropy, thermal conductivity and specific heat capacity are independent of temperature, concentration and hydrogen pressure.
5. Pressure and temperature inside the connecting tube are independent of space but are time dependent.
6. The reactors are assumed to be well insulated and no heat transfer takes place between them and to the surroundings.

4.1.3 Problem Formulation

4.1.3.1 Mass and Energy Balance Equations

Initially, all the reactors are in equilibrium with respect to the hydrogen gas. Therefore, the equilibrium pressure, P_{eq} (bar) is calculated using the van't Hoff equation (Nashizaki *et al*., 1983)

$$\frac{P_{eq}}{P_o} = exp\left[\frac{\Delta S}{R_u} - \frac{\Delta H}{R_u T} + (\varphi \pm \varphi_o) \times tan\left(\pi\left(\frac{x}{x_f} - \frac{1}{2}\right)\right) \pm \frac{\beta}{2}\right] \tag{4.1}$$

Gas pressure and temperature in the connecting pipe immediately after opening the valve are estimated from the following equations

$$P_{g,P} = \frac{P_{g,A}V_A + P_{g,B}V_B}{V_A + V_B} \qquad T_{g,P} = \frac{n_A T_A + n_B T_B}{n_A + n_B} \tag{4.2}$$

where, $P_{g,A}$, V_A, $P_{g,B}$ and V_B denote the gas pressures and volumes of the reactors A and B, respectively. Since the hydrogen is assumed to be a perfect gas, the number of moles of hydrogen in reactors A and B is calculated using the perfect gas law.

$$n_A = \frac{P_A V_A}{R_u T_A} \qquad n_B = \frac{P_B V_B}{R_u T_B} \tag{4.3}$$

The number of moles of hydrogen and gas temperature and pressure in the connecting tube at any time during the hydrogen transfer (absorption and desorption processes) are calculated using the following equations

$$n_{g,t+\delta t} = n_{g,t} + n_d - n_a \tag{4.4}$$

$$T_{g,t+\delta t} = \frac{\left(n_{g,t} - n_a\right)T_{g,a} + n_d T_{g,d}}{n_{g,t} - n_a + n_d} \tag{4.5}$$

$$P_{g,t+\delta t} = \frac{n_{g,t+\delta t} R_u T_{g,t+\delta t}}{V_A + V_B + V_P} \tag{4.6}$$

where, $n_{g,t}$, n_d *and* n_a respectively denote the number of moles of hydrogen in the connecting tube immediately after opening the valve, number of moles of hydrogen desorbed from the reactor A and number of moles of hydrogen absorbed in reactor B during time interval δt.

As stated in the physical model, the operating cycle consists of two hydrogen transfer processes (*ab* and *cd*) and two sensible heat transfer processes (*bc* and *da*). The heat and mass transfer rates during the processes *ab* and *cd* are estimated by simultaneously solving the continuity and energy equations in both the reactors. The heat transfer rates

during the processes *bc* and *da* are estimated by solving only the energy equation. These equations are discreted using finite volume method and are presented in Appendix B.

4.1.3.2 Process *ab*

During this process, hydrogen is desorbed from the reactor A by taking the heat of desorption from the heat transfer fluid at temperature T_H and absorbed at reactor B by releasing the heat of absorption to the heat transfer fluid at temperature T_M. The computational modelling of this process is discussed in the following subsections.

Reactor A (Desorption)

Mass flux (mass flow rate per unit volume) during the desorption of hydrogen is given by (Mayer *et al*., 1987)

$$\dot{m}_A = C_d \exp\left(\frac{-E_d}{R_u T_A}\right)\left(\frac{P_{eq,A} - P_{g,t+\delta t}}{P_{eq,A}}\right)\rho_{m,A} \tag{4.7}$$

where, $\rho_{m,A}$ denotes the density of hydride at any given time t. P_g the gas pressure in the connecting tube at any given time is obtained using Eq. (4.6).

Assuming thermal equilibrium between the hydride bed and hydrogen, a combined energy equation is considered instead of separate equations for both solid and gas phases (Jemni and Nasrallah, 1995a):

$$\left(\rho C_p\right)_e \frac{\partial T}{\partial t} + \left(\rho C_p\right)_g \vec{u_g}.\nabla T = k_e \nabla^2 T - \dot{m}_A \left[\frac{\Delta H}{M_g} - T\left(Cp_g - Cp_m\right)\right] \tag{4.8}$$

where,

$$\left(\rho C_p\right)_e = \left(\varepsilon \rho C_p\right)_g + \left((1-\varepsilon)\rho C_p\right)_m \tag{4.9}$$

and the effective thermal conductivity

$$k_e = \varepsilon k_g + (1-\varepsilon) k_m . \tag{4.10}$$

The hydrogen mass balance is expressed as

$$\varepsilon \frac{\partial\left(\rho_g\right)}{\partial t} + \nabla\left(\rho_g \overrightarrow{u_g}\right) = \dot{m}_A \tag{4.11}$$

where, ρ_g denotes the density of the hydrogen gas in the reactor A during the desorption process. Hydrogen density is determined using the perfect gas law. Velocity of hydrogen gas (u_g) is calculated using Darcy's law

$$\overrightarrow{u_g} = -\frac{K}{\mu_g}\nabla P_g \tag{4.12}$$

By substituting the density (ρ_g) (from perfect gas law eq.) and velocity ($\overrightarrow{u_g}$) of the gas (from Eq. 4.12) in Eq. 4.11, the gas pressures (P_g) inside the reactors are determined using the following equation

$$\left(\frac{\varepsilon M_g}{R_u T}\right)\frac{\partial P_g}{\partial t} + \left(\frac{\varepsilon M_g P_g}{R_u}\right)\frac{\partial}{\partial t}\left(\frac{1}{T}\right) - \frac{K}{\nu_g r}\frac{\partial}{\partial r}\left(r\frac{\partial P_g}{\partial r}\right) - \frac{K}{\nu_g}\frac{\partial}{\partial z}\left(\frac{\partial P_g}{\partial z}\right) = \dot{m}_A . \tag{4.13}$$

Initial and Boundary Conditions

Initially at time $t = 0$, the density of the metal hydride, temperatures of the metal hydride and hydrogen gas and hydride concentration are assumed to be uniform throughout the reactor

$$\rho_{m,A}(z,r) = \rho_{ss}\,; \quad T_{m,A}(z,r) = T_{g,A}(z,r) = T_H \;; \quad X_A(z,r) = X_{\max,A}. \tag{4.14}$$

The end boundary conditions (left and right) of the reactors are assumed to be adiabatic (shown in Fig. 4.3)

$$\frac{\partial P_g}{\partial z}(z,r,t)_{z=0} = 0; \qquad \frac{\partial T}{\partial z}(z,r,t)_{z=0} = 0 \tag{4.15}$$

$$\frac{\partial P_g}{\partial z}(z,r,t)_{z=Z} = 0; \qquad \frac{\partial T}{\partial z}(z,r,t)_{z=Z} = 0. \tag{4.16}$$

Along the centerline, where $r = r_i$, the adiabatic conditions are given as

$$P_g(z,r_i,t) = P_g. \qquad \frac{\partial T}{\partial r}(z,\ r,t)_{r=r_i} = 0 \tag{4.17}$$

The cooling fluid flows through the outer peripheral tube and therefore the convective boundary condition is applied at $r = r_o$.

$$-k_e \frac{\partial T}{\partial r}(z,r_o,t) = U\left(T_{z,r_o,t} - T_f\right) \tag{4.18}$$

where, $T_{(z,r_o,t)}$ and T_f denote the temperatures of the hydride bed at the outer radius and heat transfer fluid, respectively.

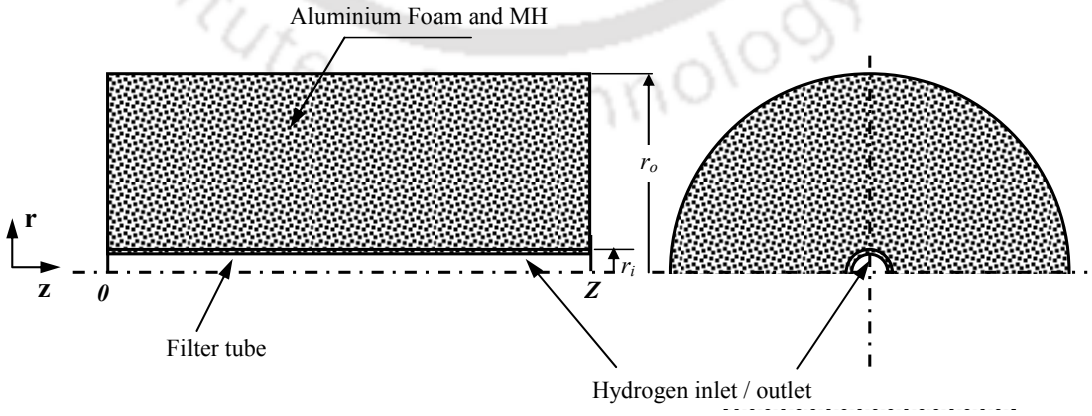

Fig. 4.3 Boundary conditions used for the numerical analysis.

In the above-mentioned boundary conditions, the variation of the cooling fluid temperature along the axial direction is assumed to be negligible. Most researches have employed a constant wall temperature condition for predicting the performance of various metal hydride based thermal machines. However, in practice, the cooling fluid temperature varies along the axial direction. Therefore, in the present work, the variable wall temperature convective boundary condition is also considered. The following equations describe the heat flow from the hydride bed to the heat transfer fluid (Muthukumar and Ramana, 2009).

$$\frac{dQ}{dt} = m_f Cp_f \left(T_{fo} - T_{fi}\right) \tag{4.19}$$

$$\frac{dQ}{dt} = UA\Delta T_{lm} = UA \frac{T_{fo} - T_{fi}}{\ln\left[\dfrac{T_{z,r_o,t} - T_{fi}}{T_{z,r_o,t} - T_{fo}}\right]} \tag{4.20}$$

$$T_{z,r_o,t} - T_{fo} = (T_{z,r_o,t} - T_{fi}) \exp\left(-\frac{UA}{m_f Cp_f}\right) \tag{4.21}$$

$$T_{fo} = T_{fi} + [T_{z,r_o,t} - T_{fi}]\left[1 - \exp\left(-\frac{UA}{m_f Cp_f}\right)\right]. \tag{4.22}$$

where, $T_{z,r_o,t}$ denotes the temperature of the hydride bed at the outer radius; U and m_f denote the overall heat transfer coefficient and the mass flow rate of heat transfer fluid.

Reactor B (Absorption)

The mass flux of hydrogen absorbed is expressed as (Mayer *et al.*, 1987)

$$\dot{m}_B = C_a \exp\left(\frac{-E_a}{R_u T_B}\right) \ln\left(\frac{P_{g,t+\delta t}}{P_{eq,B}}\right)\left(\rho_{ss} - \rho_{m,B}\right). \tag{4.23}$$

The gas pressure ($P_{g,\ t+\delta t}$) in the combined space volume is updated every time step using Eqs. 4.4 to 4.6.

The equilibrium pressure is calculated from Eq. (4.1). The rise in temperature of the reactor B is found out by using the energy equation given as

$$\left(\rho C_p\right)_e \frac{\partial T}{\partial t} + \left(\rho C_p\right)_g \vec{u}_g . \nabla T = k_e \nabla^2 T + \dot{m}_B \left[\frac{\Delta H}{M_g} - T\left(Cp_g - Cp_m\right)\right]. \tag{4.24}$$

The hydrogen mass balance during the absorption in the reactor B is expressed as

$$\varepsilon \frac{\partial\left(\rho_g\right)}{\partial t} + \nabla\left(\rho_g \overrightarrow{u_g}\right) = -\dot{m}_B \tag{4.25}$$

Hydrogen gas pressure in the reactor B is found in the same way as for the reactor A using Eq. (4.13).

Initial and Boundary Conditions

Initial conditions of the reactor B at time $t = 0$ are given as

$$\rho_{m,B}(z,r) = \rho_i\,; \quad T_{m,B}(z,r) = T_{g,B}(z,r) = T_M\ ; \quad X_B(z,r) = X_{\min,B}\,. \tag{4.26}$$

The boundary conditions used in the reactor A are the same as for the reactor B. The initial conditions stated above are used only at the first cycle.

4.1.3.3 Process *bc*

During this process, only the sensible heat transfer takes place between the hydride bed and the heat transfer fluid and no mass transfer takes place. Therefore, the governing equations for the reactors A and B become

$$\left(\rho C_p\right)_e \frac{\partial T}{\partial t}+\left(\rho C_p\right)_g \vec{u}.\nabla T = k_e \nabla^2 T. \tag{4.27}$$

The initial conditions of the sensible cooling processes are used as the final conditions of the previous desorption / absorption process.

4.1.3.4 Process *cd*

During this process, hydrogen is transferred from reactor B to reactor A at low pressure. The initial condition of this process is the final condition of the process *bc* of the respective reactors. The governing equations and boundary conditions used in this process are analogous to those for the process *ab*.

4.1.3.5 Process *da*

In the sensible heating process, the reactors A and B are heated to temperatures T_H and T_M, respectively. The final condition of this process is the initial condition of the next cycle of the process *ab*.

4.1.4 Performance Analysis

The performances of the single stage-MHHP system are characterized by the COP and SCP. These quantities are defined as

$$COP = \frac{Q_C}{Q_H} \tag{4.28}$$

where,

$$Q_C = Q_{B,cd} - Q_{A,bc} \tag{4.29}$$

Q_C denotes the net refrigeration effect obtained at the low (refrigeration) temperature, T_C. $Q_{B,cd}$ and $Q_{B,bc}$ denote the energy transfers between the heat transfer fluid and hydride bed B during processes *cd* and *bc*, respectively. $Q_{B,cd}$ denotes the product of number of moles of hydrogen desorbed from the reactor B and the enthalpy of formation of the respective hydride alloy:

$$Q_{B,cd} = n_{B,cd}\,\Delta H_{B,cd} \tag{4.30}$$

and, $Q_{B,bc}$ denotes the sensible heat energy transferred during process *bc*:

$$Q_{B,bc} = \left(m_h + m_r\right) C_{P,B} \left(T_M - T_C\right) \tag{4.31}$$

where, m_h and m_r denote the masses of metal hydride and reactor, respectively and the ratio between them is assumed to be 0.5. The energy supplied at the heat source temperature, T_H is given by

$$Q_H = Q_{A,ab} + Q_{A,da} \tag{4.32}$$

where, $Q_{A,ab}$ and $Q_{A,da}$ denote the energy supplied to the reactor A during the processes *ab* and *da*, respectively.

$$Q_{A,ab} = n_{A,ab}\,\Delta H_{A,ab} \tag{4.33}$$

$$Q_{A,ab} = \left(m_h + m_r\right) C_{P,A} \left(T_H - T_M\right) \tag{4.34}$$

where, $n_{A,ab}$ denotes the number of moles of hydrogen transferred from the reactor A to B during the process *ab* and $\Delta H_{A,ab}$ denotes the enthalpy of formation of hydride A during

the desorption of hydrogen. The specific alloy output (SCP) plays a significant role in the performance study of the MHHP system. It is defined as the net cooling capacity per unit mass of the reactor hydride B

$$SCP = \frac{Q_C}{(m_A + m_B)t} \tag{4.35}$$

where, t and m_A and m_B denote the cooling time and the masses of the hydride A and B, respectively.

4.1.5 Solution Methodology

The solution of the above-mentioned mathematical model is obtained using implicit finite volume method. The solution procedure of this system begins with the process *ab* and ends with the process *da*, so that the simulation of one complete cycle is carried out. Initially, the metal hydride heat pump system is in equilibrium and pressures inside the reactors A and B are found by using Eq. (4.1). Once the valve is opened, hydrogen gas is desorbed from the reactor A and it is absorbed in the reactor B. This process is continued until a predefined quantity of hydrogen gas is desorbed from the reactor A.

The following convergence criteria are employed in the mathematical model.

- For the coupled heat and hydrogen transfer processes (*ab* and *cd*), the hydrogen exchange between two consecutive time steps becomes less than 0.001 g.
- For the sensible heat transfer processes (*bc* and *da*), the difference between the average hydride bed temperature and the heat transfer fluid temperature becomes less than 1°C.

To find the variation in the cycle time between constant and variable wall temperature boundary conditions the average hydride bed temperature is calculated at z/Z = 0.95. The end conditions of the sensible heating process were taken as the initial conditions of the first process of the next cycle. The cycle is repeated till the processes reach stable state and then the computed values are presented.

Further, the effects of operating temperatures, such as heat source (T_H), heat sink (T_M) and refrigeration (T_C) temperatures on the performance of SS-MHHP are also presented. Table 4.2 lists the operating parameter ranges used in the present analysis. Specific heat capacity (419 kJ/kg K) and porosity (0.5) of the hydride beds are assumed as constant during both absorption and desorption processes. The initial density of the hydride alloy (with minimum hydride concentration) is taken as 8400 kg/m^3 and this value is updated in each time step during the absorption and desorption processes. The reaction rate constants and the activation energies of the selected hydride alloy pairs are listed in Table 4.3. The total alloy mass of 1.38 kg is considered in all the reaction beds except for AP 3. In order to accommodate the variation in hydrogen storage capacities of the reactors A and B in AP 3, different masses of 1.38 kg and 1.2 kg are considered respectively, for the reactors A and B.

Table 4.2 Operating parameters for the selected alloy pairs.

Parameters	**AP 1**	**AP 2**	**AP 3**	**AP 4**	**AP 5**
***T_H (K)**	383/353	443/413	433/403	413/383	413/383
***T_M (K)**	308/298	308/298	308/298	308/298	308/298
***T_C (K)**	288/278	293/283	293/283	288/243	288/278

* Operating range (maximum/minimum temperatures)

Table 4.3 The reaction rate constants and activation energies of the selected hydride alloy pairs.

Alloy pairs		Reaction rate constant (s^{-1})		Activation energy (kJ/mol H_2)	
		Abs.	Des.	Abs.	Des.
AP1	$MmNi_{4.6}Al_{0.4}$ (A) $MmNi_{4.6}Fe_{0.4}$ (B)	150 250	75 120	30.0 31.5	29.0 28.5
AP2	$LaNi_{4.61}Mn_{0.26}Al_{0.13}$ (A) $La_{0.6}Y_{0.4}Ni_{4.8}Mn_{0.2}$ (B)	230 180	25 55	35.0 30.0	32.5 27.0
AP3	$LmNi_{4.91}Sn_{0.15}$ (A) $Ti_{0.99}Zr_{0.01}V_{0.43}Fe_{0.09}$- -$Cr_{0.05}Mn_{1.5}$ (B)	195 305	30 65	30.5 31.4	28.0 29.0
AP4	$LaNi_{4.6}Al_{0.4}$ (A) $MmNi_{4.15}Fe_{0.85}$ (B)	185 300	20 40	35.0 26.0	32.0 25.0
AP5	$Zr_{0.9}Ti_{0.1}Cr_{0.9}Fe_{1.1}$ (A) $Zr_{0.9}Ti_{0.1}Cr_{0.6}Fe_{1.4}$ (B)	145 265	20 45	30.0 26.0	25.5 23.5

4.2 DOUBLE STAGE DOUBLE EFFECT METAL HYDRIDE HEAT PUMP (DSDE-MHHP)

The single-stage metal hydride heat pumps (MHHP) have a relatively low COP (range of 0.2 to 0.5) and limited operating pressure and temperature ranges. To overcome these limitations, multi-stage metal hydride systems score much attention in recent years. The performance of a double-stage, double-effect metal hydride heat pump (DSDE-MHHP) is predicted by simultaneously solving the continuity and energy equations. In this model, the effects of both conduction and convection and, thermal masses of the reaction beds are included in the energy equation. The variation in the heat transfer fluid temperature

along the axial direction and the effect of hydrogen concentration on the enthalpy of formation of the metal hydrides are also considered.

4.2.1 Physical Model and Principle of Operation

The operating principle of a DSDE-MHHP is presented in Fig. 4.4(a) - (d). It consists of three alloy pairs filled in six reactors, namely, A1, A2, B1, B2, C1 and C2. The selected metal hydride alloys for the present investigations are $LaNi_{4.1}Al_{0.52}Mn_{0.38}$ (hydride A), $LmNi_{4.91}Sn_{0.15}$ (hydride B) and $Ti_{0.99}Zr_{0.01}V_{0.43}Fe_{0.09}Cr_{0.05}Mn_{1.5}$ (hydride C). These hydride alloys are filled in two reactors each. The design details of the reaction bed are shown in Fig. 4.5 and the properties of the metal hydrides employed in the system were taken from those reported in the literature (Klein and Groll, 2002; Klein, 2007). The innermost tube (3.0 mm inner diameter with 1.5 mm thickness and 1.0 μm pore size) of 869.5 mm length acts as a filter, through which the hydrogen gas flows into (out of) the reaction bed during absorption (desorption) process. The metal hydride powder fills the space between the inner reaction tube and the filter. Aluminium foams were used for enhancing the thermal conductivity of the hydride beds. The heat transfer fluid flows between the inner and the outer peripheral tubes (1.0 mm annular gap). All the reactors operate simultaneously by exchanging the heat from/to the respective heat source/sinks. Between each coupled reactors, there is a valve to control the transfer of hydrogen between them. The system produces continuous cold output at two different pressures (medium pressure, P_M and low pressure, P_L) by supplying one heat input at a driving temperature, T_D.

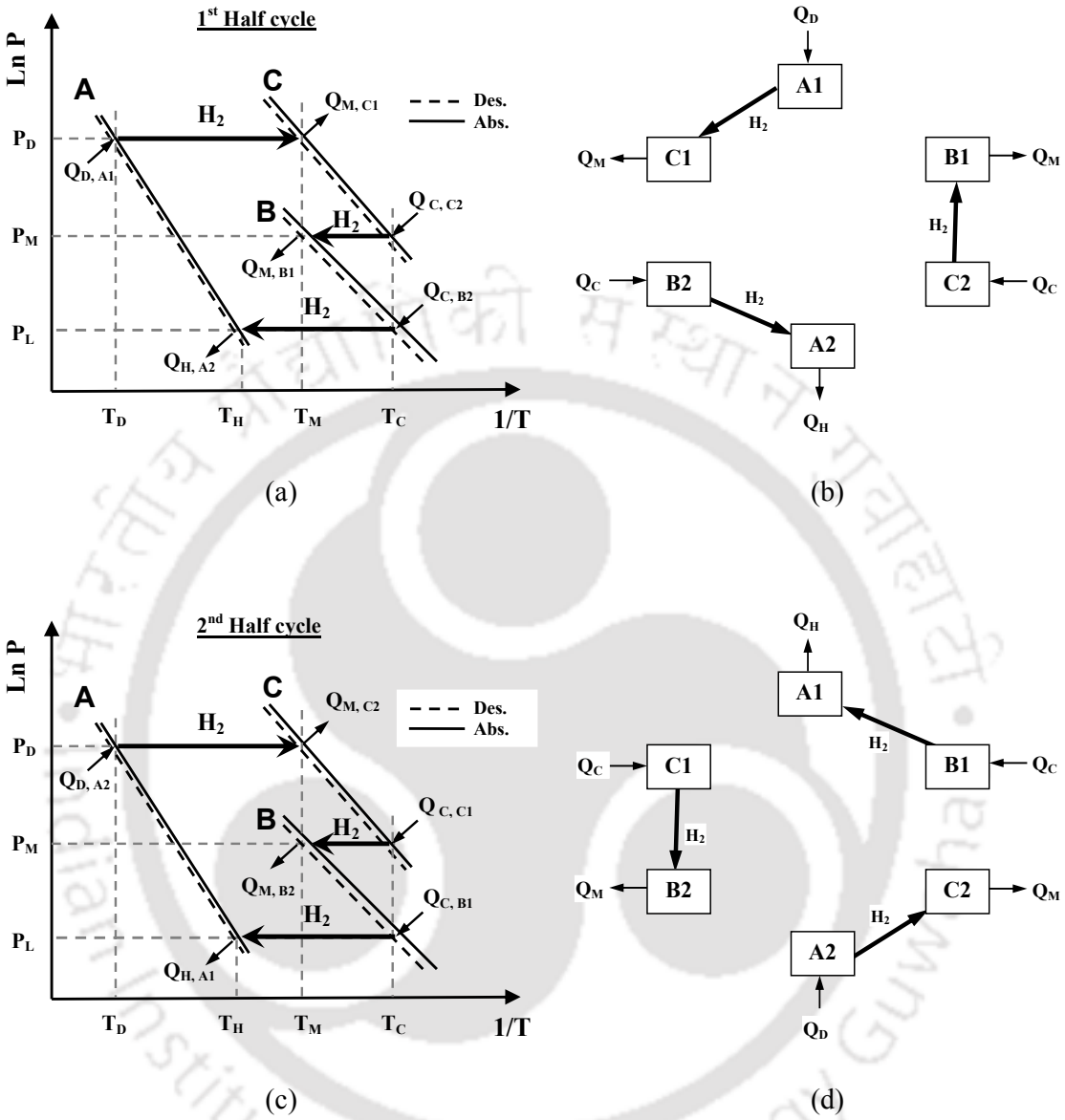

(a) Ideal van't Hoff plot for first half cycle (b) Hydrogen transfer in the first half cycle

(c) Ideal van't Hoff plot for second half cycle (d) Hydrogen transfer in the second half cycle

Fig. 4.4 Schematic of a DSDE metal hydride heat pump.

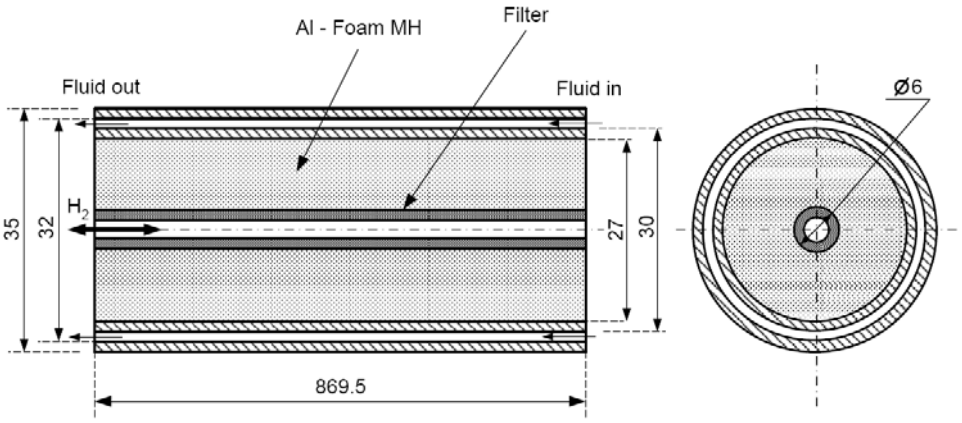

All dimensions are in mm (not to scale).

Fig. 4.5 Schematic of the reactor (Klein, 2007)

As explained in Fig. 4.4, during the first half cycle, heat input ($Q_{D,A1}$) at temperature T_D is supplied to desorb the hydrogen from the reactor A1. The desorbed hydrogen from A1 is absorbed by C1 liberating the heat ($Q_{M,C1}$) at the medium temperature, T_M. Simultaneously, hydrogen desorptions take place from the reactors B2 and C2 ($Q_{C,B2}$ and $Q_{C,C2}$) by taking the heat from the heat transfer fluid at T_C and yielding the refrigeration effects as illustrated in Fig. 4.4(a). These hydrogens are respectively absorbed by A2 and B1 liberating the heat ($Q_{H,A2}$ and $Q_{M,B1}$) at temperatures T_H and T_M, respectively. After completing this processes (allowed for a fixed time interval), valves between the coupled reactors are closed and the heat exchange takes place between the reactors A1 and A2, B1 and B2 and, C1 and C2 through the heat transfer fluids for a predetermined time. Later (sensible heat transfer processes), reactor A2 is heated to T_D and, B2 and C2 are heated to T_M. Similarly, the reactor A1 is cooled down to T_H and, B1 and C1 are cooled down to T_C.

The second half cycle will start at the end of the sensible heat transfer process. During the second half cycle, A2 desorbs hydrogen by taking the heat ($Q_{D,A2}$) at T_D, and the desorbed hydrogen is absorbed by the reactor C2 by releasing the heat of absorption ($Q_{M,C2}$) at T_M.

Similarly, hydrogen is exchanged between the reactors C1 and B2 at intermediate pressure (P_M) and, B1 and A1 at low pressure (P_L). These processes will continue for a predetermined time period. Finally, all the reactors are heated up and/or cooled down to their respective operating temperatures for continuing the next cycle of operation.

4.2.2 Selection of Metal Hydride Pairs

Performance of the MHHP systems largely depends on the selection of the suitable metal hydride alloys within the required operating pressure and temperature ranges. They must have high hydrogen exchange rates between the coupled reaction beds and high enthalpy of formation especially for refrigeration alloy to obtain large COP; low specific heat, high thermal conductivity and fast reaction kinetics to obtain higher SCP; moreover, high density and favorable equilibrium pressures are desired for compactness, and low hysteresis, flat plateau and simple activation process for good performance and easy handling. Table 4.4 shows the enthalpy and entropy of formation during both absorption and desorption of hydrogen of the selected metal hydrides.

Table 4.4 Reaction enthalpy and entropy of the metal hydride alloys (Klein, 2007).

Alloys	**ΔH (kJ/mol H_2)**		**ΔS (J/mol H_2-K)**	
	Abs.	**Des.**	**Abs.**	**Des.**
$LaNi_{4.1}Al_{0.52}Mn_{0.38}$	46.11	48.64	114.6	118.1
$LmNi_{4.91}Sn_{0.15}$	28.0	30.12	105.4	110.6
$Ti_{0.99}Zr_{0.01}V_{0.43}Fe_{0.09}Cr_{0.05}Mn_{1.5}$	20.12	25.98	97.4	112.6

Abs. – Absorption, Des. – Desorption

For the given operating temperatures, the slope and hysteresis values of the selected metal hydrides were calculated from the experimental data (PCT) reported by Klein *et al*. (2007) and the same have been incorporated in the present mathematical model. Fig. 4.6 shows the static van't Hoff plot for the DSDE-MHHP system.

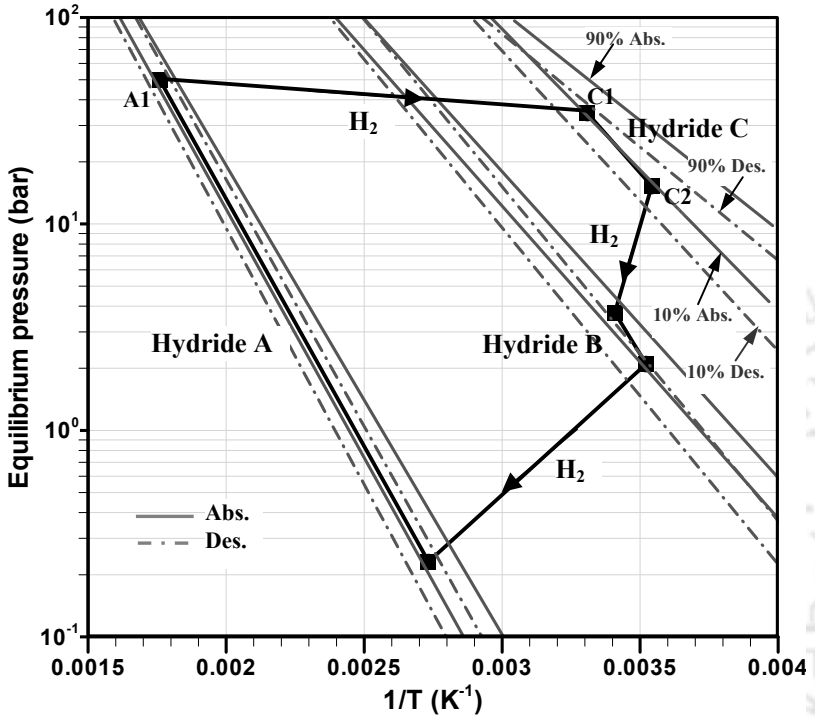

Fig. 4.6 Static van't Hoff plot for DSDE-MHHP (first half cycle).

The following assumptions have been made for developing the mathematical model for a DSDE-MHHP.

1. Initially, at the beginning of the first half cycle, all the reactors (A1, A2, B1, B2, C1 and C2) are in the equilibrium with the hydrogen gas.
2. Thermal conductivity (k) of the hydride bed is independent of concentration and pressure.

3. Heat transfer through the hydride bed is by means of unsteady, two-dimensional conduction and convection.
4. Hydrogen gas pressure (P_g) and temperature (T_g) inside the connecting pipe do not vary with space but are time dependent.
5. All the reactors are well insulated and there is no heat loss from the system to the surroundings.

4.2.3 Problem Formulation

4.2.3.1 Modeling of First Half Cycle

As stated in the physical model, hydrogen transfers take place simultaneously in the six reactors (at three pressure levels) during the first half cycle.

- A1 desorbs hydrogen by utilizing the heat $Q_{D,A1}$ at T_D and C1 absorbs by releasing the heat $Q_{M,C1}$ at T_M.
- C2 desorbs hydrogen by utilizing the heat $Q_{C,C2}$ at T_C and B1 absorbs by releasing the heat $Q_{M,B1}$ at T_M.
- B2 desorbs hydrogen by utilizing the heat $Q_{C,B2}$ at T_C and A2 absorbs by releasing the heat $Q_{M,A2}$ at T_H.

In the following section the mathematical modeling of the hydrogen exchange process between the reactors A1 and C1 is explained. The same procedure is repeated for the remaining hydrogen exchange processes between the reactors C2 and B1 and, B2 and A2. The above-mentioned processes are modeled by simultaneously solving the continuity, and energy equations for the respective reactor pairs. As already stated, initially all the reactors are assumed to be in equilibrium with respect to the hydrogen gas. Therefore, the equilibrium pressure P_{eq} (bar) is calculated using the van't Hoff equation (Eq. 4.1). Gas

pressure and temperature in the connecting pipe immediately after opening the valve are estimated from the following expressions

$$P_{g,P} = \frac{P_{g,A1}V_{A1} + P_{g,C1}V_{C1}}{V_{A1} + V_{C1}}; \qquad T_{g,P} = \frac{n_{A1}T_{A1} + n_{C1}T_{C1}}{n_{A1} + n_{C1}}; \tag{4.36}$$

where V and n denote the free volume (m^3) and the number of moles of hydrogen gas in the respective reactors (A1 and C1). n_{A1} and n_{C1} can be calculated using the real gas equation

$$n_{A1} = \frac{P_{A1}V_{A1}}{ZR_uT_{A1}}; \qquad n_{C1} = \frac{P_{C1}V_{C1}}{ZR_uT_{C1}}; \tag{4.37}$$

where, Z denotes the compressibility factor and it is expressed as a function of pressure and temperature

$$Z = f(p,T) = 1 + \left(B_0 + B_1T + B_2T^2\right)P + \left(C_0 + C_1T + C_2T^2\right)P^2 \tag{4.38}$$

where the constants B_0, B_1, B_2, C_0, C_1 and C_2 were taken from the literature (Friedlmeier, 1997)

B_0 = 0.00962 MPa^{-1} B_1 = -15.446 x 10^{-6} $MPa^{-1}K^{-1}$ B_2 = 82.314 x 10^{-10} $MPa^{-1}K^{-2}$

C_0 = 18.167 x 10^{-5} MPa^{-2} C_1 = -83.222 x 10^{-8} $MPa^{-2}K^{-1}$ C_2 = 9.527 x 10^{-10} $MPa^{-2}K^{-2}$

Eq. (4.38) is valid in the pressure and temperature ranges $0.1 < P \leq 10$ MPa and $280 \leq T \leq 428K$, respectively.

The number of moles of hydrogen present in the gas space (n_g), gas temperature (T_g) and gas pressure (P_g) in the connecting pipe at any time during the hydrogen transfer process are calculated using Eqs. 4.4 to 4.6. As explained in the physical model, desorption of

hydrogen and temperature of the hydride bed A1 are estimated using the reaction kinetics (Eq. 4.7) and energy equations (Eq. 4.8). Gas pressure at the reactor A1 is calculated using the mass balance equation (4.11). The density and velocity of the hydrogen gas can be determined using the real gas equation (Eq. 4.37) and Darcy's law (Eq. 4.12), respectively. By substituting these values into the hydrogen mass balance equation, the gas pressure in the hydride bed can be estimated using Eq. (4.39).

$$\left(\frac{\varepsilon M_g}{ZR_uT}\right)\frac{\partial P_g}{\partial t}+\left(\frac{\varepsilon M_g P_g}{ZR_u}\right)\frac{\partial}{\partial t}\left(\frac{1}{T}\right)-\left[\frac{2a}{T}\left(1+P_g\right)\right]\frac{\partial^2 P_g}{\partial r^2}-\left[\frac{a}{T}\left(1+P_g\right)\right]\frac{\partial^2 P_g}{\partial z^2}-2aP_g\frac{\partial P_g}{\partial r}\frac{\partial}{\partial r}\left(\frac{1}{T}\right)$$
$$-aP_g\frac{\partial P_g}{\partial z}\frac{\partial}{\partial z}\left(\frac{1}{T}\right)-\frac{2aP_g}{rT}\frac{\partial P_g}{\partial r}=\dot{m}_A \tag{4.39}$$

where,

$$a=\frac{KM_g}{Z\mu_g R_u} \tag{4.40}$$

where, M_g, K and μ_g denote the molecular weight of the hydrogen gas, the permeability in Darcy's law and the dynamic viscosity of the gas, respectively.

Initial and Boundary Conditions (Desorption)

Initially (t = 0), all the reactors (A1, A2, B1, B2, C1 and C2) are in the equilibrium with hydrogen at their respective operating temperatures. Hydride density, temperature and concentration of the reactor A1 are given by

$$\rho_{s,A1}(z,r)=\rho_{ss};\quad T_{s,A1}(z,r)=T_{g,A1}(z,r)=T_D;\quad X_{A1}(z,r)=X_{\max}. \tag{4.41}$$

The boundary conditions applied at the left, right and bottom walls are similar to the single-stage metal hydride heat pump (Eqs. 4.16 to 4.17). The effect of variation in heat transfer fluid temperature along the axial direction during absorption and desorption of

hydrogen was studied in the single stage heat pump (Satheesh *et al*., 2009). It was observed that the constant wall temperature convective boundary condition over predicts the numerical results. Hence, the variable wall temperature convective boundary condition (most realistic model) is considered in the double stage metal hydride heat pump. The mass flux, temperature of the hydride bed and gas pressure at the rector C1 are found in the same way as for the absorbing hydride (reactor B) in the single-stage heat pump.

Initial and Boundary Conditions (Absorption)

The initial conditions of the reactor C1 at time t = 0 are given by Eq. (4.42). The boundary conditions are similar to those for the reactor A1.

$$\rho_{s,C1}(z,r)=\rho_i\,;\quad T_{s,C1}(z,r)=T_{g,C1}(z,r)=T_M\,;\quad X_{C1}(z,r)=X_{\min}\,. \tag{4.42}$$

4.2.3.2 Internal Heat Recovery and Sensible Heat Transfer Processes

As already explained in Section 4.2.1, after the first half cycle an internal heat recovery between A1 and A2, B1 and B2 and, C1 and C2 takes place for a predetermined time period (Klein, 2007). In the present mathematical modeling, the sensible heat exchange factor for the internal heat recovery is assumed to be 0.5. After the internal heat recovery, the reactors are heated up/cooled down to their respective operating temperatures.

$$\left(\rho C_p\right)_e \frac{\partial T}{\partial t}+\left(\rho C_p\right)_g \vec{u}.\nabla T = k_e\nabla^2 T\,. \tag{4.43}$$

The initial conditions of the sensible heat transfer processes are used as the final conditions of the previous desorption / absorption processes.

4.2.3.3 Modeling of Second Half Cycle

During the second half cycle, hydrogen transfers take place in the following sequence

- A2 desorbs hydrogen by utilizing the heat $Q_{D,A2}$ at T_D and C2 absorbs by releasing the heat $Q_{M,C2}$ at T_M.
- C1 desorbs hydrogen by utilizing the heat $Q_{C,C1}$ at T_C and B2 absorbs by releasing the heat $Q_{M,B2}$ at T_M.
- B1 desorbs hydrogen by utilizing the heat $Q_{C,B1}$ at T_C and A1 absorbs by releasing the heat $Q_{M,A1}$ at T_H.

The governing equations and the boundary conditions used in these processes are analogous to those for the first half cycle. Finally, all the reactors are switched over for internal heat recovery followed by the sensible heating/cooling processes. Thus the cycle is completed. The final conditions of the first cycle process will be the initial conditions of the second first half cycle.

4.2.4 Performance Analysis

The performances of the DSDE-MHHP system are characterized by two parameters, namely, COP and SCP, and these quantities are defined as

$$COP_I = \frac{Q_{C,B2} + Q_{C,C2}}{Q_{D,A1}} \tag{4.44}$$

where, $Q_{C,B2}$ and $Q_{C,C2}$ denote the refrigeration effects obtained from the reactors B2 and C2 (B1 and C1 during second half cycle), respectively, and $Q_{D,A1}$ is the driving heat supplied to the system. They are calculated using the following Eqs. (4.45) and (4.46):

$$Q_{C,B2} = n_{d,B2}\Delta H_{d,B2} - \left[\phi C_{p,B2}\left(m_r + m_h\right)_{B2}\left(T_M - T_C\right)\right] \tag{4.45}$$

where, $n_{d,B2}$ denotes the number of moles of hydrogen desorbed from reactor B2. m_r and m_h denote the mass of the reactors and the mass of the metal hydride alloys, respectively. Similarly, the refrigeration effect obtained from the reactor C2 can be estimated. Heat supplied to the reactor A1 is expressed as

$$Q_{D,A1} = n_{d,A1}\Delta H_{d,A1} + \left[\phi C_{p,A1}\left(m_r + m_h\right)_{A1}\left(T_D - T_H\right)\right] \tag{4.46}$$

The average COP of the system is determined as

$$COP_{avg} = \frac{\left(Q_{C,B2} + Q_{C,C2}\right)_I + \left(Q_{C,B1} + Q_{C,C1}\right)_{II}}{\left(Q_{D,A1}\right)_I + \left(Q_{D,A2}\right)_{II}} \tag{4.47}$$

The cooling load (total refrigeration effect) and cooling capacity of the DSDE-MHHP are calculated using the following equations

$$Cooling\ load = \left(Q_{C,B2} + Q_{C,C2}\right)_I + \left(Q_{C,B1} + Q_{C,C1}\right)_{II} \tag{4.48}$$

$$Cooling\ capacity = \frac{Cooling\ load}{\theta_T} \tag{4.49}$$

where, θ_T denotes the complete cycle time (six processes). The specific cooling power is defined as

$$SCP = \frac{Cooling\ capacity}{m_T} \tag{4.50}$$

where, m_T denotes the total hydride mass filled in all the reaction beds.

4.2.5 Solution Methodology

The above-mentioned mathematical model is numerically solved by the finite volume method using the central difference scheme. Table 4.5 lists the thermo-physical properties, constants and, mass of the hydride alloys used for the different reaction beds. The design of the reactors geometry and the mass flow rate of heat transfer fluids (thermo-oil for reactors A1 and A2 and water-glycol mixture for reactors B1, B2, C1 and C2) used for the different reactors were taken from the literature (Klein and Groll, 2002) The present numerical investigation is carried out based on the experimental data reported by Klein and Groll (2002) and Klein (2007). In the experiments (Klein and Groll, 2002, and Klein, 2007), three pairs of reactors, consisting of four reaction beds each, were used. These reactors were connected by means of a connecting pipe with a hydrogen valve. In the numerical model, for keeping the complexity limited, the calculations are carried out for one coupled pair of reaction beds only, and not for the coupled reactors (comprising four reaction beds). The pressure drop in the connecting pipe during the hydrogen exchange processes between the hydride beds was estimated and its effect was found to be negligible. For analyzing the performance of DSDE-MHHP system, the ranges of selected operating parameters for the present study are listed in Table 4.6. The values presented in the bold with italic are the independent values when the other parameters are varied. E.g., the effect of driving temperature on system performance is studied by varying it from 558 to 598 K. During the time, the other parameters, such as heat rejection, heat sink and refrigeration temperatures are kept constant as 373, 298 and 283 K respectively. The half cycle time, mass ratio and sensible heat exchange factors are respectively 15 min, 0.65 and 0.5.

Table 4.5 Thermo-physical properties of the metal hydrides and heat transfer fluids (Klein, 2007)

Properties	**A1 (Des.)**	**A2 (Abs.)**	**B1 (Abs.)**	**B2 (Des.)**	**C1 (Abs.)**	**C2 (Des.)**
Metal Hydride						
Hydride mass (kg)	1.96	1.96	1.85	1.85	1.8	1.8
Effective density, kg/m^3	4500	4500	4250	4250	4130	4130
Molecular weight	414.3	414.3	425.6	425.6	160.3	160.3
Effective thermal conductivity (W/m K)	6.5					
Permeability (m^2)	10^{-12}					
Specific heat (J/kg K)	500					
Heat Transfer Fluid						
Mass flow rate (g/s)	14.3	12.9	9.1	11.1	14.4	8.0
Density (kg/m^3)	873	980	1030	1040	1036	1040
Specific heat (J/kg K)	2443	1884	3887	3839	3866	3839
Overall heat transfer coefficient (W/m^2 K)	330	330	645	645	645	645
Dynamic viscosity ($1x10^{-6}$) (N s/m^2)	9.5					

Table 4.6 Design and operating data range used for the numerical analysis.

Parameters	**Unit**	**Values**				
Driving temperature (T_D)	K	558	568	***578***	588	598
Heat rejection temperature (T_H)	K	***373***				
Heat sink temperature (T_M)	K	***298***	303	308	-	-
Refrigeration temperature (T_C)	K	273	***283***	293	-	-
Half cycle time (θ)	min	10	***15***	20	-	-
Mass ratio (M_R)	-	0.3	***0.65***	1.0	1.35	-
Sensible heat exchange factor (ϕ)	-	0.1	0.3	***0.5***	-	-

4.3 CROSSED VAN'T HOFF LINE METAL HYDRIDE HEAT PUMP (CV-MHHP)

The utilization of renewable energy technology, such as, solar energy and industrial waste heat has become important for the metal hydride cooling and heating systems. The following section, the crossed van't Hoff line concept metal hydride heat pump is described.

4.3.1 Physical Model and Principle of Operation

The operating principle of single-stage MHHP working with crossed van't Hoff line configuration (shown in Fig. 4.7) is analogous to the conventional MHHP system. In conventional metal hydride heat pump, during the regeneration period, the heat of absorption is rejected at atmospheric temperature, whereas in the crossed van't Hoff line configuration, the absorption heat of the refrigeration hydride (at T_D) contributes to desorb the hydrogen from the regeneration hydride during the first half cycle. This technique can significantly reduce the required heat supply to the heat pump, thereby achieving a higher coefficient of performance of the system. The design details of the reaction beds used for the present analysis are analogous to the conventional single stage metal hydride heat pump (shown in Fig. 4.1). A pair of two similar reactors (reactors A and B) is employed. Reactor A is filled with the regeneration alloy and reactor B is filled with the refrigeration alloy. The innermost porous tube of 12 mm outer diameter and 475 mm length acts as the filter tube. The purpose of the filter tube is to distribute the hydrogen uniformly throughout the reaction bed during absorption and it prevents hydride particles to be carried away by the hydrogen flow during the desorption process.

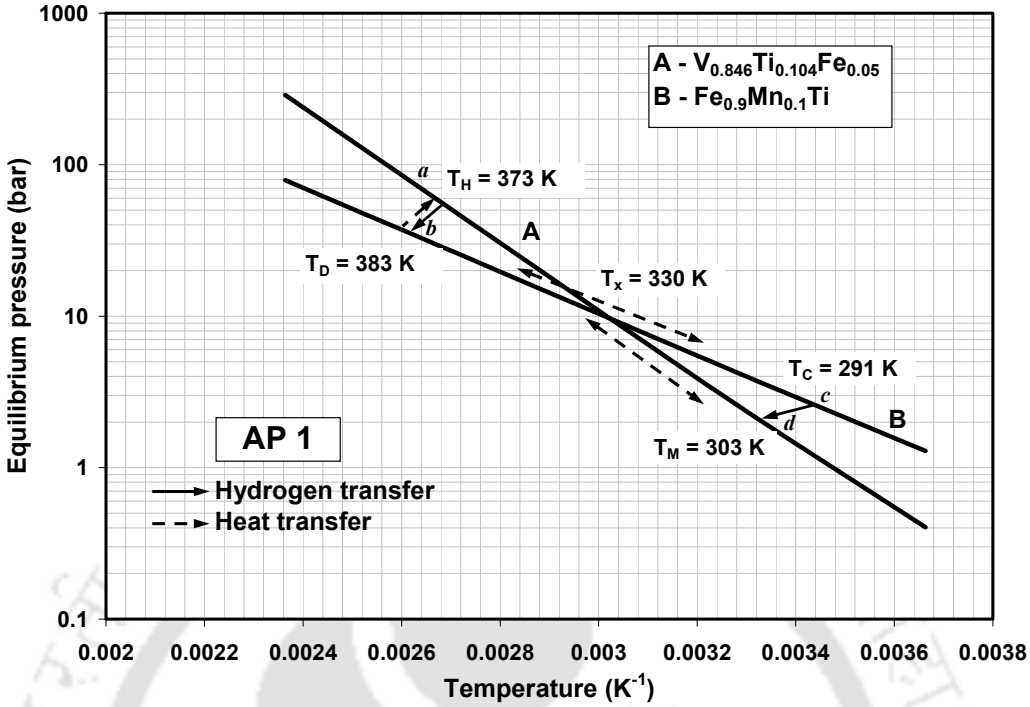

Fig. 4.7 Operation of SS-MHHP on crossed van't Hoff line configuration.

Metal hydride particles are filled in the space between the reaction bed tube and the filter tube. The heat transfer fluid flows helically around the reaction bed tube in an annular gap of 1.0 mm. The two reactors are coupled by a connecting tube with a control valve. Hydrogen gas can flow freely between the reaction beds, when the valve is open. The dimensions of the connecting tube are 300 mm length and 3 mm inner diameter. During the hydrogen transfer process, the pressure drop in the connecting pipe has been calculated and found to be negligible. The reaction beds considered in the present investigation are axi-symmetric. Hence, only the top half of the reaction bed is modeled. Thermodynamic analysis of various metal hydride alloys is studied using respective van't Hoff diagrams. Based on this, two hydride alloy pairs, namely, $V_{0.846}Ti_{0.104}Fe_{0.05}$ / $Fe_{0.9}Mn_{0.1}Ti$ (AP 1) and $V_{0.855}Ti_{0.095}Fe_{0.05}$ / $MmNi_{4.7}Al_{0.3}$ (AP 2) are selected for the present investigation and their thermodynamic properties are listed in Table 4.7.

The following assumptions are made in the present mathematical model.

1. Initially during process *ab*, the hydride beds of reactors A and B are in equilibrium with the hydrogen gas.
2. Heat transfer through the hydride bed is by means of unsteady, two-dimensional conduction and convection. The effect of radiation is negligible.
3. The thermodynamic properties of the metal hydride, such as, reaction enthalpy and entropy and thermo-physical properties, such as, thermal conductivity, are independent of temperature, concentration and hydrogen pressure.
4. Hydrogen gas pressure and temperature inside the connecting tube are independent of space but are time dependent.
5. The reactors are assumed to be well insulated and no heat transfer takes place between them and to the surroundings.

Table 4.7 Thermodynamic properties of metal hydride alloys (Libowitz *et al.* 1997)

Alloys		**ΔH (kJ/mol H_2)**		**ΔS (J/mol H_2 K)**	
		Abs.	**Des.**	**Abs.**	**Des.**
AP 1	**$V_{0.846}Ti_{0.104}Fe_{0.05}$ (A)**	42.9	43.7	148.5	151.5
	$Fe_{0.9}Mn_{0.1}Ti$ (B)	26.6	29.0	99.2	107.1
AP 2	**$V_{0.855}Ti_{0.095}Fe_{0.05}$ (A)**	43.2	44.61	140.6	143.0
	$MmNi_{4.7}Al_{0.3}$ (B)	30.55	32.05	102	108.7

Mass and energy balance equations, and the set of governing equations, initial and boundary conditions for the present mathematical model during the complete cycle of operation are similar to those for the single-stage metal hydride heat pump described in Section 4.1.3.

4.3.2 Performance Analysis

Performance of the crossed van't Hoff line SS-MHHP is described by COP and SCP. These quantities are estimated using the following equations.

$$COP = \frac{Refrigeration\ effect\ (Q_C)}{Heat\ supplied\ (Q_H)} \tag{4.51}$$

$$Q_C = (n_{H_2} \Delta H_d)_B - \left[(m_r + m_h)_B C_{P,B} (T_M - T_C) \right] \tag{4.52}$$

where, n_{H_2} denotes the number of moles of hydrogen desorbed from the reactor B. ΔH_d is the enthalpy of formation of hydride B during desorption of hydrogen. m_r and m_h denote the mass of the reactor and the mass of the hydride alloy. For predicting the performance of the system, the mass ratio (m_r / m_h) is taken as 0.5.

In the crossed van't Hoff line SS-MHHP, the heat of absorption ($Q_{a,B}$) obtained from the reactor B is utilized to drive the system. This net heat utilized from reactor B is given by Eq. (4.53).

$$Q_{a,B} = n_{H_2} \Delta H_{a,B} \tag{4.53}$$

Hence, the driving heat supplied (Q_H) to the MHHP is calculated using the following expression.

$$Q_H = n_{H_2} (\Delta H_{d,A} - \Delta H_{a,B}) + \left\{ \left[(m_r + m_h)_A C_{P,A} + (m_r + m_h)_B C_{P,B} \right] (T_D - T_M) \right\} \tag{4.54}$$

where, $\Delta H_{d,A}$ and $\Delta H_{a,B}$ denote the enthalpy of formation during desorption of hydrogen from reactor A and enthalpy of formation during absorption of hydrogen in reactor B, respectively.

The SCP of crossed van't Hoff line SS-MHHP is calculated using the following equation

$$SCP = \frac{Q_C}{(m_A + m_B)t} \tag{4.55}$$

where, m_A and m_B denote the total masses of reactors (including reactor material and hydride alloy) A and B, respectively, and t denotes the time taken for a complete cycle of operation.

4.3.3 Solution Methodology

The above-mentioned mathematical model is solved by the finite volume method using the central difference scheme. The solution procedure of this model begins with the first half cycle (process *ab*) and ends with the sensible heating process (process *da*), so that the simulation of one complete cycle is carried out. For achieving the maximum amount of hydrogen exchange between the reaction beds, the half cycle time is varied over a wide range and the optimum time duration of 25 min is fixed for the hydrogen transfer processes (*ab* and *cd*). It is observed that for the sensible heat transfer processes (*bc* and *da*) around 85% of heat is exchanged within 90 s. Therefore, the time taken for the sensible heat exchange processes is taken as 120 s. The overall heat transfer coefficient was optimized for the selected hydride bed and the corresponding value (1000 W/m^2-K) is taken for the present analysis. Depending on the hydrogen storage capacities of the selected hydride alloys, 1.0 kg of regeneration alloy and 1.3 kg of refrigeration alloy were

considered in the respective reactors A and B. For maintaining the necessary pressure difference between the reaction beds during the hydrogen transfer processes (first and second half cycles), only the heat source and refrigeration temperatures were varied over a wide range. The selected range of operating temperatures is listed in Table 4.8.

Table 4.8 Operating parameters for the selected alloy pairs.

Parameters	**AP 1**	**AP 2**
***T_H (K)**	383/368	405/390
T_D(K)	383	410
***T_M (K)**	303	303
***T_C (K)**	294/285	288/273

* Operating range (maximum/minimum temperatures)

CHAPTER 5

RESULTS AND DISCUSSION

In this chapter, the results obtained from various heat and mass transfer models, which include single-stage (SS), double stage (DS) and cross van't Hoff line (CV) metal hydride heat pump are discussed.

5.1 SINGLE STAGE METAL HYDRIDE HEAT PUMP

Systems of equations are solved using fully implicit finite volume method. A grid independence study for SS-MHHP is carried out by considering the effect of three different grid sizes on the hydride bed (reactors A and B) concentrations. It is observed from Fig. 5.1 that there is no significant change in the concentration profile for a grid size greater than 41x41. Therefore, all subsequent computations are performed by using the grid size of 41x41.

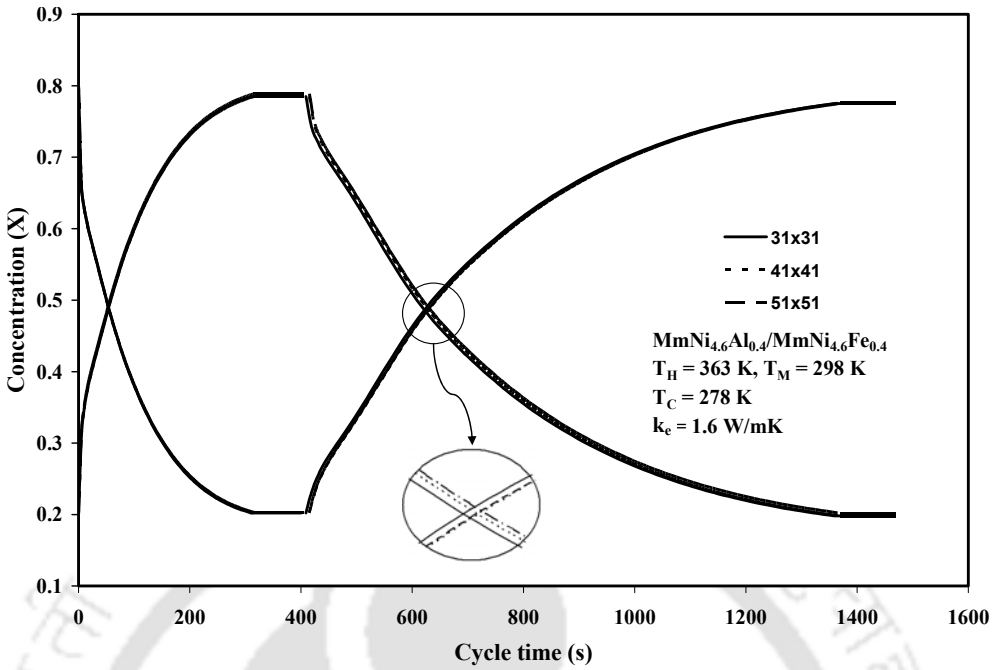

5.1 Grid independent study.

5.1.1. Validation of SS-MHHP's Thermal Model

For the validation purpose, the reactor geometry used by Ni and Liu (2007) was chosen and mathematical modelling was performed accordingly. The hysteresis and plateau slope of the PCT for the corresponding high and low temperature alloys were determined from the experimental data reported by Ni and Liu (2007). The cycle time for the processes at different heat source temperatures, thermal conductivity and bed thickness of the reactors were selected based on the experimental conditions reported by Ni and Liu (2007). Figs. 5.2 and 5.3 show that the predicted temperature profiles of the regeneration and refrigeration alloys at different source temperatures ranging from 388 K to 423 K for $LaNi_{4.61}Mn_{0.26}Al_{0.13}$ / $La_{0.6}Y_{0.4}Ni_{4.8}Mn_{0.2}$ hydride pairs match reasonably well with the experimental data of Ni and Liu (2007). A small deviation between the present computations and the experimental data is due to the assumed values of the reaction rate constants and the experimental uncertainties used in the present study. These data were not reported in the literature.

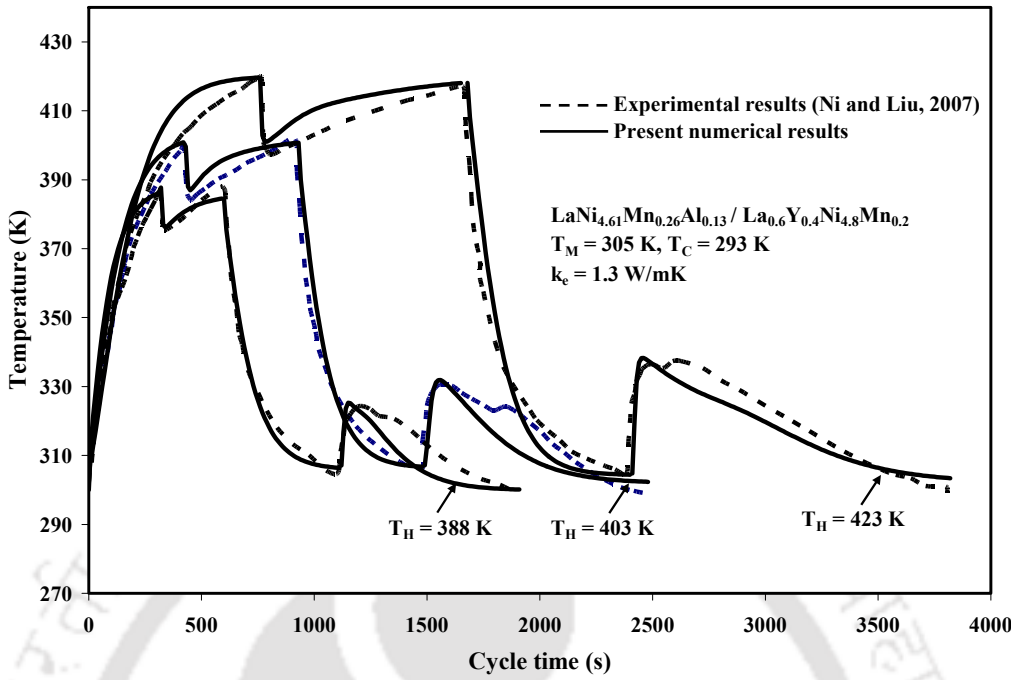

Fig. 5.2 Validation of the predicted regeneration alloy reaction bed temperature profiles at different source temperatures.

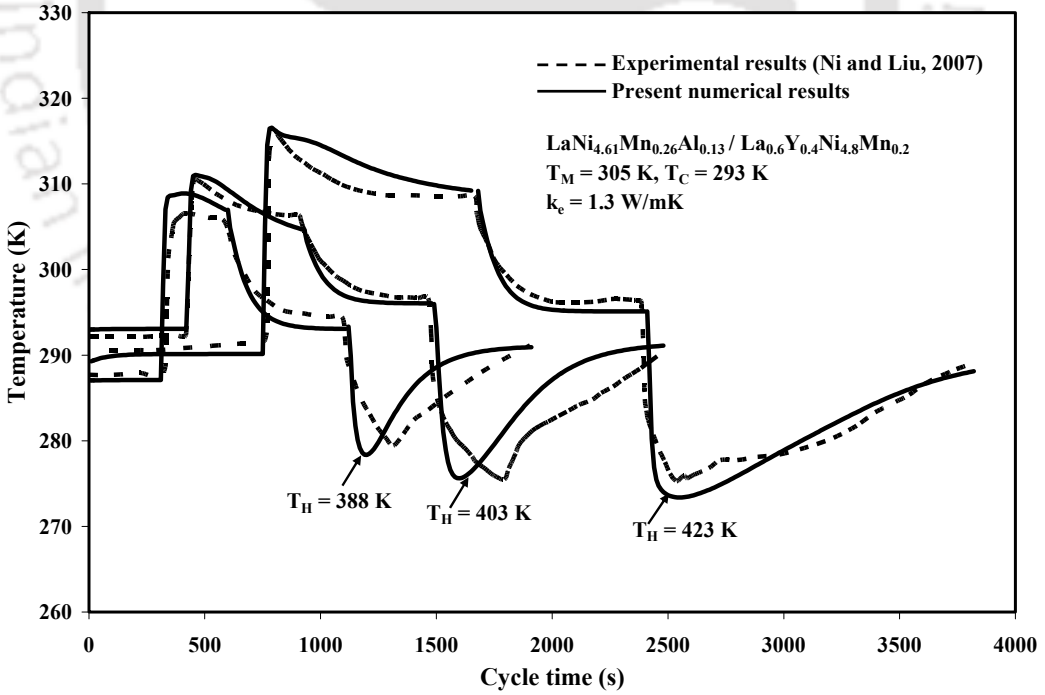

Fig. 5.3 Validation of the predicted refrigeration alloy reaction bed temperature profiles at different source temperatures.

5.1.2 Importance of Variable Wall Temperature Convective Boundary Conditions

Fig. 5.4 shows the variations of hydride concentrations in reactors A and B over a cycle for both constant and variable wall temperature boundary conditions. The concentration limits are fixed based on the PCT plot so that the minimum desorption hydride pressure of hydride A at T_H is higher than the maximum absorption pressure of hydride B at T_M. Based on the above-mentioned conditions the concentration limits are fixed as 0.2 to 0.8. It is observed from Fig. 5.4 that the model with the variable wall temperature condition takes 1765.6 s for completing a cycle, whereas the model with the constant wall temperature condition takes only 1470.0 s.

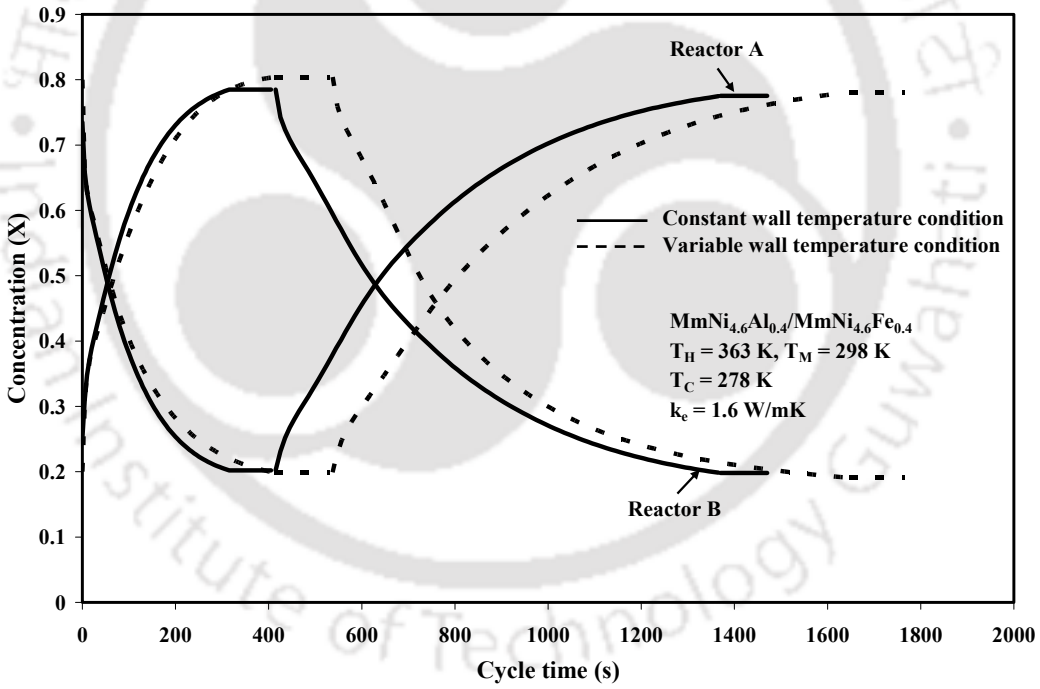

Fig. 5.4 Effect of convective boundary conditions on hydride concentrations.

It is seen that for the constant wall temperature boundary condition, the average concentration inside the reactor varies only in the radial direction. However, in the variable wall temperature boundary condition pressure, concentration and bed

temperature vary in both axial and radial directions (Muthukumar and Ramana, 2009). During process *ab*, the hydrogen starts to desorb in the reactor A in its high temperature regions and hence, hydrogen starts flowing towards the filter. Due to the supply of heat transfer fluid from the left boundary, the reactor temperature is higher at the left boundary than that at the right boundary. Hence, the concentration decreases faster at the left boundary than at the right boundary. Therefore, the desorption for the variable wall temperature condition takes more time than that for the constant wall temperature boundary condition.

It is observed from Fig. 5.4 that desorption of hydrogen (during process *ab)* at high temperature is faster than that at low temperature (during process *cd)*. This is because the pressure difference in the process *ab* is much higher than that during the process *cd*. Therefore, the reaction rate is faster and change in concentration with time is sharper during the first half cycle. For a given effective thermal conductivity, bed thickness and specific heat capacity, the time taken for sensible heat transfer processes are calculated. Times taken for all the processes are listed in Table 5.1. The difference in cycle times for the constant and variable wall temperature boundary conditions is found to be approximately 5 min.

Fig. 5.5 shows the variation in average bed temperatures of high and low temperature reactors over a cycle. It is observed that due to the poor thermal conductivity of the hydride bed the required amount of heat is not transferred from/to the heat transfer fluid. Hence the fall/rise in temperature of the reactor bed occurs as soon as the process starts, and it reaches the heat transfer fluid temperature gradually. It is observed that the difference in the equilibrium pressure between the reactors leads to rise/drop in

temperature at the initial stages. The lowest average bed temperatures obtained in the process *cd* in reactor B for the constant and variable wall temperature boundary conditions are 271 K and 269.1 K, respectively.

Table 5.1 Comparisons of cycle time for constant and variable wall temperature boundary conditions**.**

Sl. No	Processes	Constant wall boundary condition (s)	Variable wall boundary condition (s)	Difference in time	
				seconds	Percentage
1	Process *ab*	315.1	411.0	95.9	30.4
2	Sensible cooling (Process *bc*)	99.9	126.3	26.4	26.4
3	Process *cd*	954.8	1108.3	153.5	16.0
4	Sensible heating (Process *da*)	100.2	120.0	19.8	19.7
	Total cycle time	**1470.0 s**	**1765.6 s**	**295.6 s**	**20.1**

Fig. 5.6 shows the variation in hydrogen pressures in reactors A and B for both constant and variable wall temperature boundary conditions. Initially the system is in equilibrium with respect to the reactors A and B. Once the valve between the reactors is opened, due to the pressure difference, hydrogen starts to desorb from the reactor A and it is absorbed in the reactor B by releasing the heat of absorption. This process continues till both the pressures reach the equilibrium condition as illustrated in Fig. 5.6.

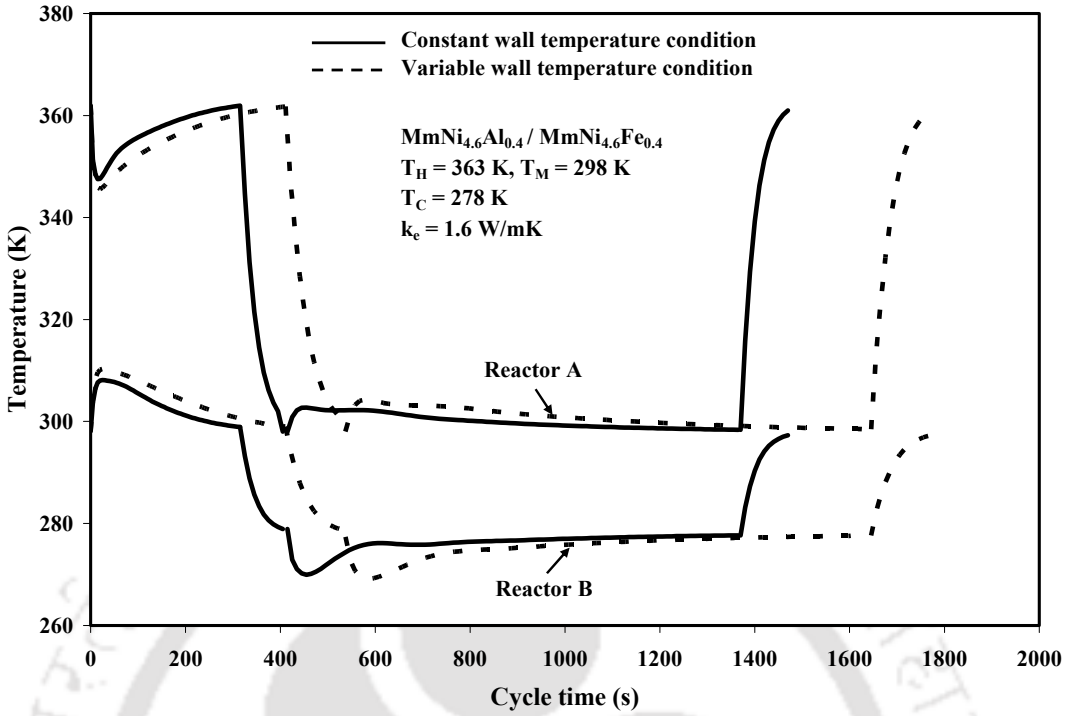

Fig. 5.5 Effect of convective boundary conditions on hydride bed temperatures.

It is observed from Fig. 5.6 that this process terminates at 15 bar (363 K) at the end of 315 s for the constant wall temperature condition and 411 s for the variable wall temperature boundary condition. During the sensible cooling process, the reactor A cools down from 363 K to 298 K and similarly reactor B cools from 298 K to 278 K. Hence the pressures of the high and low temperature reactors decrease to 2.1 and 7.2 bar, respectively. Similarly, in the process *cd* the hydrogen transfer takes place from B to A. This process terminates when both the reactors reach the equilibrium condition. Finally the heating process completes the cycle and the pressures of reactors reach the initial condition for continuing the next cycle.

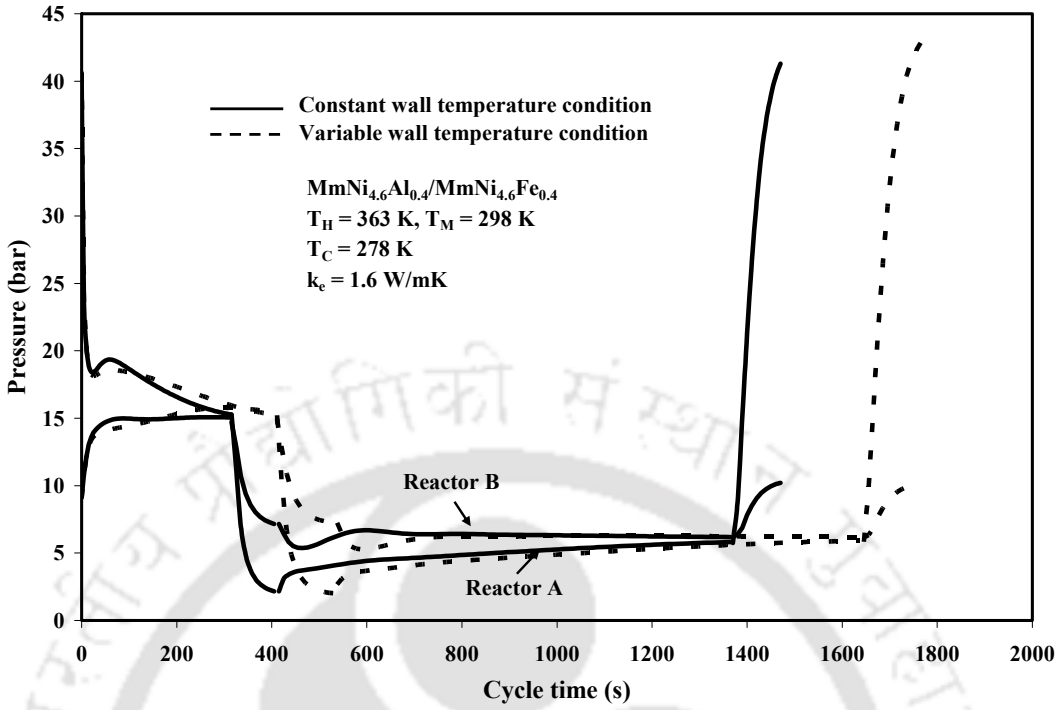

Fig. 5.6 Effect of convective boundary conditions on hydride bed pressures.

5.1.3 Various Heat Interactions during the Operation of SS-MHHP

The heat interaction (cooling/heating) between hydride bed and heat transfer fluid for a complete cycle time is shown in Fig. 5.7. Initially, the variation in the heat transfer fluid temperature is zero. Due to the exothermic/endothermic processes, heat is carried away/supplied from/to the reactors and their temperatures increase/decrease drastically and become zero at the end of the processes. It is observed from Fig. 5.7 that the change in the heat transfer fluid temperature during the process *ab* reaches the maximum value within 20 s. The maximum fall and rise in the fluid temperatures between inlet and outlet of the reactors A and B are 9.6 K and 6.5 K (corresponding to the heat interactions of 278 W and 188 W), respectively. Similarly in the process *cd*, the maximum rise and fall in fluid temperatures at reactor A and B are 3.3 K and 5 K, respectively, at 587 s. In the processes *ab* and *cd*, the heat of desorption is more than the heat of absorption.

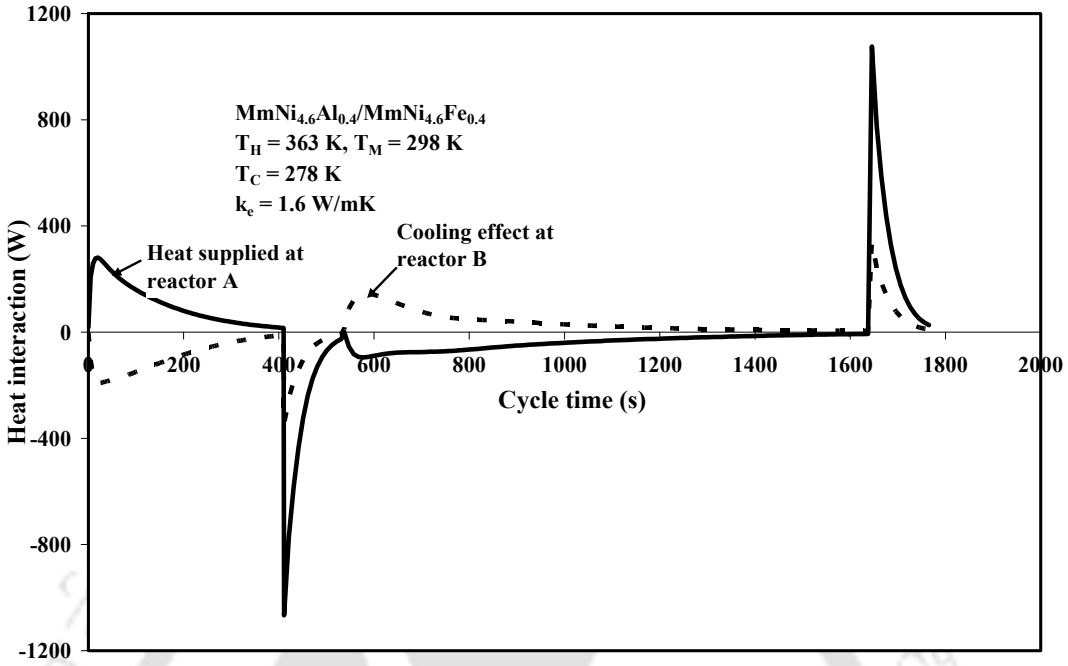

Fig. 5.7 Effect of convective boundary conditions on heat interaction.

5.1.4 Operation of SS-MHHP on Dynamic van't Hoff Plot

The actual dynamic behaviour of metal hydride heat pump considering the variable wall temperature boundary condition under the operating temperature limits of 363/298/278 K ($T_H/T_M/T_C$) is illustrated in Fig. 5.8. A large deviation between the dynamic and static van't Hoff plots is observed. It is seen from Fig. 5.8 that the path followed in the high temperature and low temperature reactors are indicated as ABCDEFA and abcdefa, respectively. ABC shows the dehydriding process, CD the sensible cooling, DEF the hydriding and FA the sensible heating process. Similarly the hydriding, cooling, dehydriding and heating processes are represented in the reactor B. Initially during the dehydriding process ABC, the pressure, temperature, and concentration decrease drastically. The temperature of the hydride bed A increases and it reaches the heat transfer fluid temperature gradually as shown in Fig. 5.8. But the pressure still decreases

and reaches the pressure equilibrium with the low temperature reactor B. Fig. 5.8 shows that the pressures at points C and c are approximately equal to 15 bar.

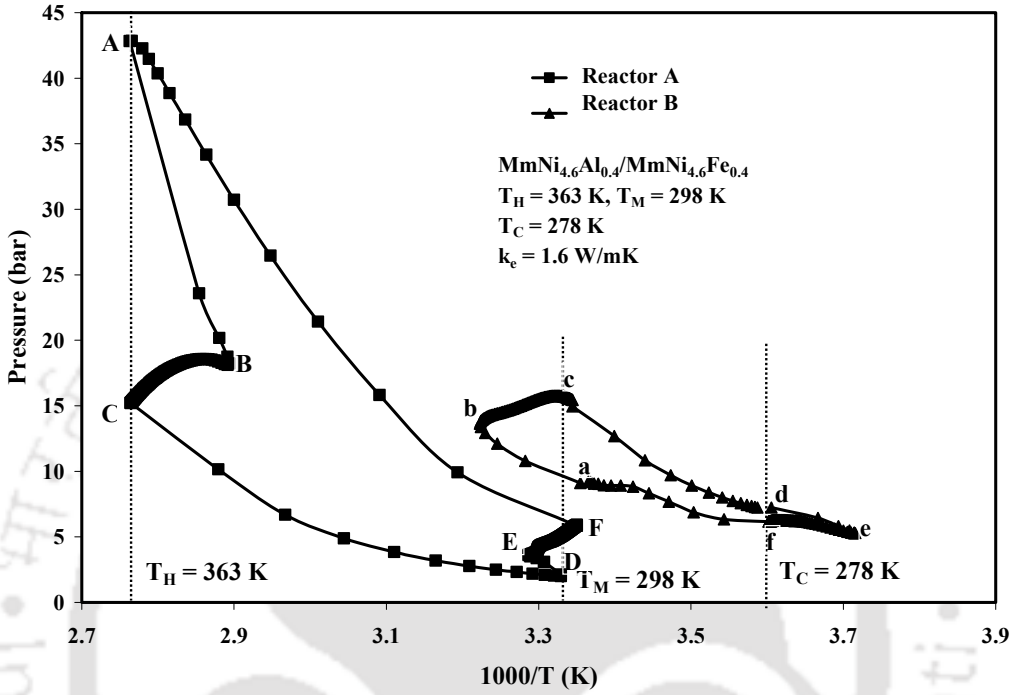

Fig. 5.8 Dynamic van't Hoff plot of the heat pump.

At the same time the concentration in the high temperature reactor decreases to 0.2. Similarly, the changes in pressure, temperature and concentration at low temperature reactor are shown in Fig. 5.8 at points a-b-c. During the sensible heat transfer processes (cooling/heating) the concentration remains the same for both the reactors. At the end of the sensible cooling process, pressures at the reactors A and B are indicated at the points D and d, respectively. When the valve between the two hydride beds is opened, dehydriding starts at low temperature reactor indicated by d-e-f. The lowest temperature obtained at point e is 269.1 K. This process stops when both the reactor pressures reach the equilibrium condition as shown in Fig. 5.8 at points F and f. During the process *da*,

hot fluid is supplied to the reactors A and B for raising their temperatures to T_H and T_M, respectively.

5.1.5 Performance Studies of SS-MHHP

In order to study the effect of heat source, heat sink and refrigeration temperatures on the performance of single stage metal hydride heat pump, the optimized values of effective thermal conductivity and overall heat transfer coefficient have been determined by varying them over a wide range. It is observed from Fig. 5.9 that for a given overall heat transfer coefficient, the cycle time is found to decrease significantly with hydride bed effective thermal conductivity up to about 4.0 W/m-K. Further increase in thermal conductivity (beyond 4.0 W/m-K) requires complicated heat transfer augmentation techniques (Groll, 1993), such as, insertion of copper bands, and aluminum foams inside the reaction bed. These techniques also increase the thermal mass of the system. It is also observed from Fig. 5.9 that for a given thermal conductivity of 4.0 W/m-K, the cycle time decreases significantly with overall heat transfer coefficient up to about 1000 W/m^2-K, and beyond this value there is no significant change in the cycle time. This indicates that for a given reactor geometry and overall heat transfer coefficient, there exists an optimum value of thermal conductivity. Therefore, the optimum values of thermal conductivity and overall heat transfer coefficient are taken as 4.0 W/m-K and 1000 W/m^2-K, respectively for further analysis of SS-MHHP.

Fig. 5.10 shows the effect of heat source temperature on the amount of hydrogen transferred between the paired reactors during the first half cycle and the COP of SS-MHHP system for the five selected hydride pairs, namely AP1, AP2, AP3, AP4 and AP5.

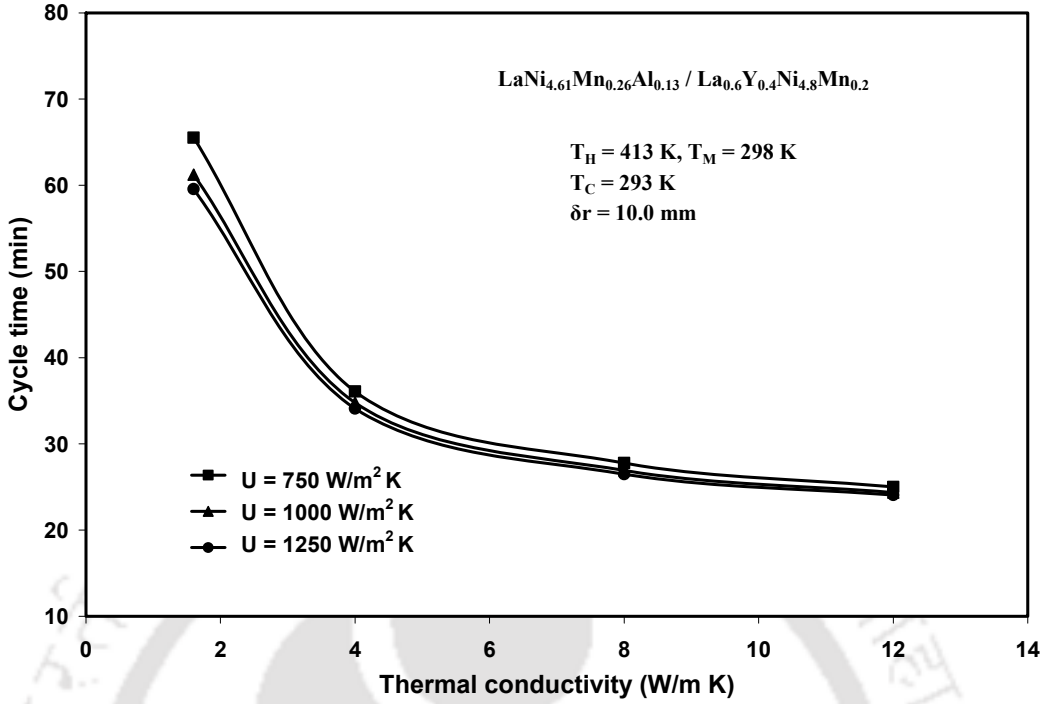

Fig. 5.9 Effect of thermal conductivity and overall heat transfer coefficient on cycle time.

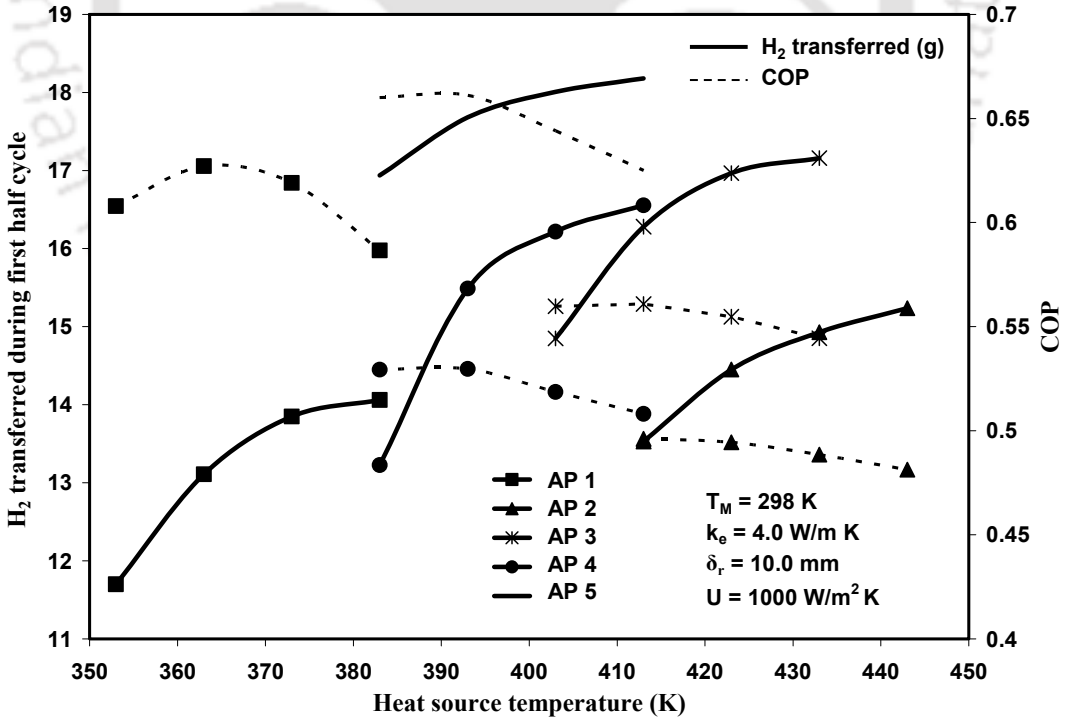

Fig. 5.10 Effect of heat source temperature on hydrogen transferred during first half cycle and COP.

For a given heat sink temperature, the amount of hydrogen transferred from the reactors A to B during the first half cycle is found to increase with heat source temperature. This behavior is due to an increase in driving potential for hydrogen transfer (difference between equilibrium and gas pressures) with heat source temperature.

It is expected that the alloy pairs AP 2 and AP 4 can transfer a significant (more than 2%) amount of hydrogen with further increase in the heat source temperature beyond 443 K and 413 K, respectively, whereas, the other alloy pairs exchanged the maximum amounts of hydrogen within the selected range of heat source temperatures. Depending on the hydride masses used in the reaction beds, maximum of about 14.0, 15.2, 17.2, 16.6 and 18.2 g of hydrogen is exchanged between the hydride pairs of AP 1, 2, 3, 4 and 5, respectively. Though the amount of hydrogen transferred during the first half cycle is found to increase with T_H, due to the fixed heat sink and refrigeration temperatures, the hydrogen transfer during the second half cycle does not change with T_H. Hence, the increase in heat source temperature is beneficial only up to a certain limit, beyond which, either refrigeration or heat sink temperatures control the amount of hydrogen transfer. It is seen from Fig. 5.10 that the COPs of all working pairs are found to increase with T_H till a certain value, after which the COP starts to decrease. This trend reveals that there exists an optimum heat source temperature for all alloy pairs. For the given operating temperatures of 363/298/288 K, 413/298/293 K, 413/298/293 K, 393/298/288 K and 393/298/288 K, the maximum values of COP obtained are 0.63, 0.5, 0.56, 0.53 and 0.66, respectively, for the alloy pairs of AP 1, AP 2, AP 3, AP 4 and AP 5.

The effect of heat source temperature on cycle time and SCP of a SS-MHHP system is illustrated in Fig. 5.11. The hydrogen transfer processes (*ab* and *cd*) and sensible heat

transfer processes (*bc* and *da*) are terminated based on the convergence criteria explained in Section 4.1.5. The summation of all the individual time durations obtained from the above four processes give the total cycle time. It is observed from Fig. 5.11 that the total cycle time decreases with heat source temperature. This is due to an increase in the driving potential for hydrogen transfer at higher temperature T_H. Therefore, the required amount of hydrogen is transferred within the shorter cycle time. For the given operating temperatures, the rates of hydrogen absorption / desorption can be increased using various methods, viz. supply of hydrogen at higher pressures through a porous tube (maintaining larger pressure difference between hydrogen supply pressure and hydride equilibrium pressure), use of heat transfer augmentation techniques, increasing the overall heat transfer coefficient, etc., Therefore, one can give more attention to the optimum utilization of hydrogen exchanged between the reactors within the shorter cycle time. For the selected alloy pairs of AP 1, AP 2, AP 3, AP 4 and AP 5, the optimum operating temperatures and the maximum SCPs are found to be 363/298/288 K, 413/298/293 K, 413/298/293 K, 393/298/288 K, 393/298/288 K and 31.8, 30.5, 53.3, 43.5, 40.9 W/kg of the total system mass (including reactor material and hydride mass), respectively.

Table 5.2 presents the effect of heat sink temperature on the performance of SS-MHHP. It is observed that the amounts of hydrogen exchanged between the paired reactors during both the first and second half cycles are found to decrease with T_M. This is due to a decrease in the driving potential at higher heat sink temperatures. Therefore, the net amount of hydrogen transfer is less at higher T_M. For a given range of heat sink temperature from 298 K to 308 K, a significant drop in hydrogen transfer between the hydride beds are observed in pairs AP 2 (31%) and AP 4 (20%) during first half cycle and in AP 1 (23.6%) during the second half cycle. It is seen from Table 5.2 that higher T_M*'s*

decrease the amount of hydrogen transferred between the paired reactors, resulting in larger cycle time. Hence, both the COP and SCP of SS-MHHP system decrease significantly with T_M.

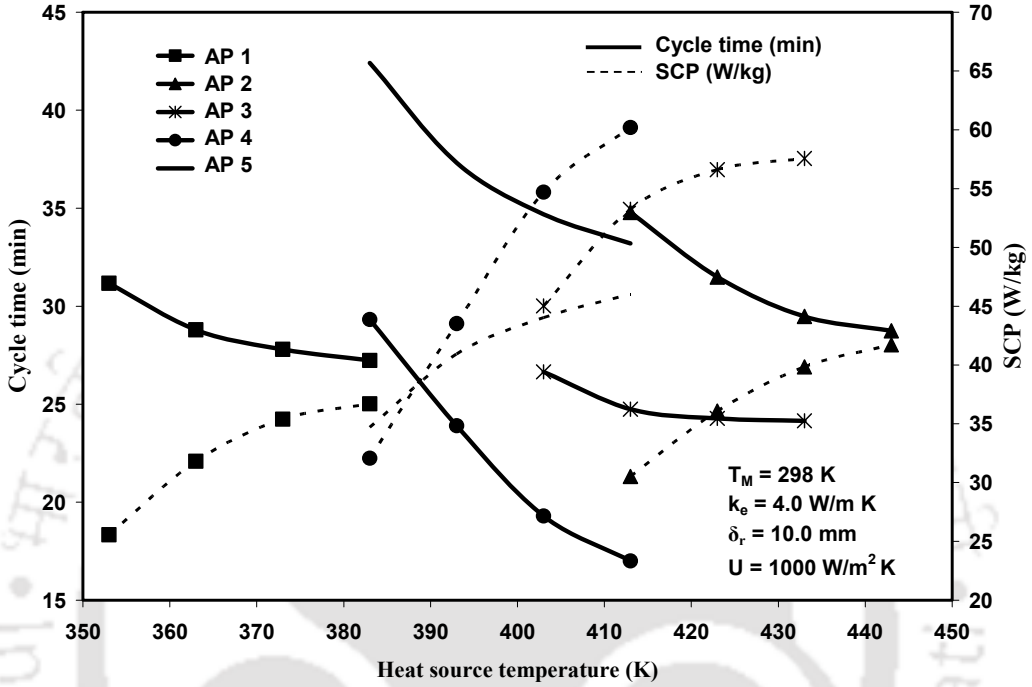

Fig. 5.11 Effect of heat source temperature on cycle time and SCP.

The effect of refrigeration temperature on the amount of hydrogen exchanged between the reactors B and A during the second half cycle and COP of SS-MHHP system is illustrated in Fig. 5.12. For a given heat sink temperature of 298 K, AP 4 starts to desorb hydrogen well above 243 K (Izhvanov *et al.,* 1996; Chernikov *et al.,* 2002). Therefore, alloy pair AP 4 is useful for any kind of refrigeration applications operating in the range of 243 K to 288 K. For a given heat sink temperature of 298 K, the amount of hydrogen exchange is increased with refrigeration temperature for all the selected alloy pairs. This is due to an increase in the driving potential for hydrogen transfer during the second half cycle. The effect of T_C on the amount of hydrogen exchanged during the first half cycle is

insignificant. Therefore, for the given T_H and T_M, the increase in T_C is beneficial, upto a certain limit (T_C at which maximum amount of hydrogen transferred from B to A). It is also observed from Fig. 5.12 that higher T_C increases the COP of SSSE-MHHP system considerably due to higher amount of hydrogen transfer between the paired reactors.

Fig. 5.13 shows the effect of refrigeration temperature on the cycle time and SCP. During the second half cycle, hydrogen exchange takes place slowly at the low pressure level. Therefore, the maximum time duration occurs during the hydrogen exchange at low pressures. Hence, this process plays a major role in controlling the total cycle time. Within range of refrigeration temperature studied, the increase in COP (19% for AP1 and 17% for AP 5) and SCP (53.6% for AP 1 and for 80% AP 5) for AP 1 and AP 5 are more significant than those for the other hydride alloy pairs.

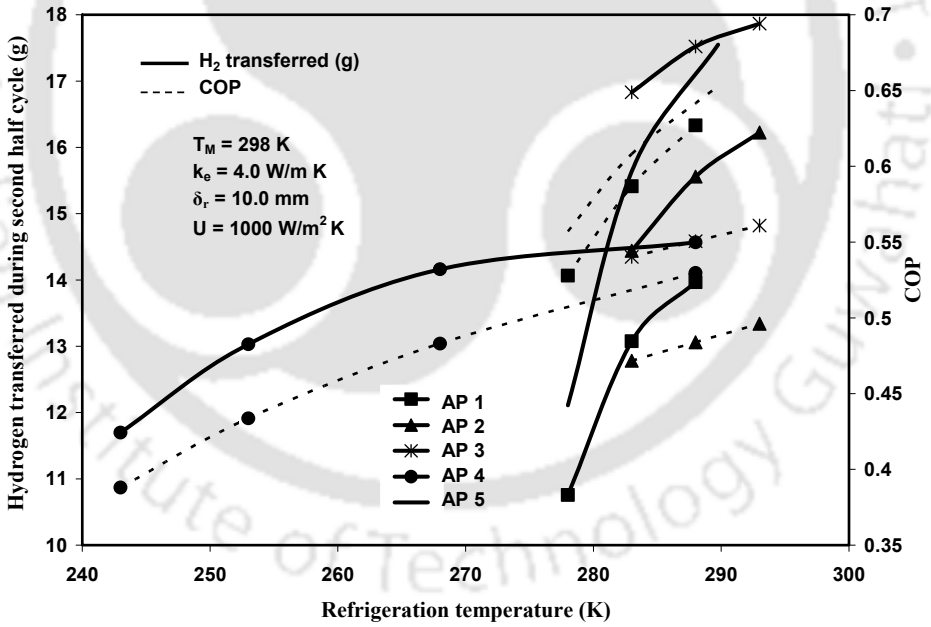

Fig. 5.12 Effect of refrigeration temperature on hydrogen transferred during second half cycle and COP.

Table 5.2 Effect of heat sink temperature on the performance of SS-MHHP for different hydride alloy pairs.

Materials	H_2 transferred (g)			Cycle time (min)			COP			SCP (W/kg)		
	298 K	303 K	308 K	298 K	303 K	308 K	298 K	303 K	308 K	298 K	303 K	308 K
AP 1	13.1 (14.0)	12.8 (12.3)	12.2 (10.7)	28.8	32.0	36.0	0.63	0.6	0.55	31.8	25.4	18.6
AP 2	13.5 (16.2)	12.0 (15.8)	9.3 (15.1)	34.8	37.0	40.0	0.5	0.47	0.42	30.5	24.6	16.7
AP 3	16.3 (17.9)	15.5 (17.5)	15.0 (17.0)	24.7	26.5	29.07	0.56	0.55	0.53	53.3	46.4	39.9
AP 4	15.5 (14.6)	14.5 (14.2)	12.5 (13.5)	24.0	25.1	27.0	0.53	0.52	0.5	43.5	39.6	31.4
AP 5	17.7 (17.6)	17.3 (16.6)	16.8 (15.0)	37.3	39.2	41.93	0.66	0.64	0.62	40.9	36.1	29.6

Note: Hydrogen transferred during second half cycle is given in the bracket.

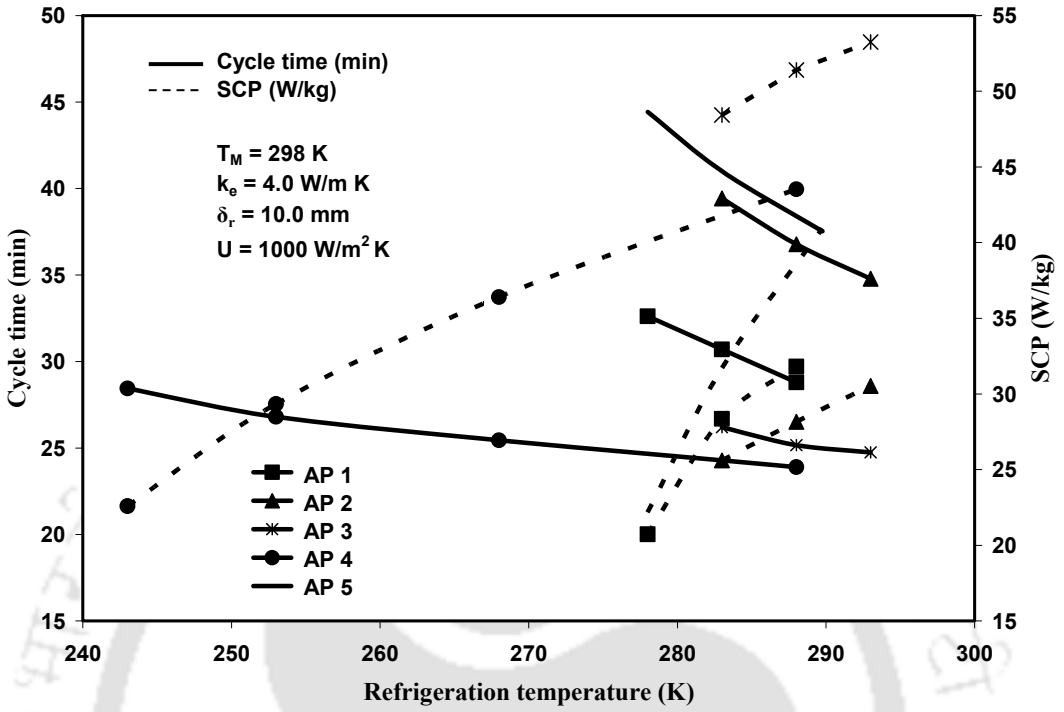

Fig. 5.13 Effect of refrigeration temperature on cycle time and SCP.

5.1.6 Summary of SS-MHHP's Thermal Modeling

An unsteady, two-dimensional mathematical model of a SS-MHHP system working with five different alloy pairs was studied. The system of equations was solved using the fully implicit finite volume method. Using the grid independent test, a 41 x 41 grid size was taken for the present investigation. As the first part of this study, the heat and hydrogen transfer aspects of the coupled reaction beds were investigated. The effects of constant and variable wall temperature convective boundary condition on the reaction bed temperature, hydrogen concentration, and the equilibrium pressure of the reaction beds were investigated. A dynamic correlation of the pressure-concentration-temperature plot was also determined. The present computational results were compared with the experimental data reported by Ni and Liu, (2007) and a good agreement between the two

was found. Further, the heat and mass transfer study was extended to study the performance investigation of SS-MHHP system for the selected hydride alloy pairs. The effects of heat source, heat sink and refrigeration temperatures on the amount of hydrogen transferred between the coupled reactors, COP and SCP of SS-MHHP system are studied. For the selected operating temperatures, a maximum COP of 0.66 is predicted for $Zr_{0.9}Ti_{0.1}Cr_{0.9}Fe_{1.1}$ / $Zr_{0.9}Ti_{0.1}Cr_{0.6}Fe_{1.4}$ hydride pair, while $LmNi_{4.91}Sn_{0.15}$ / $Ti_{0.99}Zr_{0.01}V_{0.43}Fe_{0.09}Cr_{0.05}Mn_{1.5}$ hydride pair produces the highest SCP of 53.2 W/kg of total mass of the system (including reactor material and hydride mass).

5.2 DOUBLE STAGE DOUBLE EFFECT METAL HYDRIDE HEAT PUMP

In this section, the performance prediction of double-stage double-effect metal hydride heat pump (DSDE-MHHP) system is presented. The dependence of number of grids employed in the numerical model on the variation of hydrogen concentration in reactors A1 and C1 was investigated. It is observed from Fig. 5.14 that there is no significant change in the concentration profiles beyond the grid size of 41 x 41. Hence, 41 x 41 grid size was chosen for the subsequent numerical investigations.

5.2.1 Validation of DSDE-MHHP's Thermal Model

The validations of hydride bed temperature for the six reaction beds over a complete cycle are shown in Figs. 5.15 to 5.17. As explained in Section 4.2.1, the hydrogen transfers take place between the three pairs of reaction beds simultaneously at three different pressure levels (P_D, P_M and P_L). The operating cycle consists of six processes, namely, (1) first half cycle, (2) internal heat recovery 1, (3) sensible heat transfer 1, (4) second half cycle, (5) internal heat recovery 2, and (6) sensible heat transfer 2. It is observed from Figs. 5.15 to 5.17 that the numerically predicted temperature profiles

match closely with the experimental data. A maximum deviation of about 10% was obtained between the present computational results and the experimental data. This is due to the uncertainties and heat losses in the experiments, and also the assumption of reaction rate constants and `the activation energies (listed in Table 5.3) of $LaNi_{4.1}Al_{0.52}Mn_{0.38}$ and $Ti_{0.99}Zr_{0.01}V_{0.43}Fe_{0.09}Cr_{0.05}Mn_{1.5}$, which are not reported in the literature

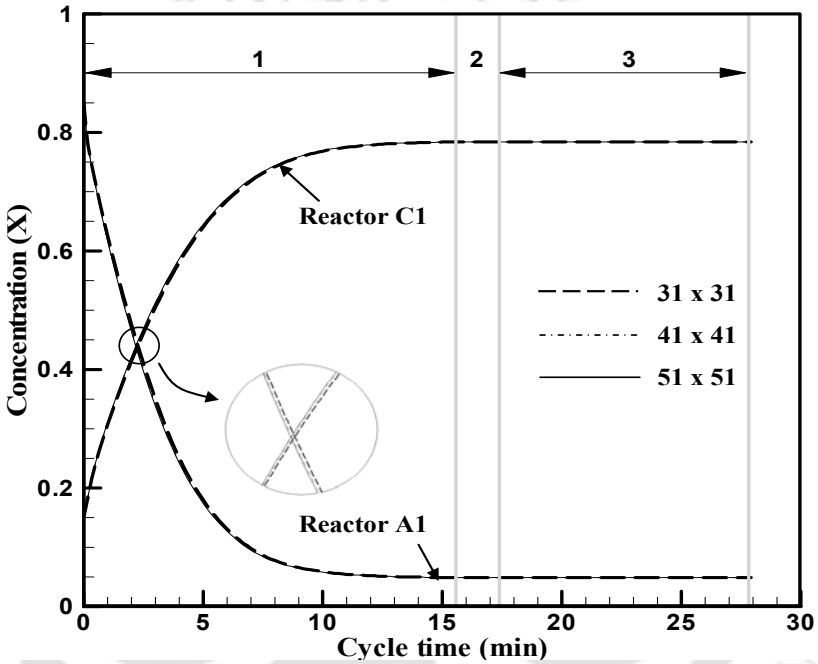

1. First half cycle 2. Internal heat recovery-1 3. Sensible heat transfer-1

Fig. 5.14 Grid independence study.

Table 5.3 Assumed activation energy and reaction rate constants of the selected metal hydrides.

Parameters	A1 (Des.)	A2 (Abs.)	B1 (Abs.)	B2 (Des.)	C1 (Abs.)	C2 (Des.)
Activation energy (kJ/mol H_2)	48.0	40.0	28.0	29.0	28.0	32.0
Reaction rate constant (s^{-1})	3.6	700	540	20	100	20

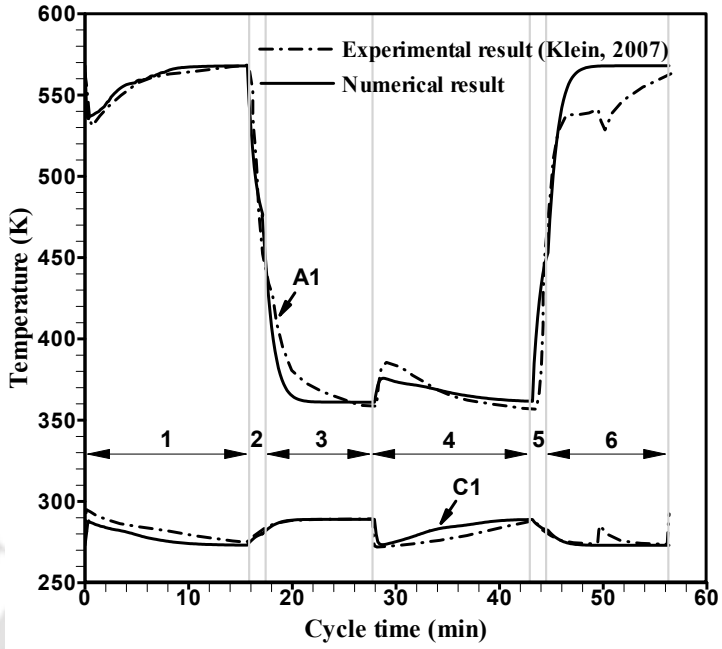

1. First half cycle 2. Internal heat recovery-1 3. Sensible heat transfer-1
4. Second half cycle 5. Internal heat recovery-2 6. Sensible heat transfer-2

Fig. 5.15 Validation of hydride bed temperatures for the reactors A1 and C1.

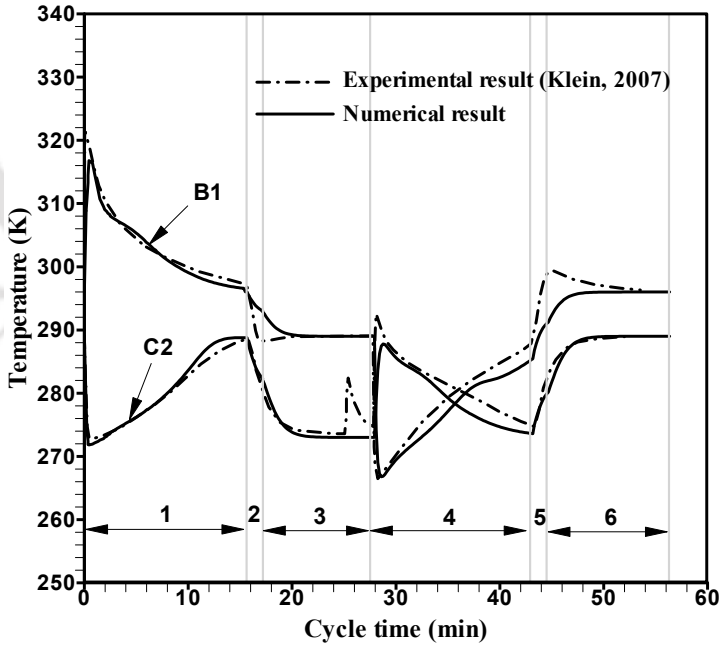

1. First half cycle 2. Internal heat recovery-1 3. Sensible heat transfer-1
4. Second half cycle 5. Internal heat recovery-2 6. Sensible heat transfer-2

Fig. 5.16 Validation of hydride bed temperatures for the reactors C2 and B1.

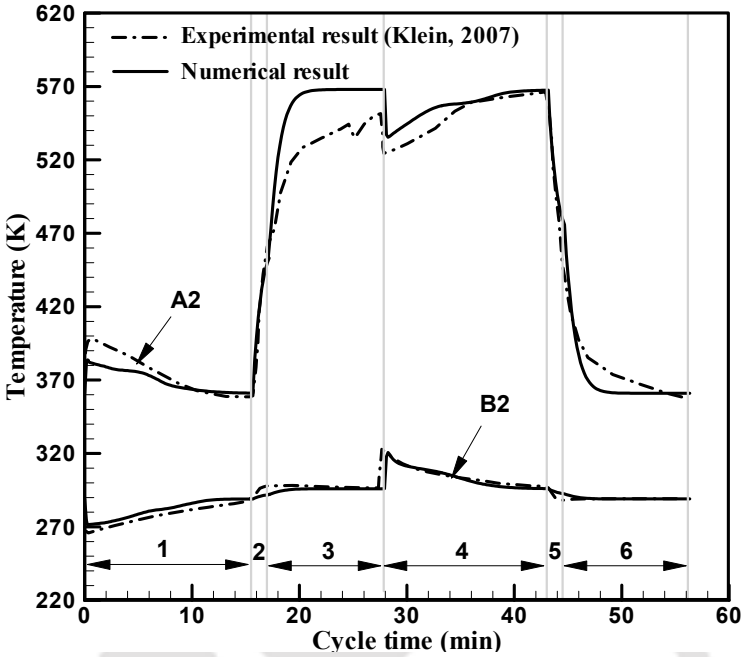

1. First half cycle 2. Internal heat recovery-1 3. Sensible heat transfer-1
4. Second half cycle 5. Internal heat recovery-2 6. Sensible heat transfer-2

Fig. 5.17 Validation of hydride bed temperatures for the reactors B2 and A2.

5.2.2 Variation of Hydride Properties and Heat Interactions during Operation of DSDE-MHHP

Fig. 5.18 illustrates the change in hydride bed pressures of all the reactors for a complete cycle. Initially, all the reactors are respectively in their hydride equilibrium pressures. Once, the hydrogen valves between the reactors are opened, a sudden change in the bed pressure is observed during the first few seconds. This is due to a large pressure difference between the paired reactors. It is observed that the system could reach a maximum pressure of about 90 bar. In practical conditions, it is difficult to handle the system with such a high pressure. Therefore, during the experiments the system was maintained below 65 bar pressure by opening the valve (flushing the excess pressure) (Klein, 2007). Due to this reason, a large deviation between the numerical and experimental results was observed during the process 6 at A1 (shown in Fig. 5.15) and the

process 3 at A2 (shown in Fig. 5.17). As illustrated in Fig. 5.18 the duration of the hydrogen exchange processes between the paired reactors are fixed similar to the experimental conditions (Klein, 2007). There is no hydrogen transfer during the internal heat recovery (2, 5) and the sensible heat transfer (3, 6) processes. During these processes, the hydride bed pressures are varied mainly due to the exchange of heat between the reaction beds and the respective heat transfer fluids.

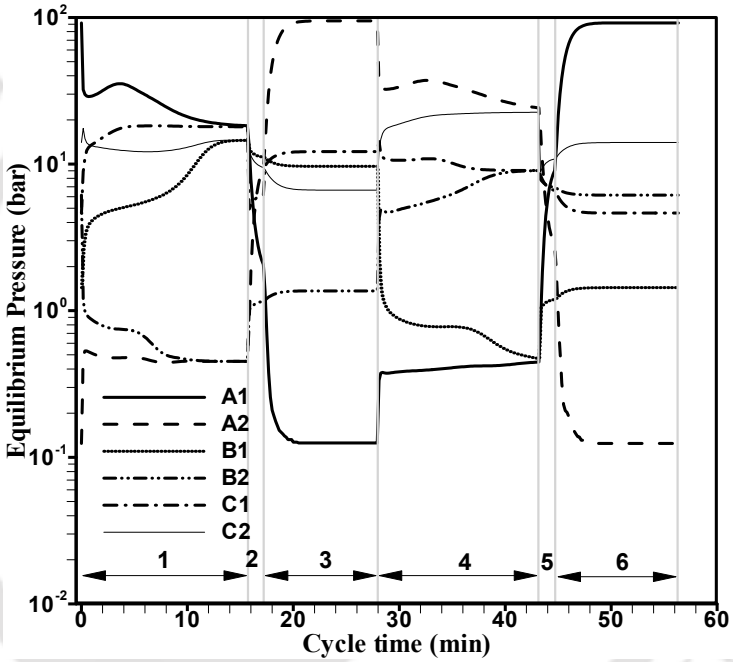

1. First half cycle 2. Internal heat recovery-1 3. Sensible heat transfer-1
4. Second half cycle 5. Internal heat recovery-2 6. Sensible heat transfer-2

Fig. 5.18 Variation in hydride bed pressures for a complete cycle.

The change in hydrogen concentrations in the metal hydride beds (A1, A2, B1, B2, C1 and C2) over a complete cycle are illustrated in Fig. 5.19. The hydrogen concentration limits are fixed based on the PCT characteristics, which has been presented in Section 4.1.2. It is observed from Fig. 5.19 that the hydrogen transfer rate mainly depends on the driving force (pressure difference) between the coupled reactors. Depending on the mass

of the alloy used, a maximum of 21 grams of hydrogen (single reaction bed) is exchanged between the paired reactors (processes 1 and 4) and only the heat exchanges take place in the remaining processes (2, 3, 5 and 6). Based on the above conditions, the average system COP is found to be 0.47 (for a complete cycle). The overall cooling power of a complete cycle is estimated to be 1.27 kW and the average specific cooling power is about 28.4 W/kg of the total hydride mass. It is found also that the numerically predicted COP of 0.47 is in good agreement with the experimental value of 0.48 (Klein, 2007).

Due to the exothermic (endothermic) reactions, the hydride bed temperatures is found to increase (decrease) rapidly during the first few seconds of the hydrogen exchange processes and then, the variations approach zero at the end of the processes as shown in Fig. 5.20. The heat removed from the reactor C1 during the first half cycle and from the reactor C2 during the second half cycle reach the maximum values shortly after the beginning of the half cycles; they complete their heat exchange with the heat transfer fluids much earlier than that by other reaction beds. This is due to the existence of a large pressure difference (driving force) between the coupled reaction beds A1 and C1, and A2 and C2 (shown in Fig. 5.18). Heat supplied to the reactor A1, and the useful cold outputs obtained from the reactors B2 and C2 are defined as positive for the first half cycle and vice versa. The maximum heat supplied to the reactor A1 (in a single reaction bed) is about 620 W with a temperature difference (heat transfer fluid inlet and outlet) of 18 K.

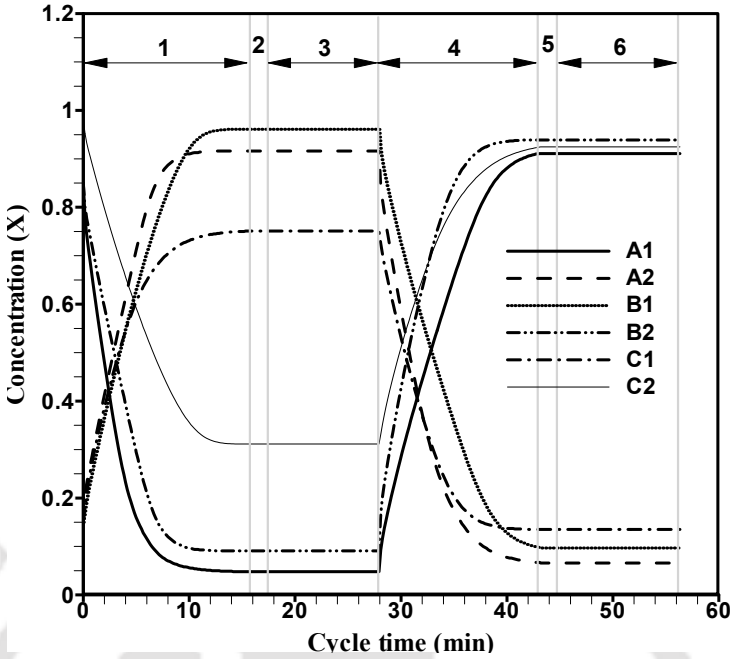

1. First half cycle 2. Internal heat recovery-1 3. Sensible heat transfer-1
4. Second half cycle 5. Internal heat recovery-2 6. Sensible heat transfer-2

Fig. 5.19 Change in hydrogen concentration for a complete cycle.

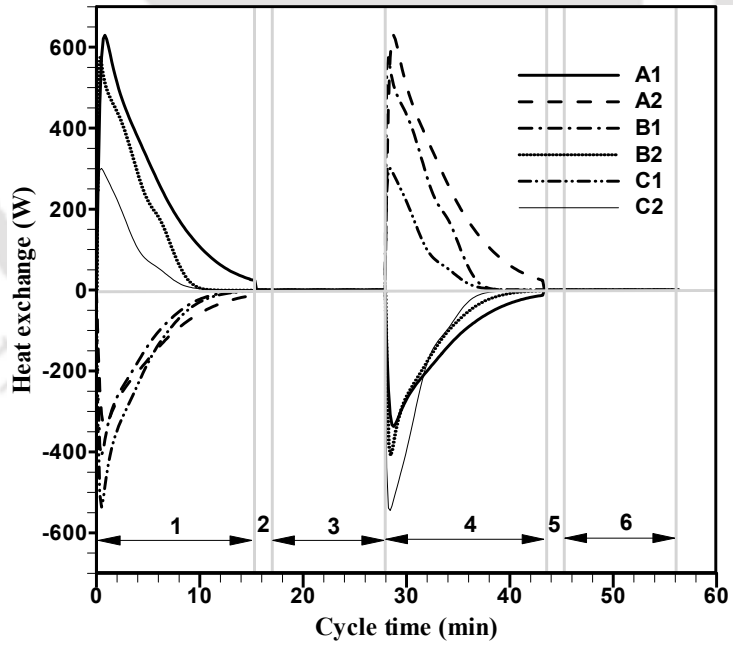

1. First half cycle 2. Internal heat recovery-1 3. Sensible heat transfer-1
4. Second half cycle 5. Internal heat recovery-2 6. Sensible heat transfer-2

Fig. 5.20 Heat exchange between the reactors and the heat transfer fluids.

5.2.3 Operation of DSDE-MHHP on Dynamic van't Hoff Plot

Fig. 5.21 shows the dynamic pressure-concentration-temperature characteristics of the reactor A1. As already explained, when the reactor A1 is heated to 568 K, it reaches the maximum pressure of about 90 bar. The paths followed by the various processes, namely, 1-2: sensible heating, 2-3-4: desorption of hydrogen and 4-5: sensible cooling, are illustrated in Fig. 5.21. When the hydrogen valve between the paired reactors (A1 and C1) is opened, due to the high pressure difference, the temperature of the reactor A1 quickly decreases down to 535 K at 29 bar (2-3 in Fig. 5.21). At the same time, the absorption of hydrogen at the reactor C1 leads to an increase in the equilibrium pressure and temperature from 4 bar at 273 K to 12 bar at 288 K (6-7 in Fig. 5.24). Later, both the reactors reach their respective heat transfer fluid temperatures. The dynamic PCT characteristics of the reactor C1 (coupled with the reactor A1 during the first half cycle) during the absorption of hydrogen is shown in Fig. 5.24. It is observed that the hydrogen exchange between the reactors A1 and C1 ceases around 19.5 bar pressure (point 4 in Fig. 5.21 and point 8 in Fig. 5.24).

The variation of hydride bed pressure, temperature, and concentration during the absorption of hydrogen (process 6-7-8) at the reactor A2 are illustrated in Fig. 5.22. During the first half cycle, the reactor A2 is coupled with the reactor B2. Initially, the reactor B2 is fully hydrided (maximum concentration) at 286 K and about 4 bar pressure and the reactor A2 is deydrided (minimum concentration) at 0.1 bar pressure and 361 K. Once the valve between these reactors is opened, the hydrogen from the reactor B2 desorbs by taking the heat from the heat transfer fluid (yielding the refrigeration effect). The lowest refrigeration temperature of 268 K is attained at 0.5 bar pressure. The desorbed hydrogen from the reactor B2 is absorbed by A2, until it reaches 0.5 bar pressure.

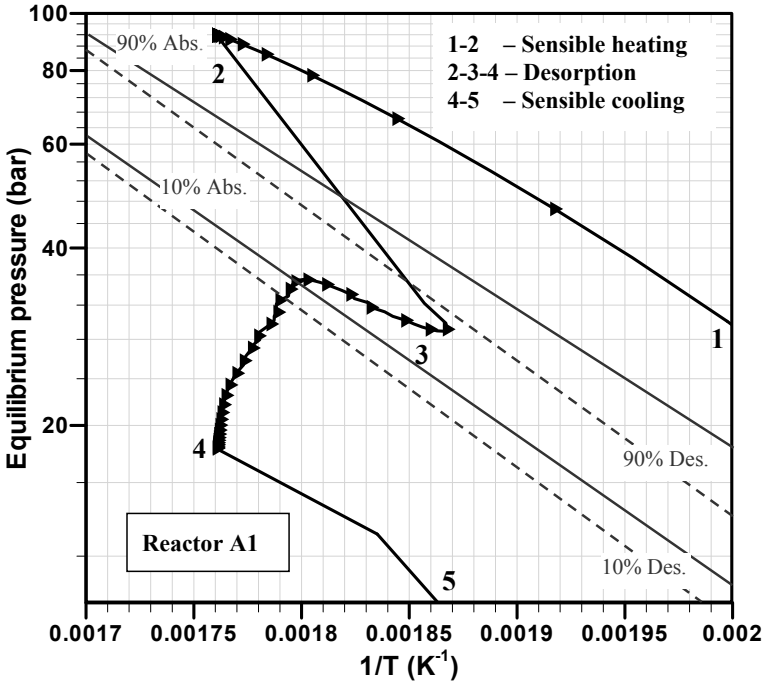

Fig. 5.21 Dynamic PCT characteristics of the reactor A1.

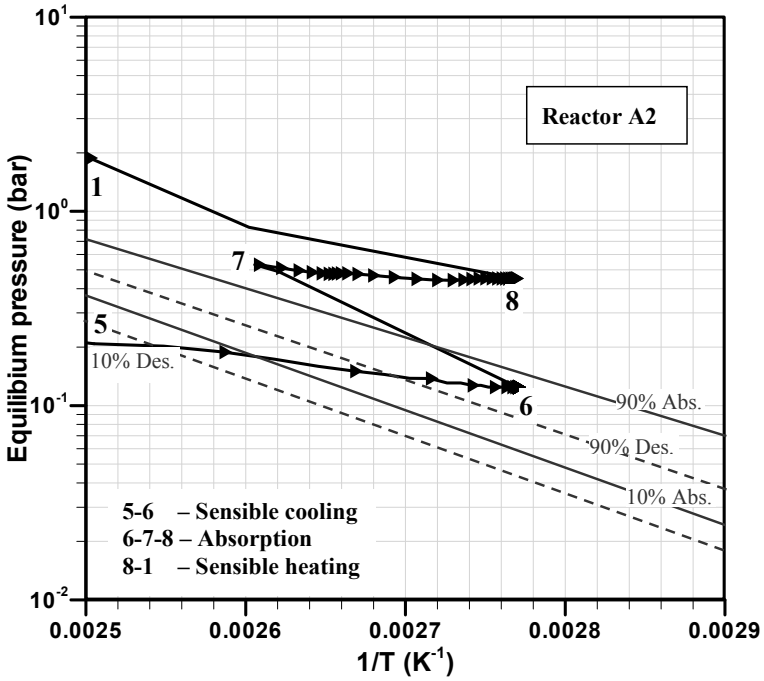

Fig. 5.22 Dynamic PCT characteristics of the reactor A2.

Similarly, the dynamic characteristics during the hydrogen exchange between the reactors C2 (desorption) and B1 (absorption) are illustrated in Figs. 5.23 and 5.24. Initially, before opening the hydrogen valve, the reactors C2 and B1 are in the respective pressures and temperatures limits of 25 bar at 289 K and 2.5 bar at 296 K. Once the processes are initiated, the desorption / absorption of hydrogen from / to the reactors C2 / B1 take place, thereby the reaction beds experience decrease / increase in the temperatures and the equilibrium pressures as shown in Figs. 5.23 and 5.24. The final condition of the first half cycle is the initial condition of the internal heat recovery 1. During these processes the heat transfer fluids are circulated between the reactors A1 and A2, B1 and B2 and, C1 and C2. After the internal heat recovery 1, the reactors are heated up / cooled down to their respective temperature limits. Later, the hydrogen transfers take place during the second half cycle between A2 and C2, C1 and B2 and, B1 and A1. Finally, all the reactors are switched over for the internally heat recovery 2, followed by the sensible heat transfer processes 2. Thus the cycle is completed. The final condition of the first cycle is the initial condition of the next first half cycle.

5.2.4 Performance investigation of DSDE-MHHP

The following section describes the performance investigation of a DSDE-MHHP working with $LaNi_{4.1}Al_{0.52}Mn_{0.38}$, $LmNi_{4.91}Sn_{0.15}$ and $Ti_{0.99}Zr_{0.01}V_{0.43}Fe_{0.09}Cr_{0.05}Mn_{1.5}$ hydride pairs. The effects of half cycle time (θ), hydride mass ratio (M_R), sensible heat exchange factor (ϕ) and operating temperatures, viz., heat source (T_D), heat sink (T_M), and refrigeration (T_C) temperatures on the amount of hydrogen transferred between the paired reactors, coefficient of performance (*COP*) and specific cooling power (*SCP*) of the DSDE-MHHP system have been investigated.

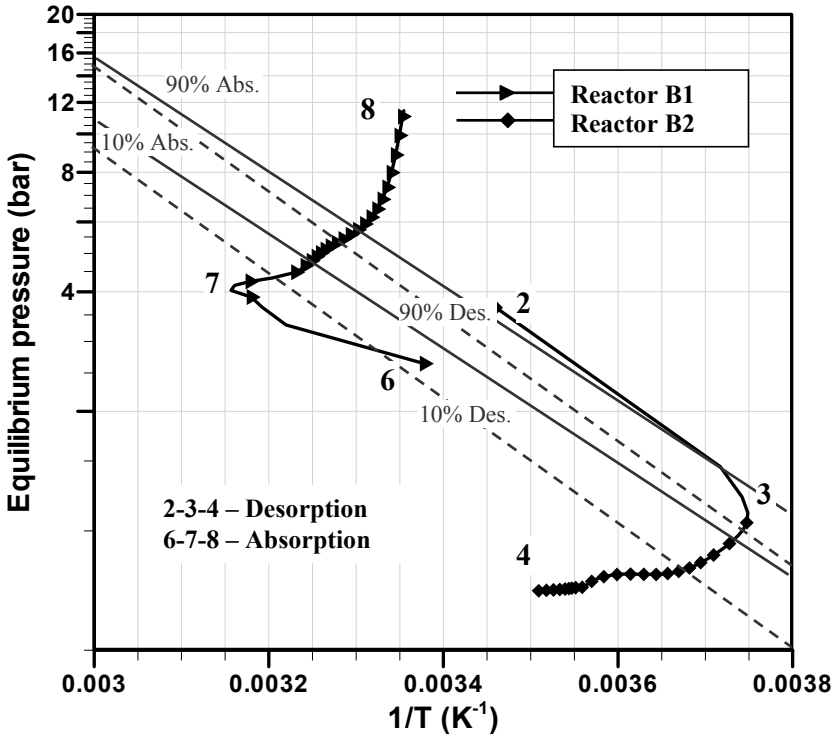

Fig. 5.23 Dynamic PCT characteristics of the reactors B1 and B2.

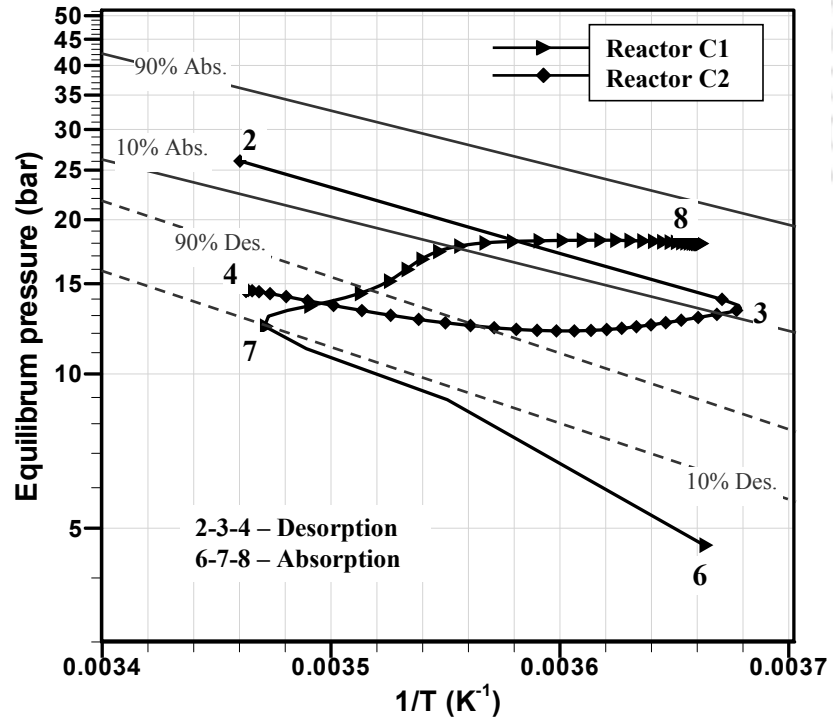

Fig. 5.24 Dynamic PCT characteristics of the reactors C1 and C2.

Fig. 5.25 shows the effect of half cycle time on the amount of hydrogen transferred between the paired reactors during the first half cycle. It is observed that the hydrogen transferred between the reactors A1 and C1, and B2 and A2 at high and low pressure increases marginally with time beyond about 10 min, while between C2 and B1 at medium pressure it increases significantly with time up to about 15 min. For given operating temperatures of 578 / 373 / 298 / 283 K, the maximum amount of hydrogen exchange that takes place between the paired reactors A1 and C1, C2 and B1, and B2 and A2 amounts to 80.4, 83.5 and 78.4 g at the respective high, medium and low pressure levels. Since all the six reactors are coupled together in a star scheme, only 78.4 g of hydrogen (lowest hydrogen exchange rate) can be exchanged in a cyclic operation. Considering the hydrogen transferred between the three pairs, an optimum half cycle time of about 15 min is fixed for further analysis.

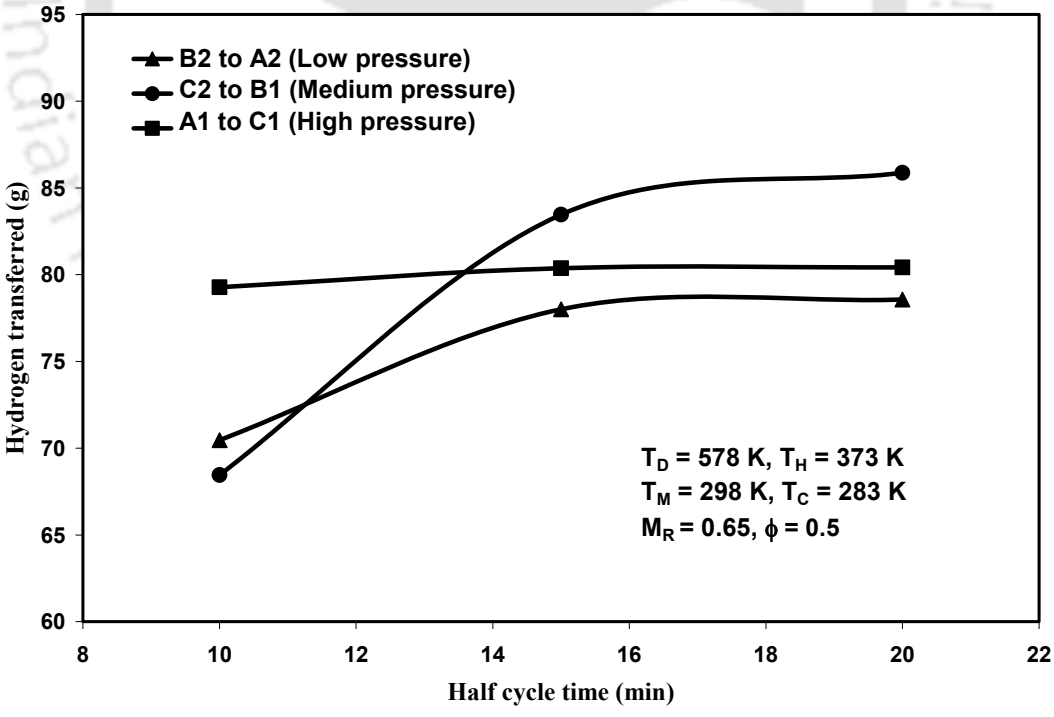

Fig. 5.25 Effect of half cycle time on the amount of hydrogen transferred between paired reactors.

Fig. 5.26 shows the effect of half cycle time on system cooling load and COP. Due to increase in amount of hydrogen transferred between the paired reactors with half cycle time, the cooling load obtained from the system at medium and low pressure levels increases up to about 15 min. Therefore, the cooling load and COP of the DSDE-MHHP system also increase up to 15 min, beyond which the increase of half cycle time does not have any significant effect, either on COP or on cooling load.

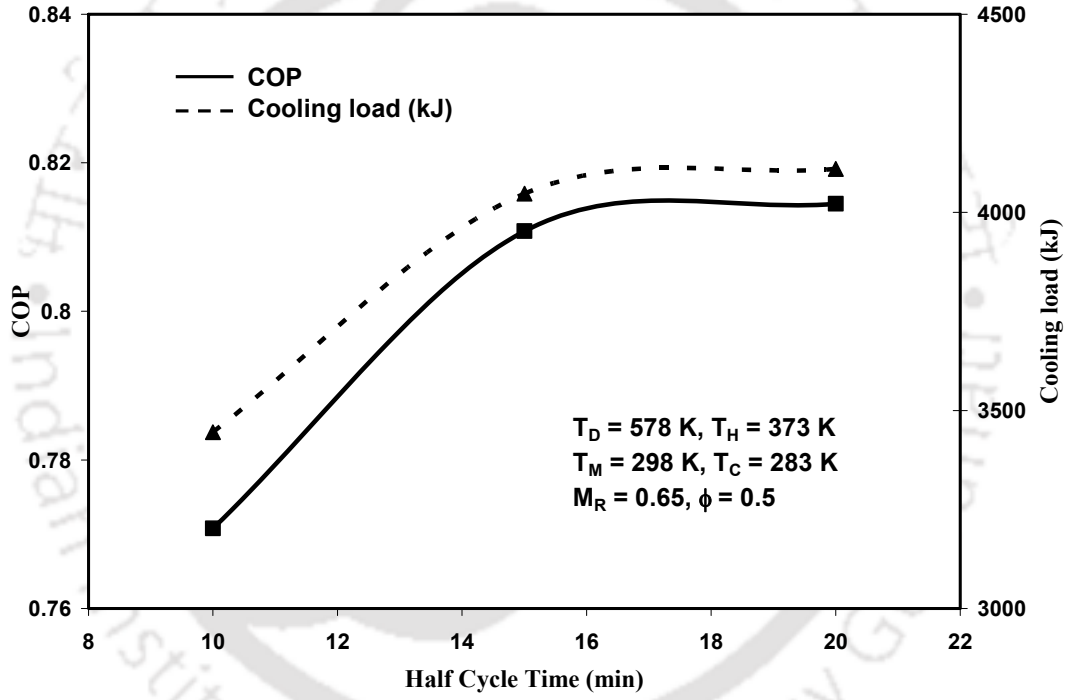

Fig. 5.26 Effect of half cycle time on COP and cooling load.

The effect of heat source temperature (T_D) on the amount of hydrogen transferred between the paired reactors and the cooling capacity is shown in Fig. 5.27. For the given operating conditions, the amount of hydrogen transferred between the reactors A1 and C1 (at high pressure level) during the first half cycle increases with heat source temperature. This is due to the increase in the equilibrium pressure difference (driving force) between

the reactors A1 and C1. As the heat sink, heat rejection and refrigeration temperatures are fixed, the influence of heat source temperature on the amount of hydrogen transferred between the paired reactors at the medium and low pressure levels is negligible (shown in Fig. 5.27).

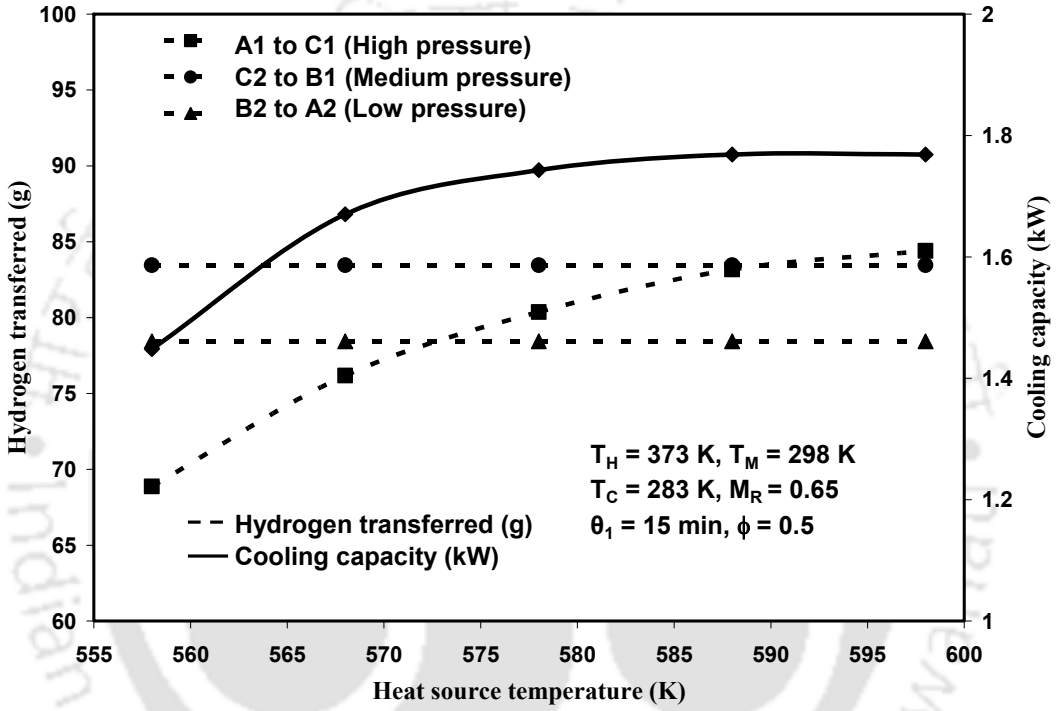

Fig. 5.27 Effect of heat source temperature on the amount of hydrogen transferred and cooling capacity.

Fig. 5.28 shows the effect of heat source temperature on COP and SCP. The average COP increases with heat source temperature up to 573 K. Further increase in T_D beyond 573 K decreases the COP. Therefore, within the range of the used temperatures of T_D (see Table 4.6), T_D = 578 K selected as an optimum value for further calculations. The increase in SCP with heat source temperature is considerable up to about 578 K and then it starts to level off, e.g., only a small increase in SCP of 1.3% is observed when the heat source temperature is increased from 578 K to 598 K. This is mainly due to the rapid desorption

of hydrogen at higher T_D. For the heat source temperature increasing from 558 K to 598 K, the SCP of the system increases from 39.1 to 47.8 W/kg of total alloy mass. The maximum cooling capacity and COP achieved at the operating temperatures of 578 / 373 / 298 / 283 K are 1.74 kW and 0.81, respectively, and the corresponding SCP is 47.2 W/kg of total hydride mass.

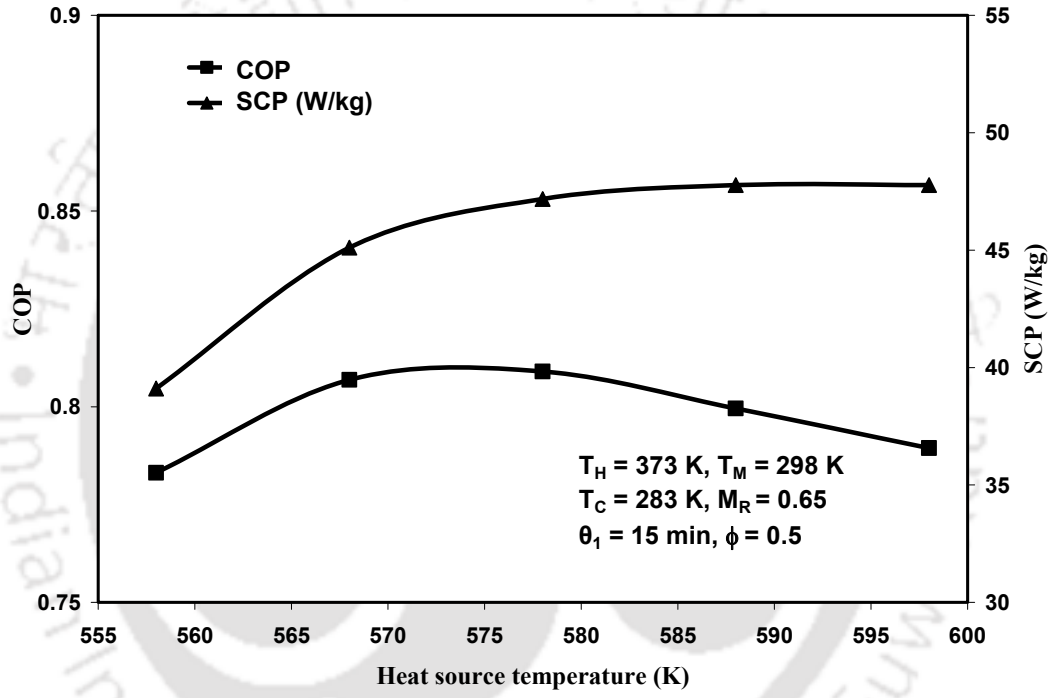

Fig. 5.28 Effect of heat source temperature on COP and SCP.

The effect of heat sink temperature on the amount of hydrogen transferred between the paired reactors and on the cooling capacity of a DSDE-MHHP system is shown in Fig. 5.29. It is observed that the amounts of hydrogen transferred between the coupled reactors A1 and C1, and C2 and B1 decrease with an increase in the heat sink temperature. This is mainly due to the decrease in the driving force between the paired reactors. Therefore, the cooling capacity (refrigeration effect) of the system also decreases. However, the effect of

T_M on the amount of hydrogen transferred between the reactors B2 and A2 (78.4 g) at low pressure is negligible. Therefore the corresponding cooling capacity at low pressure level (0.98 kW) also remains constant for T_M varying between 298 K and 306.5 K. Above T_M = 306.5 K, the amount of hydrogen exchange during the first half cycle is governed by the exchange rate between C2 and B1, which is restricted to 77.5 g at 308 K (due to a decrease in the driving potential). Hence, for the given operating temperatures of 578 / 373 / 308 / 283 K, the cooling capacity at the low pressure level is reduced to 0.95 kW. The decrease in COP and SCP of the system with heat sink temperature is illustrated in Fig. 5.30. For the heat sink temperature varying from 298 K to 308 K, the COP and SCP, are found to decrease from 0.81 and 48.2 W/kg of total hydride mass to 0.76 and 41.0 W/kg of total hydride mass, respectively.

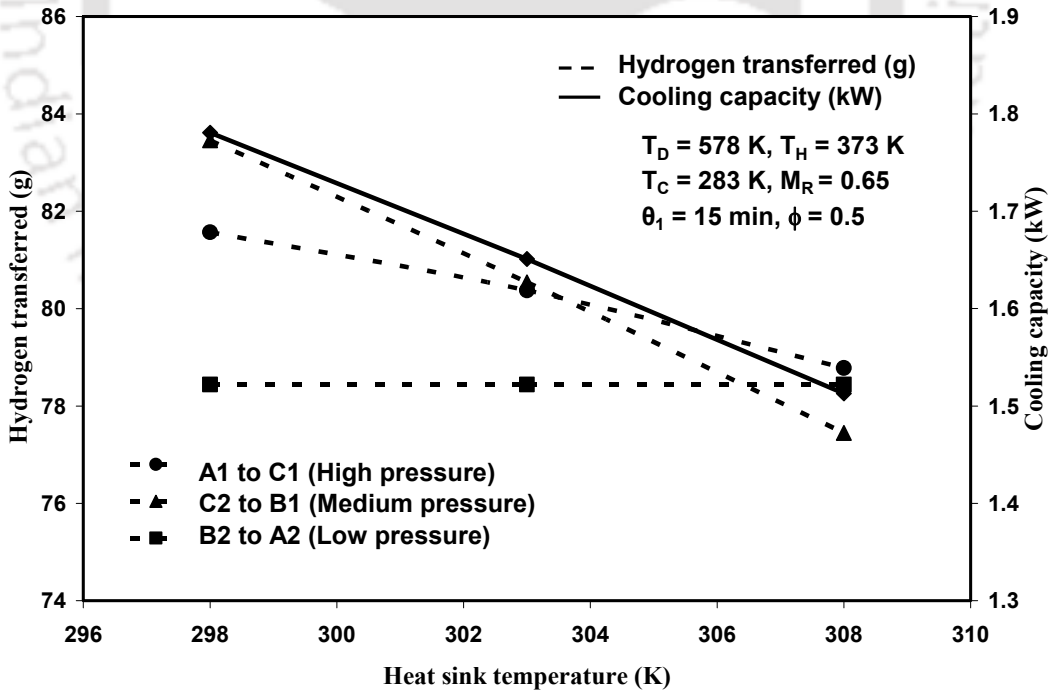

Fig. 5.29 Effect of heat sink temperature on the amount of hydrogen transferred and cooling capacity.

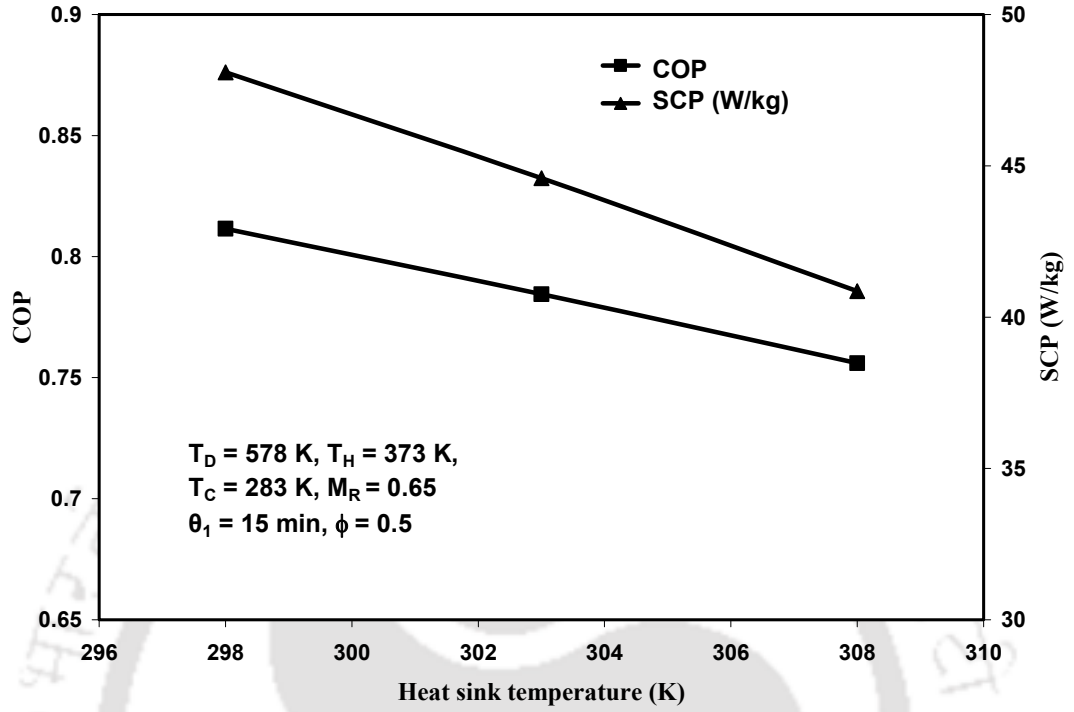

Fig. 5.30 Effect of heat sink temperature on COP and SCP.

As illustrated in Fig. 5.31, the amounts of hydrogen transferred between the paired reactors at the medium and low pressure levels increase with T_C. However, the amount of hydrogen transferred between A1 and C1 at high pressure level remains constant (at a maximum level of 80.4 g). Hence, the heat supplied to the system remains constant irrespective of the variation in the refrigeration temperature. Therefore, an increase in the refrigeration temperature increases the amount of hydrogen transferred between the paired reactors (up to 80.4 g), resulting in an increase of the cooling capacity of the entire system. It is also observed from Fig. 5.32 that the increase in COP and SCP with refrigeration temperature from 273 to 283 K is much higher than that for an increase from 283 K to 293 K. Hence, a refrigeration temperature of about 283 K can be defined as an optimum for the investigated DSDE-MHHP system.

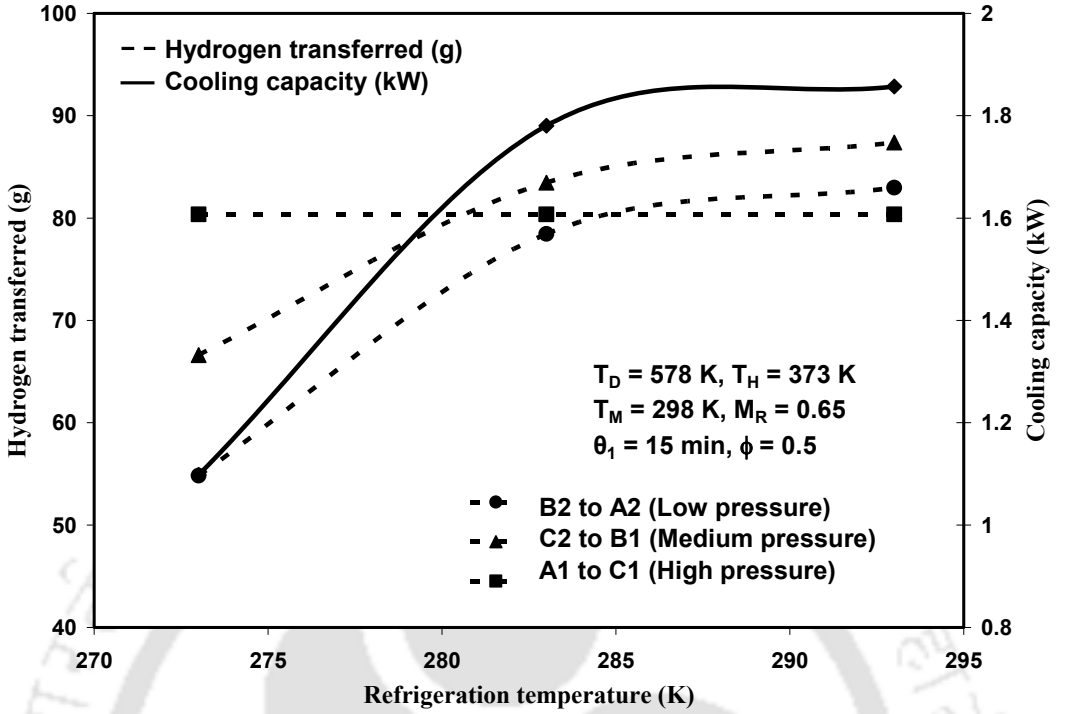

Fig. 5.31 Effect of refrigeration temperature on the amount of hydrogen transferred and cooling capacity.

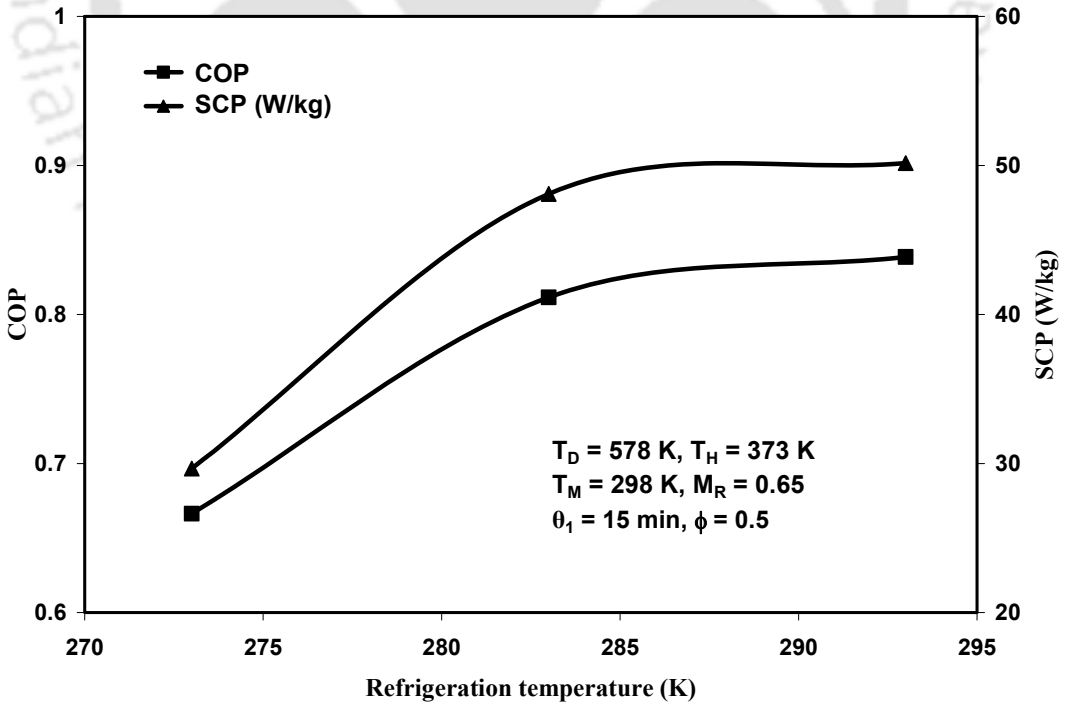

Fig. 5.32 Effect of refrigeration temperature on COP and SCP.

Fig. 5.33 shows that an increase in the mass ratio (M_R) leads to a significant reduction in the cooling capacity, COP and SCP of the DSDE-MHHP system. Higher thermal masses substantially increase the sensible heating requirement of the whole system. Therefore, the cooling capacity, COP and SCP of the system decrease from 1.8 kW, 0.87 and 61.6 W/kg of total hydride mass to 1.75 kW, 0.72 and 33.2 W/kg of total hydride mass, respectively, when the mass ratio increased from 0.3 to 1.35, i.e., these are reductions of 2.8%, 17.5% and 46.3%, respectively. Therefore, to obtain a good performance, one has to pay significant attention to the reduction of reactor mass.

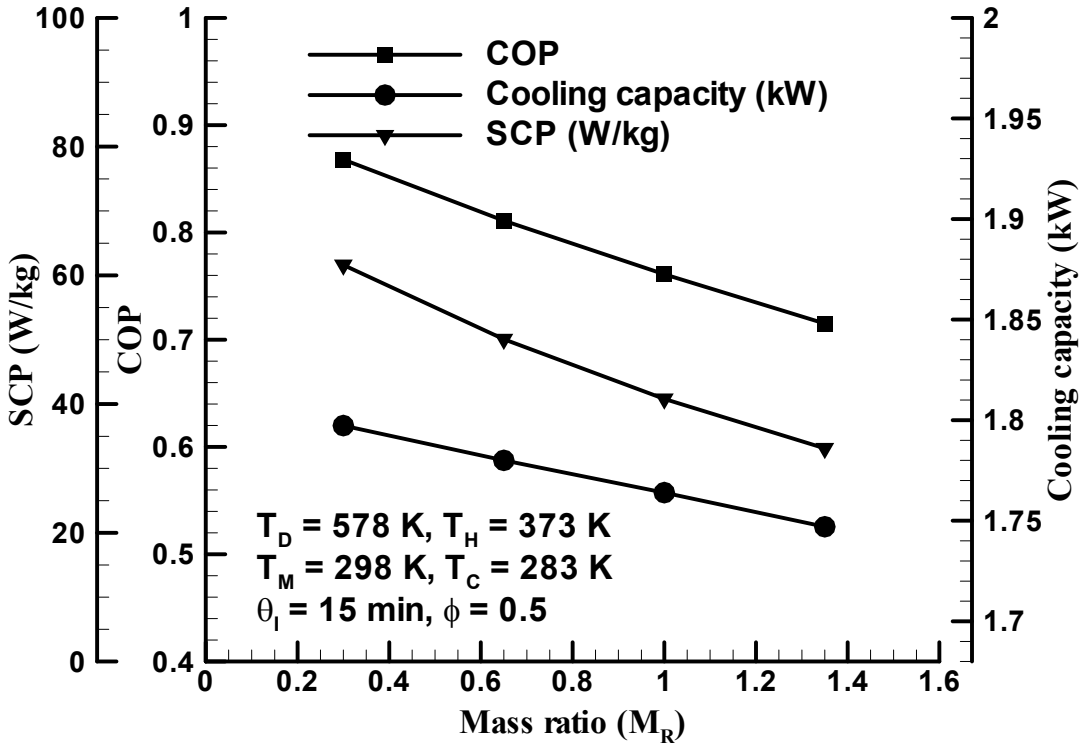

Fig. 5.33 Effect of mass ratio on cooling capacity, COP and SCP.

The sensible heat exchange (internal heat recovery) plays an important role in the performance of MHHP systems, particularly when the difference between the heat source and heat rejection temperatures is very high. Fig. 5.34 shows the effect of sensible heat exchange factor on the cooling capacity, COP and SCP of a DSDE-MHHP system. For the given operating conditions, a 50% sensible heat recovery can increase the COP remarkably by about 32%. However, sensible heat recovery increases the overall initial cost of the system, because additional heat exchangers are necessary to recover the exchanged heat between the reactors. Hence, before introducing the internal heat recovery, its economical viability must be evaluated.

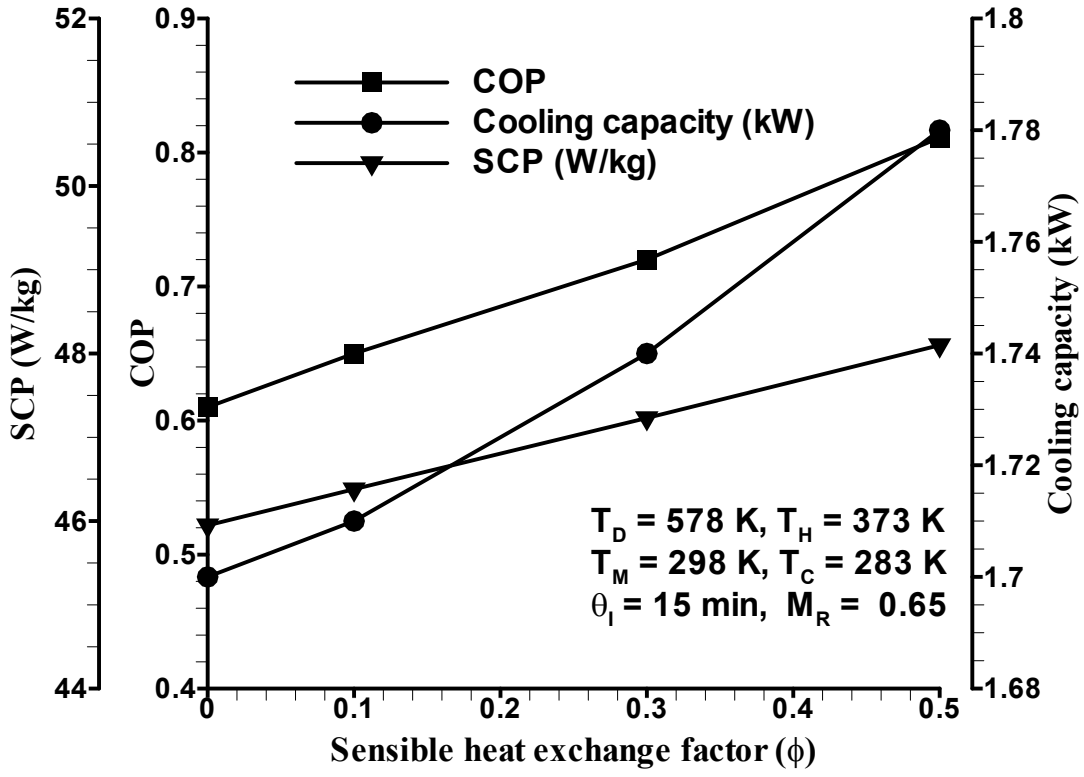

Fig. 5.34 Effect of sensible heat exchange factor on cooling capacity, COP and SCP.

5.2.5 Summary of DSDE-MHHP's Thermal Modeling

The operating cycle of a DSDE-MHHP system employing $LaNi_{4.1}Al_{0.52}Mn_{0.38}$, $LmNi_{4.91}Sn_{0.15}$ and $Ti_{0.99}Zr_{0.01}V_{0.43}Fe_{0.09}Cr_{0.05}Mn_{1.5}$ as high, medium and low temperature alloys was studied. The change in hydride bed temperatures, hydrogen concentrations and pressures for all the reactors over a complete cycle of operation, and the heat exchanged between the reactors and heat transfer fluids during the heat and hydrogen transfer processes were also investigated. The present computational results of all hydride bed temperatures were compared with the experimental data reported by Klein (2007) and a good agreement was observed between them. For the selected operating temperatures, the COP and SCP of the DSDE-MHHP system were evaluated with the experimental data. The heat and mass transfer studies were extended to predict the performance of the DSDE-MHHP using the above-mentioned hydride pair. The effects of operating temperatures T_D, T_M and T_C, half cycle time, hydride mass ratio and sensible heat exchange factor on COP and SCP of the system were investigated. In general, the present numerical model allows for obtaining the optimum operating parameters, such as, heat source, heat sink and refrigeration temperatures, half cycle time, hydride mass ratio, and sensible heat exchange factor without conducting an expensive experimental study. Further, the present model can also be useful for developing an optimal reaction bed which can provide a shorter cycle time.

5.3 CROSSED VAN'T HOFF LINE METAL HYDRIDE HEAT PUMP

This section presents a novel heat driven metal hydride heap pump operating on the principle of crossed van't Hoff configuration. It utilizes the enthalpy of formation of the refrigeration alloy to drive the single stage metal hydride heat pump. So far, no research work has been reported in the literature on the heat and mass transfer aspects of the cross

van't Hoff SS-MHHP system. Results on crossed van't Hoff MHHP is presented in the following section.

A grid independence study for the present analysis is carried out using three different grid sizes (31 x 31, 41 x 41 and 51 x 51) and a 41 x 41 grid size was found to provide good accuracy. Hence, this grid size is adopted for subsequent numerical analysis.

5.3.1 Performance Prediction of Crossed van't Hoff MHHP

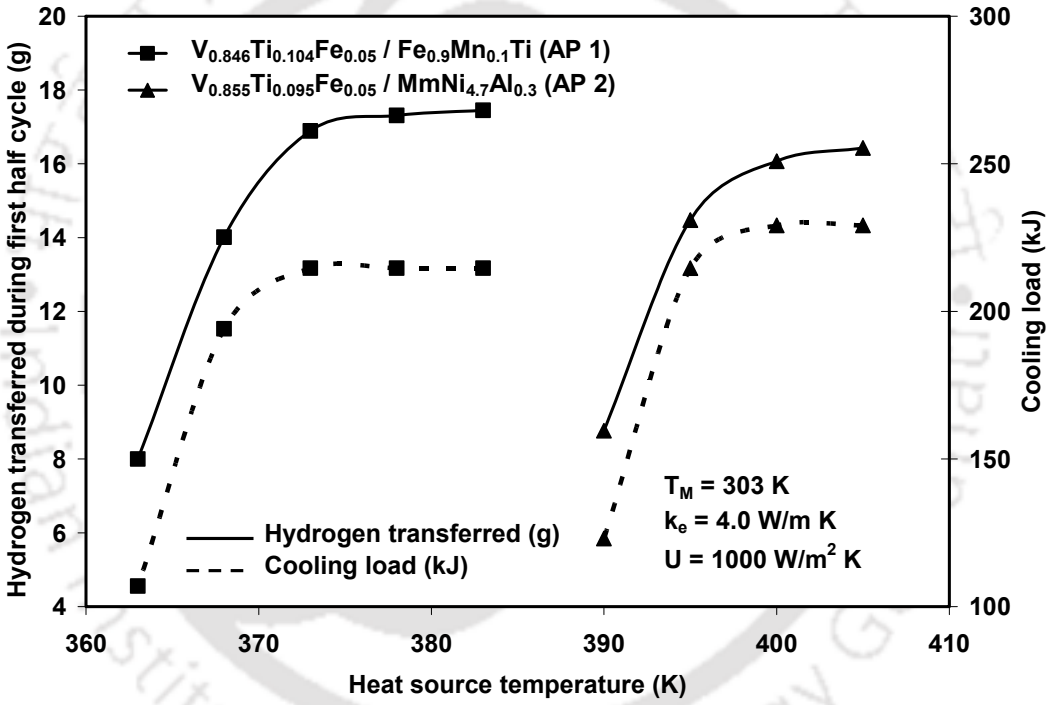

Fig. 5.35 Effect of heat source temperature on hydrogen transferred during first half cycle and cooling load.

Fig. 5.35 shows the effect of heat source temperature on the amount of hydrogen transferred between the paired reactors during the first half cycle. For the selected operating conditions, the amount of hydrogen transferred from the reactors A to B during the first half cycle increases with T_H. This is due to an increase in the pressure difference between the equilibrium pressure and gas pressure (P_{eq}-P_g) called the driving potential.

Due to fixed heat sink and refrigeration temperatures, the hydrogen transfer during the second half cycle does not change with T_H. Therefore, increasing the heat source temperature is beneficial only up to a certain limit; beyond which either the refrigeration temperature or heat sink temperature controls the hydrogen transfer. For the selected operating temperatures of 373/303/291 K and 400/303/283 K, a maximum of 16.9 and 16.0 g of hydrogen is transferred between the alloy pairs AP 1 and AP 2, respectively. It is observed from Fig. 5.35 that due to an increase in hydrogen exchanged between the paired reactors, the cooling load of the system is found to increase with T_H. The maximum cooling capacities of the selected hydride alloys pairs of AP 1 and AP 2 at 373 / 303 / 291 K and 400 / 303 / 283 K are 215 and 230 kJ, respectively.

As explained earlier, for the fixed T_M and T_C, the maximum amount of hydrogen transferred is obtained at the heat source temperatures of 373 K and 400 K for AP 1 and AP 2 hydride pairs, respectively. Therefore, the COPs of the selected hydride alloy pairs are also found to increase with the respective heat source temperatures. It is seen from Fig. 5.36 that the maximum COPs of crossed van't Hoff SS-MHHP are 0.89 and 0.86 respectively, for AP 1 and AP 2 hydride alloy pairs. For the same amount of hydrogen transfer and the operating temperatures (T_H, T_M and T_C), the maximum COP obtained from the conventional SS-MHHP ($LmNi_{4.91}Sn_{0.15}$ / $Ti_{0.99}Zr_{0.01}V_{0.43}Fe_{0.09}Cr_{0.05}Mn_{1.5}$) is only equal to 0.56 (Satheesh and Muthukumar, 2010). Therefore, while consuming the heat of absorption from the refrigeration hydride (during the first half cycle) a maximum increase in COP of about 60% can be achieved. But, the only problem is the proper selection of hydride alloy pair working in the crossed van't Hoff configuration at the required operating conditions.

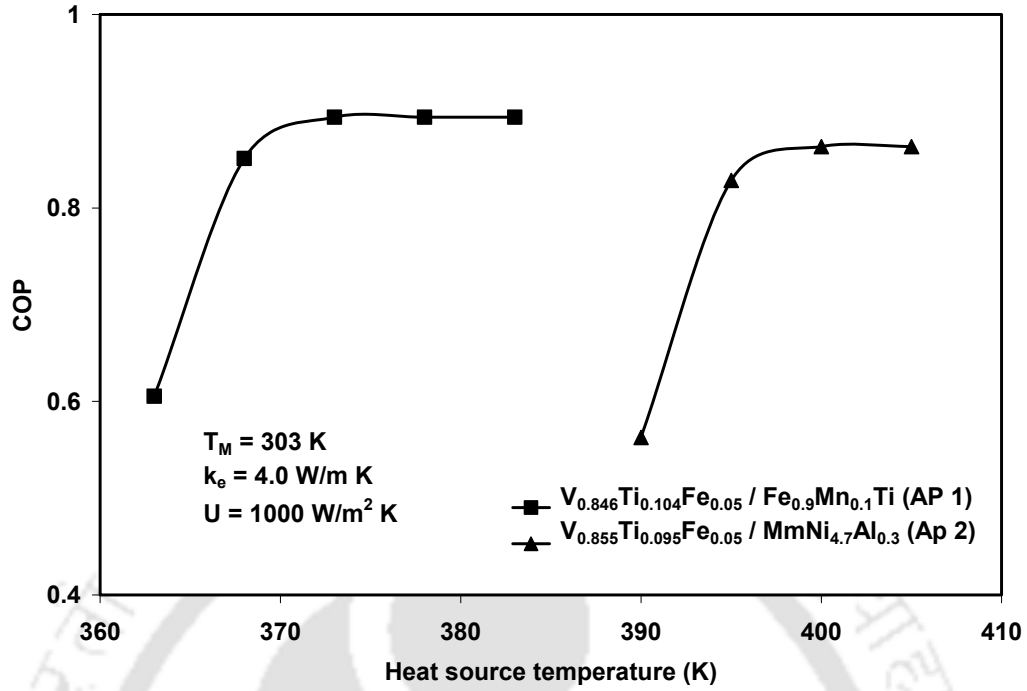

Fig. 5.36 Effect of heat source temperature on COP of MHHP operating with crossed van't Hoff configuration.

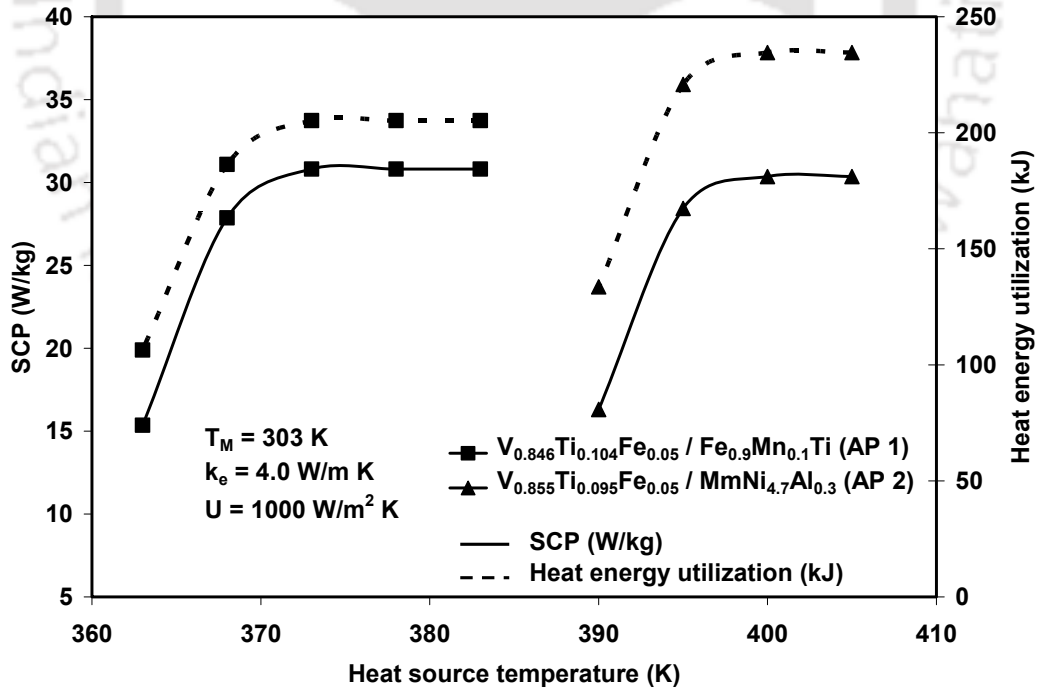

Fig. 5.37 Effect of heat source temperature on SCP and heat energy utilized during regeneration process.

The effect of heat source temperature on SCP and heat energy utilized between the hydride pairs was also investigated and the corresponding results are shown in Fig. 5.37. Due to an increase in hydrogen transferred between reactors A and B, the cooling capacity is found to increase. As a result, SCP also increases. Depending on the arrangement of heat pump (either conventional MHHP or crossed van't Hoff MHHP), the SCP does not change. It is seen from Fig. 5.37 that the maximum SCP of 30.8 and 30.5 W/kg of total system mass was achieved for AP 1 and AP 2 hydride pairs. The above SCP can also be increased by employing proper heat augmentation techniques (Groll, 1993). Heat energy utilized during the regeneration of hydrides at high pressure (P_H) for the selected hydride pair are shown in Fig. 5.37. The required heat energy to be supplied to the crossed van't Hoff MHHP is about 370 kJ (make it for per kg) and 355 kJ respectively for AP 1 and AP 2. Of these, 205.0 kJ (nearly 55%) and 234.0 kJ (nearly 65%) of heat is recovered from the refrigeration hydrides.

It is observed from Fig. 5.38 that the amounts of hydrogen transferred between the paired reactors increases with refrigeration temperature. Due to fixed T_H and T_M, the amounts of hydrogen transferred during the first half cycle (process *ab*) remains constant. Therefore, increasing the refrigeration temperature is beneficial up to a certain limit. For the selected ranges of heat source and heat sink temperatures, the optimum values of refrigeration temperatures are found out for AP 1 (291 K) and AP 2 (283 K) hydride pairs.

Figs. 5.39 and 5.40 show the effect of refrigeration temperatures on COP, SCP and heat energy utilized in the crossed van't Hoff MHHP. Due to an increase in hydrogen transfer between the reaction beds with refrigeration temperature, the performance (COP, SCP and heat energy utilized) of crossed van't Hoff MHHP is found to increase.

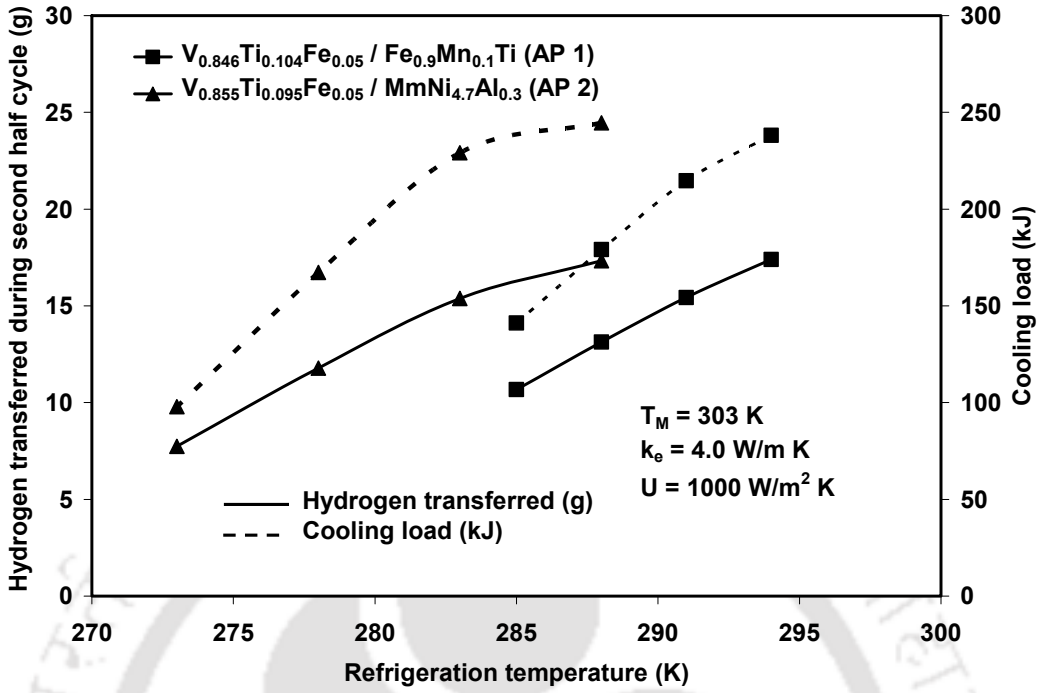

Fig. 5.38 Effect of refrigeration temperature on hydrogen transferred during second half cycle and cooling load.

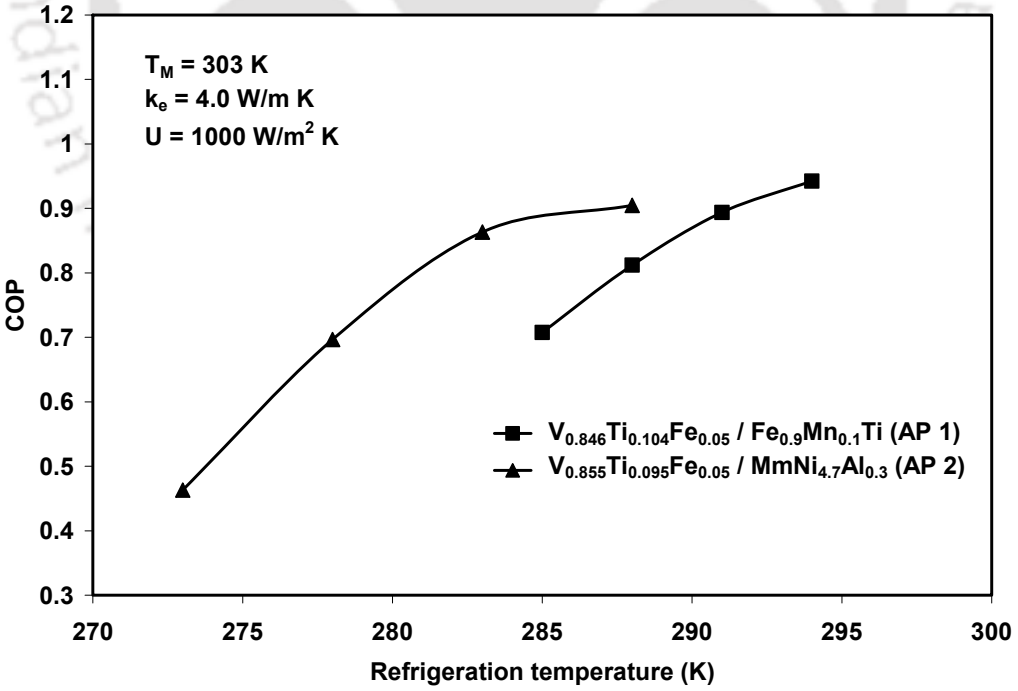

Fig. 5.39 Effect of refrigeration temperature on COP of MHHP operating with crossed van't Hoff configuration.

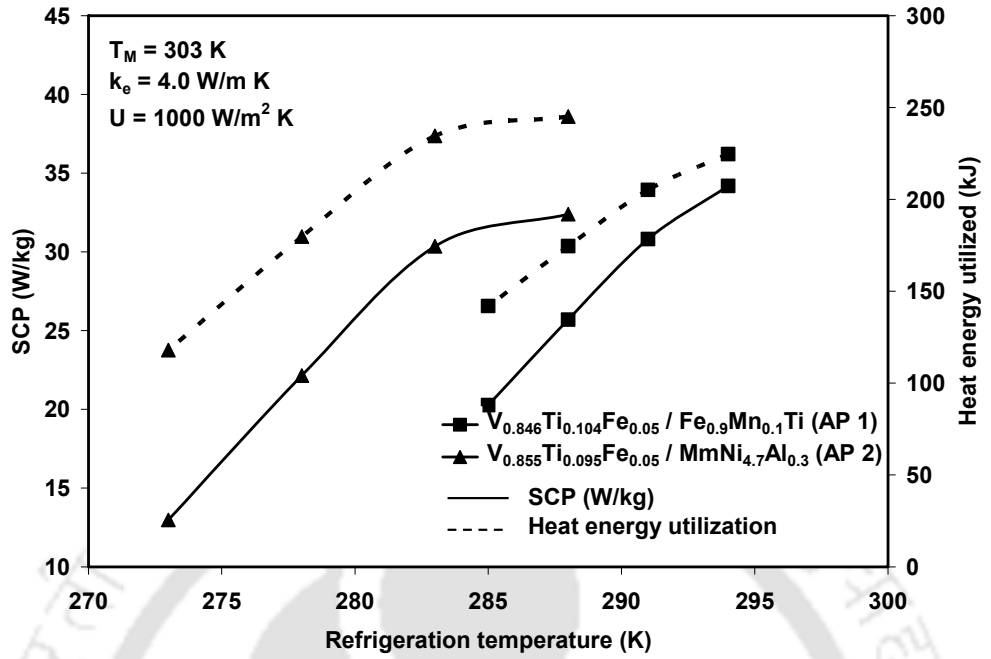

Fig. 5.40 Effect of refrigeration temperature on SCP and heat energy utilized during regeneration process.

5.3.2 Summary of Crossed van't Hoff line SS-MHHP's Thermal modeling

The operating feasibility of a crossed van't Hoff SS-MHHP working with two different hydride alloy pairs, namely, $V_{0.846}Ti_{0.104}Fe_{0.05}$ / $Fe_{0.9}Mn_{0.1}Ti$ and $V_{0.855}Ti_{0.095}Fe_{0.05}$ / $MmNi_{4.7}Al_{0.3}$ are studied. Results reveal that the crossed van't Hoff SS-MHHP gained nearly 60% higher COP than the conventional SS-MHHP. The optimum operating temperatures have been found out for the selected hydride alloy pairs. So far, no theoretical and experimental works have been reported in the literature dealing with the crossed van't Hoff MHHP. Therefore, the present study reveals the preliminary analysis for the effective utilization of heat energy which can be used for driving the MHHP applications. In future, there might be a possibility of finding the appropriate alloy pairs either from the newly synthesized hydride alloys or a modification of existing hydrides with different compositions of other metals to meet the requirement for crossed van't Hoff MHHP system.

CHAPTER 6

CONCLUSIONS

The conclusions drawn from the studies on hydriding kinetics and the performance evaluations of single-stage, double-stage and crossed van't Hoff metal hydride heat pumps are presented here.

6.1 REACTION KINETICS STUDIES

The following conclusions are drawn from the studies on reaction kinetics during the absorption of hydrogen in $LaNi_5$, $LmNi_{4.91}Sn_{0.15}$ and $LaNi_{4.7}Al_{0.3}$ hydride alloys.

1. The reaction kinetics data is modeled using different reaction kinetics models, namely, Jander diffusion model and Johnson-Mehl-Avrami model, based on the diffusion of the hydrogen atom and nucleation and growth of the hydride. Results show that the computations using the Jander diffusion model closely match the experimental data for all three alloys and therefore, the rate-controlling mechanism in the (α+β)-phase region is diffusion of hydride atom into the metal hydride.

2. The activation energies of $LaNi_5$, $LaNi_{4.7}Al_{0.3}$ and $LmNi_{4.91}Sn_{0.15}$ hydride alloys are obtained from the Arrhenius plot and their values are 27.7, 29.1 and 28.0 kJ/mol H_2, respectively, using the Jander diffusion model.

3. The reaction rate constants of the above-mentioned hydride alloys are 86, 594 and 846 s^{-1}, respectively, using the Jander diffusion model

6.2 HEAT AND MASS TRANSFER MODELS

6.2.1 Single Stage Metal Hydride Heat Pump

The following conclusions are drawn from the performance study of single-stage metal hydride heat pumps.

A computational study of a metal hydride heat pump working with five different hydride pairs, namely, $MmNi_{4.6}Al_{0.4}$ / $MmNi_{4.6}Fe_{0.4}$, $LaNi_{4.61}Mn_{0.26}Al_{0.13}$ / $La_{0.6}Y_{0.4}Ni_{4.8}Mn_{0.2}$, $LmNi_{4.91}Sn_{0.15}$ / $Ti_{0.99}Zr_{0.01}V_{0.43}Fe_{0.09}Cr_{0.05}Mn_{1.5}$, $LaNi_{4.6}Al_{0.4}$ / $MmNi_{4.15}Fe_{0.85}$ and $Zr_{0.9}Ti_{0.1}Cr_{0.9}Fe_{1.1}$ / $Zr_{0.9}Ti_{0.1}Cr_{0.6}Fe_{1.4}$ is presented.

1. A comparison of $LaNi_{4.61}Mn_{0.26}Al_{0.13}$ / $La_{0.6}Y_{0.4}Ni_{4.8}Mn_{0.2}$ hydride pair is performed by comparing the present computations with the experimental data reported in the literature (Ni and Liu, 2007) for the high temperature and low temperature reactors for a complete cycle at different heat source temperatures ranging from 388 K to 423 K. A good agreement was observed between the two.

2. The coupled heat and hydrogen transfer characteristics, such as, hydride bed temperatures, equilibrium pressures, change in hydrogen concentration between

the reaction beds, and the heat exchange between the hydride beds with heat transfer fluids are presented for $MmNi_{4.6}Al_{0.4}$ / $MmNi_{4.6}Fe_{0.4}$ hydride pair using two types of convective boundary conditions.

3. The effects of heat source, heat sink and refrigeration temperatures on the amount of hydrogen exchanged between the coupled reactors, COP and SCP of SSSE-MHHP system are studied extensively and the optimum operating temperatures of the selected metal hydride pairs are found out.

4. For a given heat sink temperature, the COP and SCP of the system are found to increase with heat source and refrigeration temperatures and decreases with heat sink temperature.

5. For the selected hydride alloy pairs, the maximum COP is found to be 0.66 for $Zr_{0.9}Ti_{0.1}Cr_{0.9}Fe_{1.1}$ / $Zr_{0.9}Ti_{0.1}Cr_{0.6}Fe_{1.4}$ at the operating temperatures of 393/298/288 K and the highest SCP of 53.2 W/kg of total mass is obtained from $LmNi_{4.91}Sn_{0.15}$ / $Ti_{0.99}Zr_{0.01}V_{0.43}Fe_{0.09}Cr_{0.05}Mn_{1.5}$, hydride pair at the operating temperatures of 413/298/293 K ($T_H/T_M/T_C$), respectively.

6.2.2 Double Stage Double Effect Metal Hydride Heat Pump

The following conclusions are drawn from the performance study of the double-stage double-effect metal hydride heat pump system.

The operation and performance investigations of a double-stage double-effect metal hydride heat pump working with $LaNi_{4.1}Al_{0.52}Mn_{0.38}$, $LmNi_{4.91}Sn_{0.15}$ and $Ti_{0.99}Zr_{0.01}V_{0.43}Fe_{0.09}Cr_{0.05}Mn_{1.5}$ are presented. Computationally predicted temperature profiles of the reaction beds are compared with experimental data (Klein, 2007) and a good agreement is observed between the two.

1. The change in hydride bed temperatures, hydrogen concentrations and pressures for all the reactors over a complete cycle of operation, and the heat exchanged between the reactors and heat transfer fluids during the heat and hydrogen transfer processes are presented. The dynamic PCT characteristics of all reactors are also presented.

2. The lowest refrigeration temperature of 268 K is attained at 0.5 bar pressure.

3. The effects of various operating temperatures, half cycle time, hydride mass ratio and sensible heat exchange factor on COP and SCP of the system are studied.

4. The effect of the driving heat and refrigeration temperatures on system COP is more significant than that of the heat sink temperature.

5. Based on the operating conditions, the about optimum half cycle time is fixed at 15 min.

6. For the given operating temperatures of 578 / 373 / 298 / 283 K (T_D / T_H / T_M / T_C), the COP and SCP of the system are found to be 0.81 and 48.1 W/kg of the total alloy mass, respectively.

7. A decrease of the mass ratio from 1.35 to 0.3 enhances the COP and SCP by about 17.5% and 46.3%, respectively. Recovery of 50% sensible heat improves the COP by 32%.

6.2.3 Crossed van't Hoff line Single Stage Metal Hydride Heat Pump

The following conclusions are drawn from the performance study of crossed van't Hoff line concept single-stage metal hydride heat pump system.

1. The operating feasibility of a crossed van't Hoff line configured single-stage MHHP working with two different hydride alloy pairs, namely, $V_{0.846}Ti_{0.104}Fe_{0.05}$ / $Fe_{0.9}Mn_{0.1}Ti$ and $V_{0.855}Ti_{0.095}Fe_{0.05}$ / $MmNi_{4.7}Al_{0.3}$ are studied.

2. For the selected operating temperatures of 373 / 303 / 291 K and 400 / 303 / 283 K, the COP, SCP of the crossed van't Hoff line MHHP are found to be 0.89 and 30.8 W/kg of total mass, and 0.86 and 30.3 W/kg of total mass, respectively for $V_{0.846}Ti_{0.104}Fe_{0.05}$ / $Fe_{0.9}Mn_{0.1}Ti$ and $V_{0.855}Ti_{0.095}Fe_{0.05}$ / $MmNi_{4.7}Al_{0.3}$ hydride pairs.

3. Results reveal that the COP increases by approximately 35% between the conventional and crossed van't Hoff line MHHP systems.

APPENDIX – A

REACTION KINETICS STUDIES EXPERIMENTAL SET-UP

Generally, gravimetric or volumetric methods are used to investigate the reaction kinetics of metal hydride alloys. The reaction kinetics of the selected metal hydride samples were measured at IKE, University of Stuttgart, Germany using the volumetric method (Fu, 2007; Muthukumar *et al.,* 2009). This measurement is based on the principle that a closed, sealed system contains hydrogen either in gaseous state or bound in the metal hydride. If the volume is known, the gaseous amount can be calculated by measuring the respective temperature and pressure using a real gas equation. Fig. A.1 shows the experimental set-up used for reaction kinetics measurement of the selected metal hydride alloys. The experimental set-up is divided into two main sections: area 1 (left part of the

set-up) and area 2 (right part of the set-up), which are separated during the hydriding process through valves A10 (during the dehydriding process A7), A11 and A13.

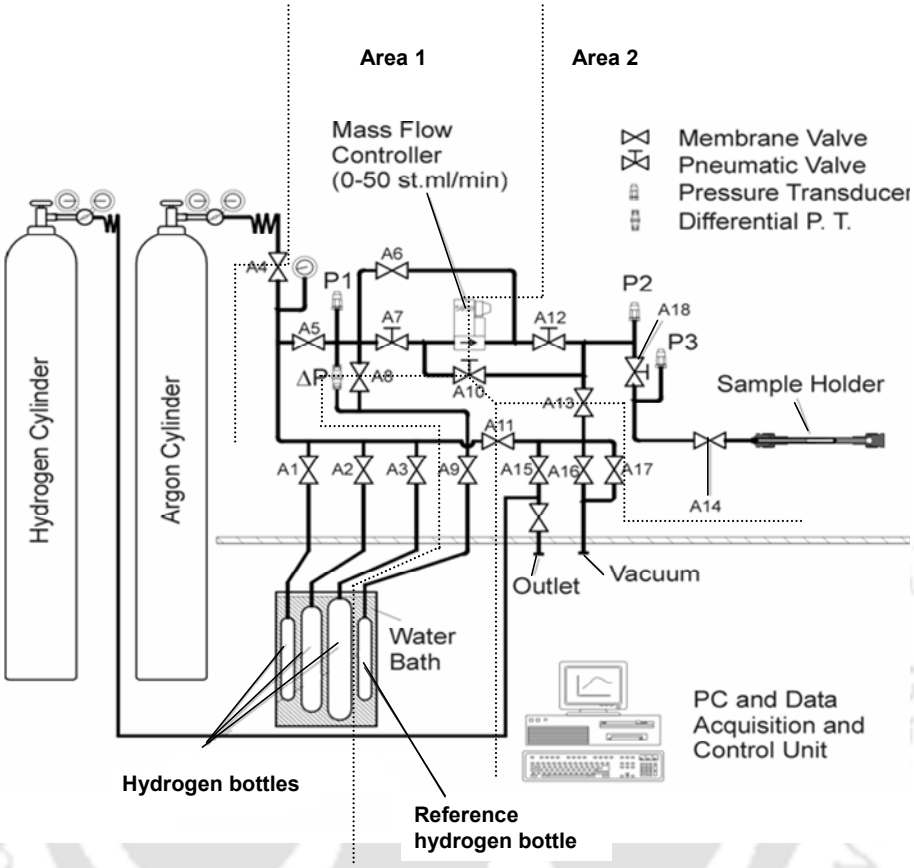

Fig.A.1 Experimental set-up used for measuring the hydriding reaction kinetics (Muthukumar *et al*., 2009)

Through pressure reducer and valve A4, the system can be filled with H_2 for reaction kinetics measurement and activation or with argon for volume determination, respectively. Through valves A1, A2 and A3, the hydrogen reservoir bottles R1, R2 and R3 respectively, are connected. The gas bottles are maintained at a constant temperature in a water bath. The reactor containing the metal hydride is connected to the set-up through valves A14 and A18. P1, P2 and P3 are absolute pressure transducers (resolution 0.01 bar). Additionally, to increase the overall accuracy of the measurement, a differential

pressure transducer (ΔP) is installed which measures the pressure difference between area 1 and a reference hydrogen bottle. This can be bypassed via valve A8. The transducer (accuracy = 0.5 % F.S.) works up to a differential pressure of 2 bar. All measured values are recorded using a PC with a data logging system. The reactor is kept in a thermostat (heating and cooling) to maintain a constant temperature.

Fig. A.2 shows the details of the reactor used for the present analysis. The rector is made up of a copper block having a 3 mm central hole. A 1 gram of metal hydride is filled into this hole. The left side of the reactor is fitted with an O - ring and a screw including a metal sheathed `K´ type thermocouple having a time constant of 0.1 s (resolution 0.1 °C), which is used to measure the temperature of the reaction bed. The right side of the reactor is connected to a filter assembly which prevents the metal hydride powder from being carried away by the hydrogen gas during desorption. Heat generated during absorption is rejected to the large copper mass (viz. conduction heat transfer), and thereby nearly isothermal reaction condition is maintained in the metal hydride bed during hydriding/dehydriding processes. After connecting the reactor to the set up, the volume of the tubes between valves A14 and A18 and the reactor volume are determined because these volumes can change after the installation of a new reactor. Before starting the absorption and desorption, an activation process of the metal hydride may be necessary to generate clean surface areas of the particles. Temperature, pressure and the number of cycles of this procedure depend on the respective material. In our case, of the order of 10 to 15 activation cycles were carried out. Initially, the whole set-up is evacuated to 10^{-3} mbar, and all valves are closed after evacuation.

At the beginning of the experiment, the area containing the metal hydride (area 2) is evacuated (the metal hydride completely discharged) and area 1 is pressurized to the desired level. Then, the separating valves (A7 and A12) are opened and hydrogen flows from area 1 to area 2. A hydrogen uptake of the sample is determined from the loss of gaseous hydrogen (measured by the differential pressure transducer). Due to the instantaneous high flow rate and the rapidly changing pressure at the beginning of the experiment, the system is not in thermodynamic equilibrium. Depending on the experimental conditions (supply pressure), the first measured data (first 1 or 2 s) are therefore not valid until hydrogenation reaches equilibrium with the set-up. By recording the pressure changes in both the areas and the temperatures, the amount of hydrogen absorbed is calculated using a real gas equation. Temperature fluctuations in the metal hydride bed during the experiments are within 2 K. The step by step procedure for estimating the amount of hydrogen absorbed and desorbed is available in the literature (Fu, 2007; Muthukumar *et al.,* 2009). The estimated uncertainty involved in the calculation of the hydrogen storage capacity is ± 6.5%.

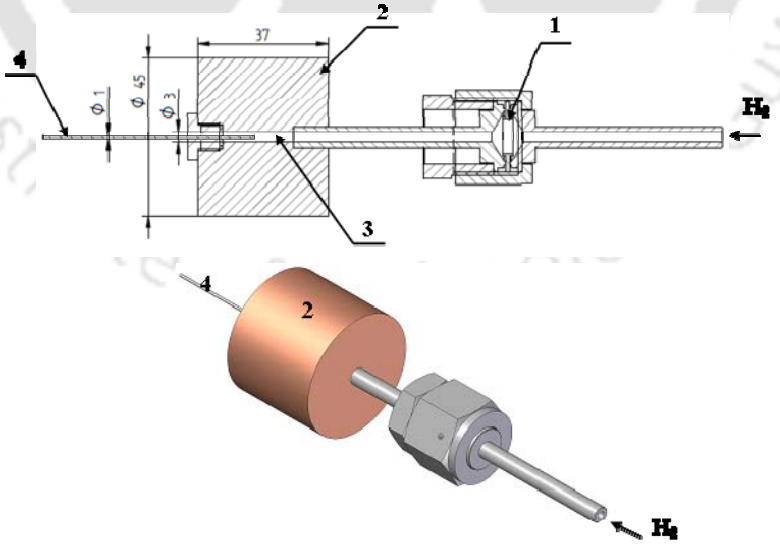

1. Filter 2. Copper mass 3. Metal hydride 4. Thermocouple

Fig.A.2 Schematic of the reactor

APPENDIX – B

DISCRETIZATION OF GOVERNING EQUATIONS

The mathematical model of the coupled heat and mass transfer in a paired reaction beds is solved numerically using the finite volume method and it is presented in Section 4.1. Two-dimensional cylindrical reactors (reaction beds) are considered in the cylindrical coordinate system. The reaction beds are assumed to axisymmetric. Hence, only the top half of the reaction bed is considered for the present investigation. As a first step in the finite volume method, the domain is to be divided into discrete control volumes. Each nodal point is surrounded by a control volume. The boundaries (or faces) of control volumes are positioned mid-way between adjacent nodes. Near the edge of the domain the physical boundaries coincide with the control volume boundaries. A general nodal

point is identified by P and its neighbour points in a two-dimensional geometry is identified as north, south, east and west and they are denoted respectively by N, S, E and W. The north side face of the control volume is referred to be '*n*'. Similarly south, east and west are denoted as *s*, *e* and *w*, respectively. The distance between the nodes W and P, and between nodes P and E is denoted by ΔZ. Similarly, the distance between and N and P, and P and S is denoted by ΔR. The distances between the control volumes faces *n*, *s*, *e* and *w* are denoted as Δr and Δz, respectively.

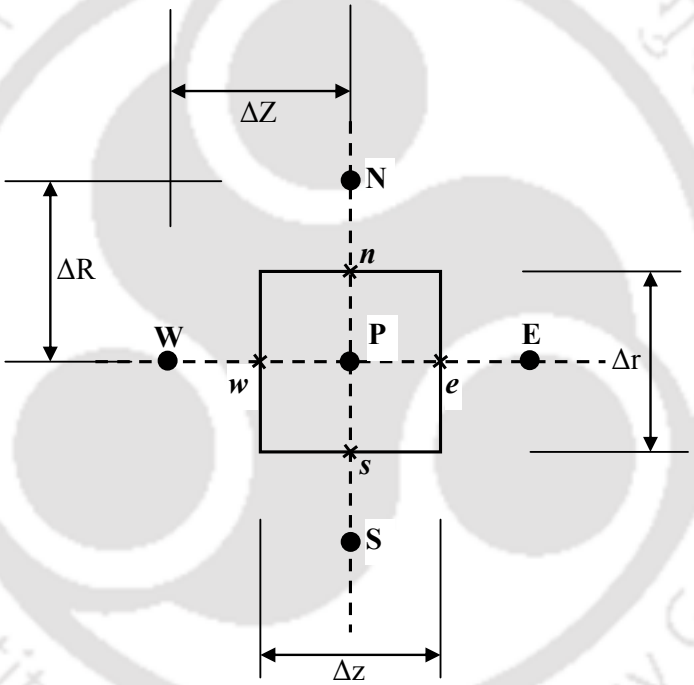

Fig. B.1 Two-dimensional grid generation technique

B.1 Energy Equation

$$\left(\rho C_p\right)_{eff}\frac{\partial T}{\partial t}=\frac{1}{r}\frac{\partial}{\partial r}\left(rk_e\frac{\partial T}{\partial r}\right)+\frac{\partial}{\partial z}\left(k_e\frac{\partial T}{\partial Z}\right)-\left(\rho C_p u\right)_{g,r}\frac{\partial T}{\partial r}-\left(\rho C_p u\right)_{g,z}\frac{\partial T}{\partial z}$$
$$-\dot{m}_{H_2}\left[\frac{\Delta H}{M_g}-T\left(C_{P,g}-C_{p,s}\right)\right] \quad \text{(B.1)}$$

Integrating over the control volume

$$\begin{aligned}\left(\rho C_p\right)_{eff}\frac{T_P^{n+1}-T_P^n}{\Delta t}r_P\Delta r\Delta z = &\left(rk_{eff}\frac{\partial T}{\partial r}\right)_n\Delta z-\left(rk_{eff}\frac{\partial T}{\partial r}\right)_s\Delta z+r\left(k_{eff}\frac{\partial T}{\partial z}\right)_e\Delta r\\ &-r\left(k_{eff}\frac{\partial T}{\partial z}\right)_w\Delta r-\left(r\left(\rho C_p u\right)_{g,r}T\right)_n\Delta z+\left(r\left(\rho C_p u\right)_{g,r}T\right)_s\Delta z\\ &-\left(r\left(\rho C_p u\right)_{g,z}T\right)_e\Delta r+\left(r\left(\rho C_p u\right)_{g,z}T\right)_w\Delta r-\dot{m}_{H_2}\frac{\Delta H}{M_g}r_p\Delta r\Delta z\\ &+\dot{m}_{H_2}\left(C_{P,g}-C_{P,s}\right)r_p\Delta r\Delta z T_P^{n+1}\end{aligned} \tag{B.2}$$

The central difference scheme is applied for the convection term. Hence Eq. (B.2) can be written as

$$\begin{aligned}a_p^o\left(T_P^{n+1}-T_P^n\right) = &D_n\left(T_N^{n+1}-T_P^{n+1}\right)-D_s\left(T_P^{n+1}-T_S^{n+1}\right)+D_e\left(T_E^{n+1}-T_P^{n+1}\right)\\ &-D_w\left(T_P^{n+1}-T_W^{n+1}\right)-F_n\left(\frac{T_N^{n+1}+T_P^{n+1}}{2}\right)+F_s\left(\frac{T_P^{n+1}+T_S^{n+1}}{2}\right)\\ &-F_e\left(\frac{T_E^{n+1}+T_P^{n+1}}{2}\right)+F_w\left(\frac{T_P^{n+1}+T_W^{n+1}}{2}\right)+S_u+S_P T_P^{n+1}\end{aligned} \tag{B.3}$$

Where,

$$D_n=\frac{r_n k_{eff}\Delta z}{\Delta R};\qquad D_s=\frac{r_s k_{eff}\Delta z}{\Delta R};\qquad D_e=\frac{r_e k_{eff}\Delta r}{\Delta Z};\qquad D_w=\frac{r_w k_{eff}\Delta r}{\Delta Z}; \tag{B.4}$$

$$F_n=r_n\Delta z\left(\rho C_p u\right)_{g,r};\quad F_s=r_s\Delta z\left(\rho C_p u\right)_{g,r};\quad F_e=r_e\Delta r\left(\rho C_p u\right)_{g,z};\quad F_w=r_w\Delta r\left(\rho C_p u\right)_{g,z}; \tag{B.5}$$

$$a_P^o=\frac{\left(\rho C_p\right)_{eff}r_P\Delta r\Delta z}{\Delta t}; \tag{B.6}$$

$$S_u=-\frac{\dot{m}_{H_2}\Delta H r_p\Delta r\Delta z}{M_g};\qquad S_P=\dot{m}_{H_2}\left(C_{P,g}-C_{P,s}\right)r_p\Delta r\Delta z; \tag{B.7}$$

$$a_P T_P^{n+1} = a_N T_N^{n+1} + a_S T_S^{n+1} + a_E T_E^{n+1} + a_W T_W^{n+1} + a_p^o T_P^n + S_u; \quad \text{(B.8)}$$

where,

$$a_P = a_P^o + D_n + D_s + D_e + D_w + F_n - F_s + F_e - F_w - S_p; \quad \text{(B.9)}$$

B.2 Continuity Equation

Absorption or desorption of hydrogen to or from the metal hydride is obtained from the conservation of mass expressed using the following equation

$$\varepsilon \frac{\partial(\rho_g)}{\partial t} + \nabla\left(\rho_g \overrightarrow{u_g}\right) = \pm \dot{m}_{H_2} \quad \text{(B.10)}$$

where, + sign denotes the absorption of hydrogen to the metal hydride and – sign denotes desorption of hydrogen. ρ_g denotes the density of the hydrogen gas at any time (t) and u_g the velocity of the hydrogen in the reaction bed.

Metal hydride particles are of porous form. Velocity inside the porous region is calculated using the Darcy's law

$$\overrightarrow{u_g} = -\frac{K}{\mu_g} \nabla P_g \quad \text{(B.11)}$$

By substituting the density (ρ_g) and velocity (u_g) of the gas in Eq. (B.12) the gas pressure (P_g) inside the reactors are determined using the following equation

$$\left(\frac{\varepsilon M_g}{R_u T}\right)\frac{\partial P_g}{\partial t} + \left(\frac{\varepsilon M_g P_g}{R_u}\right)\frac{\partial}{\partial t}\left(\frac{1}{T}\right) - \frac{K}{\nu_g r}\frac{\partial}{\partial r}\left(r\frac{\partial P_g}{\partial r}\right) - \frac{K}{\nu_g}\frac{\partial}{\partial z}\left(\frac{\partial P_g}{\partial z}\right) = \dot{m}_{H_2} \quad \text{(B.12)}$$

$$\frac{\varepsilon M_g}{R_u T}\left(\frac{P_g^{n+1}-P_g^n}{\Delta t}\right) r_p \Delta r \Delta z + \left(\frac{\varepsilon M_g P_g^{n+1}}{R_u}\right)\left(\frac{1}{T_g^{n+1}}-\frac{1}{T_g^n}\right) r_p \Delta r \Delta z$$
$$-\left(\frac{Kr}{\nu_g}\frac{\partial P_g}{\partial r}\right)_n \Delta z + -\left(\frac{Kr}{\nu_g}\frac{\partial P_g}{\partial r}\right)_s \Delta z - \frac{K}{\nu_g}\left(\frac{\partial P_g}{\partial z}\right)_e \Delta r + \frac{K}{\nu_g}\left(\frac{\partial P_g}{\partial z}\right)_w \Delta r \qquad \text{(B.13)}$$
$$= -\dot{m}_{H_2}\, r_p \Delta r \Delta z$$

$$a_P^o\left(P_P^{n+1}-P_P^n\right) + S_P P_P^{n+1} - D_n\left(P_N^{n+1}-P_P^{n+1}\right) + D_s\left(P_P^{n+1}-P_S^{n+1}\right)$$
$$- D_e\left(P_E^{n+1}-P_P^{n+1}\right) + D_w\left(P_P^{n+1}-P_W^{n+1}\right) = -\dot{m}_{H_2}\, r_p \Delta r \Delta z \qquad \text{(B.14)}$$

where,

$$D_n = \frac{Kr_n \Delta z}{\nu_g \Delta R}; \qquad D_s = \frac{Kr_s \Delta z}{\nu_g \Delta R}; \qquad D_e = \frac{Kr_e \Delta r}{\nu_g \Delta Z}; \qquad D_w = \frac{Kr_w \Delta r}{\nu_g \Delta Z}; \qquad \text{(B.15)}$$

$$a_P^o = \frac{\varepsilon M_g r_P \Delta r \Delta z}{R_u T_g \Delta t}; \qquad \text{(B.16)}$$

$$S_u = -\dot{m}_{H_2}\, r_p \Delta r \Delta z; \qquad S_P = \frac{\varepsilon M_g r_p \Delta r \Delta z}{R_u}\left(\frac{1}{T_P^{n+1}}-\frac{1}{T_P^n}\right); \qquad \text{(B.17)}$$

$$a_P P_P^{n+1} = a_N P_N^{n+1} + a_S P_S^{n+1} + a_E P_E^{n+1} + a_W P_W^{n+1} + a_p^o P_P^n + S_u; \qquad \text{(B.18)}$$

where,

$$a_P = a_P^o + D_n + D_s + D_e + D_w + S_p; \qquad \text{(B.19)}$$

REFERENCES

Abraham, K., M.P. Maiya and **S.S. Murthy** (2003) Performance analysis of a single stage four bed metal hydride cooling system, part C: Influence of combined heat and mass recovery, *Int. J. Thermal Sciences*, 42, pp.1021–1027.

Aldas, K., M.D. Mat and **Y. Kaplan** (2002) A three-dimensional mathematical model for absorption in a metal hydride bed, *Int. J. Hydrogen Energy*, 27, pp.1049–1056.

Anil Kumar, E., M.P. Maiya and **S.S. Murthy** (2007) Influence of aluminium content on the dynamic characteristics of mischmetal based hydrogen storage alloys, *J. Alloys and Compounds*, 32, pp.2382–2389.

Askri, F., A. Jemni and **S.B. Nasrallah** (2003) Study of two-dimensional and dynamic heat and mass transfer in a metal-hydrogen reactor, *Int. J. Hydrogen Energy*, 28, pp.537–557.

Askri, F., A. Jemni and **S.B. Nasrallah** (2004a) Prediction of transient heat and mass transfer in a closed metal-hydrogen reactor, *Int. J. Hydrogen Energy*, 29, pp.195–208.

Askri, F., A. Jemni and **S.B. Nasrallah** (2004b) Dynamic behavior of metal-hydrogen reactor during hydriding process, *Int. J. Hydrogen Energy*, 29, pp.635–647.

Askri, F., M.B. Salah, A. Jemni and **S.B. Nasrallah** (2009) Heat and mass transfer studied on metal-hydrogen reactor filled with $MmNi_{4.6}Fe_{0.4}$, *Int. J. Hydrogen Energy*, 34, pp.6705–6711.

Balakumar, M., S.S. Murty, M.V. K. Murthy and **M.V.C. Sastri** (1985) A comparative thermodynamic study of metal hydride heat transformers and heat pumps, *Heat Recovery Systems and CHP*, 5, pp.527–534.

Bjurstrom, H., and **S. Suda** (1989) The metal hydride heat pump: dynamics of hydrogen transfer, *Int. J. Hydrogen Energy*, 14, pp.19–28.

Boser, O (1976) Hydrogen sorption in $LaNi_5$, *J. Less-Common Metals*, 46, pp.91–99.

Bronfman, N., J. Bloch, M.H. Mintz, Sarussi and **I. Jacob** (1991) Kinetics of hydrogen absorption in the intermetallic $Zr(Al_{0.2}Fe_{0.8})_2$, *J. Alloys and Compounds*, 177, pp.183–191.

Chernikov, A.S., L.A. Izhvanov, A.I. Solovey, V.P. Frolov and **I.Y. Shanin** (2002) An installation for water-cooling based on a metal hydride heat pump, *J. Alloys and Compounds*, 330–332, pp.907–910.

Cui, X.Y., Q. Li, K.C. Chou, S.L. Chen, G.W. Lin and **K.D. Xu** (2008) A comparative study on the hydriding kinetics of Zr-based AB_2 hydrogen storage alloys, *Intermetallics*, 16, pp.662–667.

Dantzer, P and **E. Orgaz** (1986) Thermodynamics of the hydride chemical heat pump-II, How to select a pair of alloys, *Int. J. Hydrogen Energy*, 11, pp.797–806.

Dehouche, Z., W.D. Jong, E. Willers, A. Isselhorst and **M. Groll** (1998) Modeling and simulation of heating/Air conditioning systems using the multi-hydride thermal-wave concept, *Applied Thermal Engineering*, 18, pp.457–480.

Demircan, A., M. Demiralp, Y. Kaplan, M.D. Mat and **T.N. Veziroglu** (2005) Experimental and theoretical analysis of hydrogen absorption in $LaNi_5$-H_2 rectors, *Int. J. Hydrogen Energy*, 30, pp.1437–1446.

Dhaou, H., F. Askri, M.B. Salah, A. Jemni, B.S Nasrallah and **J. Lamloumi** (2007) Measurement and modelling of kinetics of hydrogen sorption by $LaNi_5$ and two related pseudobinary compounds, *Int. J. Hydrogen Energy*, 32, pp.576–587.

Dogan, A., Y. Kaplan and **T.N. Veziroglu** (2004) Numerical investigation of heat and mass transfer in a metal hydride bed, *Applied Mathematics and Computation*, 150, pp.169–180.

Fedorov, E.M., Y.I. Shanin and **L.A. Izhvanov** (1999) Simulation of hydride heat pump operation, *Int. J. Hydrogen Energy*, 24, pp.1027–1032.

Fleming, W.H., J.A. Khan and **C.A. Rhodes** (2001) Effective heat transfer in a metal hydride based hydrogen separation process, *Int. J. Hydrogen Energy*, 26, pp.711–724.

Førde, T., E. Næss and **V.A. Yartys** (2009) Modelling and experimental results of heat transfer in a metal hydride store during hydrogen charge and discharge, *Int. J. Hydrogen Energy*, 34, pp.5121–5130.

Fu, Y (2007) Investigation on hydrogen storage properties of Mg-based nanostructured composites, *PhD Thesis*, IKE, University of Stuttgart, Germany.

Gambini, M (1993) Metal hydride energy systems performance evaluation, Part A: Dynamic analysis model of heat and mass transfer, *Int. J. Hydrogen Energy*, 19, pp.67–80.

Gambini, M., M. Manno and **M. Vellini** (2008) Numerical analysis and performance assessment of metal hydride-based hydrogen storage systems, *Int. J. Hydrogen Energy*, 33, pp.6178–6187.

Goodell, P.D and **G.D. Sandrock** (1980) Kinetics and dynamic aspects of rechargeable metal hydrides, *J. Less-Common Metals*, 73, pp.135–142.

Gopal, M.R and **S.S. Murthy** (1992) Prediction of heat and mass transfer in annular cylindrical metal hydride beds, *Int. J. Hydrogen Energy*, 17, pp.795–805.

Gopal, M.R and **S.S. Murthy** (1995a) Prediction of metal-hydride refrigerator performance based on reactor heat and mass transfer, *Int. J. Hydrogen Energy*, 20, pp.607–614.

Gopal, M.R and **S.S. Murthy** (1995b) Studies on heat and mass transfer in metal hydride beds, *Int. J. Hydrogen Energy*, 20, pp.911–917.

Gopal, M.R and **S.S. Murthy** (1995c) Performance of metal hydride cooling system, *Int. J. Refrigeration*, 18, pp.413–420.

Gopal, M.R (1996) Thermodynamic and heat transfer studies on metal hydride heat pumps and heat transformers, *PhD Dissertation*, IIT Madras, India.

Gopal, M.R and **S.S. Murthy** (1999) Experiments on a metal hydride cooling system working with ZrMnFe/$MmNi_{4.5}Al_{0.5}$ pair, *Int. J. Refrigeration*, 22, pp.137–149.

Goudy A.J., D.G. Stokes and **J.A. Gazzillo** (1983) The effect of heat transfer on the desorption kinetics of $LaNi_5H_6$. *J. Less-Common Metals*, 91, pp.149–158.

Goudy, A.J and **R.A. Wallingford** (1984) Desorption kinetics of $LaNi_5$, $LaNi_{4.7}Al_{0.3}$, (CFM)Ni_5 and $MmNi_{4.5}Al_{0.5}$ hydrides, *J. Less-Common Metals*, 99, pp.249–256.

Groll, M., W. Supper, U. Mayer and **O. Brost** (1987) Heat and mass transfer limitations in metal hydride reaction beds, *Int. J. Hydrogen Energy*, 12, pp.89–97.

Groll, M (1993) Reaction beds for dry sorption machines, *Heat Recovery Systems and CHP*, 13, pp.341–346.

Gruen, D.M., M.H. Mendelsohn and **I. Sheft** (1978) Metal hydrides as chemical heat pumps, *Solar Energy*, 21, pp.153–156.

Guo, Z and **H.J. Sung** (1999) Technical note conjugate heat and mass transfer in metal hydride beds in the hydriding process, *Int. J. Heat and Mass Transfer*, 42, pp.379-382.

Ha, M.Y., I.K. Kim, H.D. Song, S. Sung and **D.H. Lee** (2004) A numerical study of thermo-fluid phenomena in metal hydride beds in the hydriding process, *Int. J. Heat and Mass Transfer*, 47, pp.2901–2912.

Holt, A., E.C. Edgar and **J.B. Firth** (1913) Zeitschrift für Physikalische Chemie, 82, 513.

Huang, P., A.J. Goudy and **J.T. Koh** (1989) Hydrogen absorption-desorption kinetics of $MmNi_5$ and their related compounds, *J. Less-Common Metals*, 155, pp.111–118.

Huston, E.L and **G.D. Sandrock** (1980) Engineering properties of metal hydrides, *J. Less-Common Metals*, 74, pp.435–443.

Imoto, T., T. Yonesaki, S. Fujitani, I. Yonezu, N. Hiro, K. Nasak and **T. Saito** (1996) Development of an F-class refrigeration system using hydrogen-absorbing alloys. *Int. J. Hydrogen Energy*, 21, pp.451–455.

Isselhorst, A and **M. Groll** (1995) Two-stage metal hydride heat transformer laboratory model, *J. Alloys and Compounds*, 231, pp.888–894.

Isselhorst, A (1995) Heat and mass transfer in coupled hydride reaction beds, *J. Alloys Compounds,* 231, pp.871–879.

Jang, K.J., G.A. Fateev, J.G. Park, S.C. Han, P. Lee and **J.Y. Lee** (2001) Simulation of the metal hydride heat pump system with the single and double reactors, *Int. J. Hydrogen Energy*, 26, pp.231–241.

Jemni, A and **S.B. Nasrallah** (1995a) Study of two dimensional heat and mass transfer during absorption in a metal-hydrogen reactor, *Int. J. Hydrogen Energy*, 20, pp.43–52.

Jemni, A and **S.B. Nasrallah** (1995b) Study of two dimensional heat and mass transfer during desorption in a metal-hydrogen reactor, *Int. J. Hydrogen Energy*, 20, pp.881–891.

Kang, B.H and **A. Kuznetsov** (1995) Thermal modelling and analysis of a metal hydride chiller for air conditioning, *Int. J. Hydrogen Energy*, 20, pp.665–674.

Kesavan, T.R., R. Ramesh, K.V.S. Rama Rao and **T.P. Das** (1996) Hydrogen absorption studies in $Zr_{0.4}Ho_{0.8}Fe_{0.2}$, *J. Alloys and Compounds*, 244, pp.164–169.

Kim, K.J and **K.T. Feldman** (1997a) Heat-driven hydride slurry heat pumps, *Int. J. Refrigeration*, 20, pp.339–351.

Kim, K.J., K.T. Feldman and **A. Razani** (1997b) Cooling and power efficiency diagrams for compressor-driven, metal-hydride slurry air conditioners, *Energy,* 22, pp.787–796.

Kim, K.J., K.T. Feldman, G. Lloyd and **A. Razani** (1997) Compressor-driven metal-hydride heat pumps, *Applied Thermal Engineering,* 17, pp. 551–560.

Kim, S.R and **J.Y. Lee** (1991) The effect of thermal cycling on the hydriding rate of $MmNi_{4.5}Al_{0.5}$, *Int. J. Less-Common Metals*, 161, pp.37–47.

Klein, H.-P and **M. Groll** (2002) Development of a two-stage metal hydride system as topping cycle in cascading sorption systems for cold generation, *Applied Thermal Engineering*, 22, pp.631–639.

Klein, H.-P (2007) Operational performance of a double stage metal hydride sorption system for cold generation, *PhD Thesis*, IKE, University of Stuttgart, Germany.

Koh, J.T., A.J. Goudy, P. Huang and **G.A. Zhou** (1989) A comparison of the hydriding and dehydriding kinetics of $LaNi_5$ hydride, *J. Less-Common Metals*, 153, pp.89–100.

Lee. S.G., Y.K. Kim and **J.Y. Lee** (1995) Operating characteristics of metal hydride heat pump using Zr-based laves phases, *Int. J. Hydrogen Energy*, 20, pp.77–85.

Li. Q., K.C. Chou, Q. Lin, L.J. Jiang and **F. Zhan** (2004) Influence of the initial hydrogen pressure on the hydriding kinetics of the $Mg_{2-x}Al_xNi$(x = 0, 0.1) alloys, *Int. J. Hydrogen Energy*, 29, pp.1383-1388.

Libowitz. G.G., K.T. Feldman Jr. and **C. Stein** (1997) Thermodynamic properties of metal hydrides for novel heat pump configuration, *J. Alloys and Compounds*, 253-254, pp.673–676.

Lucas, G.G and **WC. S.L. Richards** (1984) Mathematical modelling of hydrogen storage systems, *Int. J. Hydrogen Energy*, 9, pp.225–231.

Magnetto, D., S. Mola, D.H. Da Costa, M. Golben and **M.A. Rosso** (2006) metal hydride mobile air conditioning system, *SAE International*, (2006-01-1235).

Martin, M., C. Gommel, C. Borkhart and **E. Fromm** (1996) Absorption and desorption kinetics of hydrogen storage alloys, *J. Alloys and Compounds*, 238, pp.193–201.

Marty, P., J.F. Fourmigue, P.D. Rango, D. Fruchart and **J. Charbonnier** (2006) Numerical simulation of heat and mass transfer during the absorption of hydrogen in a magnesium hydride, *Energy Conversion and Management*, 47, pp.3632–3643.

Mat, M.D and **Y. Kaplan** (2001) Numerical study of hydrogen absorption in an $LmNi_5$ hydride reactor, *Int. J. Hydrogen Energy*, 26, pp.957–963.

Mayer, U., M. Groll and **W. Supper** (1987) Heat and mass transfer in metal hydride reaction beds: Experimental and theoretical results, *J. Less-Common Met*als, 131, pp.235–244.

Mazumdar, S., M.R. Gopal and **S. Bhattacharyya** (2005) Compressor driven metal hydride cooling and heating systems, *International Conference on Solid State Hydrogen Storage – Materials and Applications*, Hyderabad, India; Jan. 31–Feb. 1.

Mellouli, S., F. Askri, H. Dhaou, A. Jemni and **S.B. Nasrallah** (2009) Parametric studies on a metal hydride cooling system, *Int. J. Hydrogen Energy*, 34, pp.3945–3952.

Mellouli, S., F. Askri, H. Dhaou, A. Jemni and **S.B. Nasrallah** (2010) Numerical simulation of heat and mass transfer in metal hydride hydrogen storage tanks for fuel cell vehicles, *Int. J. Hydrogen Energy*, 35(4), pp.1693–1705.

Melnichuk, M., N. Silin, G. Andreasen, H.L. Corso, A. Visintin and **H.A. Peretti** (2010) Hydrogen discharge simulation and testing of a metal-hydride container, *Int. J. Hydrogen Energy*, 35, pp.5855–5859.

Ming, L., E. Lavendar and **A.J. Goudy** (1997) The hydriding and dehydriding kinetics of some RCo_5 alloys. *Int. J. Hydrogen Energy*, 22, pp.63–66.

Mintz, M.H (1991) Mixed mechanisms controlling hydrogen-metal reactions under steady state conditions: the diffusion-interface mechanism, *J. Alloys and Compounds*, 176, pp.77–87.

Miyamoto, M., K. Yamaji and **Y. Nakata** (1983) Reaction kinetics of $LaNi_5$, *J. Less-Common Metals*, 89, pp.111–116.

Mungole, M.N and **R. Balasubramaniam** (1998) Hydrogen desorption kinetics in $MmNi_{4.2}Al_{0.8}$-H systems, *Int. J. Hydrogen Energy*, 23, pp.349–353.

Murthy, S.S and **M.V.C. Sastri** (1992) Thermodynamic analysis of two-stage ternary metal hydride heat pumps, *Int. J. Hydrogen Energy*, 17, pp.731–735.

Muthukumar, P., M.P. Maiya and **S.S. Murthy** (2005) Experiments on a metal hydride-based hydrogen storage device, *Int. J. Hydrogen Energy*, 30, pp.1569–1581.

Muthukumar. P., U. Madhavakrishna and **A. Dewan** (2007) Parametric studies on a metal hydride based hydrogen storage device, *Int. J. Hydrogen Energy*, 32, pp.4988–4997.

Muthukumar. P and **S.V. Ramana** (2009) Numerical simulation of coupled heat and mass transfer in metal hydride-based hydrogen storage reactor, *J. Alloys and Compounds*, 472, pp.466–472.

Muthukumar. P., M. Linder, R. Mertz and **E. Laurien** (2009) Measurement of thermodynamic properties of some hydrogen absorbing alloys, *Int. J. Hydrogen Energy*, 34, pp.1873-1879.

Muthukumar, P., A. Satheesh, M. Linder, R. Mertz and **M. Groll** (2009c) Studies on hydriding kinetics of some La-based metal hydride alloys, *Int. J. Hydrogen Energy,* 34, pp.7253–7262.

Nagel, M., Y. Komazaki and **S. Suda** (1986) Dynamic behaviour of paired metal hydrides: I. Experimental method and results, *J. Less-Common Metals*, 120, pp.45–53.

Nagel, M., Y. Komazaki, M. Uchida S. Suda and **Y. Matsubara** (1984) Operating characteristics of a metal hydride heat pump for generating cooled air, *J. Less-Common Metals*, 104, pp.307–314.

Nakagawa, T., A. Inomata, H. Aoki and **T. Miura** (2000) Numerical analysis of heat and mass transfer characteristics in the metal hydride bed, *Int. J. Hydrogen Energy*, 25, pp.339–350.

Ni, J and **H. Liu** (2007) Experimental research on refrigeration characteristics of a metal hydride heat pump in auto air-conditioning, *Int. J. Hydrogen Energy*, 32, pp.2567–2572.

Nishizaki, T., K. Miyomoto and **K. Yoshida** (1983) Coefficient of performance of hydride heat pumps, *J. Less-Common Metals*, 89, pp.559–566.

Orgaz, E and **P. Dentzer** (1986) Thermodynamics of the HCHP-111: Considerations for multistage operation, *J. Less-Common Metals*, 131, pp.385–398.

Park. J.M and **J.Y. Lee** (1990) Hydrogenation characteristics of the $Zr_{1-x}Ti_xCr_{1-y}Fe_{1+y}$ laves phase alloys, *J. Less Common Metals*, 160, pp.259–271.

Park, J.G., K.J. Jang, P.S. Lee and **J.Y. Lee** (2001) The operating characteristics of the compressor-driven metal hydride heat pump system, *Int. J. Hydrogen Energy*, 26, pp. 701–706

Park, J.G., S.C. Han, H.Y. Jang, S.M. Lee, P.S. Lee and **J.Y. Lee** (2002) The development of compressor-driven metal hydride heat pump (CD-MHHP) system as an air conditioner, *Int. J. Hydrogen Energy*, 27, pp. 941–944.

Patankar S.V (1980) Numerical Heat Transfer and Fluid Flow, Hemisphere, New York.

Paya, J., M. Linder, E. Laurien and **J.M. Corberan** (2009) Dynamic model and experimental results of a thermally driven metal hydride cooling system, *Int. J. Hydrogen Energy*, 34, pp.3173–3184.

Phate, A.K., M.P. Maiya and **S.S. Murthy** (2007) Simulation of transient heat and mass transfer during hydrogen sorption in cylindrical metal hydride beds, *Int. J. Hydrogen Energy*, 32, pp.1969–1981.

Qin, F., J. Chen, M. Lu, Z. Chen, Y. Zhou and **K. Yang** (2007) Development of a metal hydride refrigeration system as an exhaust gas-driven automobile air conditioner, *Renewable Energy*, 32, pp.2034–2052.

Reilly, J.J (1979) Metal hydride technology, *Z. Phys. Chemie N.F*, 117, pp.655–681.

Ron. M (1984) A hydrogen heat pump as a bus air conditioner, *J. Less-Common Metals*, 104, pp.259–278.

Rudman, P.S (1983) Hydriding and dehydriding kinetics, *J. Less-Common Metals*, 89, pp.93–110.

Sieverts, A (1914) Palladium und Wasserstoff II, *Z. Phys. Chem*, 88, pp.451.

Skripnyuk, V.M and **M. Ron** (2003) Hydrogen desorption kinetics in intermetallic compounds C2, C51 and C52 with Laves phase structure, *Int. J. Hydrogen Energy*, 28, pp.303–309.

Srinivas, G., V. Sankaranarayanan and **S. Ramaprabhu** (2008) Kinetics of hydrogen absorption in $Ho_{1-x}Mm_xCo_2$ alloys, *J. Alloys and Compounds*, 448, pp.159–165.

Suda, S (1984) Experimental evaluation of heat pump performance in connection with metal hydride properties, *J. Less-Common Metals*, 104, pp.211–222.

Suda, S., Y. Komazaki, H. Narasaki and **M. Uchida** (1991) Development of a double-stage heat pump: Experimental and analytical survey, *J. Less-Common Metals*, 172-174, pp.1092–1110.

Sun, D.W (1996) Thermodynamic analysis of the operation of two-stage metal-hydride heat pumps, *Applied Energy*, 54, pp. 29–47.

Sun, D.W., M. Groll and **R. Werner** (1992) Selection of alloys and their influence on the operational characteristics of a two-stage metal hydride heat transformer, *Heat Recovery System and CHP*, 12, pp.49–55.

Sun, D.W and **S.J. Deng** (1990) Numerical solution of the two dimensional non-steady heat and mass transfer problem in metal hydride beds, *Int. J. Hydrogen Energy*, 15, pp.807–816.

Supper, W., M. Groll and **U. Mayer** (1984) Reaction kinetics in metal hydride reaction beds with improved heat and mass transfer, *J. Less-Common Metals*, 104, pp.279–286.

Veerraju, C and **M.R. Gopal** (2010) Heat and mass transfer studies on plate fin-and-elliptical tube type metal hydride reactors, *Applied Thermal Engineering*, 30, pp.673–682.

Wang, X.L and **S. Suda** (1990) Dehydriding kinetics study of $LaNi_{4.7}Al_{0.3}$ hydride by a step-wise method, *J. Less-Common Metals*, 159, pp.83–90.

Website: http://hydpark.ca.sandia.gov/

Werner, R (1988) Two-stage metal hydride heat transformer lab model, In M. Groll, and R. Werner (eds.) Proc of Int. Workshop on Metal Hydrides for Hydrogen Storage, Purification and Thermodynamic devices, Stuttgart, Germany, Sept 1-2, pp.91-101.

Willers, E and **M. Groll** (1999a) Evaluation of metal hydride machines for heat pumping and cooling applications, *Int. J. Refrigeration*, 22, pp.47–58.

Willers, E and **M. Groll** (1999b) The two-stage metal hydride heat transformer, *Int. J. Hydrogen Energy*, 24, pp.269–276.

Willers, E., M. Wanner and **M. Groll** (1999) A multi-hydride thermal wave device for simultaneous heating and cooling, *J. Alloys and Compounds*, 293–295, pp.915–918.

Winter, C.J (2009) Hydrogen energy–abundant efficient, clean: a debate over the energy-system-of-change, *Int. J. Hydrogen Energy*, 34, pp.S1–S52.

Ye, J., L. Jiang, Z. Li, X. Liu, S. Wang and **X. Li** (2010) Numerical analysis of heat and mass transfer during absorption of hydrogen in metal hydride based hydrogen storage tanks, *Int. J. Hydrogen Energy*, 35, pp.8216–8224.

Zarynow, A., A.J. Goudy, R.G. Schweibenz and **K.R. Clay** (1993) The effect of the partial replacement of nickel in $LaNi_5$ hydride with iron, cobalt, and copper on absorption and desorption kinetics. *J. Less-Common Metals*, 172-174, pp.1009–1017.

Zhang, W., J. Cimato and **A.J. Goudy** (1993) The hydriding and dehydriding kinetics of some $LaNi_{5-x}Al_x$ alloys. *J. Alloys and Compounds*, 201, pp.175–179.

Züttel A (2003) Material for hydrogen storage, *Materials Today*, 6, pp.24–33.

List of Publications

List of publication based on the present thesis work

International Journal Publications

1. **Muthukumar, P., A. Satheesh**, **U. Madhavakrishna** and **A. Dewan** (2009) Numerical investigation of coupled heat and mass transfer during desorption of hydrogen in metal hydride beds, *Energy Conversion and Management,* 50, pp.69–75.

2. **Satheesh, A., P. Muthukumar** and **A. Dewan** (2009) Computational study of metal hydride cooling system, *Int. J. Hydrogen Energy*, 34, pp.3164–3172.

3. **Muthukumar, P., A. Satheesh, M. Linder, R. Mertz** and **M. Groll** (2009) Studies on hydriding kinetics of some La-based metal hydride alloys, *Int. J. Hydrogen Energy,* 34, pp.7253–7262.

4. **Satheesh, A** and **P. Muthukumar** (2010) Simulation of double-stage double-effect metal hydride heat pump, *Int. J. Hydrogen Energy*, 35, pp.1474–1484.

5. **Satheesh, A** and **P. Muthukumar** (2010) Performance investigations of single-stage metal hydride heat pump, *Int. J. Hydrogen Energy,* 35, pp. 6950–6958.

6. **Satheesh, A** and **P. Muthukumar** (2010) Performance investigation of double-stage metal hydride heat pump, *Applied Thermal Engineering, 30,* pp. 2698–2707.

7. **Satheesh, A., P. Muthukumar** and **M. Groll** (2010) Feasibility study of crossed van't Hoff line concept for single-stage metal hydride heat pump, *Communicated to Applied Thermal Engineering*.

National/International Conferences

1. **Satheesh, A., P. Muthukumar** and **A. Dewan** (2008) Numerical investigation of coupled heat and mass transfer during desorption of hydrogen in metal hydride beds, *Centenary – International Conference on Advances in Mechanical Engineering*, IISc Bangalore, 02–04 July.

2. **Satheesh, A., P. Muthukumar, M. Linder, R. Mertz** and **E. Laurien** (2009) Reaction kinetics studies on $LmNi_{4.91}Sn_{0.15}$ hydride, *International Conference on Hydrogen and Hydrogen storage methods and Materials*, IISc Bangalore, 03–06 Jan.

3. **Satheesh, A., P. Muthukumar** and **A. Dewan** (2009) Modelling of metal hydride based cooling system, *National Conference on Refrigeration and Air Conditioning*, IIT Madras, 08–10 Jan.

4. **Satheesh, A., P. Muthukumar, A. Dewan** and **M. Groll** (2009) Performance investigation of a double stage double effect metal hydride heating and cooling system, *World Hydrogen Technologies Convention*, IIT Delhi, 26–28 Aug.

5. **Satheesh, A** and **P. Muthukumar** (2009) Operation and performance investigation of a double-stage double-effect metal hydride heat pump, *International Symposium on Hydrogen in Matter*, IIT Madras, 13–16 Dec.

6. **Satheesh, A., P. Muthukumar** and **A. Dewan** (2010) Performance analysis of metal hydride based cooling systems, *20th National and 9th International ISHMT-ASME Heat and Mass transfer Conference*, IIT Bombay, 04–06 Jan.

7. **Satheesh, A., P. Muthukumar** and **M. Groll** (2010) Feasibility study of crossed van't Hoff line concept for single-stage metal hydride heat pump, *International Symposium on Innovative Materials for Processes in Energy Systems 2010 - For Fuel Cells, Heat Pumps and Sorption Systems*, Singapore, Nov. 30th- Dec. 01st, 2010.